DISCOVERY OF NOVEL MURAYMYCIN ANTIBIOTICS AND
INSIGHT INTO THE BIOSYNTHETIC PATHWAY

_____

DISSERTATION
_____

A dissertation submitted in partial fulfillment of the
requirements for the degree of Doctor of Philosophy in the
College of Pharmacy
at the University of Kentucky

By
Zheng Cui
Lexington, Kentucky
Director: Dr. Steven G. Van Lanen, Professor of Pharmaceutical Sciences
Lexington, Kentucky
2017

ABSTRACT OF DISSERTATION

DISCOVERY OF NOVEL MURAYMYCIN ANTIBIOTICS AND
INSIGHT INTO THE BIOSYNTHETIC PATHWAY

New antibiotics with novel targets or mechanisms of action are needed to counter the steady emergence of bacterial pathogens that are resistant to antibiotics used in the clinic. MraY, a promising novel target for antibiotic development, initiates the lipid cycle for the biosynthesis of peptidoglycan cell wall, which is essential for the survival of most, if-not-all, bacteria. MraY is an enzyme that catalyzes the transfer and attachment of phospho-MurNAc-pentapeptide to a lipid carrier, undecaprenylphosphate. Muraymycins are recently discovered lipopeptidyl nucleoside antibiotics that exhibit remarkable antibiotic activity against Gram-positive as well as Gram-negative bacteria by inhibiting MraY. We conducted a thorough examination of the metabolic profile of *Streptomyces* sp. strain NRRL 30473, a known producer of muraymycins. Eight muraymycins were isolated and characterized by a suite of spectroscopic methods, including three new members of muraymycin family named B8, B9 and C5. Muraymycins B8 and B9, which differ from other muraymycins by having an elongated fatty acid side chain, showed potent antibacterial activity against *Escherichia coli* Δ*tolC* mutant and pM IC_{50} against *Staphylococcus aureus* MraY. Muraymycin C5, which is characterized by an N-acetyl modification of the disaccharide's primary amine, greatly reduced its antibacterial activity, which possibly indicates this modification is used for self-resistance.

In addition to the discovery of new muraymycins, eleven enzymes from the biosynthetic pathway were functionally assigned and characterized *in vitro*. Six enzymes involved in the biosynthesis of amino ribofuranosylated uronic acid moiety of muraymycin were characterized: Mur16, a non-heme, Fe(II)-dependent α-ketoglutarate: UMP dioxygenase; Mur17, an L-threonine: uridine-5′-aldehyde transaldolase; Mur20, an L-methionine:1-aminotransferase; Mur26, a low specificity pyrimidine nucleoside phosphorylase; Mur18, a primary amine-requiring nucleotidylyltransferase; Mur19, a 5-amino-5-deoxyribosyltransferase. A one-pot enzyme reaction was utilized to produce this disaccharide moiety and its 2″-deoxy analogue. Two muraymycin-modifying enzymes that confer self-resistance were functionally assigned and characterized: Mur28, a TmrB-like ATP-dependent muraymycin phosphotransferase, and Mur29, a muraymycin nucleotidyltransferase. Notably, Mur28 preferentially phosphorylates the intermediate, aminoribofuranosylated uronic acid, in

the muraymycin biosynthetic pathway to produce a cryptic phosphorylated-dissacharide intermediate. Mur23 and Mur24 were assigned as two enzymes that modify the cryptic phosphorylated intermediate by attachment of an aminopropyl group. Mur24 catalyzes the incorporation of butyric acid into the phosphorylated-disaccharide. Following the incorporation, Mur23 catalyzes a PLP-dependent decarboxylation. Finally, Mur15, which belongs to the cupin family, is functionally assigned as a non-heme, Fe(II)-dependent α-ketoglutarate dioxygenase that catalyzes the β-hydroxylation of a leucine moiety in muraymycin D1 to form muraymycin C1. Mur15 can also hydroxylate the γ-position of leucine moiety to muraymycins with fatty acid chain in β-position.

KEYWORDS: nucleoside antibiotics, muraymycin, translocase I (MraY), antibiotic resistance, biosynthesis

<div align="right">

Zheng Cui
_____
Student's Signature
12/14/2017
_____
Date

</div>

DISCOVERY OF NOVEL MURAYMYCIN ANTIBIOTICS AND
INSIGHT INTO THE BIOSYNTHETIC PATHWAY

By

Zheng Cui

Steven G. Van Lanen		
Director of Dissertation		
David Feola		
Director of Graduate Studies		
12/14/2017		
Date		

献给我的奶奶姥姥爸爸妈妈，我爱你们

Dedicated to my grandmas and parents for their unconditional love

ACKNOWLEDGEMENTS

TABLE OF CONTENTS

LIST OF TABLES

LIST OF FIGURES

LIST OF FIGURES IN SUPPORTING INFORMATION

LIST OF ABBREVIATIONS

DMSO	dimethyl sulfoxide
2D	two dimensional
ACC	1-aminocyclopropanecarboxylic acid
AdoMet	*S*-adenosyl-L-methionine
ADR	5″-amino-5″-deoxyribose
AMP	adenosine monophosphate
AQC	6-aminoquinolyl-*N*-hydroxysuccinimidyl carbamate
Arg	arginine
Asp	aspartic acid
ATP	adenosine triphosphate
COSY	correlation spectroscopy
CTP	cytidine triphosphate
dATP	2′-deoxy-adenosine triphosphate
dTTP	2′-deoxy-thymidine triphosphate
E. coli	*Escherichia coli*
GlyU	(5′S,6′S)-5′-C-glycyluridine
GTP	guanosine triphosphate
h	hour
His$_6$	hexa-histidine
HMBC	heteronuclear multiple-bond correlation spectroscopy
HPLC	high performance liquid chromatography
HR-ESI-MS	high resolution-electrospray ionization-mass spectrometry
HSQC	heteronuclear single-quantum correlation spectroscopy
IPTG	β-D-1-thiogalactopyranoside
kD	kilodalton
LC-MS	liquid chromatography-mass spectrometry
Leu	leucine
L-VG	L-vinylglycine

MBP	maltose binding protein
MBTH	3-methyl-2-benzothiazolinone hydrazone hydrochloride
MeOH	methanol
Met	methionine
MIC	minimum inhibitory concentration
min	minute
MTA	methylthioadenosine
MW	molecular weight
NDP	nucleotidyl diphosphate
NMR	nuclear magnetic resonance
NOESY	nuclear overhauser effect spectroscopy
NRPS	nonribosomal peptide synthetase
NTP	nucleotidyl triphosphate
OD	optical density
PCR	polymerase chain reaction
PHOS	phosphate
PLP	pyridoxal phosphate
rt	room temperature
S. aureus	*Staphylococcus aureus*
SAR	structural-activity relationship
SDS	sodium dodecyl sulfate
SMM	[(3*S*)-3-Amino-3-carboxypropyl] (dimethyl)-sulfonium iodide
TEA	triethylamine
TFA	trifluoroacetic acid
TOCSY	total correlation spectroscopy
UDP	uridine diphosphate
UMP	uridine monophosphate
UTP	uridine triphosphate
UV/Vis	ultraviolet/visible

α-KB   α-ketobutyrate

α-KG   α-ketoglutarate

Chapter 1 : Introduction and Background

1.1 Muraymycins Discovery

Muraymcyins were discovered from a *Streptomyces* sp. organism guided by cell-wall specific biological assays by Wyeth-Research in 2001.[1] Structural elucidation revealed that the muraymycin family belongs to the lipopeptidyl nucleoside antibiotic family. The 22 muraymycins that were discovered have a common peptide-appended, ribofuranoside uronic acid core structure (Figure 1.1). Discovered members of this family differ in one or more of three components: the fatty acyl chain, the aminoribose and the terminal amino acid in the peptide chain. Muraymycin A1 with a guanidino fatty acyl side chain is the most potent member of the family and showed good activity against *Staphylococcal* (MIC 2 to 16 μg/mL), *Escherichia coli imp* mutant (MIC <0.03 μg/mL) and *Staphylococcus aureus* in infected mice (ED$_{50}$ 1.1 mg/kg).[2]
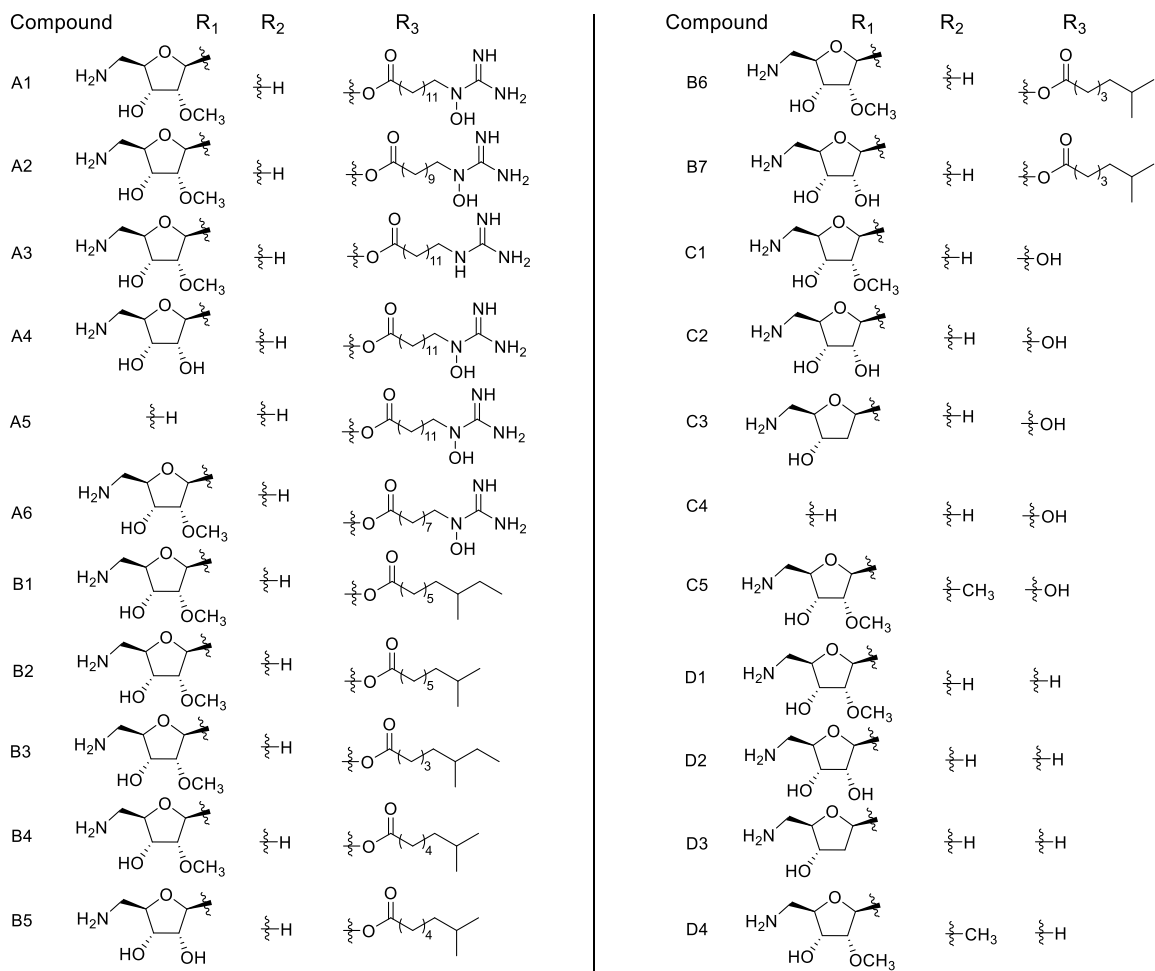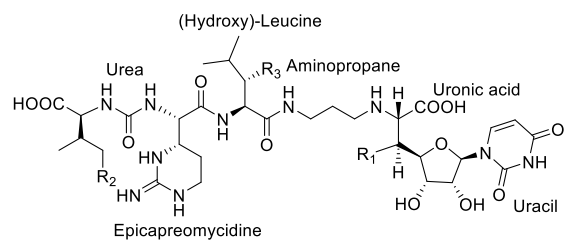
Figure 1.1 Structure of muraymycin.

1.2 Targets of Muraymycin

Muraymycins inhibit peptidoglycan cell wall biosynthesis of Gram-positive as well as Gram-negative bacteria by inhibiting the activity of bacteria translocase I (MraY). MraY catalyzes the transfer and attachment of phospho-MurNAc-pentapeptide to a lipid carrier, undecaprenylphosphate, to form undecaprenyl-diphodpho-MurNAc-pentapeptide, also called Lipid I (Figure 1.2).[3] Recently, the crystal structure of MraY from the Gram-negative bacteria *Aquifex aeolicus* (MraY$_{AA}$) in complex with muraymycin D2 was solved.[4] Surprisingly, muraymycin D2 didn't interact with any of the conserved amino acid residues (Asp117, Asp118, and Asp265) of MraY$_{AA}$, which is essential for catalytic activity from previous studies.[5] Instead, muraymycin D2 bound with the nucleoside-binding pocket, which was formed by large conformational rearrangement of loops C and D of MraY$_{AA}$.[4, 6]

Recently, Kurosu's group reported that besides MraY, muraymycin D1 also inhibited a second, distinct bacterial transferase, polyprenyl phosphate-GlcNAc-1-phosphate transferase (WecA), which is an essential enzyme in the biosynthesis of cell wall components of *Mycobacterium tuberculosis* in both replicating and nonreplicating states.[7]
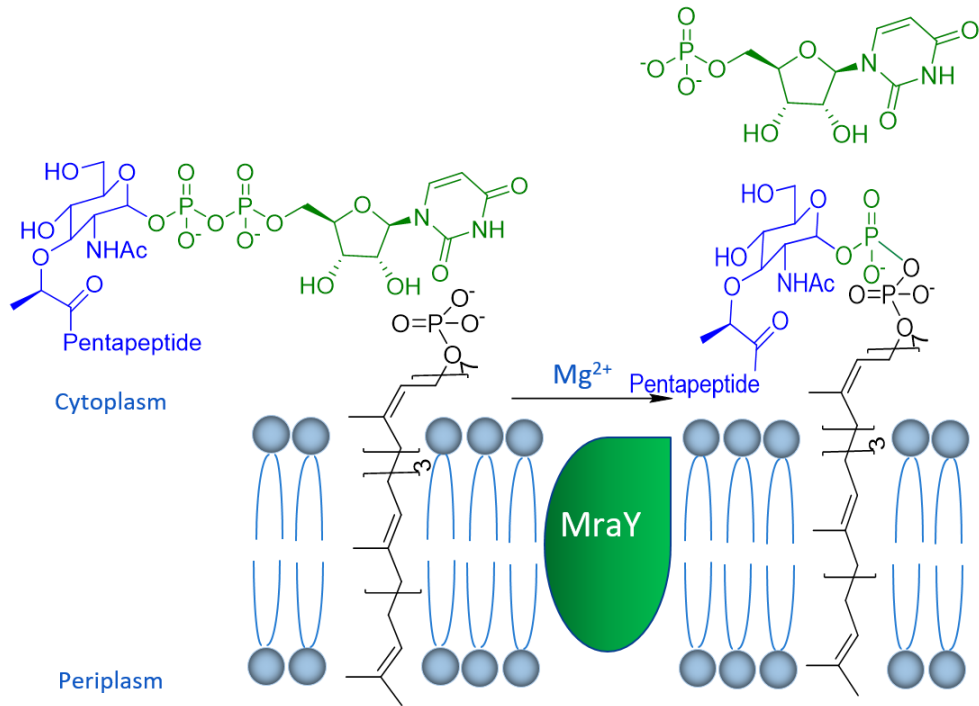
Figure 1.2 Translocase I (MraY) catalyzed reaction.

1.3 SAR of Muraymycins

Antibacterial activity of the 22 discovered muraymycins showed that better activity was observed for acylated muraymycins, especially with longer and charged fatty acyl chains.Various structurally diverse muraymycin analogues have been synthesized, and, many of them showed comparable activity with natural muraymycins (Table 1.1). A graphical summary of SAR of muraymycin is shown in Figure 1.3 based on the activity of naturally occurring muraymycins and chemically synthesized or semisynthesized analogues.[7-17] The SAR is, to some extent, consistent with the crystal structure of the binding pattern of muraymycin D2 with $MraY_{AA}$.[4]

Table 1.1 Summary of synthesized muraymycin analogues with good activity.

Compound	IC_{50} (µM)		MIC (µg/mL)	
1	MurX	0.011	*M. tuberculosis*	1.56[7] (1.68 µM)
2	MurX	0.011	*M. tuberculosis*	1.56[7] (1.68 µM)
3	MurX	0.0096	*M. tuberculosis*	6.25 [7] (6.74 µM)
4	MraY	0.0011	*P. aeruginosa* ATCC25619	>64[18]
5	MraY	0.0008	*P. aeruginosa* ATCC25619	>64[8]
6	MraY	0.0007	*P. aeruginosa* ATCC25619	>64[8]
7	MraY	0.00024	*P. aeruginosa* ATCC25619	64[8] (68.0 µM)
8	MraY	0.00022	*P. aeruginosa* ATCC25619	8[8] (8.5 µM)
9	MraY	0.00014	*P. aeruginosa* ATCC25619	8[8] (9.18 µM)
10	MraY	0.00060	*P. aeruginosa* ATCC25619	8[8] (9.18 µM)
11	MraY	1.7-2.7	*E. coli* Δ*tolC* 50 [13] (65.1 µM)	
12	MraY/ MurG	~5.9[12]	NA	
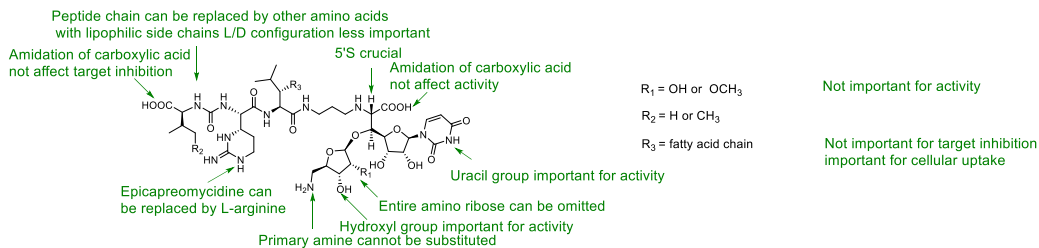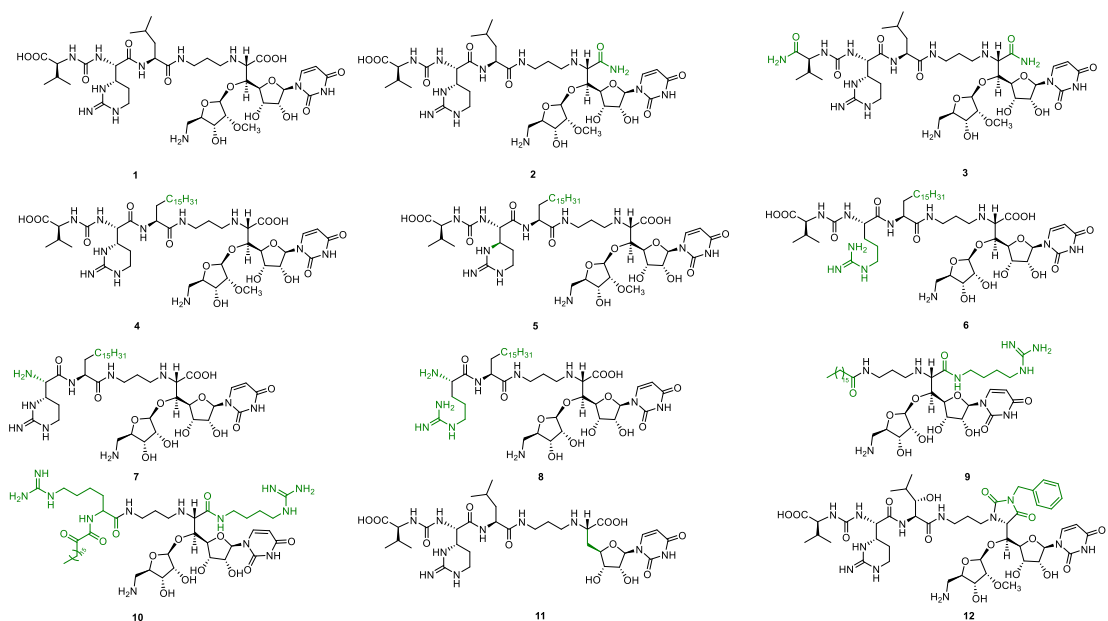
Figure 1.3 SAR results for structural variations of muraymycin scaffold.

1.4 Muraymycin Related Nucleoside Antibiotics

Besides muraymycin, many other nucleoside antibiotics are known to inhibit peptidoglycan biosynthesis by targeting MraY. Four review articles[10, 19-21] provide a broad overview of these nucleoside antibiotics. Figure 1.4 shows the structures of representative members of the different classes of nucleoside antibiotics inhibiting MraY.

Muraymycin A1

FR-900493

A-90289 B

Sphaerimicin A

A-500359 A

Pacidamycin S
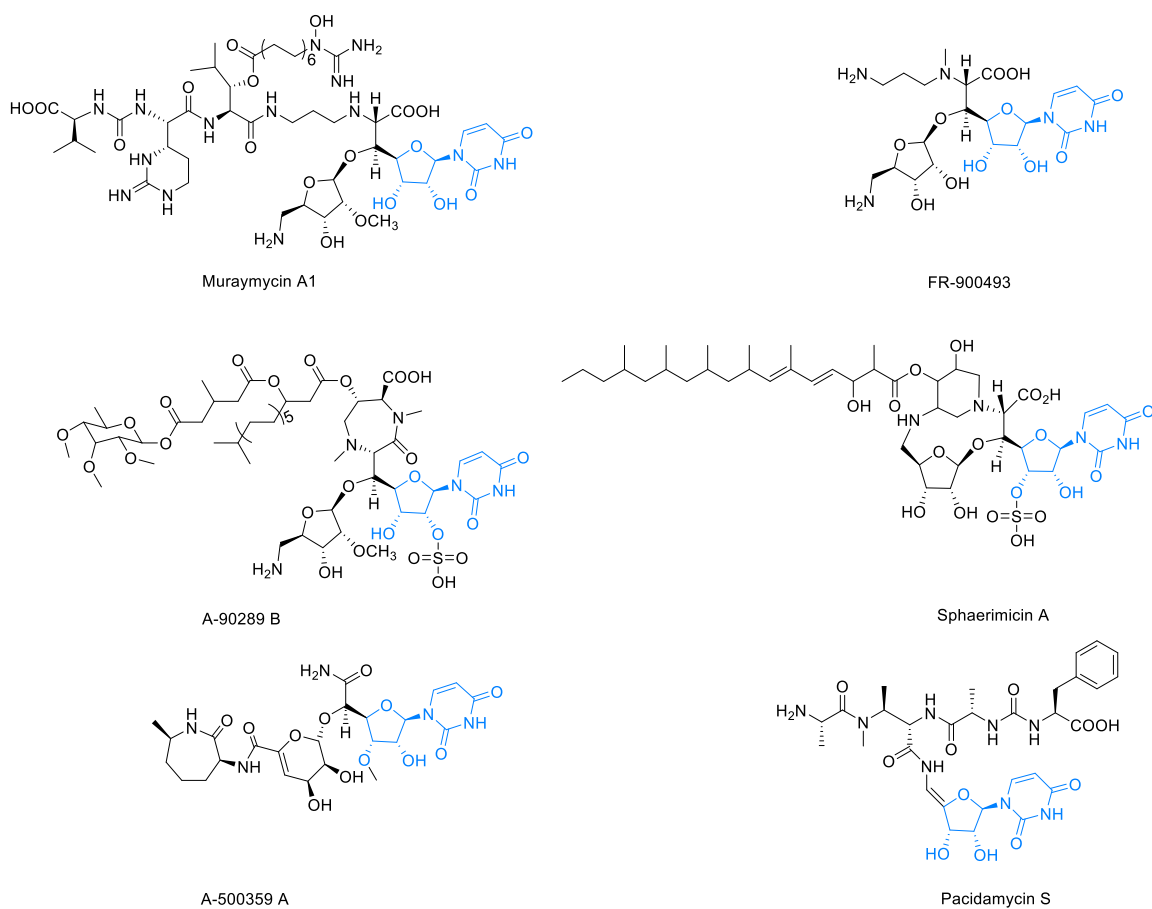
Figure 1.4 Structure of representative members from different classes of nucleoside antibiotics that target MraY. Similarities are highlighted in blue.

1.5 Biosynthetic Gene Cluster of Muraymycin

The muraymycin biosynthetic gene cluster was identified by the Deng group in 2010 from *Streptomyces* sp. NRRL30471.[22] 18F3 cosmid was introduced into *S. lividans* TK24 for heterologous production of muraymycin. The minimal muraymycin biosynthetic gene cluster (*mur12-mur34*) was determined by gene disruption (Figure 1.5). Mur34 was identified as a negative regulator involved in muraymycin biosynthesis.[23] The function of the other genes in the cluster was preliminarily assigned by BLAST analysis.
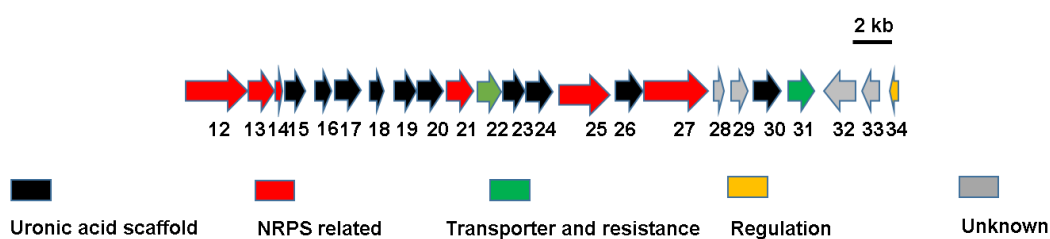
Figure 1.5 The gene cluster identified for muraymycin biosynthesis.

1.6 Contents of the Dissertation

Our over-arching goal is to delineate the biosynthetic pathway of muraymycin in order to develop analogues through chemoenzymatic synthesis and mutasynthesis. Prior work has identified the gene cluster involved in the biosynthesis of muraymycin.[22] However, the enzymatic mechanism of the muraymycin scaffold assembly has not been elucidated. This dissertation consists of seven chapters. Chapter 1 is the introduction of murymycins while chapter 7 discusses the future direction of the projects. In chapter 2, we report the isolation, structural elucidation, and biological activity of muraymycins. Three new muraymycin congeners were isolated and the antibacterial activity was evaluated. Chapters 3 to 6 focus on studying biosynthetic mechanism of the alkyl-ribofuranosylated glycyl-uridine scaffold and fatty acid side chain of muraymycin. In chapter 3, six enzymes that are responsible for the biosynthesis of the ribofuranosylated glycyl-uridine moiety of muraymycin were functionally assigned. In chapter 4, unique resistance pattern of muraymycin was defined. A complementary nucleotidyltransferase and phosphotransferase modifies identical position of muraymycin, but shows distinct temporal order. In chapter 5, two enzymes that are functionally assigned to modify the cryptic phosphorylated intermediate by attachment of an aminopropyl group are characterized. In chapter 6, one enzyme belonging to the cupin family is functionally assigned as an Fe(II)- and α-KG-dependent dioxygenase to catalyze the hydroxylation of the peptide moiety of muraymycins.

Chapter 2 : Antibacterial Muraymycins from *Streptomyces* sp. NRRL 30473

2.1 Introduction

Muraymycins, initially reported as a mixture of nineteen congeners from the fermentation broth of *Streptomyces* sp. NRRL 30471,[1] were discovered using biological assays to identify inhibitors of Lipid II and peptidoglycan cell wall biosynthesis.[1-2, 24-25] Muraymycin A1, one of the more potent of the congeners, was shown to have good activity against *Staphylococcal* (MIC 2 to 16 μg/mL) and *E. coli imp* mutant (MIC <0.03 μg/mL), and was further shown to be effective in a murine model of *Staphylococcus aureus* infection (ED$_{50}$ 1.1 mg/kg). Follow-up efforts have revealed that muraymycins likely exhibit antibacterial activity by directly inhibiting translocase I (MraY). MraY initiates the lipid cycle of cell wall biosynthesis by catalyzing the transfer and attachment of phospho-MurNAc-pentapeptide from UDP-MurNAc-pentapeptide to a lipid carrier, undecaprenylphosphate, to form UMP and undecaprenyl-diphospho-MurNAc-pentapeptide, also referred to as Lipid I.[7, 9, 13-14, 26] Notably, several muraymycin synthetic variants have been screened against MraYs from different species, achieving IC$_{50}$ values as low as 0.7 nM. However, only two naturally occurring muraymycins have been directly tested against MraY to date: muraymycin D1 and D2, both prepared by total synthesis and yielding IC$_{50}$ values of 10 nM and 2.8 nM, respectively.[7, 14] Our understanding of muraymycin structure-activity relationship from these studies has recently been reviewed.[10]

Muraymycins have several unique structural features when compared with clinically used antibiotics. They are classified as lipopeptidyl nucleoside antibiotics, consisting of a

(5′S,6′S)-glycyluridine (GlyU) core that is modified with two distinct components: an

aminoribose attached by a traditional O-glycosidic bond and an unusual peptide attached by a

propylamine linker.[1, 27] The different congeners have been categorized into four types (series

A-D) based on structural variation of a Leu residue of the peptide moiety. The D series, which

includes the aforementioned muraymycins D1 and D2, contain an unmodified L-Leu and are

structurally the simplest. The C series of muraymycins contain a (3S)-3-hydroxy-L-Leu, and

the A and B series are O-acylated variants of the hydroxylated L-Leu. The B series are

characterized by a branched, saturated fatty acid ranging from seven to ten linear carbons

(represented by muraymycin B2 in Figure 1) and the A series characterized by a terminal

guanidinium-substituted fatty acid ranging from fourteen to sixteen linear atoms in length

(represented by muraymycin A1 in Figure 1).[1]

As part of our on-going efforts to characterize the inhibitory properties and establish

structure-activity relationships of naturally occurring muraymycins toward the target MraY, we

report the discovery, structural elucidation, and activity of three new muraymycins (**1-3**) from

Streptomyces sp. NRRL30473 and NRRL 30477, two strains previously derived from

Streptomyces sp. NRRL 30471 by random, chemical mutagenesis. Importantly, a complete

suite of 1D and 2D NMR spectroscopic analysis was performed, and the entirety of the NMR

spectral data is provided in the public domain for the first time for any muraymycin congener.

Compounds **1** and **2**, named muraymycin B8 and B9, respectively, differ from other

muraymycins by having an elongated fatty acid side chain. Both are shown to be potent

inhibitors of *Staphylococcus aureus* and *Aquifex aeolicus* MraY *in vitro*. Compound **3**, named

muraymycin C6, is characterized by an N-acetyl modification of the primary amine of the

aminoribose. The inhibitory activity of **3** against MraY is significantly reduced, which is consistent with an important role of this amine in target binding and suggests acetylation as a possible means of self-resistance by the producing strain.

2.2 Materials and Methods

2.2.1 General Experimental Procedures

UV spectra were recorded on an Ultraspec 8000 spectrometer (GE, Pittsburgh, PA, USA). All NMR data was recorded at 400 MHz for ^{1}H and 100 MHz for ^{13}C with Varian Inova NMR spectrometers (Agilent, Santa Clara, CA), and 600 MHz for ^{1}H and 150 MHz for ^{13}C with an Agilent DD2 NMR spectrometer (Agilent, Santa Clara, CA). LC-MS was conducted with an Agilent 6120 Quadrupole MSD mass spectrometer (Agilent Technologies, Santa Clara, CA) equipped with an Agilent 1200 Series Quaternary LC system and an Eclipse XDB-C18 column (150 × 4.6 mm, 5 μm). HR-ESI-MS spectra were recorded on an AB SCIEX Triple TOF 5600 System (AB Sciex, Framingham, MA, USA). Analytic HPLC was performed with Waters Alliance 2695 separation module (Milford, MA) equipped with a Waters 2998 diode array detector and an analytical Apollo C_{18} column (250 mm x 4.6 mm, 5 μm). Semipreparative HPLC was performed with a Waters 600 controller and pump (Milford, MA) equipped with a 996 diode array detector, 717 plus autosampler, and an Apollo C_{18} column (250 × 10 mm, 5 μm) purchased from Grace (Deerfield, IL). All solvents used were of ACS grade and purchased from Pharmco-AAPER (Brookfield, CT). Sephadex LH-20 (25-100 *μ*m) was purchased from GE Healthcare (Little Chalfont, United Kingdom). A solution of resazurin sodium salt (Alfa aesar B21187) was prepared to 1 mg/mL in sterile distilled water.

2.2.2 Fermentation, Extraction, Isolation and Purification

Streptomyces sp. NRRL 30473 and NRRL 30477 were cultivated on MS agar plates at 28 °C for 7 days. Chunks of the corresponding agar with bacterial growth were added to five 250 mL Erlenmeyer flasks, each containing 50 mL TSBG (Tryptic soy broth (Difco) supplemented with 20 g/L glucose), at 30 °C on a rotary shaker (250 rpm) for 72 h. The cultures were used to inoculate 200 flasks (250 mL), each containing 50 mL PM-1 medium.[28] PM-1 was composed of glucose 2%, soluble starch 1%, pressed yeast 0.9%, peptone 0.5%, meat extract 0.5%, NaCl 0.5%, CaCO$_3$ 0.3% and CB-442 (NOF Co., Ltd.) 0.01% (pH 7.4, before sterilization). The fermentation was continued for 7 days at 23 °C on a rotary shaker (210 rpm).

All culture flasks were combined and centrifuged at 6000 x g for 15 min to separate the mycelium and water phase. The mycelial-cake portion was extracted with methanol (3 ×1 L) by sonication, and the organic phase was evaporated to afford 15 g of brown crude extract. Amberlite XAD-16 (4%, Sigma) resin was added to the water phase and stirred for 12 h. The resin was washed with water until the effluent became colorless, and then eluted with 3 L of methanol. The MeOH extract was concentrated under reduced pressure to obtain a crude extract (12 g). Components of the mycelium crude extract and water phase crude extract were subjected to Sephadex LH-20 column, and methanol was used to elute compounds at a flow rate at 2 mL/min to yield twelve fractions. Fraction I was further purified by using a semipreparative HPLC (CH$_3$CN−H$_2$O, 0.01 % TFA; flow rate: 3.0 mL/min)to yield **1** (6 mg) and **2** (2 mg). Compound **3** (4 mg) and muraymycin C1 (5 mg) were isolated from fraction II by semipreparative HPLC (CH$_3$CN−H$_2$O, 0.01 % TFA; flow rate: 3.0 mL/min).

muraymycin B8 (1): white amorphous powder; UV (MeOH) λ_{max} (log ε) 260 (3.83) nm; ^{13}C and ^{1}H NMR data, see Tables 1 and 2; (+)-HR-ESI-MS: *m/z* 1184.6757 [M + H]$^{+}$ (calcd for $C_{64}H_{94}N_{11}O_{18,}$ 1184.6778).

muraymycin B9 (2): white amorphous powder; UV (MeOH) λ_{max} (log ε) 258 (1.93) nm; ^{13}C and ^{1}H NMR data, see Tables 1 and 2; (+)-HR-ESI-MS: *m/z* 1156.6458 [M + H]$^{+}$ (calcd for $C_{62}H_{90}N_{11}O_{18,}$ 1156.6465).

muraymycin C6 (3): white amorphous powder; UV (MeOH) λ_{max} (log ε) 261 (3.95) nm; ^{13}C and ^{1}H NMR data, see Tables 1 and 2; (+)-HR-ESI-MS: *m/z* 988.4598 [M + H]$^{+}$ (calcd for $C_{40}H_{66}N_{11}O_{18,}$ 988.4587).

2.2.3 DNA Extraction, Genome Sequencing, and Analysis

A single colony of *Streptomyces* sp. NRRL30473 from MS agar was used to inoculate 50 mL TSBG in a 250 mL baffled flask and cultured for 3 days at 30 °C. Cells were harvested via centrifugation and washed once with TE buffer and resuspended with 5 mL of 2 mg/mL lysozyme (dissolved in TE buffer). Cells were incubated at 30 °C for 30 min and then 1.2 mL 0.5 M EDTA was added and mixed. Proteinase K (6 ml of 0.2 mg/mL) was added to the solution and incubated at 37 °C for 2 h. DNA was extracted using phenol-chloroform with the protocol shared by Pacific Biosciences with minor modifications. Phenol/chloroform/isoamyl alcohol solution (7 mL of 25: 24: 1) was added, and the mixture rotated for 10 min. The top aqueous solution was transferred after centrifugation and 7 mL chloroform/isoamyl alcohol solution (24:1) was added. After rotating for 5 min, the top aqueous solution was transferred after centrifugation. The solution was treated with RNase for 1 h at 37 °C. After mixing with 0.25

volume of 5 M NaCl, 30% PEG6000 was added to final concentration of 10%. Precipitated

DNA was transferred with glass tube to a new tube and rinsed with 70% ethanol and air dried.

DNA was re-dissolved in 2 mL TE buffer and stored at 4 °C.

2.2.4 Antimicrobial Bioactivities

The protocol used for the determination of the minimum inhibitory concentration (MIC)

was as described previously with minor modifications.[29] The bacterial strains *S. aureus* subsp.

aureus (Newman strain), *E. coli* Δ*tolC* mutant JW5503 (*E. coli* genetic stock center), and *E.

coli* BL21(DE3) were used as model strains for antimicrobial susceptibility assays. All strains

were grown in appropriate liquid or on agar plates using LB media (BD244620) for *S. aureus*

and LB media supplemented with 50 µg/mL kanamycin for *E. coli* Δ*tolC* mutant. Individual

strains were grown in 5 mL of medium for 16 h at 37 °C with shaking (250 rpm), and then were

diluted X1000 into 4.5 mL of medium and incubated until OD_{600} reaching 0.4. An aliquot of the

suspensions was diluted X1000. Aliquots (90 µL) of each diluted culture and transferred into

the individual well of a 96-well plate supplied with 5 µL of the tested compound. Maximum

final concentration of 256 µg/mL or 32 µg/mL with serial dilutions was maintained to obtain

the antimicrobial activities and compared to the negative control 1% DMSO or water alone.

The culture plates were incubated at 37 °C for 16 h with shaking (160 rpm) for *E. coli* strains

and (50 rpm) for *S. aureus*. The OD_{600} of each well measured using BioTek™ Synergy™ 2

Multi-Mode Microplate Readers. The acquired OD_{600} values were normalized to the negative

control wells (100% viability). Resazurin solution (5 µL) was also added to each well, and the

plates were shaken for 10 s and incubated at 37 °C for another 3 h to allow resazurin to convert

to resorufin by viable bacteria. The minimal concentration of the tested compound that caused

growth inhibition was recorded as the MIC. The MIC assay with *S. aureus* was carried out by Prof. Christian Ducho's lab in Department of Pharmacy, Pharmaceutical and Medicinal Chemistry, Saarland University.

2.2.5 MraY Inhibition Assay

MraY inhibition to determine IC_{50} was carried out by Prof. Christian Ducho's lab in Department of Pharmacy, Pharmaceutical and Medicinal Chemistry, Saarland University.

Overexpression of MraY from *S. aureus*. The overexpression of *Sa*MraY in *E. coli* was performed as described, and a crude membrane preparation was employed for *in vitro* MraY assays.[13]

Overexpression of MraY from *Aquifex aeolicus*. For the overexpression of AaMraY from in *E. coli*, the plasmid previously reported by Lee and co-workers[4-5] was used. This plasmid contained the codon-optimized mraY gene from *Aquifex aeolicus* encoding a fusion protein with decahistidine maltose-binding protein (His-MBP) and a PreScission protease cleavage site for removal of the tag. The plasmid was transformed into C41 (DE3) *E. coli* cells and MraY was expressed in terrific broth (TB) medium containing 35 μg/mL kanamycin. Protein expression was induced at OD_{600} ~1.0 at 37 °C for 3 h using 0.4 mM isopropyl-β-D-thiogalactopyranoside (IPTG). Cells were harvested by centrifugation at 5750 x g. All further steps were carried out at 4 °C. The cells were resuspended in 10-20 mL resuspension buffer per liter culture (resuspension buffer: 50 mM Tris-HCl (pH 8.0), 150 mM NaCl, 2 mM β-mercaptoethanol (BME), lysozyme, DNAse I and one cOmplete™ EDTA-free Protease Inhibitor Cocktail tablet), the cells were lysed by sonication (30% amplitude, 3/10 s pulse, 7/10

s pause for 15 min). n-Dodecyl-β-D-maltoside (DDM, 30 mM) was added and the resultant

lysate was stirred for 2 h. After centrifugation at 30000 x g for 45 min, the cleared lysate was

loaded onto pre-equilibrated TALON Superflow™ resin (~0.5 mL/L culture), imidazole was

added to a final concentration of 7 mM and the mixture was rotated at 4 °C overnight.

Subsequently, the resin was washed with 20 column volumes of washing buffer (50 mM Tris-

HCl (pH 8.0), 150 mM NaCl, 2 mM BME, 10 mM imidazole, 1 mM DDM) and eluted with

10-20 mL elution buffer (50 mM Tris-HCl (pH 8.0), 150 mM NaCl, 2 mM BME, 250 mM

imidazole, 1 mM DDM). Dithiothreitol (DTT, final concentration of 1 mM),

ethylenediaminetetraacetic acid (EDTA, final concentration of 1 mM) and PreScission protease

(ratio to His-MBP-MraY 1:100) were added and the solution was incubated at 4 °C overnight.

The cleaved protein was separated on a HiLoad 16/600 Superdex 200 pg in a buffer containing

20 mM Tris-HCl (pH 8.0), 150 mM NaCl, 2 mM DTT and 5 mM n-decyl-β-D-maltopyranoside

(DM). The resultant solution was employed as a source of solubilized and purified AaMraY for

in vitro MraY assays.

Fluorescence-based MraY assay. *In vitro* MraY assays were performed using our

previously reported adapted version[30] of Bugg's fluorescence-based method.[31-36] Fluorescence

intensity over time was measured at $\lambda_{ex} = 355$ nm and $\lambda_{em} = 520$ nm (BMG Labtech

POLARstar Omega, 384-well plate format). Each well contained a total volume of 20 μL with

100 mM Tris-HCl buffer (pH 7.5), 200 mM KCl, 10 mM MgCl$_2$, 0.1% Triton X-100, 0-5%

DMSO, 50 mm undecaprenyl phosphate, 7.5 mm dansylated Park's nucleotide (synthetic or

semi-synthetic),[30] a protein preparation (see below) and the potential inhibitor at various

concentrations.

For *Sa*MraY, 1 μL of a crude membrane preparation with a total protein concentration of 1.0 mg/mL was used and the reaction was initiated by the addition of the protein preparation. For *Aa*MraY, 1 μL of a solution of purified protein was used and preincubated with the assay mixture (including the inhibitor but excluding the dansylated Park's nucleotide) at rt for 30 min. The reaction was then initiated by the addition of Park's nucleotide. Concentrations of the purified *Aa*MraY was 0.1 mg/mL. The protein preparations of SaMraY and AaMray showed comparable activity in the absence of inhibitors.

MraY activity at a certain inhibitor concentration was determined by a linear fit of the fluorescence intensity curve from 0 to 2 min. This measure of enzymatic activity was plotted against the logarithmic inhibitor concentration and fitted with a sigmoidal fit using the formula shown below, thus furnishing the reported IC$_{50}$ values.

$$y \ = \ A1 \ + \ \frac{(A2 - A1)}{1 \ + \ 10^{\log(x_0 - x) \cdot p}}$$

2.3 Results

Initial attempts to produce muraymycins using the published fermentation conditions[1,24] were unsuccessful. Hence, a few different media were examined. Using analytical scale fermentation with LC-MS analysis, production of muraymycins was observed using PM-1 media, which was previously employed for the production of capuramycin, a structurally distinct nucleoside antibiotic from a different *Streptomyces* sp.[28] As a consequence, a 100 mL seed culture of *Streptomyces* sp. strain NRRL 30473 was grown for three days and used to inoculate 10 L of PM-1 media. After fermentation for seven days, followed by extraction, fractionation, and resolution of the components within the crude extract, five known muraymycins were identified by LC-MS analysis (A1, B1, B2, B3, and B6). Two congeners, muraymycins B8 (**1**, yield: 0.6 mg/L) and B9 (**2**, yield: 0.2 mg/L), with masses that did not match prior reports, were purified by reverse-phase HPLC. Using identical fermentation conditions with Streptomyces sp. strain NRRL 30477, one new congener, muraymycin C6 (**3**, yield: 0.4 mg/L), and one known muraymycin C1 (yield: 0.5 mg/L) were obtained and likewise isolated for structural elucidation and activity testing.
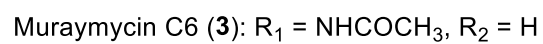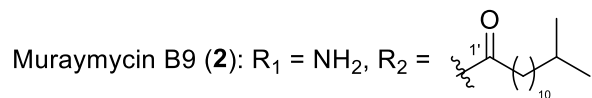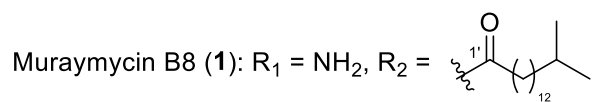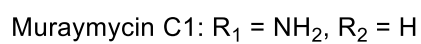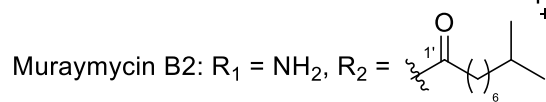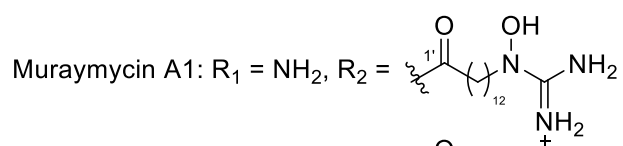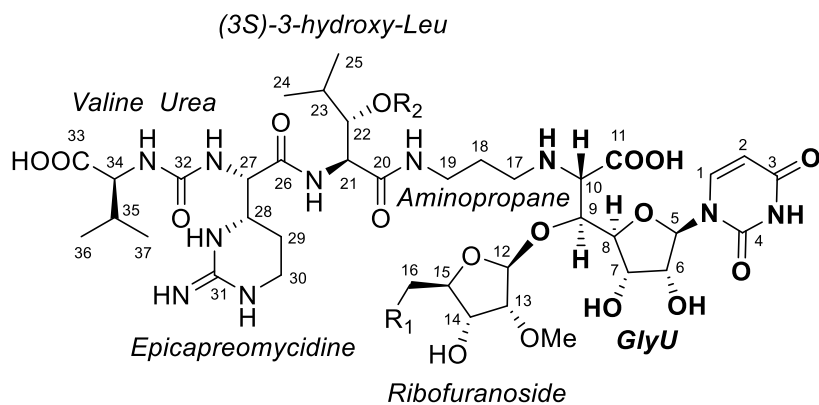
Figure 2.1 Structures of representative muraymycins.

2.3.1 Structure Elucidation

The molecular formula of **1** ($C_{64}H_{93}N_{11}O_{18}$) was determined by HR-ESI-MS (Figure S2.1). An initial analysis of the ^{13}C and ^{1}H NMR data (Tables 2.1 and 2.2) in conjunction with the HSQC spectra in DMSO-d_6 showed the presence of 54 carbon resonances, which were ascribed to 7 methyls (including 1 methoxyl), 18 methylenes, 18 methines, 1 double bond and 9 amide/acid carbonyls (Figures S2.2-S2.3). The NMR and UV data for **1** displayed typical features of a muraymycin compound, including the GlyU nucleoside, ribofuranoside, aminopropane, epicapreomycidine, urea, valine and hydroxy-leucine. Further interpretation of the 1D and 2D NMR data (including ^{1}H-^{1}H COSY, HSQC, HMBC and TOCSY; Figures S2.4-S2.7) revealed the structure of **1**, which was quite similar with muraymycin B1[1], except for the fatty acid chain, which was identified as 14-methyl-pentadecanoic acid through 2D NMR (Figure 2.2). A strong HMBC correlation from H-22 (δ_H 4.92) to C-1′ (δ_C 172.0) unambiguously determined the position of pentadecanoic acyl group on hydroxy-leucine. Based on the NOESY spectrum (Figure S2.8), the relative configuration of **1** was assigned to be identical with that reported for muraymycin B1.[1] Thus, the structure of compound **1** was established as a new member of the muraymycin B family and subsequently named muraymycin B8.

Compound **2** was assigned the molecular formula $C_{62}H_{89}N_{11}O_{18}$ on the basis of HR-ESI-MS (Figure S2.9). A difference of C_2H_4 with **1** and their similar NMR spectroscopic data was suggestive of **2** as a muraymycin B congener (Figures S2.10-S2.11). The fatty acid chain for **2** was identified as 12-methyl-tridecanoic acid from a thorough analysis of the 2D NMR data (Figures 2.12-S2.14). The relative configuration of **2** was also established by NOESY (Figure S2.15). Compound **2** was designated as muraymycin B9.

The UV and NMR spectroscopic data for **3** ($C_{40}H_{65}N_{11}O_{18}$) revealed characteristic features of muraymycin (Tables 2.1 and 2.2, and Figures S2.16-2.22) and were similar to that reported for muraymycin C1,[1] which was likewise isolated from this strain (Figures S2.23-S2.28).[2] Specifically, **3** displayed an extra acetyl substitution of a methyl (δ_C 21.9 and δ_H 1.85) and a carbonyl (δ_C 174.1). The key HMBC correlations from H$_2$-16 (δ_H 3.05 and 3.41) to δ_C 174.1 established the *N*-acetyl at C-16. Based upon this analysis, the structure of **3** was established as 16-*N*-acetyl-muraymycin C1, a new muraymycin C congener and subsequently named muraymycin C6. Of note, 16-N-acetyl-muraymycin C1 was previously prepared from muraymycin C1 via chemical semisynthesis,[24] and the 1H NMR spectrum of the naturally occurring congener matched the semisynthetic variant.
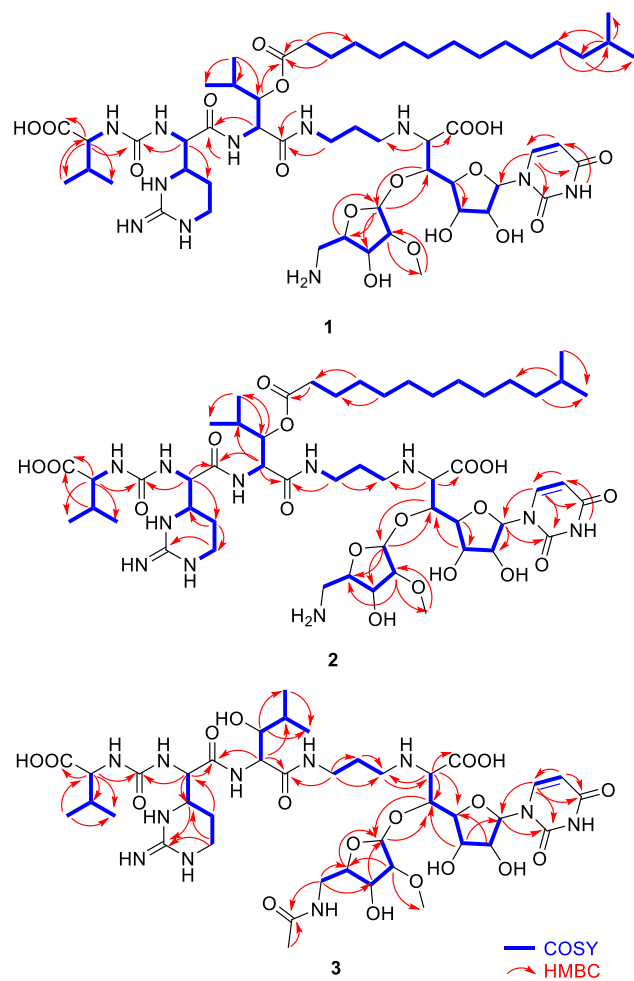
Figure 2.2 ^{1}H-^{1}H COSY (▬) and selected HMBC (→) correlations of **1**−**3**.

Table 2.1 ^{13}C NMR data (100 MHz) of compounds **1−4**.

no.	**1**[a]	**2**[a, b]	**3**[c]	C1[c]	no.	**1**[a]	**2**[a, b]	**3**[c]	C1[c]
1	141.6,	141.5, CH	141.9, CH	142.3, CH	21	53.4,	53.4, CH	56.1, CH	56.0, CH
2	101.7,	101.7, CH	101.9, CH	102.2, CH	22	75.0,	75.0, CH	74.4, CH	74.6, CH
3	163.1, C	163.1, C	165.9, C	165.9, C	23	27.8,	27.8, CH	29.1, CH	29.2, CH
4	150.3, C	150.3, C	151.2, C	151.2, C	24	15.7,	15.7, CH$_3$	14.6, CH$_3$	14.7, CH$_3$
5	90.6,	90.6, CH	91.1, CH	91.8, CH	25	19.6,	19.6, CH$_3$	18.7, CH$_3$	18.7, CH$_3$
6	72.6,	72.5, CH	72.8, CH	72.5, CH	26	169.5, C	169.5, C	171.2, C	171.1, C
7	70.0,	69.9, CH	69.0, CH	69.1, CH	27	54.8,	54.8, CH	55.3, CH	55.4, CH
8	82.8,	82.8, CH	83.4, CH	83.7, CH	28	50.0,	50.0, CH	49.1, CH	49.1, CH
9	76.3,	76.3, CH	76.4, CH	76.3, CH	29	20.4,	20.4, CH$_2$	20.3, CH$_2$	20.3, CH$_2$
10	62.5,	62.5, CH	63.6, CH	62.8, CH	30	35.6,	35.6, CH$_2$	35.6, CH$_2$	35.7, CH$_2$
11	168.8, C	168.7, C	169.9, C	170.3, C	31	153.7, C	153.7, C	153.6, C	153.6, C
12	105.2,	105.1, CH	106.5, CH	106.7, CH	32	157.5, C	157.5, C	158.7, C	158.7, C
13	84.1,	84.1, CH	83.9, CH	83.6, CH	33	173.7, C	173.6, C	177.3, C	176.4, C
14	71.8,	71.7, CH	70.1, CH	70.5, CH	34	57.5,	57.5, CH	59.4, CH	58.6, CH
15	79.3,	79.3, CH	82.9, CH	79.6, CH	35	30.3,	30.3, CH	30.1, CH	29.9, CH
16	42.1,	42.0, CH	41.7, CH	42.2, CH	36	19.1,	19.1, CH$_3$	18.5, CH$_3$	18.3, CH$_3$
17	45.5,	45.5, CH$_2$	45.4, CH$_2$	45.6, CH$_2$	37	17.4,	17.4, CH$_3$	16.6, CH$_3$	16.6, CH$_3$
18	25.5,	25.4, CH$_2$	25.2, CH$_2$	25.0, CH$_2$	14-OCH$_3$	57.5,	57.4, CH$_3$	57.8, CH$_3$	57.9, CH$_3$
19	36.1,	36.0, CH$_2$	35.8, CH$_2$	35.8, CH$_2$	16-			174.1, C	
20	169.2, C	169.1, C	172.5, C	172.5, C	16-			21.9, CH$_3$	

Fatty acid for **1**

O / 1' 172.0 / 33.5 / 24.5 / 28.5-29.3 / 8 / 26.8 / 38.5 / 27.4 / 22.5 / 22.5

Fatty acid for **2**

O / 1' 172.0 / 33.5 / 24.4 / 28.4-29.2 / 6 / 26.7 / 38.4 / 27.3 / 22.5 / 22.5
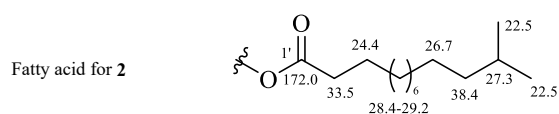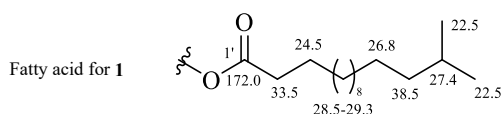
[a]measured in DMSO-d_6; [b]measured at 150 MHz; [c]measured in D$_2$O.

Table 2.2 ^{1}H NMR data (400 MHz, J in Hz) of compounds **1−3** and muraymycin C1.

no.	1[a]	2[a,b]	3[c]	C1[c]	no.	1[a]	2[a,b]	3[c]	C1[c]
1	7.75, d (8.0)	7.75, d (9.5)	7.62, d (6.4)	7.54, d (5.7)	25	0.79[e]	0.79[e]	0.76, d (5.3)	0.77, d (5.4)
2	5.70[d]	5.68[d]	5.73, d (6.4)	5.72, d (6.4)	27	4.39, m	4.38, m	4.19, m	4.20, d (6.2)
5	5.66[d]	5.66[d]	5.65, d (2.2)	5.62, d (2.3)	28	3.60, m	3.61, m	3.71, m	3.71, m
6	4.13, m	4.14, m	4.23, m	4.25, m	29	1.70, m	1.71, m	1.72, m	1.72, m
7	3.98, m	3.99, m	4.11, m	4.12, m	30	3.19, 3.29, m	3.19, 3.29, m	3.15, m	3.12, 3.19, m
8	4.10, m	4.11, m	4.09, m	4.18, m	34	4.03, m	4.03, m	3.86, m	3.93, m
9	4.42, m	4.42, m	4.30, m	4.43, dd (0.8, 3.1)	35	2.02, m	2.03, m	1.96, m	1.98, m
10	3.58, m	3.57, m	3.73, m	3.92, m	36	0.86[e]	0.86[e]	0.75, d (5.2)	0.76, d (5.4)
12	5.11, br s	5.11, br s	5.03, d (2.5)	5.11, d (1.9)	37	0.82[e]	0.82[e]	0.70, d (5.8)	0.72, d (5.4)
13	3.54, m	3.54, m	3.64, m	3.68, m	3-NH	11.42, s	11.39, s		
14	4.03, m	4.05, m	4.04, m	4.08, m	13-OCH$_3$	3.27, s	3.28, s	3.22, s	3.25, s
15	3.95, m	3.94, m	3.85, m	3.95, m	16-NH$_2$	8.02, br s	8.02, br s		
16	3.03, m	3.03, m	3.05, 3.41, m	2.95, 3.13, m	16-NHCO$\underline{CH_3}$			1.85, s	
17	2.87, 2.94, m	2.88, 2.95, m	2.98, m	2.95, 3.03, m	19-NH	8.23, br s	8.21, br s		
18	1.73, m	1.73, m	1.77, m	1.74, m	21-NH	8.50, d (8.2)	8.47, d (9.6)		
19	2.93, 3.16, m	2.92, 3.17, m	3.16, m	3.05, 3.18, m	27-NH	6.65, d (8.2)	6.66, d (9.3)		
21	4.44, m	4.44, m	4.14, m	4.14, m	30-NH	8.02, br s	8.02, br s		
22	4.92, dd (2.7, 6.4)	4.92, dd (1.1, 5.8)	3.48, dd (3.3, 6.7)	3.47, dd (3.5, 6.6)	31-NH	7.84, br s	7.83, br s		
23	1.89, m	1.90, m	1.58, m	1.57, m	32-NH	6.50, d (9.5)	6.50, d (10.1)		
24	0.82[e]	0.82[e]	0.65, d (5.3)	0.64, d (5.4)					

Fatty acid for **1**
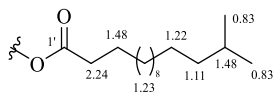
Fatty acid for **2**
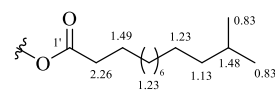
^{a}measured in DMSO-d_6; ^{b}measured at 600 MHz; ^{c}measured in D$_2$O; ^{d,e}overlapped signals.

2.3.2 Antimicrobial Bioactivity

The newly isolated muraymycins were evaluated for inhibition of MraY activity. An in vitro fluorescence-based assay for MraY was previously developed,[35-39] which we have adapted and optimized for screening.[30] In short, this assay required the synthesis of a dansylated derivative of the MraY substrate UDP-MurNAc-pentapeptide to generate a fluorescent readout, and overproduction of recombinant *S. aureus* and *A. aeolicus* MraY. The MraY homologue from *S. aureus* (*Sa*MraY) was used as a crude membrane preparation as attempts to solubilize and purify the protein resulted in loss of activity. In contrast, the solubilization and purification of the MraY homologue from *Aquifex aeolicus* (*Aa*MraY) was feasible,[4-5] and the protein was used accordingly in the *in vitro* assays for MraY inhibition. The results for the inhibitory activities (IC_{50} values) of the new muraymycins **1-3** along with the known compound muraymycin C1 are listed in Table 2.3. To summarize, **1**, **2**, and muraymycin C1 had potent IC_{50} values ranging from 4-22 pM against *Sa*MraY and 68-350 pM against *Aa*MraY, which is significantly lower than IC_{50} values reported for synthetic analogues and naturally occurring muraymycins D1 and D2 (D1, 11 nM against crude *Mycobacterium tuberculosis*;[7] D2, 10 nM against purified MraY from *Bacillus subtilis*,[14] and 2.8 nM against *Sa*MraY[26]). The comparable IC_{50} values with or without the acid chain is consistent with prior conclusions that a long chain, aliphatic component might not significantly contribute to MraY inhibition.[10] Contrastingly, when compared with muraymycin C1, compound **3** showed reduced activity against both enzymes. This result is consistent with a significant role of the intact aminoribosyl group for MraY binding, which was postulated based upon analysis of the X-ray structure of muraymycin D2 in complex with *Aa*MraY.[4] It has been found that a conformational rearrangement occurs

upon muraymycin D2 binding that generates a pocket for opportune interactions with the aminoribose.[4-5]

We also examined the bacterial growth inhibition of **1-3** against *S. aureus* and two strains of *E. coli*. Interestingly, the longer fatty acid side chains of **1** and **2** converted the B series from inactive against *S. aureus* (MIC > 32 μg/mL for muraymycin B2 and B6)**1, 3** to active against *S. aureus* (MIC = 2-6 μg/mL for muraymycin B8 and B9). Furthermore, the lack of a fatty acid side chain for **3** yielded an inactive compound. Taken together with the IC_{50} values for MraY inhibition, this result suggests that the fatty acid unit indeed plays a role in cellular uptake as suggested.[40] In contrast to the MIC data against *S. aureus*, the addition of the fatty acid side chain and increase in its length slightly reduced the activity against both efflux-deficient *E. coli ΔtolC* (MIC for the B series range from 1-4 μg/mL) and efflux-competent *E. coli* BL21(DE3) (MIC from 8-64 μg/mL). Similarly to the trends observed with the IC_{50} values, however, acetylation of muraymycin C1 at the aminoribose significantly reduced the MIC against all strains.

Self-resistance mechanisms to muraymycins remain undefined. The discovery and assessment of muraymycin C6 suggests that acetylation might be such a mechanism, not unlike acetyltransferases involved in aminoglycoside resistance. Interestingly, two potential resistance genes that encode enzymes predicted to covalently modify muraymycins are found in the biosynthetic gene cluster.[22] However, neither would be expected to catalyze acetylation: *mur28* is predicted to encode a TmrB-like ATP-dependent phosphotransferase and *mur29* a putative nucleotidyltransferase. Thus, the role of these two genes and relationship to resistance and/or acetylation, if any, await further examination.

Table 2.3 *In vitro* MraY assays and antimicrobial activities

compounds	*S. aureus* MraY	*A. aeolicus* MraY	*S. aureus* growth inhibition	*E. coli ΔtolC* growth inhibition	*E. coli* BL21(DE3) growth inhibition
	IC_{50} (pM)	IC_{50} (pM)	MIC (µg/mL)	MIC (µg/mL)	MIC (µg/mL)
1	4.0 ± 0.7	$(6.8\pm0.5)\times10^1$	2	4	64
2	22.1 ± 3.2	$(3.2\pm0.2)\times10^2$	6	2	32
3	93 ± 8	$(1.8\pm0.4)\times10^3$	>32	16	256
muraymycin C1	15.7 ± 1.2	$(3.5\pm0.4)\times10^2$	>32	1	8

2.4 Discussion

2.4.1 Synthesized Muraymycin B9 Analogue with Good Antibacterial Activity

Tanino et al.[18] reported the synthesis and biological evaluation of muraymycin analogues with different lipophilic side chain (Figure 2.3). Among these analogues, MRY1 with similar lipophilic side chain as muraymycin B8 showed the best activity. Compared to MRY3, which showed no activity to methicillin-resistant *S. aureus* and vancomycin-resistant *E. faecalis* up to 64 µg/mL, the MIC of MRY1 to both strains were 2~4 µg/mL, which was 2~4 times lower than MRY2, suggesting that long aliphatic side chain without aromatic ring is preferred for the target inhibition.
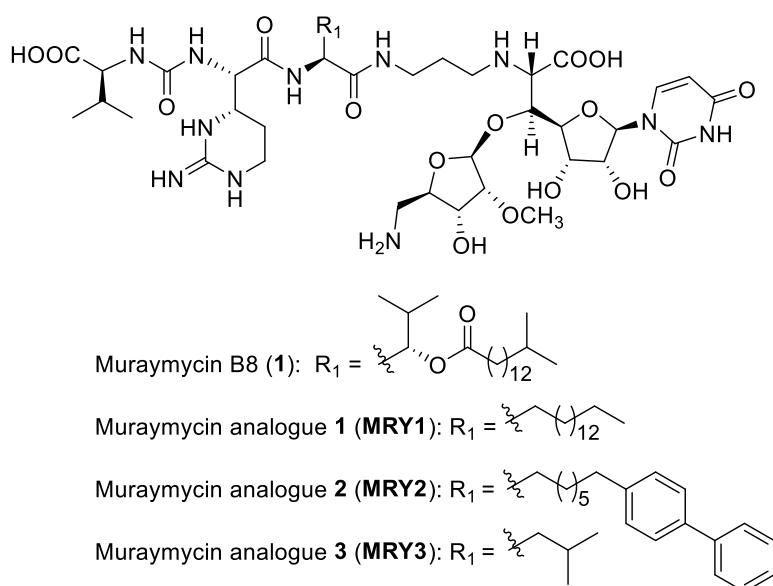
Figure 2.3 Structures of synthesized muraymycin analogues.

2.4.2 Resistant Modifications of Muraymycin

The isolation of muraymycin C6, the acetylated muraymycin C1, is proposed to be one of the resistance modification of muraymycins. We sequenced the genome of *Streptomyces* sp. NRRL30473. AntiSMASH analysis[41-42] enabled us to identify the muraymycin biosynthetic gene cluster, which spans ~31 kb on a single contig (~96 kb). However, a gene encoding an N-acetyltransferase was not found in the biosynthetic gene cluster. The *N*-acetylation modification is possibly catalyzed by a *N*-acetyltransferase located outside the gene cluster. Genome sequencing of *Streptomyces* sp. NRRL30473 also showed several *N*-acetyltransferases located outside the gene cluster, one of which might be responsible for the modification.

Moreover, two muraymycin resistance genes were found in the biosynthetic gene cluster of muraymycin from *Streptomyces* sp. NRRL 30473, one encoding a TmrB-like ATP-dependent muraymycin phosphotransferase, and another encoding a muraymycin nucleotidyltransferase. As the disaccharide moiety of muraymycin is technically an aminoglycoside, the three kinds of aminoglycoside resistance modification[43-44] are also discovered in muraymycin. Functional assignment of muraymycin phosphotransferase and muraymycin nucleotidyltransferase is presented in chapter 4.

2.5 Conclusion

With the goal of developing a muraymycin production platform and expanding upon the known family of muraymycins, we examined the metabolic profile of *Streptomyces* sp. strain NRRL 30473 and *Streptomyces* sp. strain NRRL 30477. Four muraymycins were characterized by a suite of spectroscopic methods, including three new members of the

muraymycin family: B8, B9 and C6 (**1−3**). Muraymycin B8 and B9 showed promising antibacterial activity and pM inhibition against *Sa*MraY and *Aa*MraY. Remarkably, the newly discovered muraymycins B8 and B9 were the first congeners of the B series to display antibacterial activity against *S. aureus*. In our hands muraymycin B8 and B9 have activity against *S. aureus* that is comparable to or better than muraymycin A1,[45] which was previously noted as the most potent muraymycin,[1-2] hence warranting a continued evaluation of these new muraymycins as antistaphylococcal antibiotics. Contrastingly, muraymycin C6, the first N-acetylated version of muraymycin to be isolated, showed reduced activity in all screens suggesting acetylation might be a mechanism of self-resistance.

2.6 Supporting Information
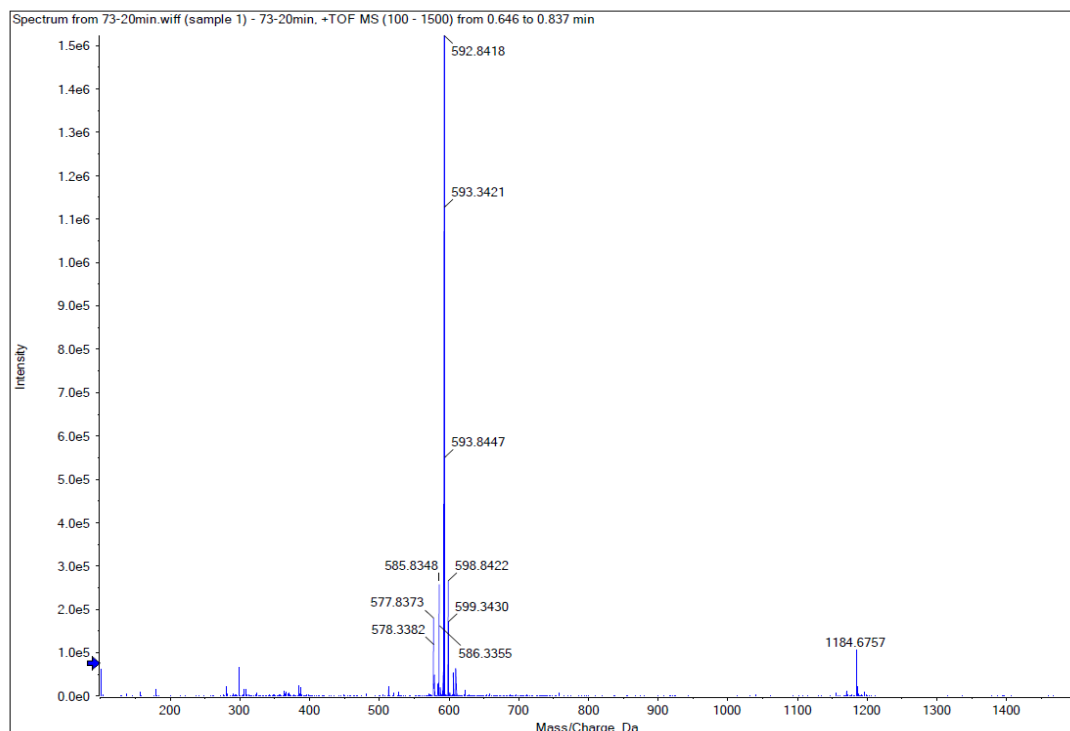
Figure S2.1 (+)-HR-ESI-MS (positive mode) of muraymycin B8 (**1**).
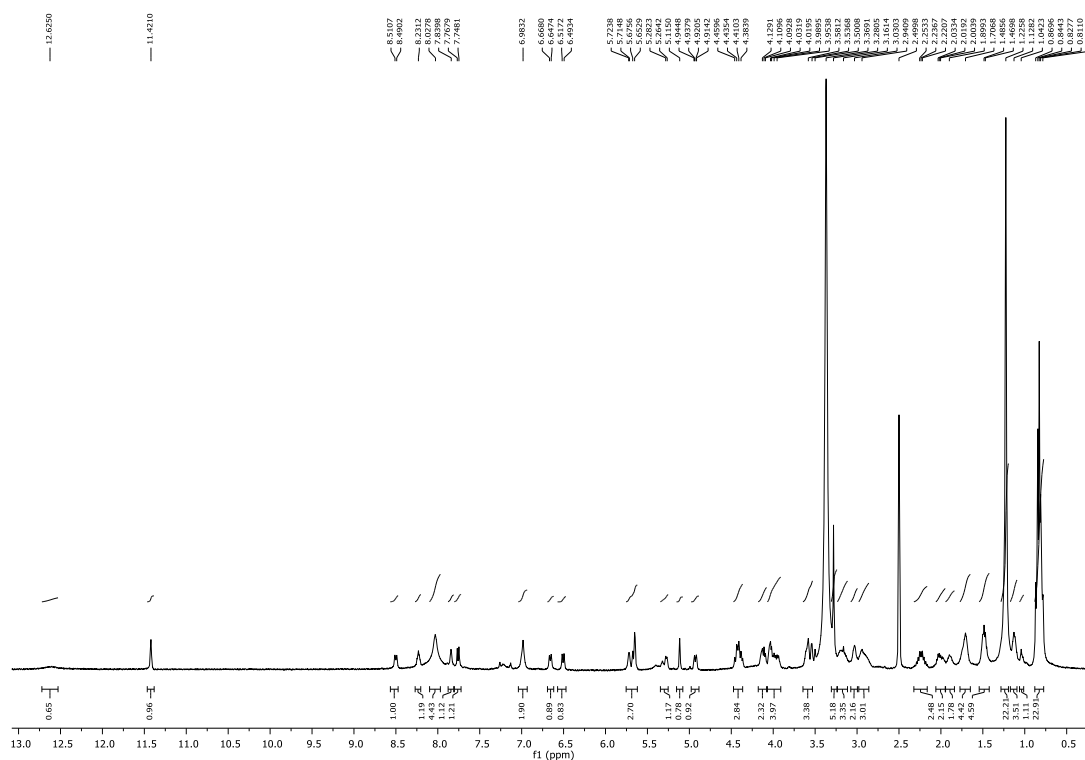
Figure S2.2 ^{1}H NMR spectrum (DMSO-d_6, 400 MHz) of muraymycin B8 (**1**).
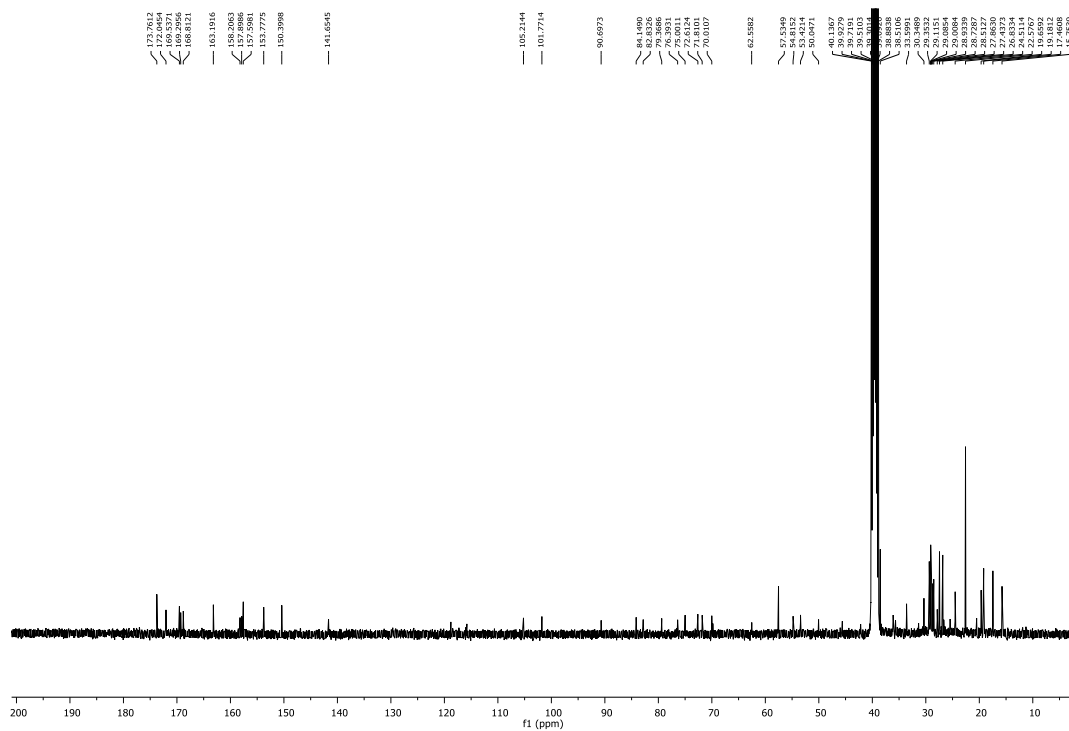
Figure S2.3 ^{13}C NMR spectrum (DMSO-d_6, 100 MHz) of muraymycin B8 (**1**).
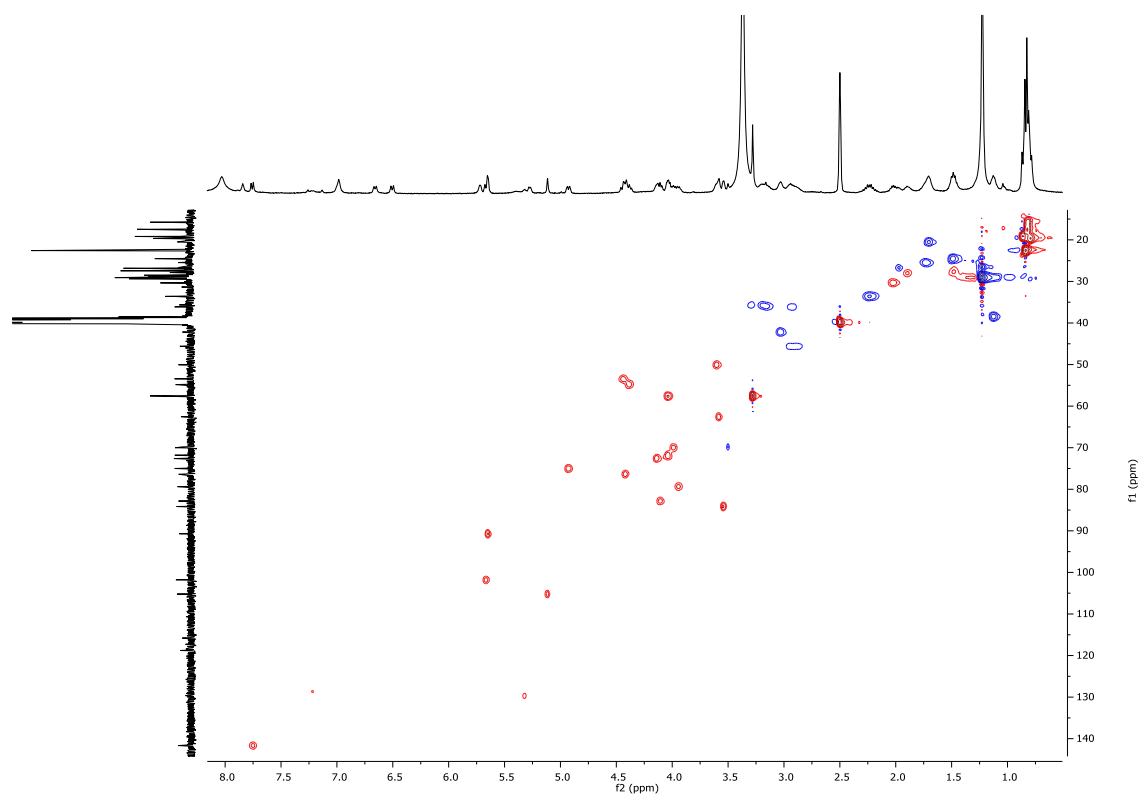
Figure S2.4 HSQC spectrum (DMSO-d_6, 400 MHz) of muraymycin B8 (**1**).
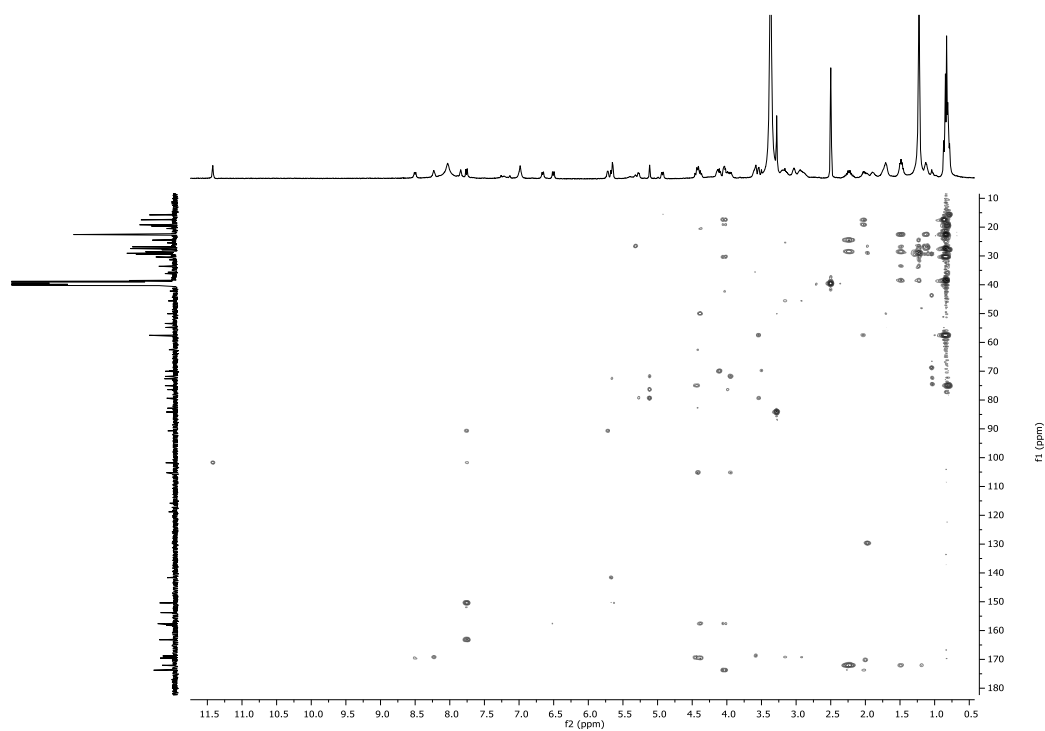
Figure S2.5 HMBC spectrum (DMSO-*d₆*, 400 MHz) of muraymycin B8 (**1**).
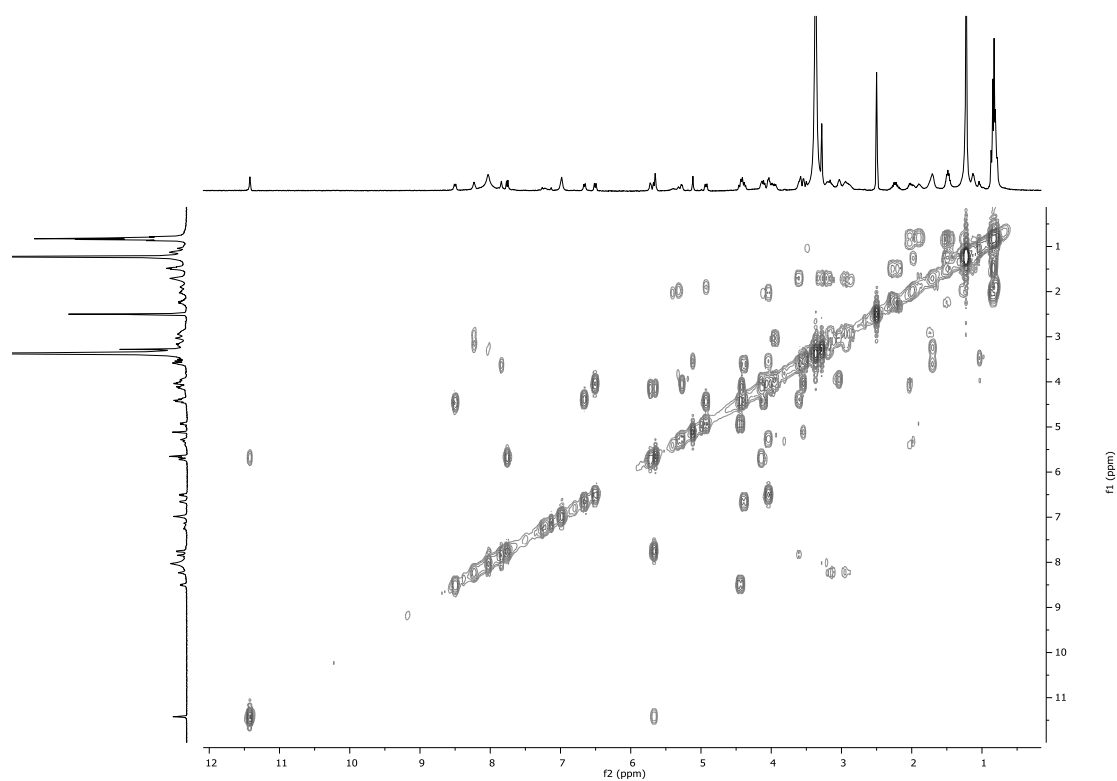
Figure S2.6 ¹H-¹H COSY spectrum (DMSO-*d₆*, 400 MHz) of muraymycin B8 (**1**).
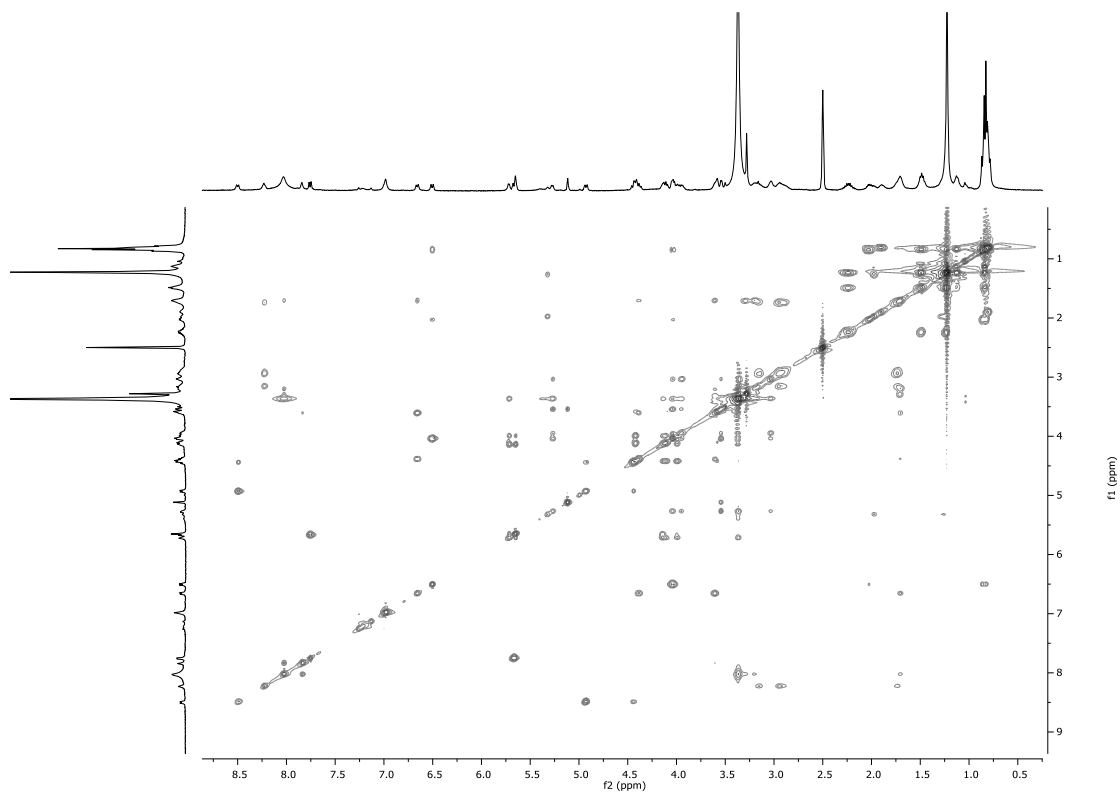
Figure S2.7 TOCSY spectrum (DMSO-d*6*, 400 MHz) of muraymycin B8 (**1**).
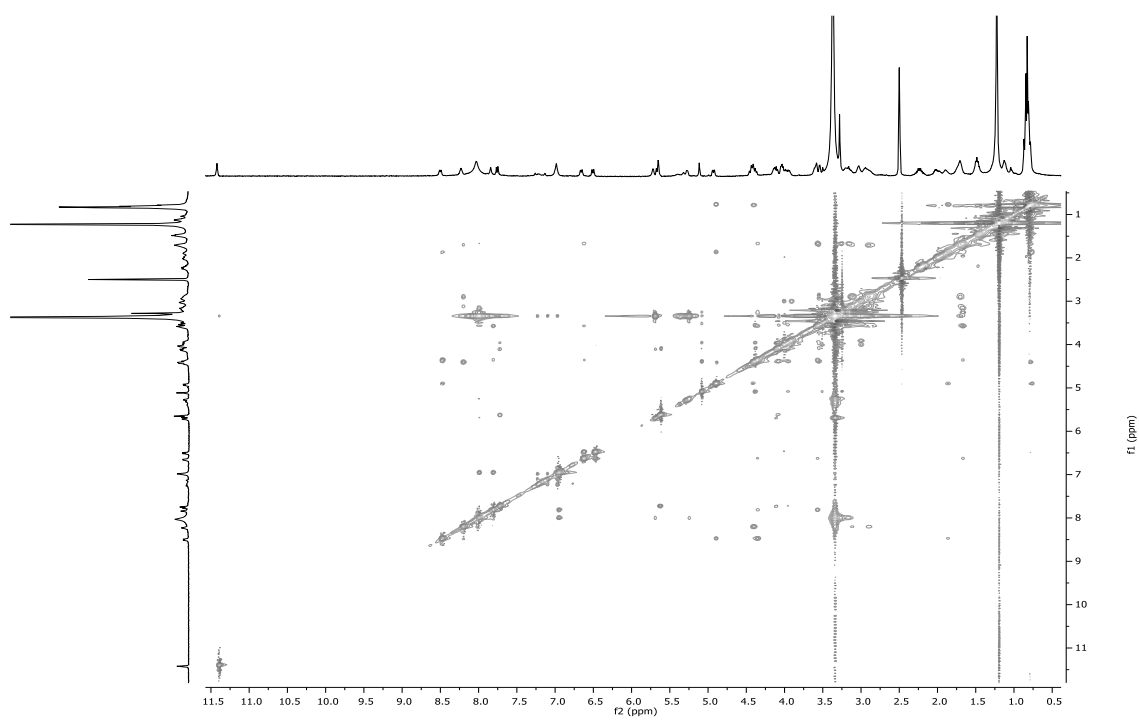
Figure S2.8 NOESY spectrum (DMSO-*d6*, 400 MHz) of muraymycin B8 (**1**).
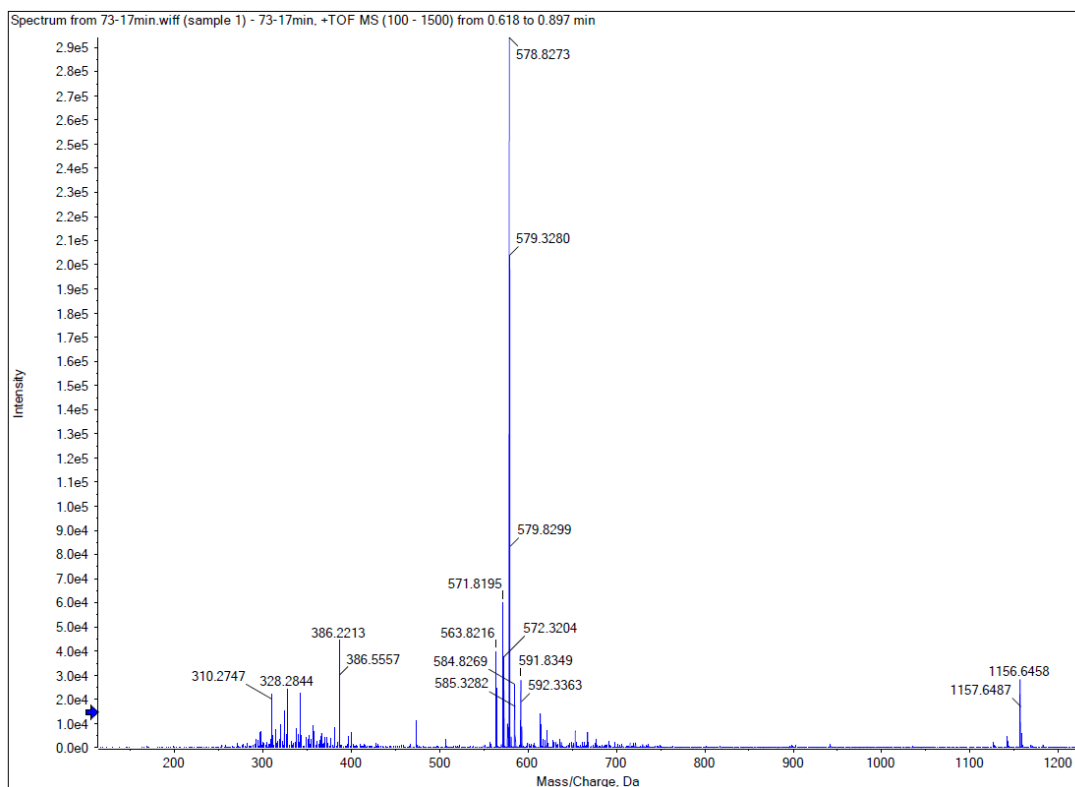
Figure S2.9 (+)-HR-ESI-MS (positive mode) of muraymycin B9 (**2**).
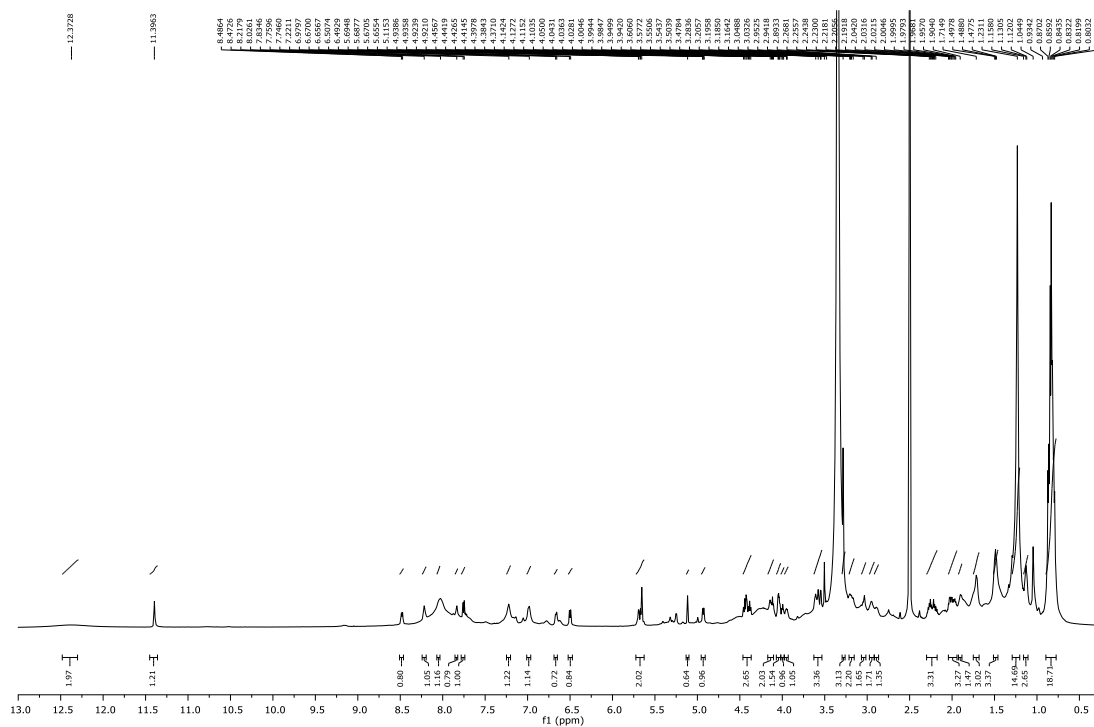
Figure S2.10 ^{1}H NMR spectrum (DMSO-d_6, 600 MHz) of muraymycin B9 (**2**).
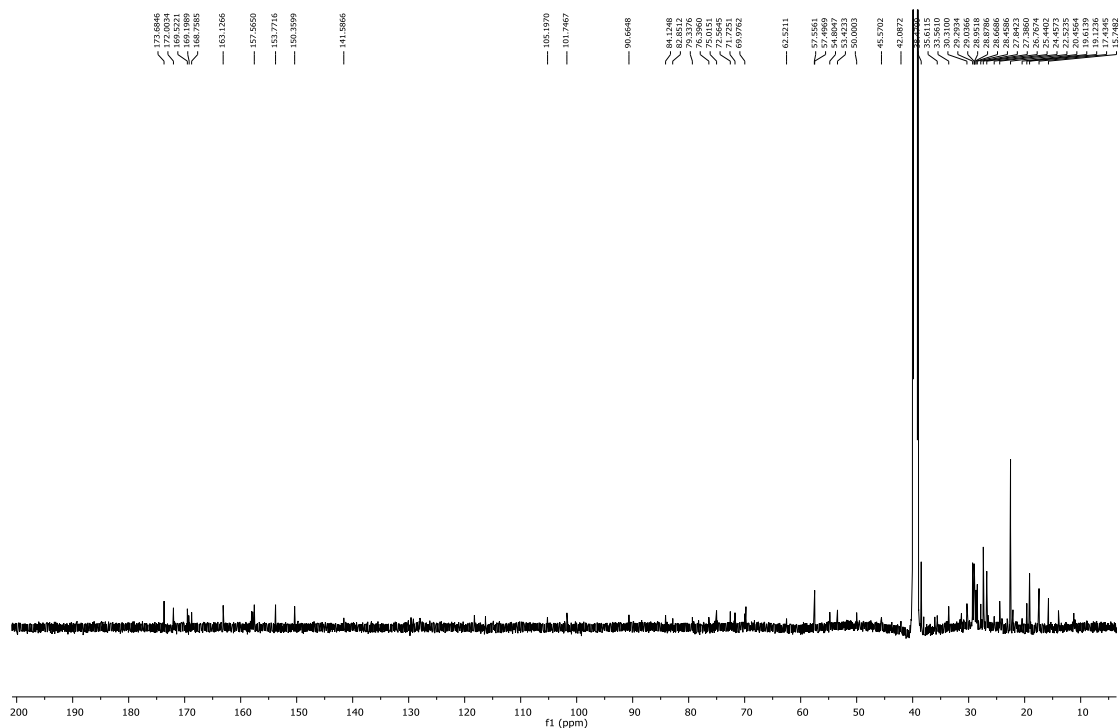
Figure S2.11 ^{13}C NMR spectrum (DMSO-d_6, 150 MHz) of muraymycin B9 (**2**).
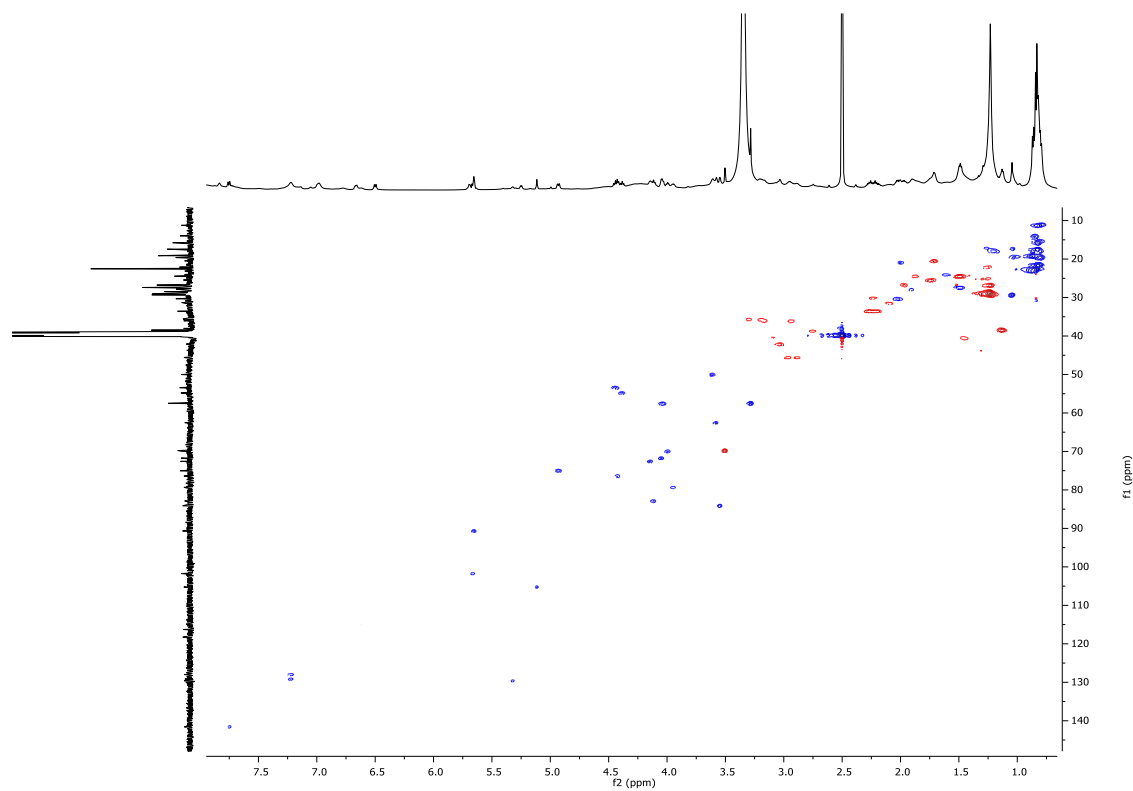
Figure S2.12 HSQC spectrum (DMSO-d_6, 600 MHz) of muraymycin B9 (**2**).
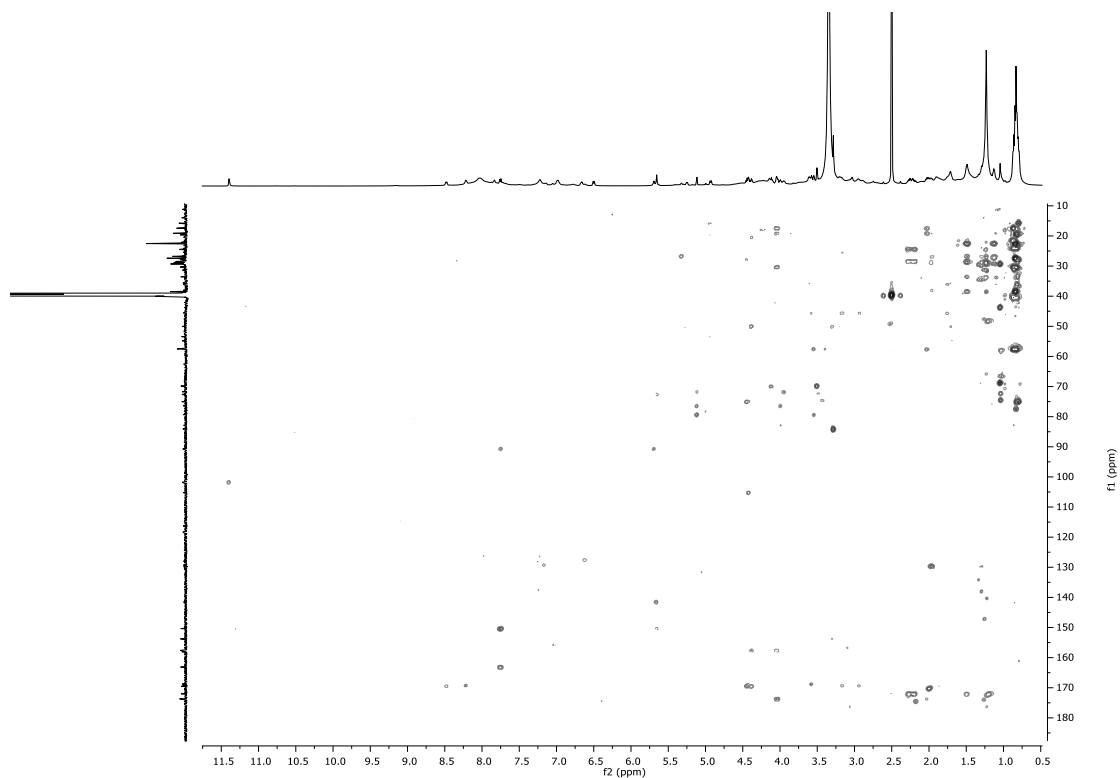
Figure S2.13 HMBC spectrum (DMSO-d_6, 600 MHz) of muraymycin B9 (**2**).
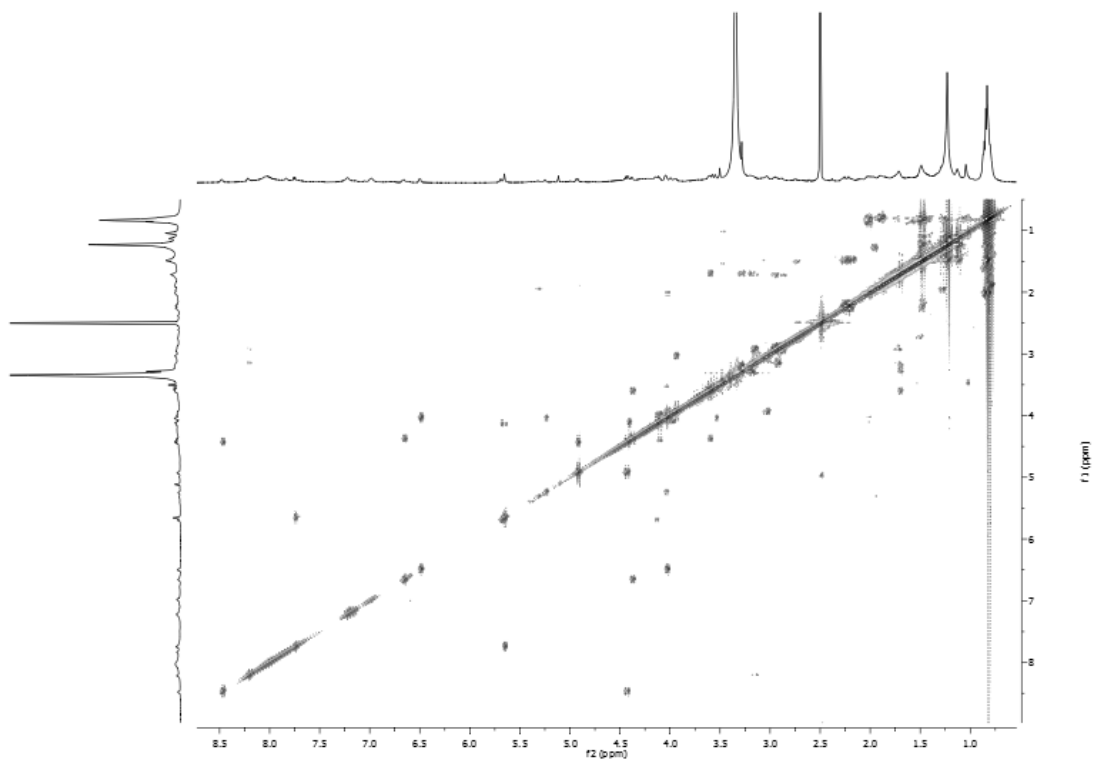
Figure S2.14 ^{1}H-^{1}H COSY spectrum (DMSO-d_6, 600 MHz) of muraymycin B9 (**2**).
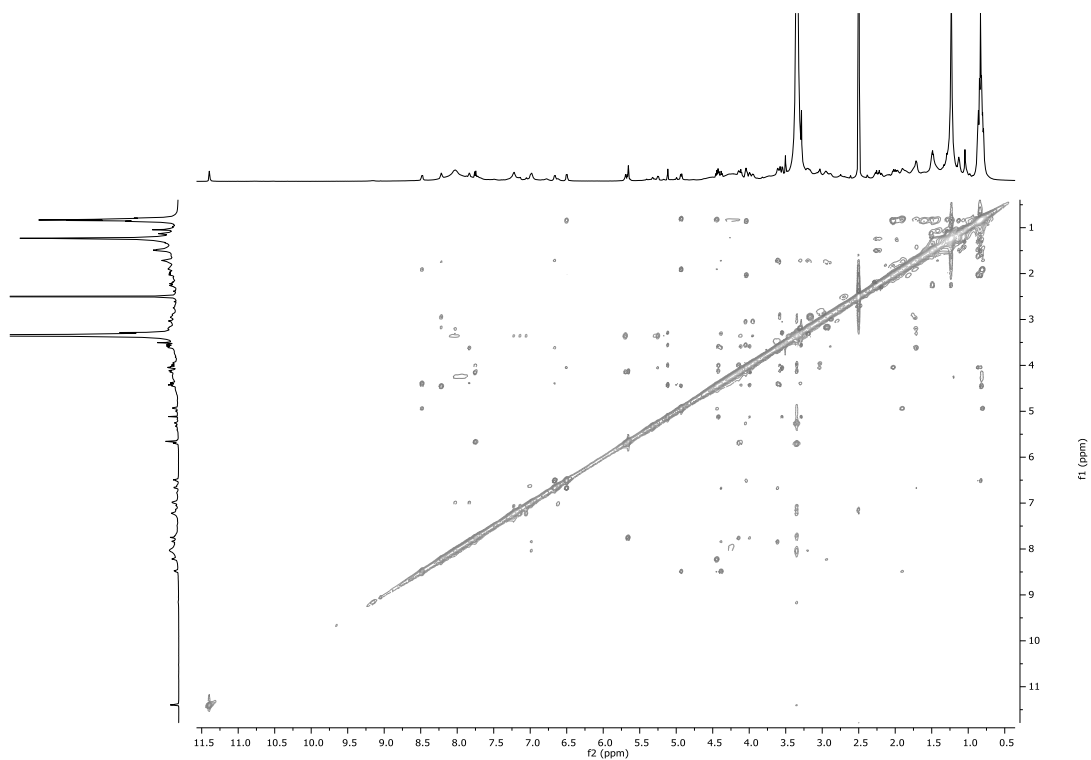
Figure S2.15 NOESY spectrum (DMSO-d_6, 600 MHz) of muraymycin B9 (**2**).
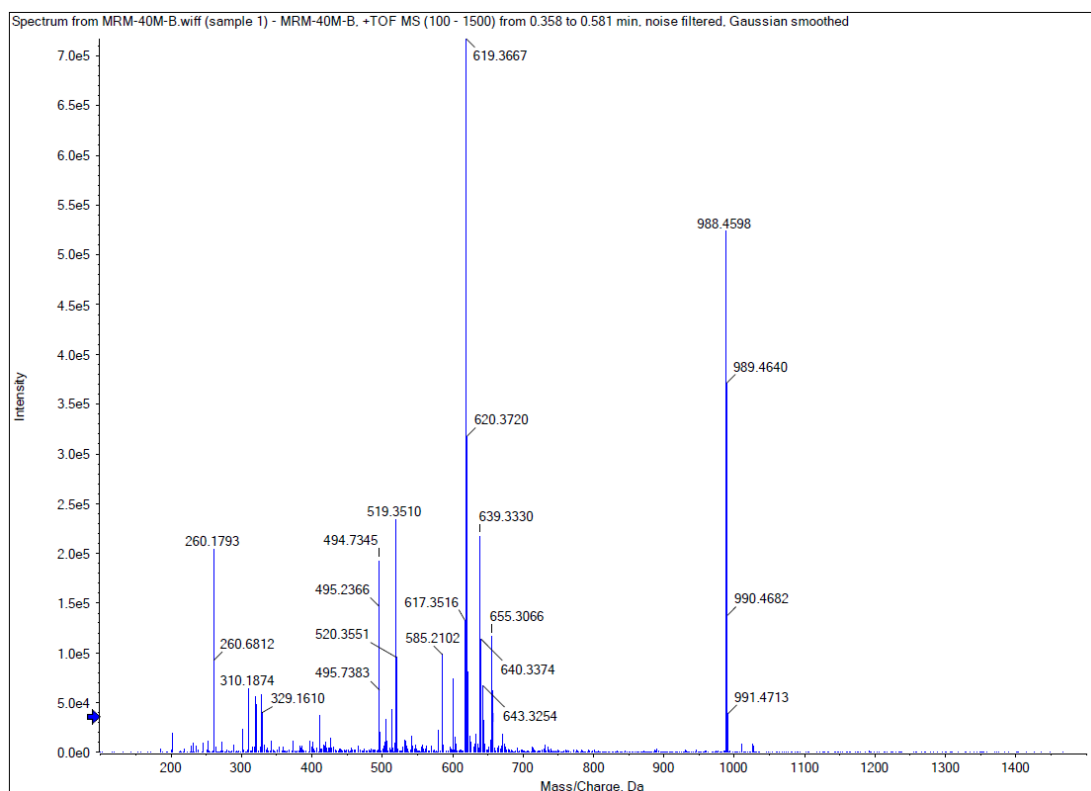
Figure S2.16 (+)-HR-ESI-MS (positive mode) of muraymycin C6 (**3**).
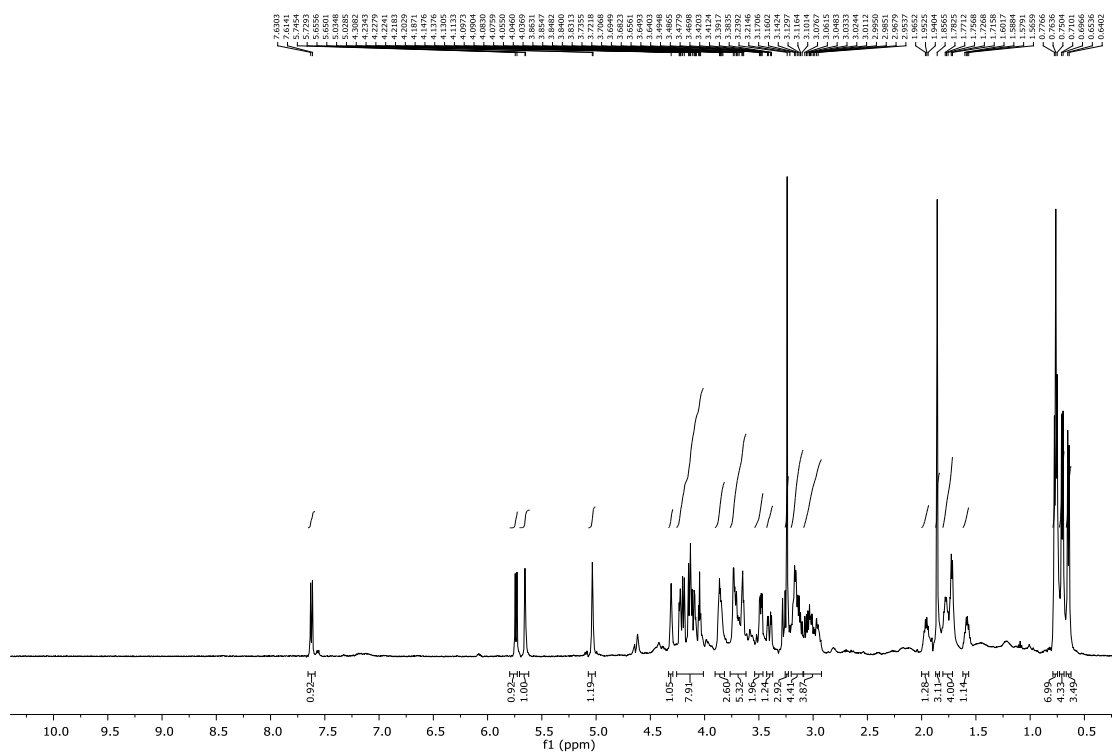
Figure S2.17 ^{1}H NMR spectrum (D$_2$O, 400 MHz) of muraymycin C6 (**3**).
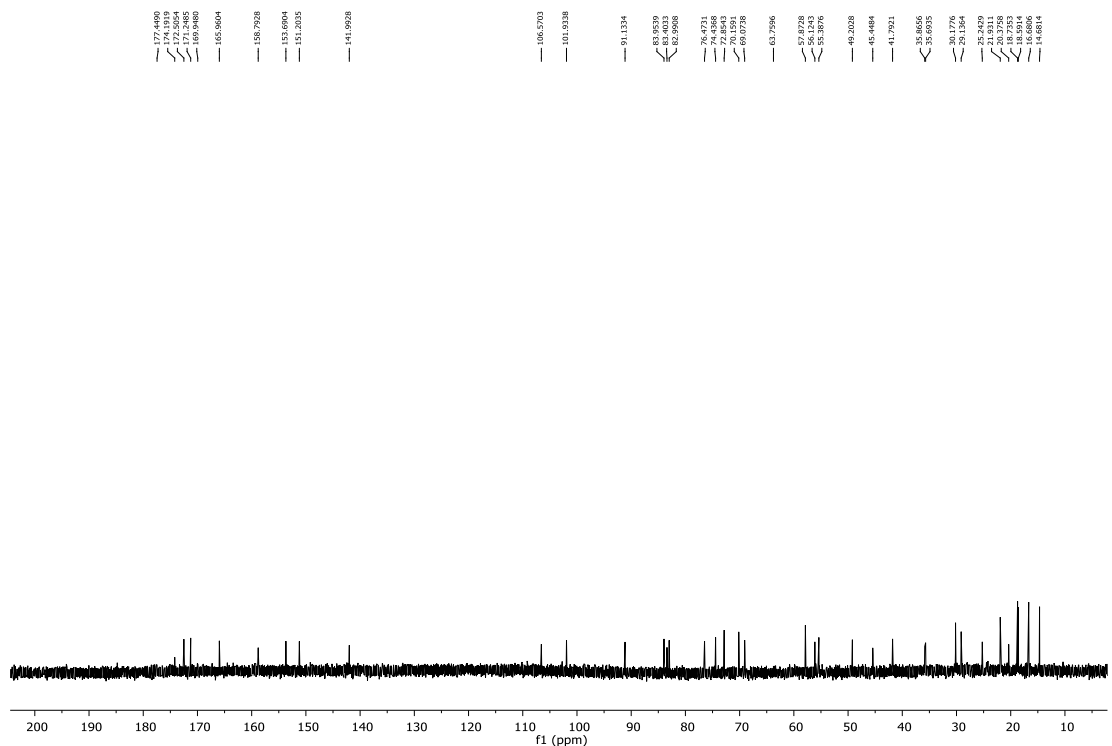
Figure S2.18 ^{13}C NMR spectrum (D$_2$O, 100 MHz) of muraymycin C6 (**3**).
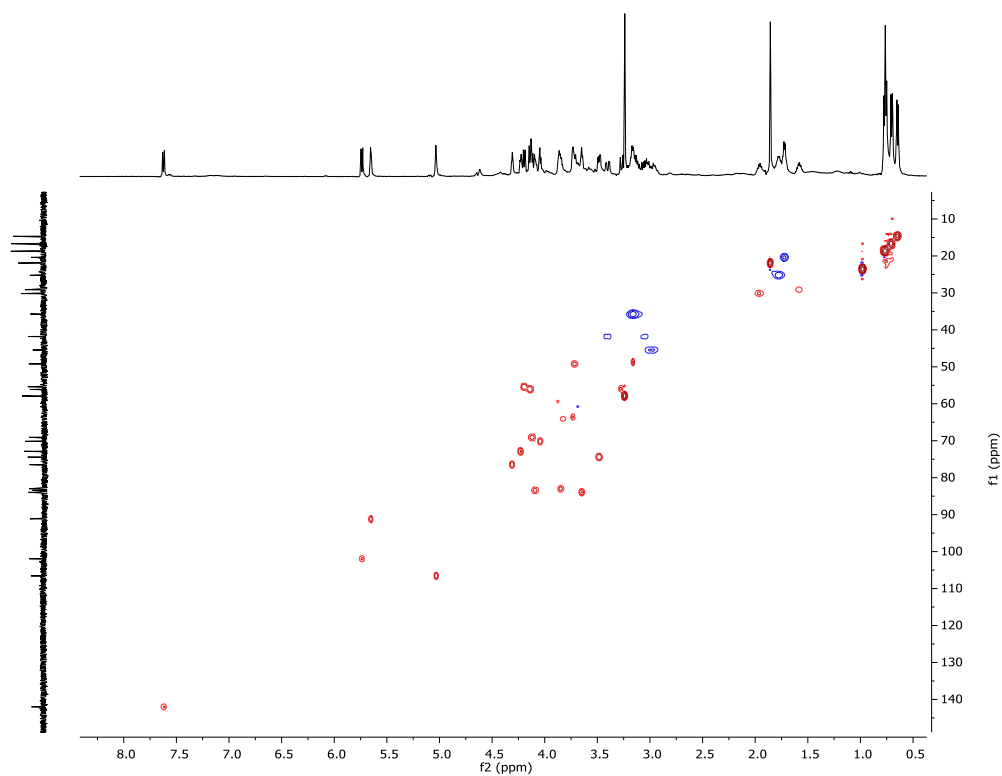
Figure S2.19 HSQC spectrum (D$_2$O, 400 MHz) of muraymycin C6 (**3**).
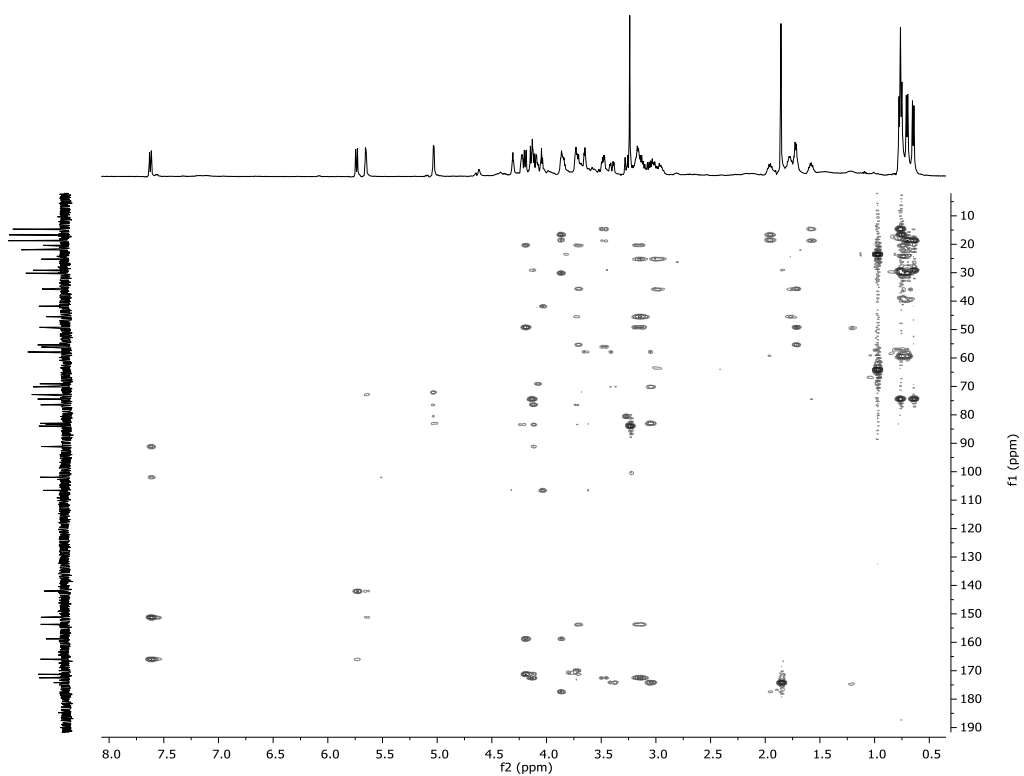
Figure S2.20 HMBC spectrum (D$_2$O, 400 MHz) of muraymycin C6 (**3**).
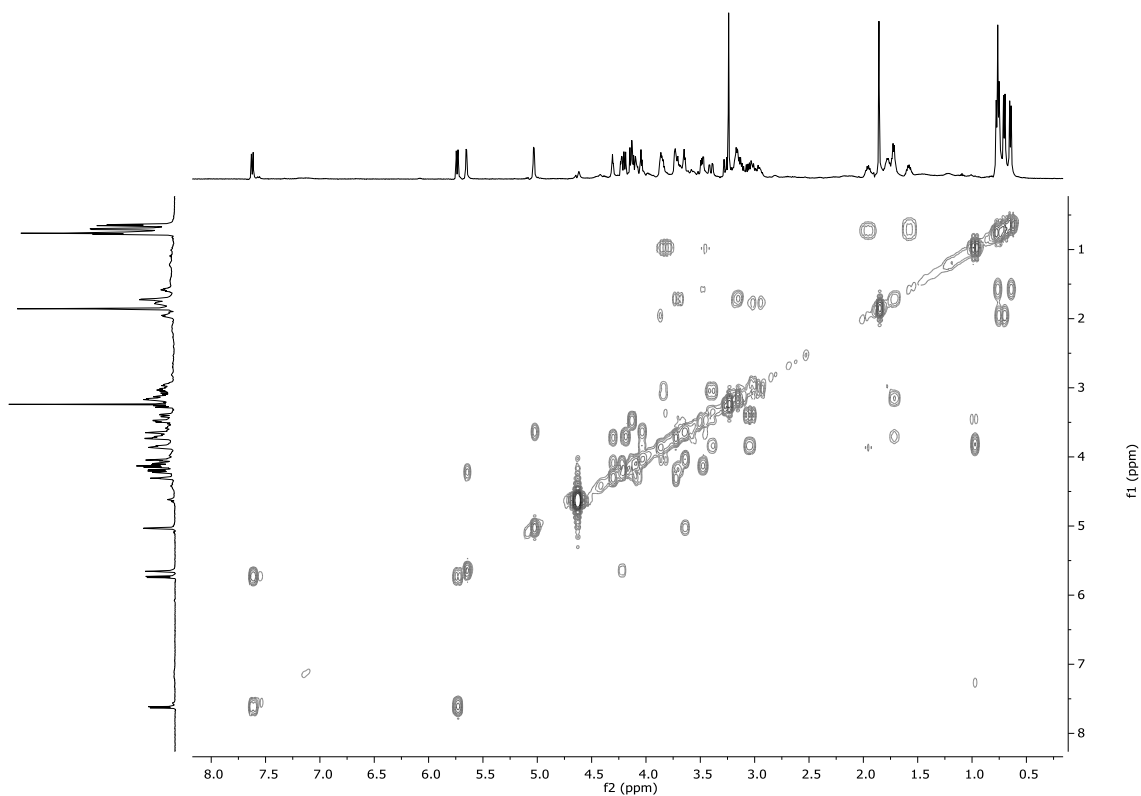
Figure S2.21 ^{1}H-^{1}H COSY spectrum (D$_2$O, 400 MHz) of muraymycin C6 (**3**).
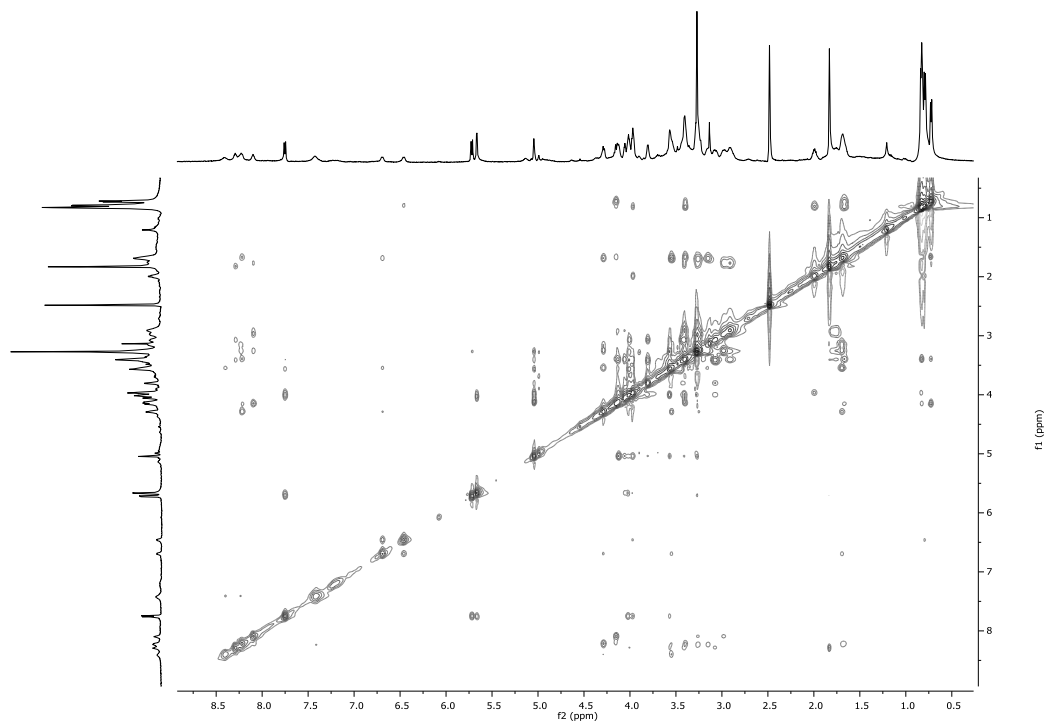
Figure S2.22 NOESY spectrum (D$_2$O, 400 MHz) of muraymycin C6 (**3**).
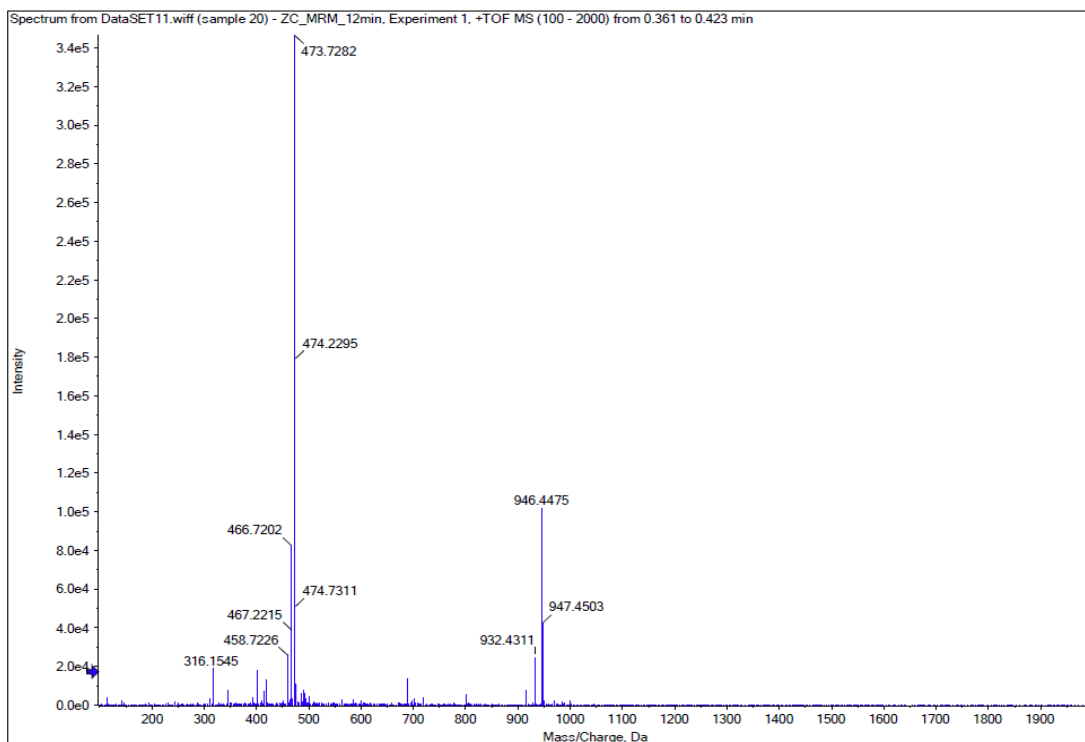
Figure S2.23 (+)-HR-ESI-MS (positive mode) of muraymycin C1 (**4**).
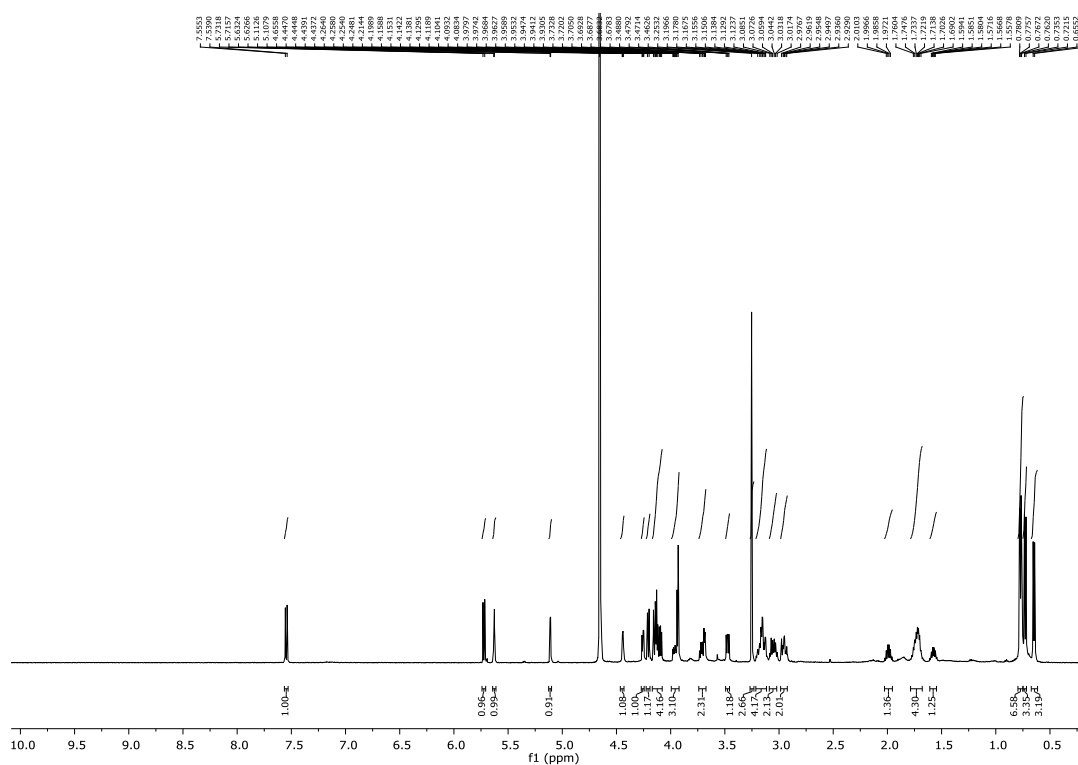
Figure S2.24 ^{1}H NMR spectrum (D$_2$O, 400 MHz) of muraymycin C1 (**4**).
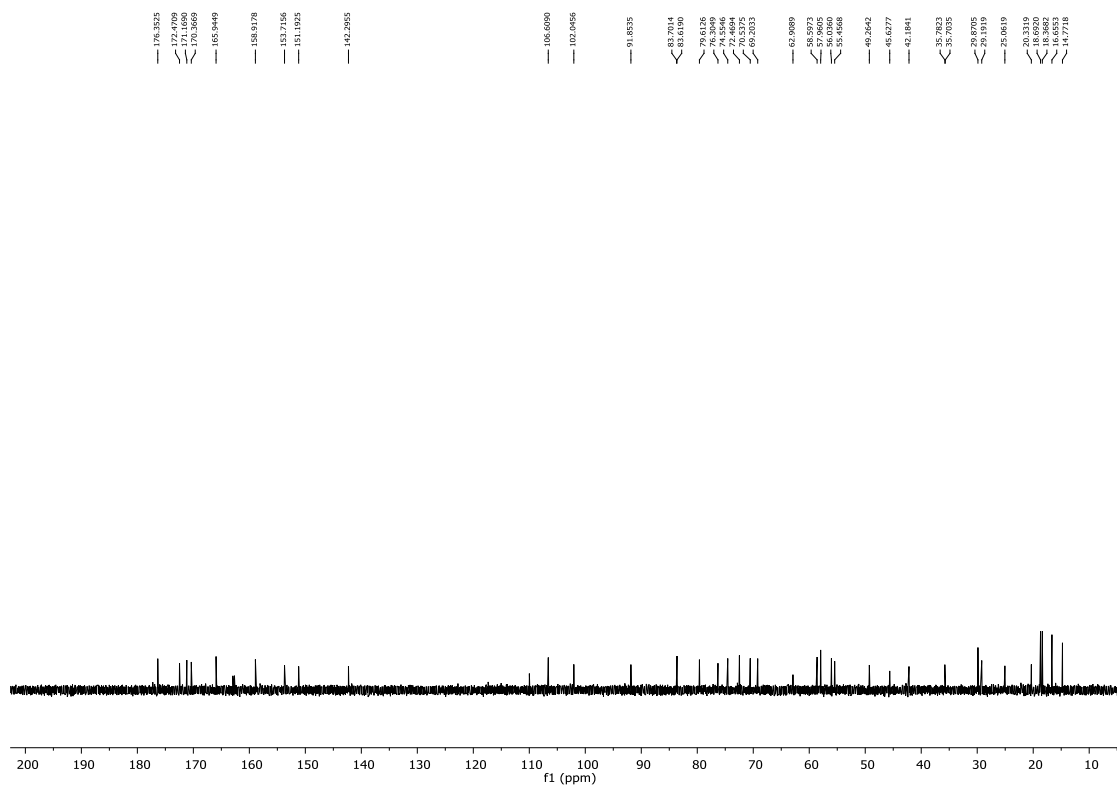
Figure S2.25 ^{13}C NMR spectrum (D$_2$O, 100 MHz) of muraymycin C1 (**4**).
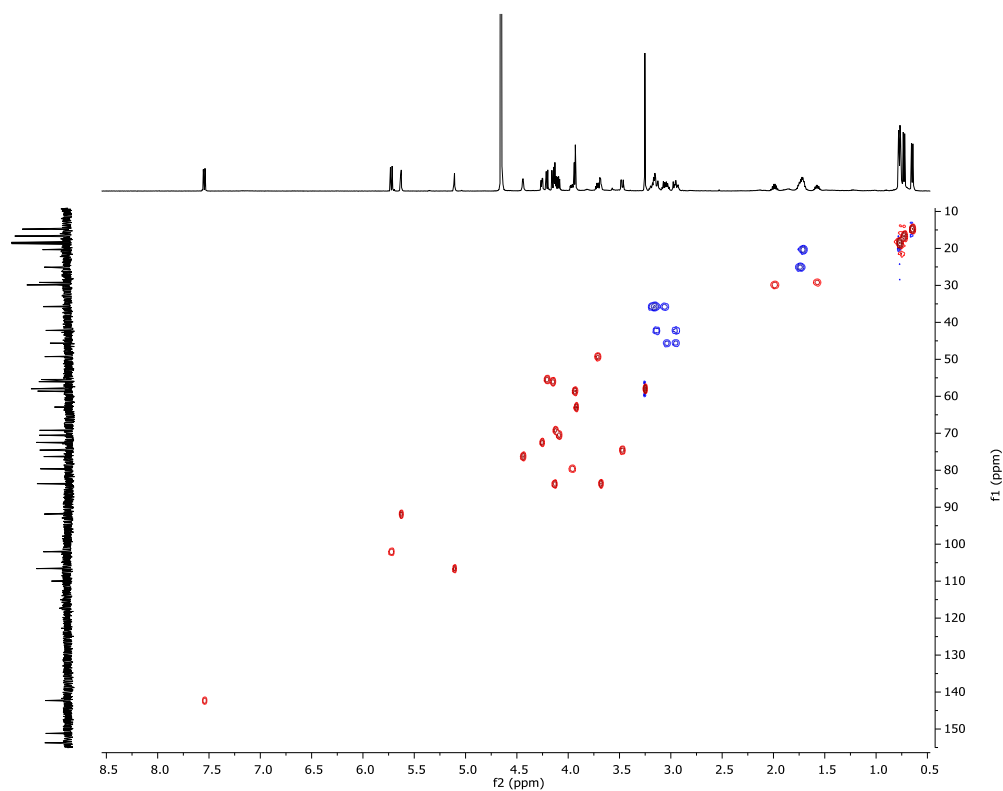
Figure S2.26 HSQC spectrum (D$_2$O, 400 MHz) of muraymycin C1 (**4**).
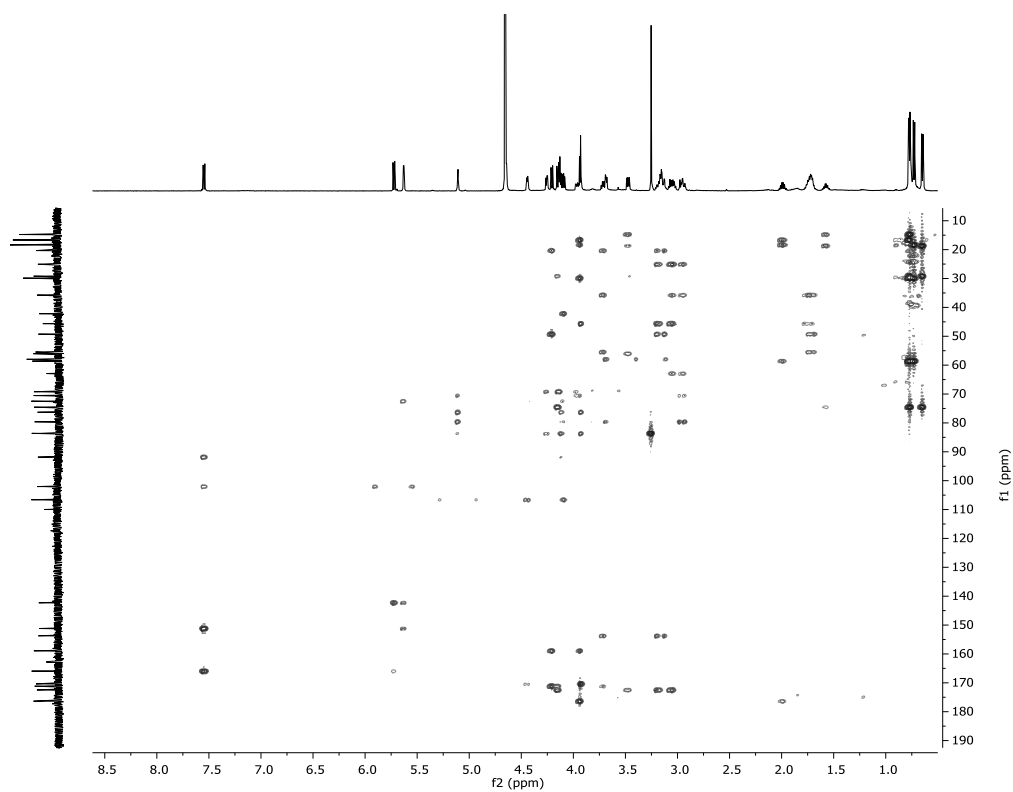
Figure S2.27 HMBC spectrum (D$_2$O, 400 MHz) of muraymycin C1 (**4**).
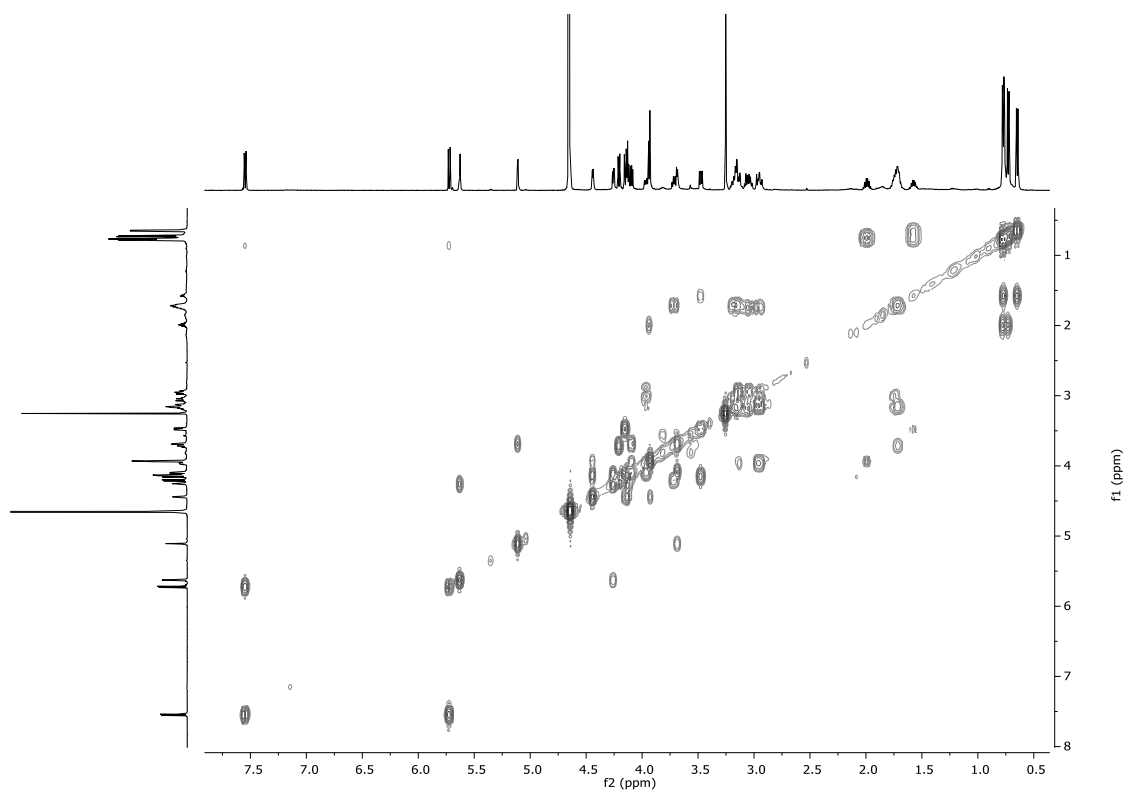
Figure S2.28 ^{1}H-^{1}H COSY spectrum (D$_2$O, 400 MHz) of muraymycin C1 (**4**).

Chapter 3 : Enzymatic Formation of Ribofuranosylated Glycyl-uridine Scaffold of Antibiotic Muraymycin

3.1 Introduction

According to bioinformatics analysis of the muraymycin gene cluster, six enzymes, Mur16 (encoding a putative dioxygenase), Mur17 (encoding a putative transaldolase), Mur20 (encoding a putative aminotransferase), Mur26 (encoding a putative phosphorylase), Mur18 (encoding a putative nucleotidylyltransferase) and Mur19 (encoding a putative glycosyltransferase) are proposed to be critical for the biosynthesis of the core structure, ribofuranosylated glycyl-uridine, of muraymycin. Respective enzyme homologs from the biosynthetic pathway of A-90289, a structurally related nucleoside antibiotic (Figure 3.1), have been characterized (Figure 3.2).[46-51] As muraymycin has similar disaccharide scaffold with A-90289, we expect the muraymycin homologs to have a similar function. However, unlike A-90289, the muraymycin nucleoside is not 2′-*O*-sulfated and the 2″-OH of the aminoribose is differentially modified, suggesting the possibility that the homologues have unique biochemical properties. Moreover, the ribosyltransferase in the biosynthetic pathway of A-90289 was only tested by utilizing its surrogate acceptor. In this chapter, the function of the six enzymes (Mur16, 17, 18, 19, 20 and 26) was identified and characterized. The ribosyltransferase Mur19 in muraymycin biosynthetic pathway and LipN in A-90289 biosynthetic pathway were also tested, for the first time, with its genuine aminoribose acceptor. A one-pot enzymatic reaction was utilized to produce this disaccharide moiety and its 2″-deoxy analogue.
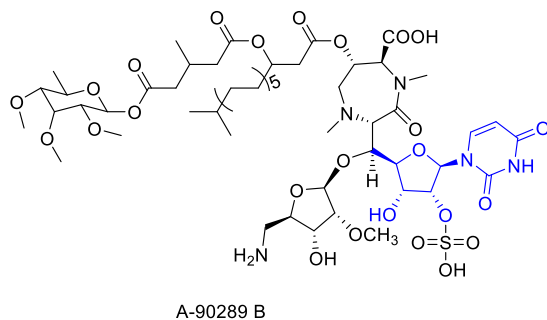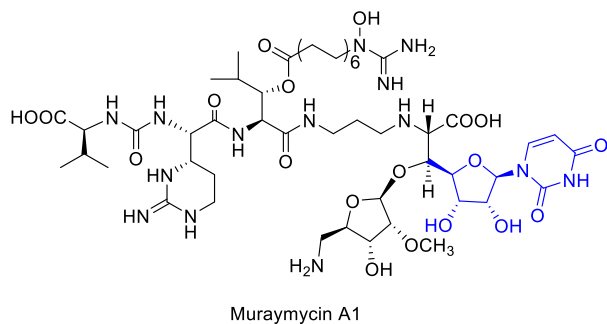
Figure 3.1 Structure of muraymycin A1 and A-90289A containing similar ribofuranosylated glycyl-uridine moiety.
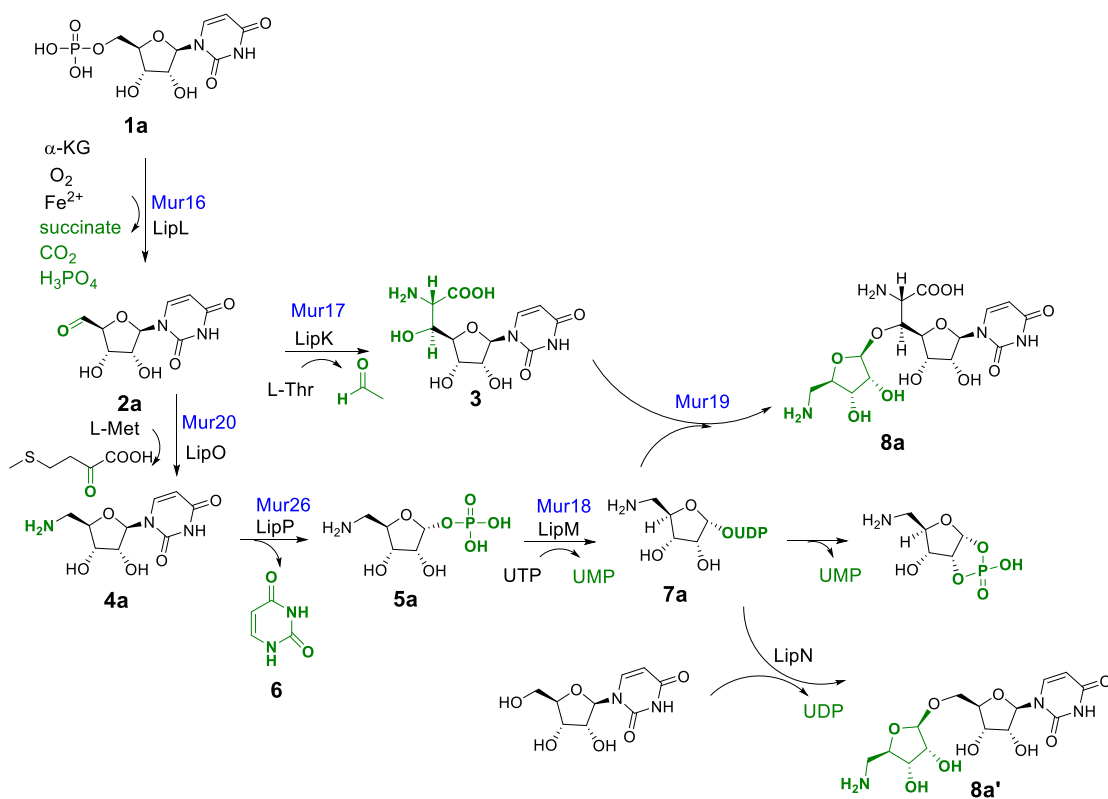
Figure 3.2 Proposed biosynthetic pathway towards ribofuranosylated glycyl-uridine moiety. Enzymes that were previously functionally characterized were labeled in black.

3.2 Materials and Methods

3.2.1 Cloning, Overexpression and Purification of Proteins

The genes *mur16, 17, 18, 19, 20* and *26* were amplified by PCR from genomic DNA extracted from *Streptomyces* sp. NRRL30473 using Phusion Hot Start II DNA Polymerase from Thermo Scientific with supplied HF buffer. Purified PCR products were ligated to pET30 Xa/LIC (Novagen) or pXY200 following the standard protocol and confirmed by DNA sequencing (ACGT, INC).

Plasmids pET30-*mur16*, pET30-*mur18*, pET30-*mur20* and pET30-*mur26* were introduced into *E. coli* BL21(DE3) cells, and the transformed strains were grown in LB supplemented with 50 μg/mL kanamycin. Following inoculation of 500 mL of LB with 50 μg/mL kanamycin, the cultures were grown at 37 °C until the cell density reached an OD_{600} ~ 0.5 when expression was induced with 0.1 mM IPTG. Cells were harvested after an overnight incubation at 18 °C and lysed in Buffer A (100 mM KH_2PO_4, 300 mM NaCl, 10 mM imidazole, pH 8.3) using a Qsonica sonicator (Qsonica LLC, Newtown, CT) for sonication for a total of 6 min at 40% amplitude with 30 s pulses separated by 30 s rest periods. Following centrifugation the protein was purified using affinity chromatography with HisPurTM Ni-NTA agarose (Thermo Scientific, Rockford, IL), and proteins were eluted with increasing concentrations of imidazole in Buffer A. Purified proteins were concentrated and buffer exchanged into Buffer B (25 mM KH_2PO_4, 100 mM NaCl, pH 8.3) using Amicon Ultra 10000 MWCO centrifugal filter (Millipore) and stored as glycerol stocks (40%) at -20 °C. Protein purity was assessed as by 12% acrylamide SDS-PAGE; His_6-tagged proteins were utilized without further modifications.

Protein concentration was determined using UV/Vis spectroscopy, and the extension coefficients were calculated using the ProtParam tool available from ExPASY.

Plasmids pXY200-*mur17* and pXY200-*mur19* were transformed into *S. lividans* TK24 using PEG-mediated protoplast transformation and plated on R2YE supplemented with 50 μg/mL apramycin. After 6 days at 28 °C, positive transformants were confirmed by colony PCR using InstaGene Matrix from Bio-Rad (Hercules, CA) and LA-Taq polymerase with GC buffer I.

The recombinant strain was utilized to inoculate 50 mL R2YE containing 50 μg/mL apramycin, grown for 3 days at 28 °C at 250 rpm, and 2 mL transferred to fresh 100 mL containing 50 μg/mL apramycin. Following growth for 3 days at 28 °C at 250 rpm, protein expression was induced by addition of thiostrepton (5 μg/mL) and the culture was incubated for another 24 h before harvesting. The cells from 400 mL of culture were collected by centrifugation. The pellet was thoroughly resuspended in ice-cold Buffer A supplemented with 4 mg/mL of lysozyme was subsequently added to the suspension. After incubation at 30 ℃ for 30 min, the cell suspension was mixed by pipetting and lysed using a Qsonica sonicator (Qsonica LLC, Newtown, CT) for sonication for a total of 10 min at 40% amplitude with 30 s pulses separated by 30 s rest periods. The protein purification and storage was as described above.

3.2.2 Synthesis of 2'-Methoxy-UMP, **1c**.

The synthesis of **1c** followed a previously described procedure.[52] Pyrophosphoryl chloride (0.1 mL) was added to a cool solution (4 °C) of 2′-O-methyluridine (52 mg) in m-

cresol (2 mL). The mixture was stirred for 2 h at 4 °C and diluted with ice water (7 mL). The product was extracted with diethyl ether (3 mL). The aqueous layer was adjusted to pH = 2 with 4 N sodium hydroxide. After freeze-drying, the product was purified by semipreparative HPLC (Waters 600) with gradient shown in Table S3.7 to yield 30 mg.
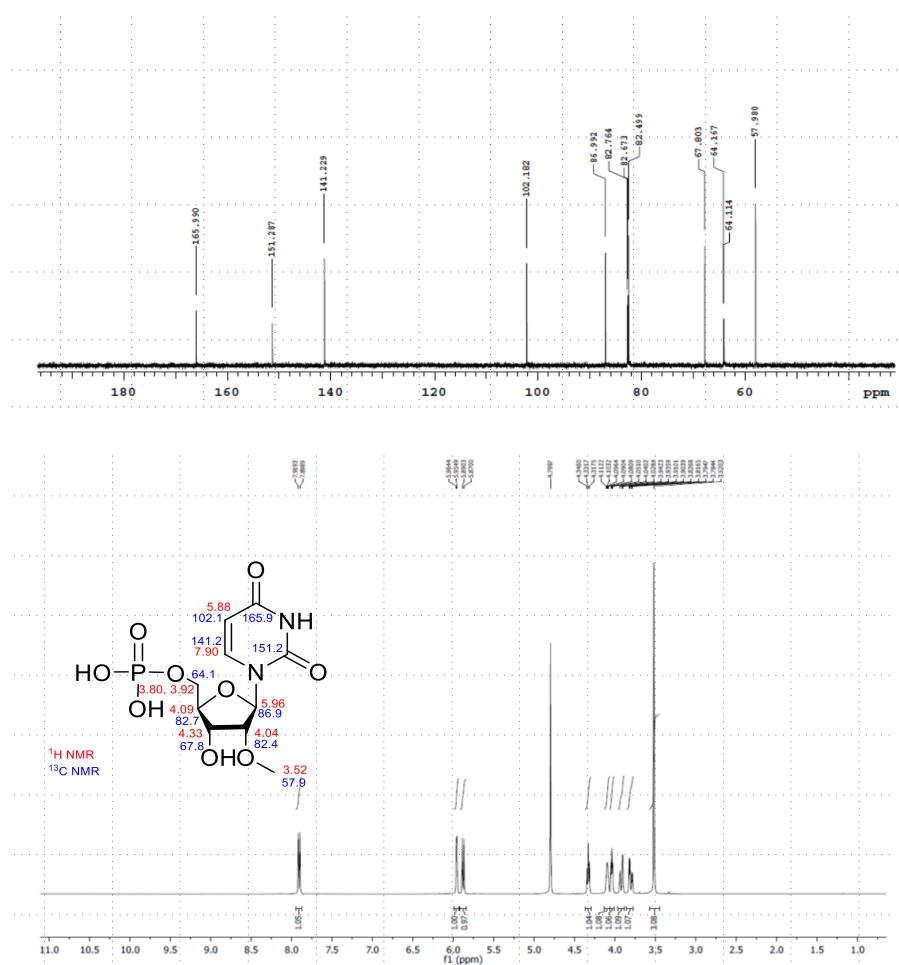
Figure 3.3 ^{13}C NMR spectrum (D$_2$O, 100 MHz) and ^{1}H NMR spectrum (D$_2$O, 400 MHz) of 2′-methoxy-UMP.

3.2.3 Activity Assay of Mur16

Reactions consisted of 50 mM HEPES (pH 7.5), 2.5 mM α-KG, 2 mM ascorbic acid, 0.2 mM FeCl$_2$, 1 mM UMP, dUMP or 2′-methoxy-UMP, and 100 nM Mur16 at 30 °C. Reactions were terminated by ultrafiltration using Amicon® Ultra centrifugal filter units. Following

centrifugation to remove protein, the reaction was analyzed by HPLC or LC-MS with the gradient shown in Table S3.2.

3.2.4 Kinetics of Mur16

To determine the kinetic constants with respect to UMP and dUMP, reactions were carried out in 50 mM Tris-HCl (pH 7.5), 2 mM α-KG, 2 mM ascorbic acid, 0.4 mM FeCl$_2$ with variable concentration of UMP (1 µM-500 µM), dUMP (1 µM-500 µM) or 2′-methoxy-UMP and 40 nM Mur16 at 30 °C for 4 min and analyzed under initial velocity conditions using the malachite green binding assay or at 30 °C for 1 h and analyzed by HPLC with gradient shown in Table S3.2 at 260 nm. Each data point represents three replicate end point assays. Kinetic constants were obtained by nonlinear regression analysis using GraphPad Prism 7 (GraphPad Software, La Jolla, CA).

3.2.5 Activity Assay of Mur17

Reactions of Mur17 consisted of 50 mM HEPES (pH 7.5), 2 mM uridine-5′-aldehyde **2a**, 5 mM L-threonine, 0.1 mM PLP and 1 µM Mur17 at 30 °C. Following removal of the protein by ultrafiltration, the reaction was analyzed by LC-MS.

AQC, 6-aminoquinolyl-*N*-hydroxysuccinimidyl carbamate, a derivatizing reagent for amines, was used for the modification of 5′- and 6′-epimers of GlyU (synthesized by Christian Ducho's lab[53]). The reaction (20 µL) was mixed with 60 µL of 0.2 M sodium borate buffer (pH8.8) and 20 µL of 3 mg/mL AQC acetonitrile solution. The mixtures were incubated at 55 °C for 10 min and then allowed to cool to rt. The AQC-derivatized samples (50 µL) were applied to LC-MS with the gradient shown in Table S3.3.

51

3.2.6 Activity Assay of Mur20

Reactions of Mur20 consisted of 50 mM potassium phosphate (pH 7.5), 1 mM uridine aldehyde with different 2′ modification (**2a** synthesized by previous lab members**, 2b or 2c**), 1 mM L-amino acid (methionine, alanine, arginine, etc.) and 1 μM Mur20 or LipO at 30 °C. Following removal of the protein by ultrafiltration, the reaction was analyzed by LC-MS with the gradient shown in Table S3.2.

To identify the production of α-keto-γ-methylthio butyric acid, reaction mixtures or the positive control (α-keto-γ-methylthio butyric acid) were treated with reagent 3-methyl-2-benzothiazolinone hydrazone hydrochloride (MBTH) according to the method described by Tanaka.[54] Following removal of the protein by ultrafiltration, 50 μL reaction mixtures were mixed with 50 μL of 1 M sodium acetate (pH 5.0) and 50 μL of 8 mM MBTH aqueous solution. The mixtures were then incubated at 50 °C for 30 min and then analyzed by LC-MS with the gradient shown in Table S3.4 with detection at 350 nm.

3.2.7 Activity Assay of Mur26

Reactions of Mur26 consisted of 50 mM potassium phosphate (pH 7.5), 2 mM 5′-amino-5′deoxy-uridine with different 2′ modification (**4a, 4b, 4c**) and 1 μM Mur26 or LipP at 30 °C. Following removal of the protein by ultrafiltration, reactions were analyzed by LC-MS with the gradient shown in Table S3.2.

3.2.8 Activity Assay of Mur18

Reactions of Mur18 consisted of 50 mM potassium phosphate (pH 7.5), 2 mM 5′-amino-5′-deoxy-uridine **4a** or 5′-amino-2′, 5′dideoxy-uridine **4b** (synthesized by previous lab

members), 5 mM $MgCl_2$, 2 mM UTP, 1 μM Mur26 or LipP and 1 μM Mur18. Following

removal of the protein by ultrafiltration, reactions were analyzed by HPLC with the gradient

shown in Table S3.5 or Table S3.6.

3.2.9 Activity Assay of Mur19

Reactions of Mur19 consisted of 50 mM potassium phosphate (pH 7.5), 2 mM 5′-

amino-5′-deoxy-uridine **4a** or 5′-amino-2′, 5′-dideoxy-uridine **4b**, 5 mM $MgCl_2$, 2 mM UTP or

2′-F-dUTP, 1 mM GlyU **3**, 1 μM Mur26 or LipP, 1 μM Mur18 or LipM and 1 μM Mur19 or

LipN. Following the removal of the protein by ultrafiltration, reactions were analyzed by HPLC

with the gradient shown in Table S3.5.

Large-scale production of **8b** (30 mL reaction) was identical to reactions

described above using **3**, **4b** and UTP. The isolation of AQC-modified **8b** was carried

out with semipreparative HPLC with the gradient shown in Table S3.8 with detection.

3.2.10 MIC assay of AQC modified **8b**

The protocol used for the determination of the minimum inhibitory

concentration (MIC) was as described previously with minor modifications.[29]

Escherichia coli Δ*tolC* mutant JW5503 (*E. coli* genetic stock center) was used as model

strains for antimicrobial susceptibility assays. *E. coli* Δ*tolC* mutant were grown in 5

mL of LB medium with 50 μg/mL kanamycin for 16 h at 37 °C with shaking (250 rpm),

and then were diluted (x1000) into 4.5 mL of medium and incubated until OD_{600}

reaching 0.4. An aliquot of the suspension was diluted (x1000) and 90 μL aliquots of

diluted culture were transferred into the individual well of a 96-well plate supplied with

10 μL of the AQC modified **8b**. Maximum final concentration of 32 μg/mL with serial dilutions was added to obtain the antimicrobial activities and compared to the negative control containing water alone. Resazurin solution (5 μL) was added to each well, and the plates were shaken for 10 s and incubated at 37 °C for another 3 h to allow resazurin to convert to resorufin by viable bacteria. The minimal concentration of the tested compound that caused growth inhibition was recorded as the MIC.

3.2.11 One-Pot Enzymatic Reaction for the Biosynthesis of **8a**

Reactions consisted of 50 mM Hepes buffer (pH 7.5), 2.5 mM α-KG, 2 mM ascorbic acid, 0.2 mM FeCl$_2$, 4 mM UMP, 2 mM L-threonine, 0.1 mM PLP, 2 mM L-methionine, 1 mM MgCl$_2$, 2 mM UTP, 1 μM Mur16, Mur17, LipO, LipP, Mur18 and Mur19 was added accordingly. Following removal of the protein by ultrafiltration, reactions were analyzed by HPLC with the gradient shown in Table S3.5.

3.2.12 One-Pot Enzymatic Reaction for the Biosynthesis of **8b**

Reactions consisted of 50 mM HEPES buffer (pH 7.5), 2.5 mM α-KG, 2 mM ascorbic acid, 0.2 mM FeCl$_2$, 4 mM dUMP, 100 μM GlyU, 0.1 mM PLP, 2 mM L-methionine, 1 mM MgCl$_2$, 2 mM UTP. 1 μM Mur16, LipO, LipP, Mur18 and Mur19 was added accordingly. Following removal of the protein by ultrafiltration, reactions were analyzed by HPLC with the gradient shown in Table S3.5.

3.3 Results and Discussion

3.3.1 Functional Assignment of Mur16 as a Non-heme, Fe(II)-dependent α-Ketoglutarate: UMP Dioxygenase

Bioinformatic analysis revealed that Mur16 has a sequence similarity to dioxygenases including LipL and Cpr19,[55-56] which utilizes UMP, α-KG and $FeCl_2$ to form uridine-5′-aldehyde.[25,36] The *mur16* gene was cloned and expressed in *E. coli* BL21(DE3) to yield soluble protein (Figure S3.1). Using HPLC for detection, the activity of Mur16 was tested with UMP and a new peak corresponding to uridine-5′-aldehyde, **2a** was formed in the presence of α-KG and $FeCl_2$ (Figure 3.4A, Figure S3.2A). Mur16 also catalyzed oxidative decarboxylation of α-KG to form succinate from the LC-MS result (Figure S3.3A). The enzyme-coupled assay to detect succinate production was also employed to confirm the production of succinate. Mur16 was previously proposed to utilize L-arginine as substrate,[22] however, LC-MS analysis and the enzyme-coupled assay to detect succinate revealed that L-arginine cannot be utilized by Mur16 (Figures S3.3B-C).

Different from LipL, which was unable to utilize deoxy-or 2′modified ribonucleoside monophosphate, Mur16 can also utilize dUMP, **1b** and 2′-methoxy-UMP, **1c** as substrates to form corresponding aldehyde **2b** and **2c** (Figures 3.4B-C, S3.2B-C). Mur16 was found to have optimal activity at 2 mM ascorbate using 40 µM $FeCl_2$ (Figure 3.5A). Steady-state kinetic analysis with substrate UMP and dUMP was performed using the malachite green binding assay to detect phosphate formation. Single-substrate kinetic experiments of Mur16 with UMP and dUMP revealed typical Michaelis-Menten kinetics, yielding kinetic constants of $K_m = 20.81 \pm 3.93$ µM and $k_{cat} = 4.37 \pm 0.23$ s^{-1} with UMP and $K_m = 6.30 \pm 2.13$ µM and $k_{cat} = 2.3 \pm 0.16$ s^{-1} with dUMP (Figures 3.5B-C). However, kinetic experiments of Mur16 with **1c** showed strong substrate inhibition with the increased concentration of **1c** (Figure 3.5D), which indicated that the 2′-methyl group was added in a later step in the muraymycin biosynthetic pathway.
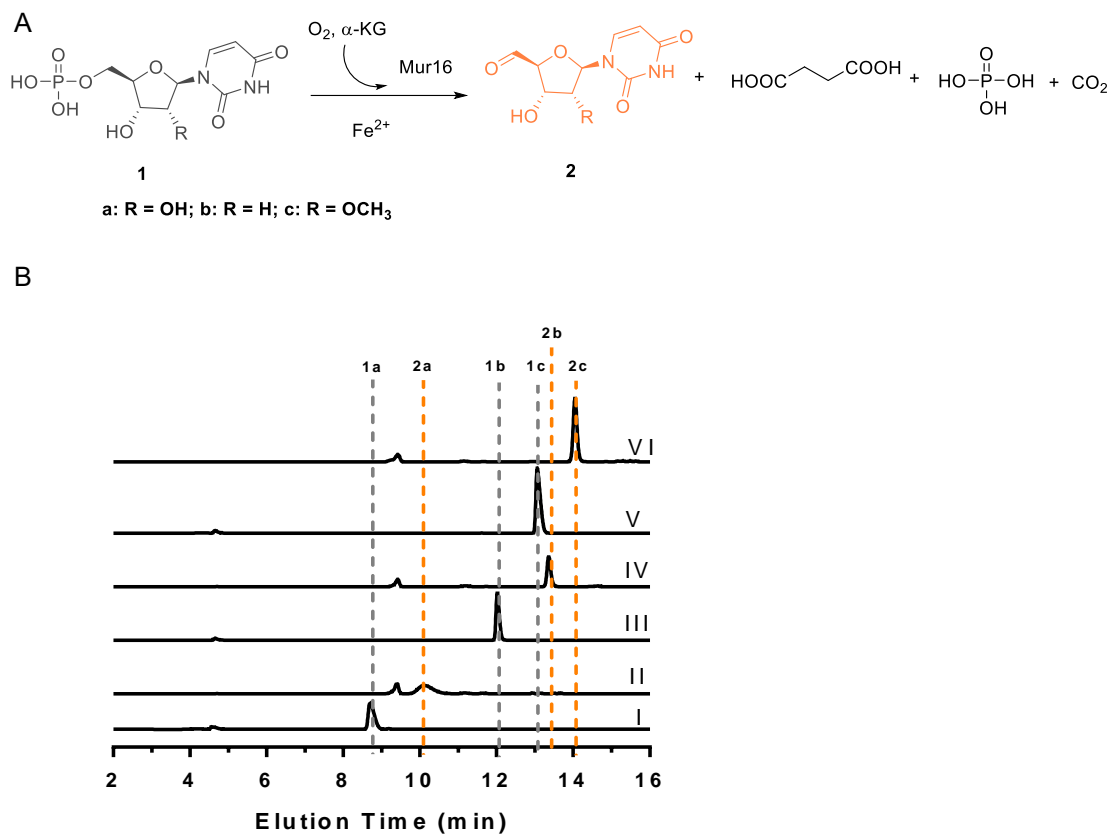
Figure 3.4 Characterization of Mur16.

(A) Reaction catalyzed by Mur16. (B) HPLC analysis using UMP (**1a**) after I, 12 h reaction w/ UMP, w/o Mur16; II, 12 h reaction w/ UMP, w/o Mur16; III, 12 h reaction w/ dUMP (**1b**), w/o Mur16; IV, 12 h reaction w/dUMP, w/o Mur16; V, 12 h reaction w/ 2′-methoxy-UMP (**1c**), w/o Mur16; VI, 12 h reaction w/ 2′-methoxy-UMP, w/ Mur16.
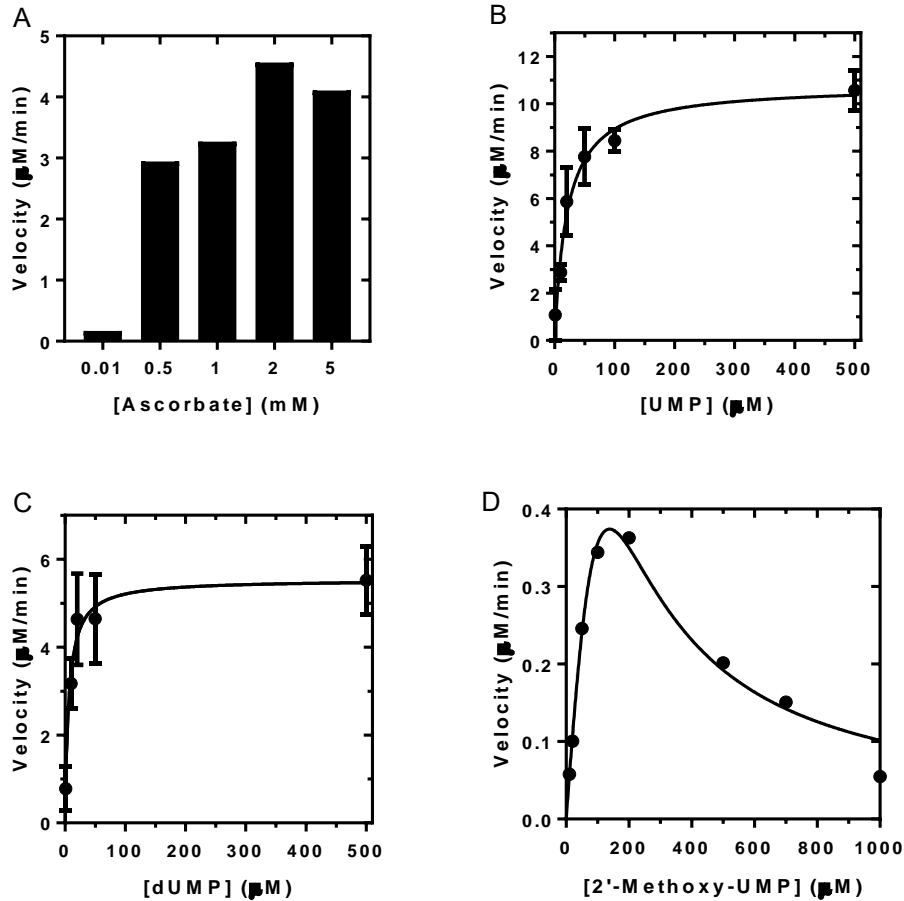
Figure 3.5 Activity optimization and kinetic analysis of Mur16.

(A) Optimal activity of Mur16 with respect to varied ascorbate in reactions containing of 40 µM FeCl$_2$ and 40 nM Mur16. (B) Single-substrate kinetic analysis using variable UMP (1 µM-500 µM), near saturating α-KG and 40 nM Mur16. (C) Single-substrate kinetic analysis using variable dUMP (1 µM-500 µM), near saturating α-KG and 40 nM Mur16. (D) Single-substrate kinetic analysis using variable 2′-methoxy-UMP (1 µM-1000 µM), near saturating α-KG and 40 nM Mur16.

57

3.3.2 Functional Assignment of Mur17 as an L-Threonine: Uridine-5′-aldehyde Transaldolase

Bioinformatic analysis of Mur17 revealed sequence similarity to LipK[49], which was previously assigned as a transaldolase that utilizes uridine-5'-aldehyde **2a** and L-threonine to generate GlyU, **3** (Figure 3.6A). Similar to LipK, the gene product of *mur17* was only soluble when expressed in *S. lividans* TK24 (Figure S3.1). Activity tests analysis using HPLC with uridine-5'-aldehyde revealed a new peak (Figure 3.6B). LC-MS analysis of the purified new peak revealed an $(M+H)^+$ ion at $m/z = 318.1$, consistent with the product of LipK (Figure S3.4). However, Mur17 cannot utilize **2b** or **2c** as substrate, which potentially explains why all discovered muraymycin congeners have the same GlyU core structure. 6-aminoquinolyl-*N*-hydroxysuccinimidyl carbamate (AQC) modification, which generates 6-quinolinylaminocarbonyl amines without alteration of the stereochemistry of the starting material, of synthetically prepared 5′- and 6′-epimers of **3** all showed different elution time (Figure S3.5). LC-MS analysis of AQC modified Mur17 reaction revealed enzymatic produced **3** showed same elution time with (5′S, 6′S)-**3**, which confirmed the stereo chemical assignment of **3** (Figure S3.6).

A
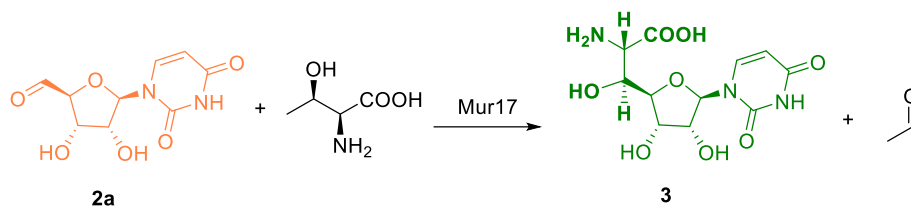
B
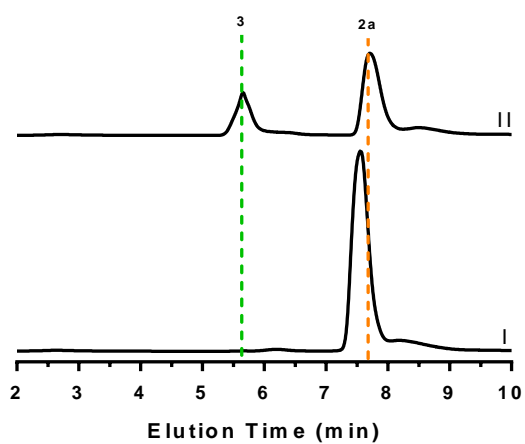
Figure 3.6 Characterization of Mur17.
(A) Reaction catalyzed by Mur17. (B) HPLC analysis using uridine aldehyde (**2a**) after I, 12 h reaction without Mur17; II, 12 h reaction.

3.3.3 Functional Assignment of Mur20 as an L-Methionine: 2-Aminotransferase.

Bioinformatic analysis revealed that Mur20 has a sequence similarity to LipO[47], which was previously assigned as a pyridoxal-phosphate (PLP)-dependent aminotransferase that catalyzes amino transfer utilizing nucleoside **2** as the amine acceptor (Figure 3.7A). The *mur20* gene was cloned and expressed in *E. coli* BL21(DE3) to yield soluble protein (Figure S3.1). HPLC analysis of the activity test of Mur20 with **2a** and L-methionine revealed a new peak (Figure 3.7B) with $(M+H)^+$ ion at $m/z = 244.0902$ (Figure S3.7), corresponding to amino uridine, **4a**, which is consistent with the product of LipO. Reagent 3-methyl-2-benzothiazolinone hydrazone hydrochloride (MBTH) was used to confirm the production α-keto-γ-methylthiol butyric acid from L-methionine in the transamination reaction (Figure S3.8). Further analysis revealed that 2′-deoxy-5′-uridine aldehyde **4b** and 2′-methoxy-5′-uridine aldehyde **4c** were also amine acceptors of Mur20 (Figures 3.7C-D, S3.9A-B). Several other potential amine donors like AdoMet, L-Arg or L-Ala can also be utilized as the amine donors by Mur20. However, GlyU cannot serve as amine donor for the reaction, which possibly indicated that GlyU was the acceptor of the glycosyltransferase in later steps.
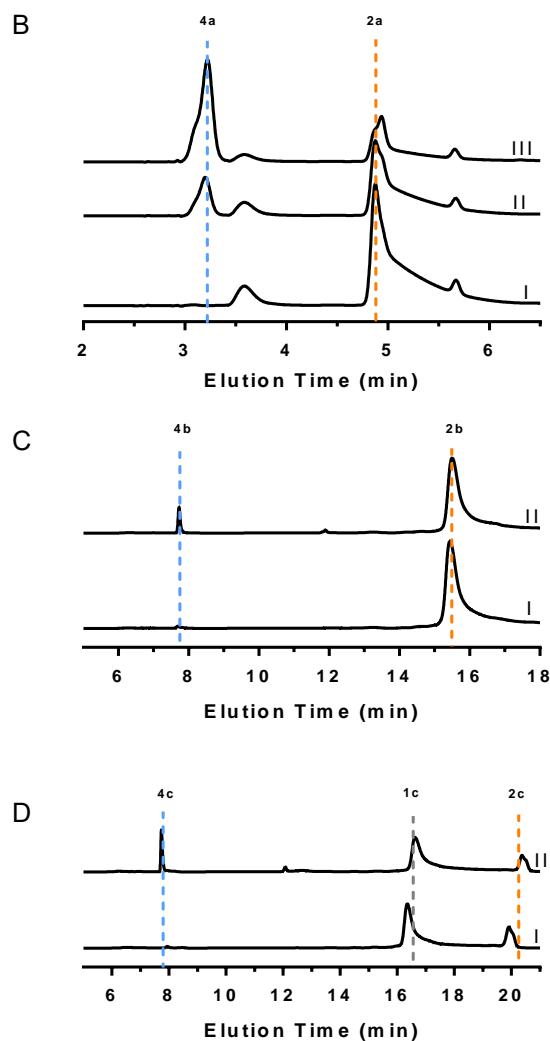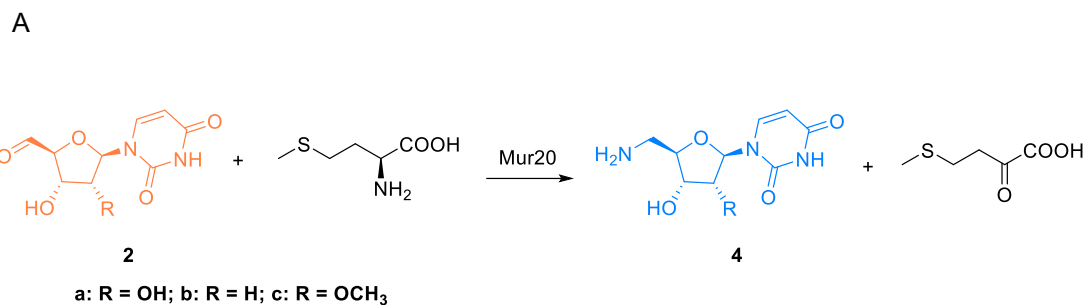
Figure 3.7 Characterization of Mur20.

(A) Reaction catalyzed by Mur20. (B) HPLC analysis using uridine aldehyde (**2a**) after I, 6 h reaction without Mur20; II, 6 h reaction with Mur20; III, 6 h reaction with LipO. (C) LC-MS analysis using 2′-deoxy uridine aldehyde (**2b**) after I, 6 h reaction without Mur20; II, 6 h reaction with Mur20. (D) LC-MS analysis using 2′-methoxy uridine aldehyde (**1c**) after I, 6 h reaction with Mur16; II, 6 h reaction with Mur16 and Mur20.

3.3.4 Functional Assignment of Mur26 as a Low Specificity Uridine Nucleoside Phosphorylase

Bioinformatic analysis of Mur26 revealed a sequence similarity to LipP[47], which catalyzes the phosphorolysis of uridine or 5′-amino-5′-deoxy uridine to generate the respective ribose-1-phosphate and uracil. The *mur26* gene was cloned and expressed in *E. coli* to yield soluble protein (Figure S3.1). Activity tests revealed that, identically to LipP, Mur26-catalyzed reaction proceeded with uridine, 5′-amino-5′-deoxy-uridine **4a** and 2′,5′-dideoxy-5′-amino-uridine **4b** (Figures 3.8, S3.10). Additional activity tests revealed that Mur26 didn't utilize 2′-methoxy-5′-amino-5′-deoxy-uridine **4c**, which, combined with the kinetic experiment of Mur16 with **1c**, supported the proposal that the 2′-methylation happened as a later step during muraymycin biosynthesis.

A

4

a: R = OH; b: R = H

5

6

B

Elution Time (min)
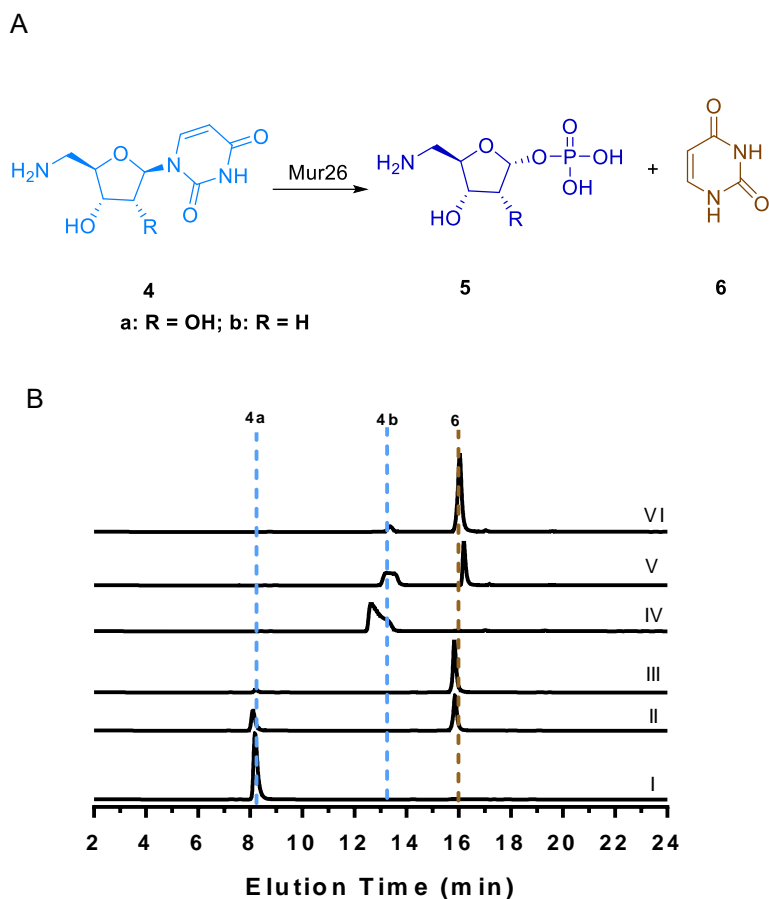
Figure 3.8 Characterization of Mur26.
(A) Reaction catalyzed by Mur26. (B) LC-MS analysis of reaction catalyzed by Mur26. I, 6 h reaction w/ 5′-deoxy-5′-amino-uridine (**4a**) w/o Mur26; II, 6 h reaction w/ **4a** w/ Mur26; III, 6 h reaction w/ **4a** w/ LipP; IV, 6 h reaction w/ 2′, 5′-dideoxy-5′-amino-uridine (**4b**) w/o Mur26; V, 6 h reaction w/ **4b** w/ Mur26; VI, 6 h reaction w/ **4b** w/ LipP.

3.3.5 Functional Assignment of Mur18 as a Primary Amine-requiring Nucleotidylyltransferase.

Bioinformatic analysis revealed that Mur18 has a sequence similarity to LipM[47, 51], which has already been demonstrated as nucleotidylyltransferase by utilizing 5′-amino-5′-deoxy-α-D-ribose-1-phosphate **5a** or 5′-amino-2′,5′-dideoxy-α-D-ribose-1-phosphate **5b** and UTP to generate the activated sugar. Different from LipM, which was only soluble when expressed in *S. lividans* TK64, Mur18 is soluble when expressed in *E. coli* with either an *N*-terminal His6-tag or C terminal His6-tag, which makes it easier for the ongoing crystal structure

study. Activity test revealed that Mur18 utilized **5b**, which was generated in situ with LipP from

4b and UTP, to generate UDP-5-amino-2, 5-dideoxyribose **7b** (Figures 3.9- S3.11).
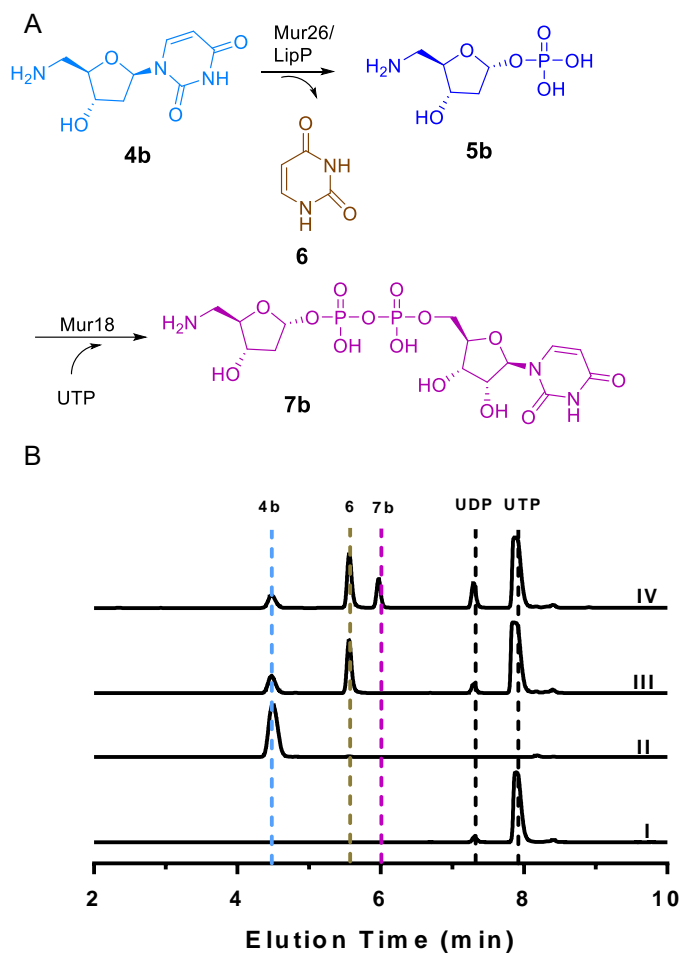
Figure 3.9 Characterization of Mur18.

(A) Reaction catalyzed by Mur26 (or LipP) and Mur18. (B) HPLC analysis of Mur18 reaction. I, UTP; II, 2′, 5′-dideoxy-5′- amino-uridine (**4b**); III, 6 h reaction with LipP; IV, 6 h reaction with LipP and Mur18.

3.3.6 Functional Assignment of Mur19 as a GlyU: 5-Amino-5-Deoxyribosyltransferase

Bioinformatic analysis revealed that Mur19 has a sequence similarity to LipN[47], which has already been characterized as a ribosyltransferase that utilizes uridine as a surrogate acceptor and the genuine sugar donor **7a** (generated in situ with LipP and LipM) as substrates. Both muraymycin and A-90289 have the GlyU moiety, which can be produced by Mur17 or LipK, and thus, we propose that GlyU is the genuine sugar acceptor for both Mur19 and LipN. Similar to LipN, soluble Mur19 was only obtained in *S. lividans* TK24 by heterologous expression. HPLC analysis of Mur19 reactions using genuine acceptor **3** and in situ generated sugar donor **7a** revealed a new peak, which co-eluted with chemically synthesized standard **8a** (Figure 3.10).
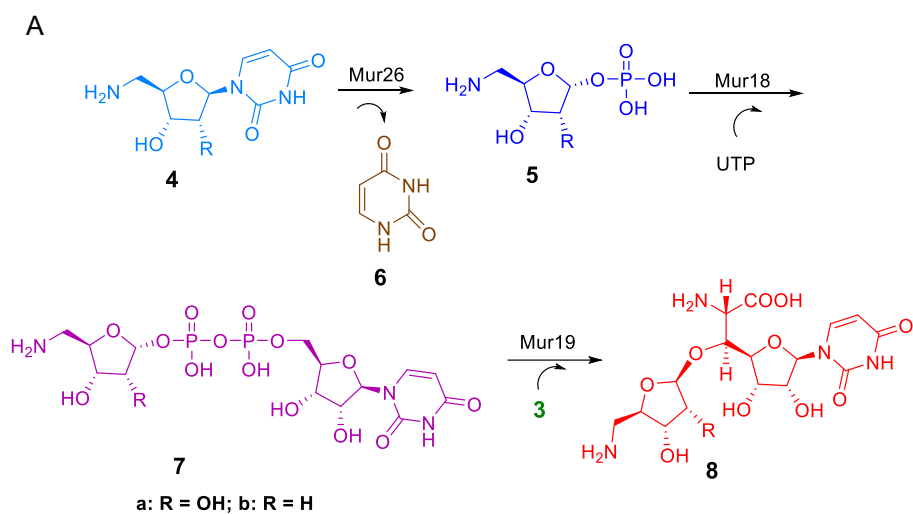
Figure 3.10 Characterization of Mur19.

(A) Reaction catalyzed by Mur26, Mur18 and Mur19. (B) HPLC analysis of Mur19 reaction. I, chemically synthesized **8a**; II, 6 h reaction with Mur26; III, 6 h reaction with Mur26 and Mur18; IV, 6 h reaction with Mur26, Mur18 and Mur19.

2′-Fluoro-2′-deoxyuridine-5′-triphosphate (2′-F-dUTP), was used to replace UTP in order to form a more, stable activated sugar **7a′** and **7b′**. Activity tests showed that 2′-F-dUTP can be utilized by Mur18 to generate activated aminoribose, which was utilized by Mur19 to generate **8a** and **8b** (Figure 3.11). The production of **8b** was confirmed by HR-ESI-MS and ^{1}H NMR after large-scale purification of AQC derived reaction (Figures S3.12-S3.14). Activity of LipN with genuine sugar acceptor GlyU was also tested for the first time. Surprisingly, different from Mur19, LipN only accepted activated 5′-amino-5′-deoxy-amino ribose to generate **8a**, while **8b** cannot be generated by LipN (Figure 3.12).
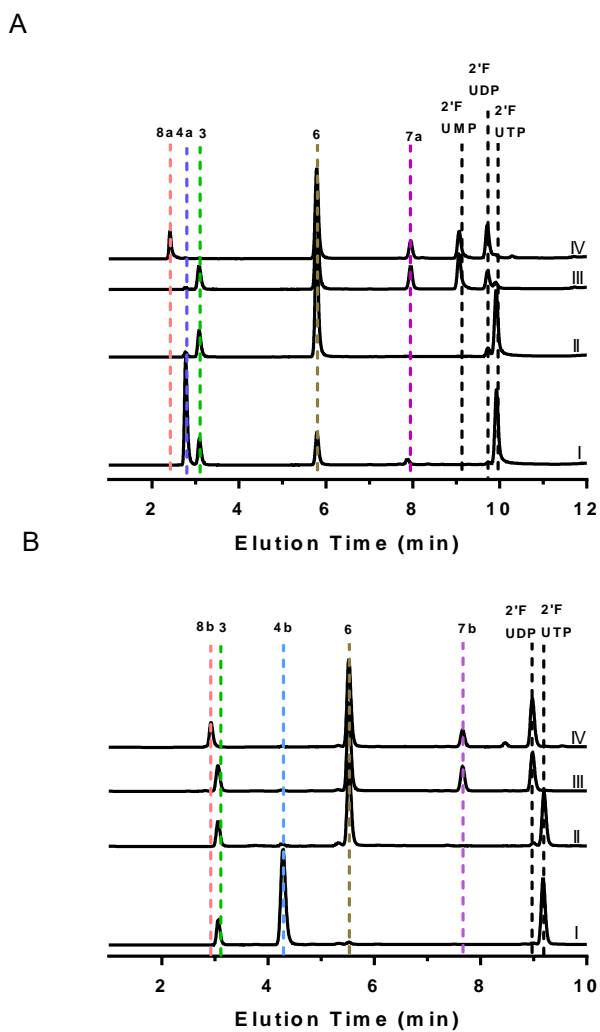
Figure 3.11 Characterization of Mur19 with 2'-fluoro-2'-deoxyuridine-5'-triphosphate.
(A) HPLC analysis of Mur19 reaction with **4a**. I, 6 h reaction without enzyme; II, 6 h reaction with LipP; III, 6 h reaction with LipP and Mur18; IV, 6 h reaction with LipP, Mur18, and Mur19.
(B) HPLC analysis of Mur19 reaction with **4b**. I, 6 h reaction without enzyme; II, 6 h reaction with LipP; III, 6 h reaction with LipP and Mur18; IV, 6 h reaction with LipP, Mur18, and Mur19.
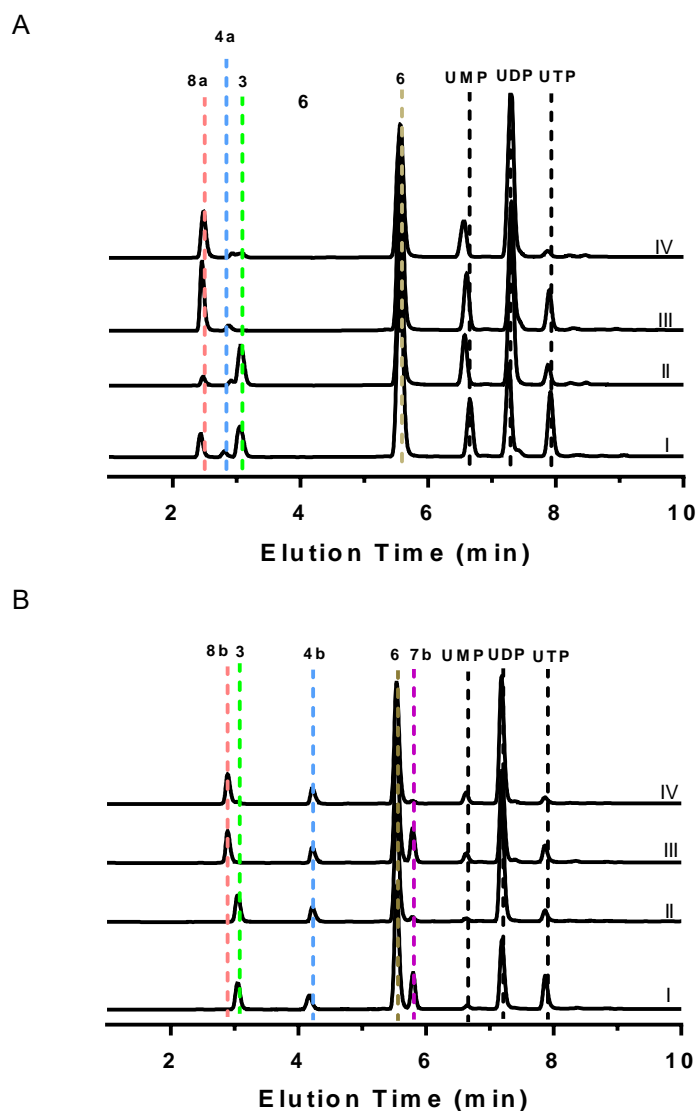
Figure 3.12 Comparison of substrate promiscuity of Mur19 and LipN with **4a** and **4b**.
(A) Comparison of substrate promiscuity of Mur19 and LipN with **4a**. I, 6 h reaction with LipP, LipM and LipN; II, 6 h reaction with LipP, Mur18 and LipN; III, 6 h reaction with LipP, LipM and Mur19; IV, 6 h reaction with LipP, Mur18 and Mur19. (B) Comparison of substrate promiscuity of Mur19 and LipN with **4b**. I, 6 h reaction with LipP, LipM and LipN; II, 6 h reaction with LipP, Mur18 and LipN; III, 6 h reaction with LipP, LipM and Mur19; IV, 6 h reaction with LipP, Mur18 and Mur19.

3.3.7 One-Pot Six-enzyme Synthesis of Ribofuranosylated Uronic Acid Moiety of Muraymycin

Aminoribofuranosylated uronic acid **8a** was generated *in vitro* by six proteins Mur16, Mur17, LipO, LipP, Mur18 and Mur19 using UMP as the starting substrate (Figure 3.13). With the addition of each enzyme, a new peak corresponding to respective product was revealed in the HPLC traces except for the product of Mur18 **7a**, which was unstable and degraded into UMP via intramolecular attack of the 2-hydroxy group of the aminoribosyl unit on the proximal phosphate as our group has previously reported.[47] The degradation product UMP was further utilized by Mur16 followed by LipO and LipP, which resulted in the generation of twice the amount of uracil. HPLC analysis of the six-enzyme one pot reaction revealed a small new peak corresponding to the generation of **8a**.

2″-Deoxy-aminoribofuranosylated uronic acid **8b** was also generated using dUMP and GlyU as starting substrates by five enzymes Mur16, LipO, LipP, Mur18 and Mur19. Mur17 was omitted in this reaction with the supplementation of its product GlyU because Mur17 couldn't utilize 2′-deoxy-uridine aldehyde **2b**, generated by Mur16 from dUMP, as a substrate. The generation of UDP-5-amino-2,5-dideoxyribose **7b** by Mur18 was observable in HPLC traces. HPLC analysis of the five-enzyme one pot reaction revealed a small new peak corresponding to the generation of **8b** (Figure 3.14, Figures S3.11-S3.13).

Different from the one-pot enzymatic reaction I (reaction to produce **8a)**, the equilibration of the reaction shows the similar amount of **3,4a** and **8a**, one pot enzymatic reaction II (reaction to produce **8b**) uses up all the synthetic **3** to produce **8b**, and the excess of dUMP was totally converted to **2b** rather than **4b** or uracil. It seems that, by only adding the

UMP as start substrate, six enzymes added in one pot reaction I created a balance for the production of **8a** with similar amount of **3** and **4a**.
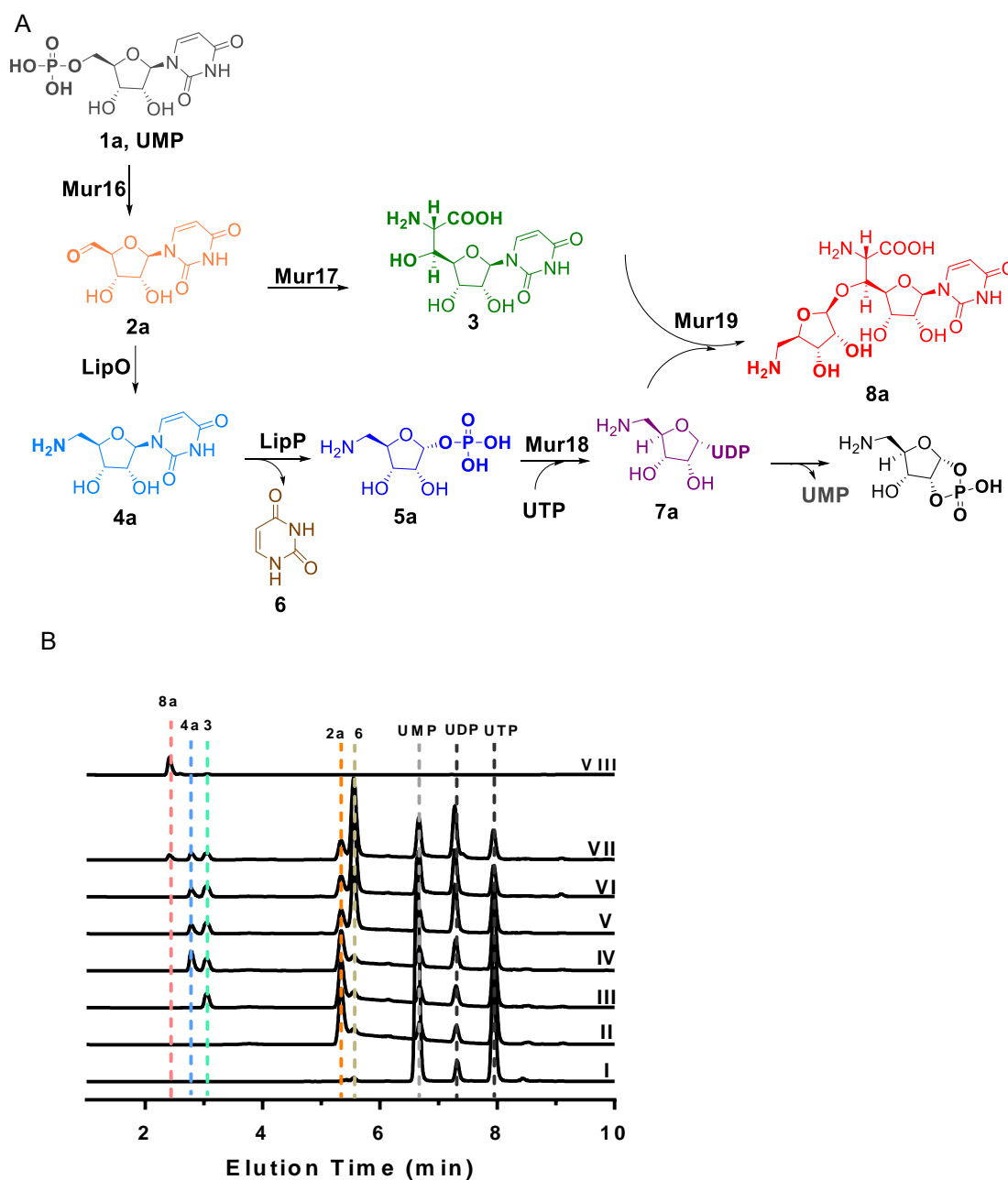
Figure 3.13 Characterization of one-pot enzymatic reaction with UMP and UTP as start substrates.
(A) One pot enzymatic reaction catalyzed by Mur16, Mur17, LipO, LipP, Mur18 and Mur19.
(B) HPLC analysis of one pot enzymatic reaction. I, no enzyme control; II, 12 h reaction with Mur16; III, 12 h reaction with Mur16 and Mur17; IV, 12 h reaction with Mur16, Mur17 and LipO; V, 12 h reaction with Mur16, Mur17, LipO and LipP; VI, 12 h reaction with Mur16, Mur17, LipO, LipP and Mur18; VII, 12 h reaction with Mur16, Mur17, LipO, LipP, Mur18 and Mur19; VIII, **8a** standard.

71
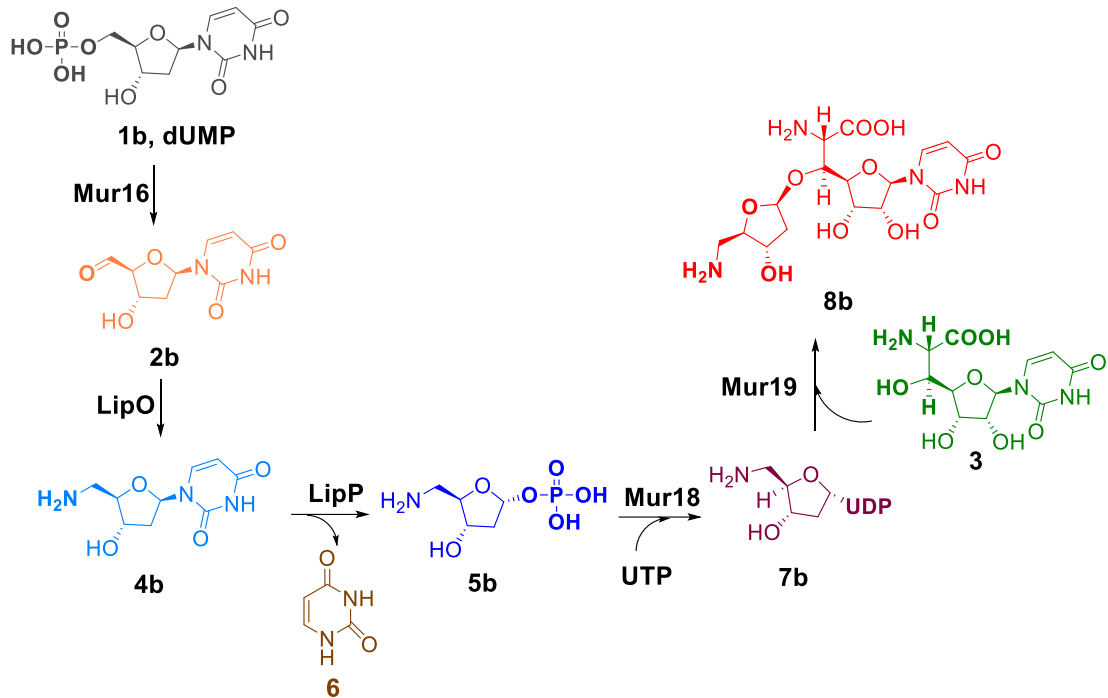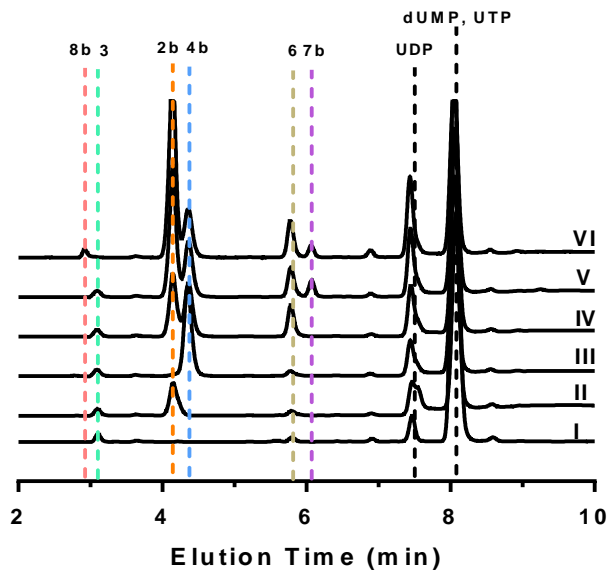
Figure 3.14 Characterization of one-pot enzymatic reaction with GlyU, 2′-deoxy-UMP, UTP as start substrates.

(A) One pot enzymatic reaction catalyzed by Mur16, Mur17, LipO, LipP, Mur18 and Mur19.
(B) HPLC analysis of one pot enzymatic reaction. I, no enzyme control; II, 12 h reaction with Mur16; III, 12 h reaction with Mur16 and LipO; IV, 12 h reaction with Mur16, LipO and LipP; V, 12 h reaction with Mur16, LipO, LipP and Mur18; VI, 12 h reaction with Mur16, LipO, LipP, Mur18 and Mur19.

3.4 Conclusion

In this chapter, six enzymes were functionally assigned and characterized: Mur16, a non-heme, Fe(II)-dependent α-ketoglutarate: UMP dioxygenase; Mur17, an L-threonine: uridine-5′-aldehyde transaldolase; Mur20, an L-methionine: 1-aminotransferase; Mur26, a low specificity pyrimidine nucleoside phosphorylase; Mur18, a primary amine-requiring nucleotidylyltransferase; Mur19, a 5-amino-5-deoxyribosyltransferase. Substrates promiscuity for each enzyme was studied. Substrate promiscuity was preliminarily discussed. For the first time a one pot enzyme reaction was utilized to produce two distinct disaccharide moieties, both of which are potential biosynthetic intermediates that lead to the mature muraymycins (Figure 3.15).
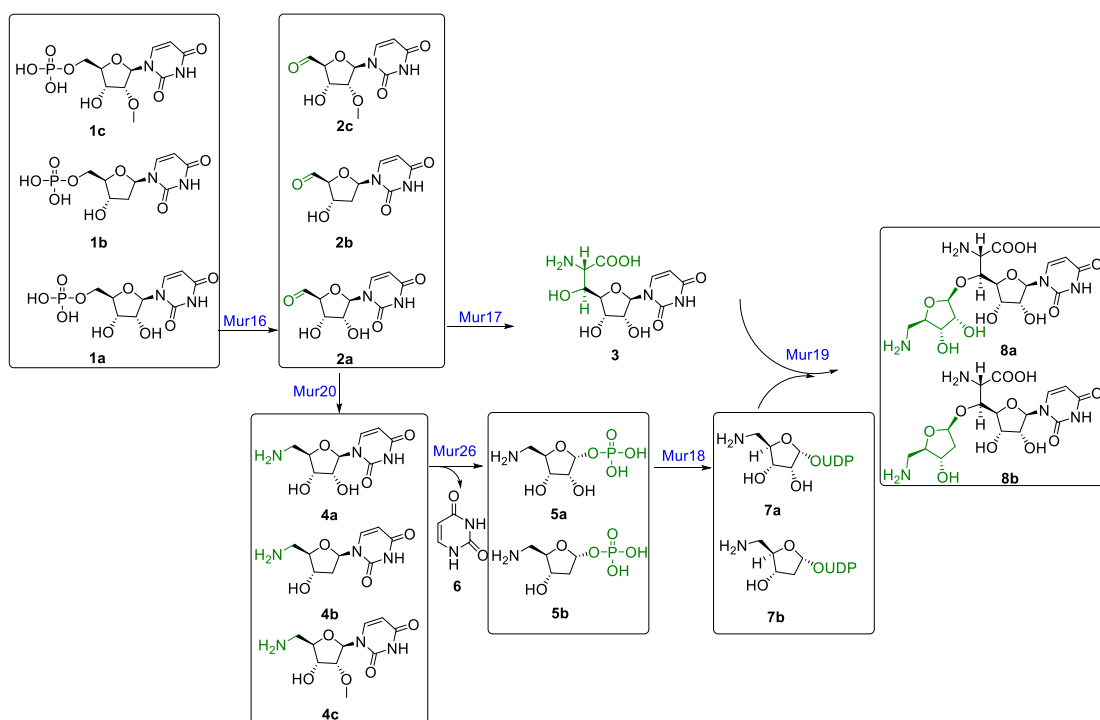
Figure 3.15 Biosynthetic pathway and substrate promiscuity towards ribofuranosylated glycyl-uridne moiety of muraymycins.

3.5 Supporting Information

Table S3.1 Primers used in this study.

Primer	Sequence	Note
*mur16*_pET30F	5′- GGTATTGAGGGTCGCGTGGTCCGCGCTGAC -3′	Used for *mur16* expression
*mur16*_pET30R	5′- AGAGGAGAGTTAGAGCC TCAGGGGCTCTCCAG-3′	
*mur17*_NdeI	5′- GATAGGCATATGACCTCTTCGGACGACTGC-3′	Used for *mur17* expression from *S. lividans* TK24
*mur17*_BamHI	5′- CGAGTTGGATCCTCAGCCATGGAAGAGTCCGG-3′	
*mur18*_pET30F	5′-GGTATTGAGGGTCGCATGGCTGACTTCGCCGAACC-3′	Used for *mur18* expression
*mur18*_pET30R	5′- AGAGGAGAGTTAGAGCCTCATGACCAGCTCCCCGGA-3′	
*mur19*_NdeI	5′-AAAAAACATATGAGCCGCCCGACAAGAGT-3′	Used for *mur19* expression from S. *lividans* TK24
*mur19*_BamHI	5′- AAAAAAGGATCCTCACAGGGTCGTAGTTCTCAG-3′	
*mur20*_pET30F	5′- GGTATTGAGGGTCGC GTGAGCCCCCAGAGCG-3′	Used for *mur20* expression
*mur20*_pET30R	5′- AGAGGAGAGTTAGAGCC TCAGGCCGTCGCCTCG-3′	
*mur26*_pET30F	5′- GGTATTGAGGGTCGC ATGAGCACCTCCCTCGCG-3′	Used for *mur26* expression
*mur26*_pET30R	5′- AGAGGAGAGTTAGAGCCTCACAGGACGGAGTGCACC-3′	

Table S3.2 Gradient used for HPLC or LC-MS analysis of reactions with an analytical Apollo C18 column (250 mm x 4.6 mm, 5 μm).

Solvent A = ddH$_2$O with 0.1% formic acid; Solvent B = acetonitrile with 0.1% formic acid; A260

Time (min)	% Solvent B	Flow Rate (mL/min)
0	1	0.5
16	20	0.5
28	100	0.5
37	100	0.5
38	1	0.5
41	1	0.5

Table S3.3 Gradient used for LC-MS analysis of AQC modified reactions with an analytical Acclaim[TM] 120 C18 column (100 mm x 4.6 mm, 5 μm).

Solvent A = ddH$_2$O with 0.1% formic acid; Solvent B = acetonitrile with 0.1% formic acid; A260

Time (min)	% Solvent B	Flow Rate (mL/min)
0	1	0.4
40	20	0.4
41	100	0.4
44	100	0.4
45	1	0.4
47	1	0.4

Table S3.4 Gradient used for LC-MS analysis of MBTH modified reaction with an analytical Acclaim[TM] 120 C18 column (100 mm x 4.6 mm, 5 μm).

Solvent A = ddH$_2$O with 0.1% formic acid; Solvent B = acetonitrile with 0.1% formic acid; A350.

Time (min)	% Solvent B	Flow Rate (mL/min)
0	10	0.4
10	40	0.4
20	100	0.4
27	100	0.4
28	10	0.4
30	10	0.4

Table S3.5 Gradient used for HPLC analysis of reactions with an analytical Apollo C18 column (250 mm x 4.6 mm, 5 μm).

Solvent A = 40 mM acetic acid-triethylamine pH 6.5; Solvent B = 40 mM acetic acid-triethylamine, 20% methanol, pH 6.5; A260

Time (min)	% Solvent B	Flow Rate (mL/min)
0	0	1.0
8	100	1.0
18	60	1.0
19	60	1.0

Table S3.6 Gradient used for HPLC analysis of reactions with an analytical ZIC®-HILIC column (250 mm x 4.6 mm, 5 μm).

Solvent A = ddH2O with 0.1% formic acid; Solvent B = acetonitrile with 0.1% formic acid; A260

Time (min)	% Solvent B	Flow Rate (mL/min)
0	80	0.4
12	50	0.4
26	50	0.4
27	80	0.4
35	80	0.4

Table S3.7 Gradient used for semipreparative HPLC analysis of reactions with an analytical Apollo C18 column (250 mm x 10 mm, 5 μm).

Solvent A= ddH$_2$O with 0.025% trifluoroacetic acid; Solvent B= acetonitrile with 0.025% trifluoroacetic acid; A260

Time (min)	% Solvent B	Flow Rate (mL/min)
0	3	3.5
8	10	3.5
9	100	3.5
13	100	3.5
14	3	3.5
16	3	3.5

Table S3.8 Gradient used for semipreparative HPLC analysis of reactions with an analytical Apollo C18 column (250 mm x 10 mm, 5 μm).

Solvent A= ddH2O with 0.025% trifluoroacetic acid; Solvent B= acetonitrile with 0.025% trifluoroacetic acid; A260

Time (min)	% Solvent B	Flow Rate (mL/min)
0	12	4
15	12	4
16	100	4
19	100	4
20	12	4
24	12	4
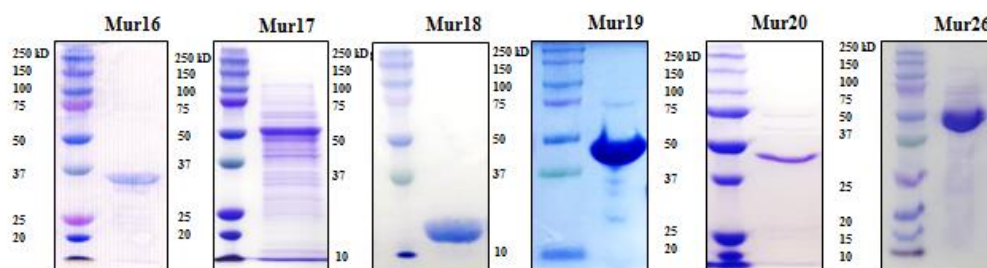
Figure S3.1 SDS-PAGE analysis of protein Mur16, Mur17, Mur18, Mur19, Mur20 and Mur26. Mur 16 (expected MW of 33 kD), Mur18 (expected MW of 25 kD), Mur20 (expected MW of 46 kD) and Mur26 (expected MW of 48 kD) purified from *E. coli* BL21 (DE3) and Mur17 (expected MW of 47 kD), Mur19 (expected MW of 42 kD) purified from *Streptomyces lividans* TK24. All proteins have N-terminal hexahistidine tag.
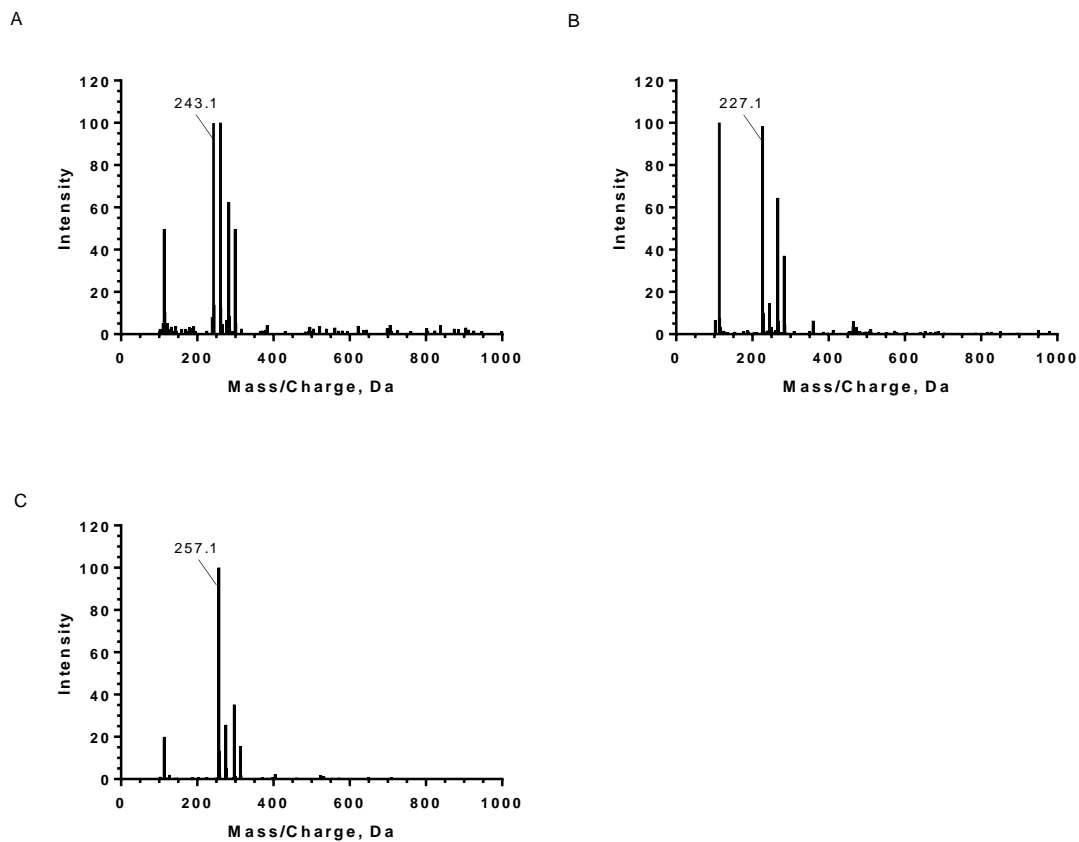
Figure S3.2 LC-MS analysis of Mur16 catalyzed reactions.

(A) Mass spectrum for the ion peak eluting at time t = 10.274 min of Mur16 reaction with UMP (uridine aldehyde expected (M+H)$^+$ ion at *m/z* = 243.06, found: 243.1). (B) Mass spectrum for the ion peak eluting at time t = 13.404 min of Mur16 reaction with dUMP (2′- deoxy-uridine aldehyde expected (M+H)$^+$ ion at *m/z* = 227.07, found: 227.1). (C) Mass spectrum for the ion peak eluting at time t = 14.116 min of Mur16 reaction with 2′-methoxy-UMP (2′-methoxy-uridine aldehyde expected (M+H)$^+$ ion at *m/z* = 257.22, found: 257.1).

A

B

C
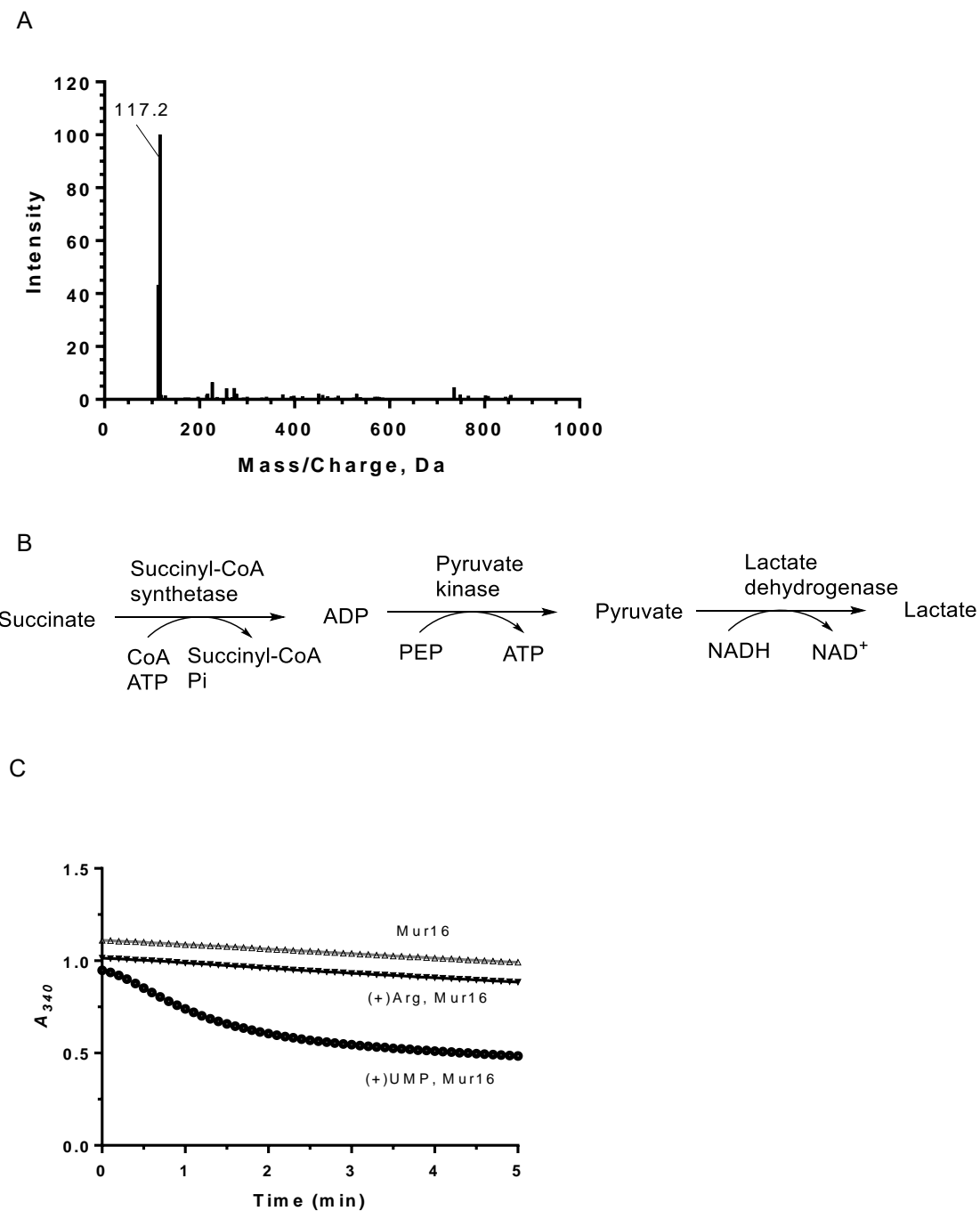
Figure S3.3 Detection of succinate production using LC-MS and an enzyme coupled reaction. (A) Mass spectrum for the peak at elution time t = 14.358 min corresponding to succinate (succinate expected (M-H)⁻ ion at m/z = 117.02, Found: 117.2). (B) Scheme of reactions catalyzed by three additional enzymes that lead to oxidation of NADH for detection by UV/Vis spectroscopy at 340 nm. (C) Mur16-catalyzed reaction with or without addition of UMP. In presence of UMP, the production of succinate is faster.
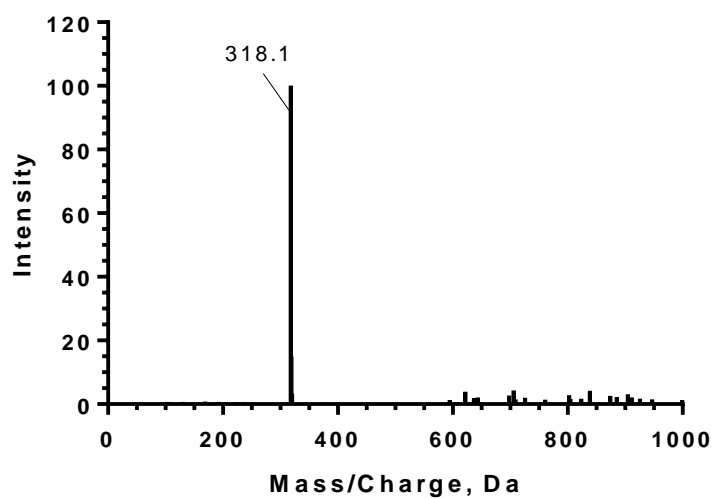
Figure S3.4 LC-MS analysis of Mur17 catalyzed reactions.

Mass spectrum for the ion peak eluting at time t = 7.111 min of Mur17 reaction with uridine aldehyde (GlyU expected (M+H)$^+$ ion at m/z = 318.09, found: 318.1).

A
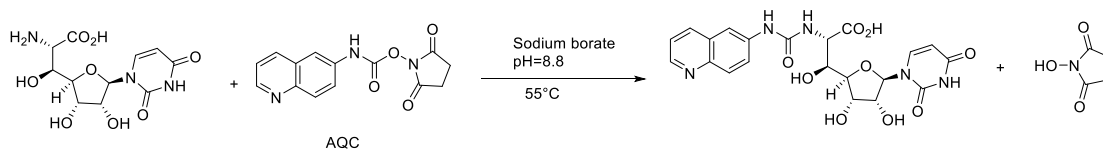
B
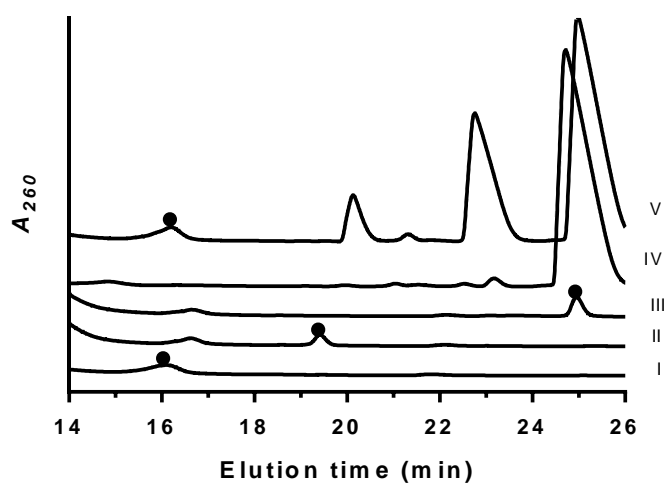
Figure S3.5 Comparative analysis of enzymatic and synthetic 3 diastereomers.
(A) Primary amine of **3** reacts with AQC. (B) LC-MS analysis of AQC modified Mur17 reaction and synthetic **3** diastereomers. I, Synthetic (5′S, 6′S)-**3** modified by AQC; II, (5′S, 6′R)-**3** modified by AQC; III, (5′R, 6′S)-**3** modified by AQC; IV, AQC modified reaction using uridine aldehyde w/o Mur17; V, AQC modified reaction using uridine aldehyde w/ Mur17.
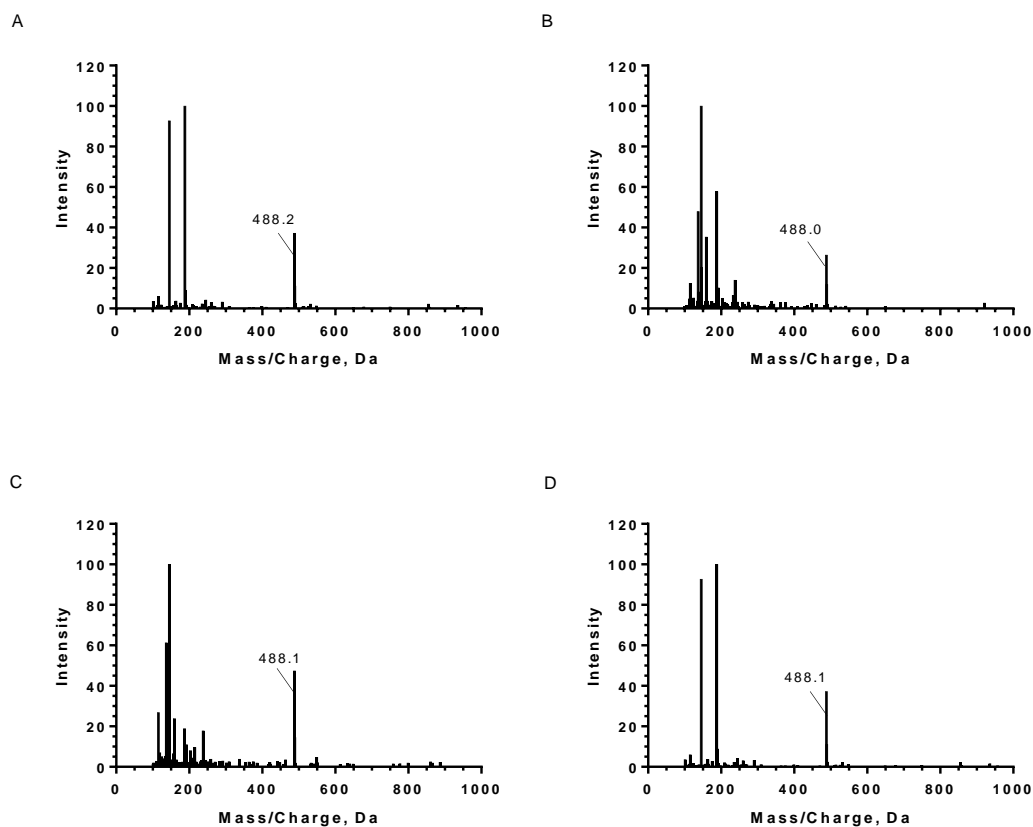
Figure S3.6 LC-MS analysis of AQC modified GlyU epimers and Mur17 catalyzed reactions. (A) Mass spectrum for the ion peak eluting at time t = 16.169 min of AQC modified Mur17 reaction (aqc modified (5′S, 6′S)-**3**, expected $(M+H)^+$ ion at m/z = 488.14, found: 488.2). (B) Mass spectrum for the ion peak eluting at time t = 16.169 min of AQC modified synthetic (5′S, 6′S)-**3** (AQC modified synthetic (5′S, 6′S)-**3**, expected $(M+H)^+$ ion at m/z = 488.14, found: 488.0). (C) Mass spectrum for the ion peak eluting at time t = 19.484 min of AQC modified synthetic (5′S, 6′R)-**3** (AQC modified synthetic (5′S, 6′R)-**3**, expected $(M+H)^+$ ion at m/z = 488.14, found: 488.1). (D) Mass spectrum for the ion peak eluting at time t = 25.081 min of AQC modified synthetic (5′R, 6′S)-**3**.
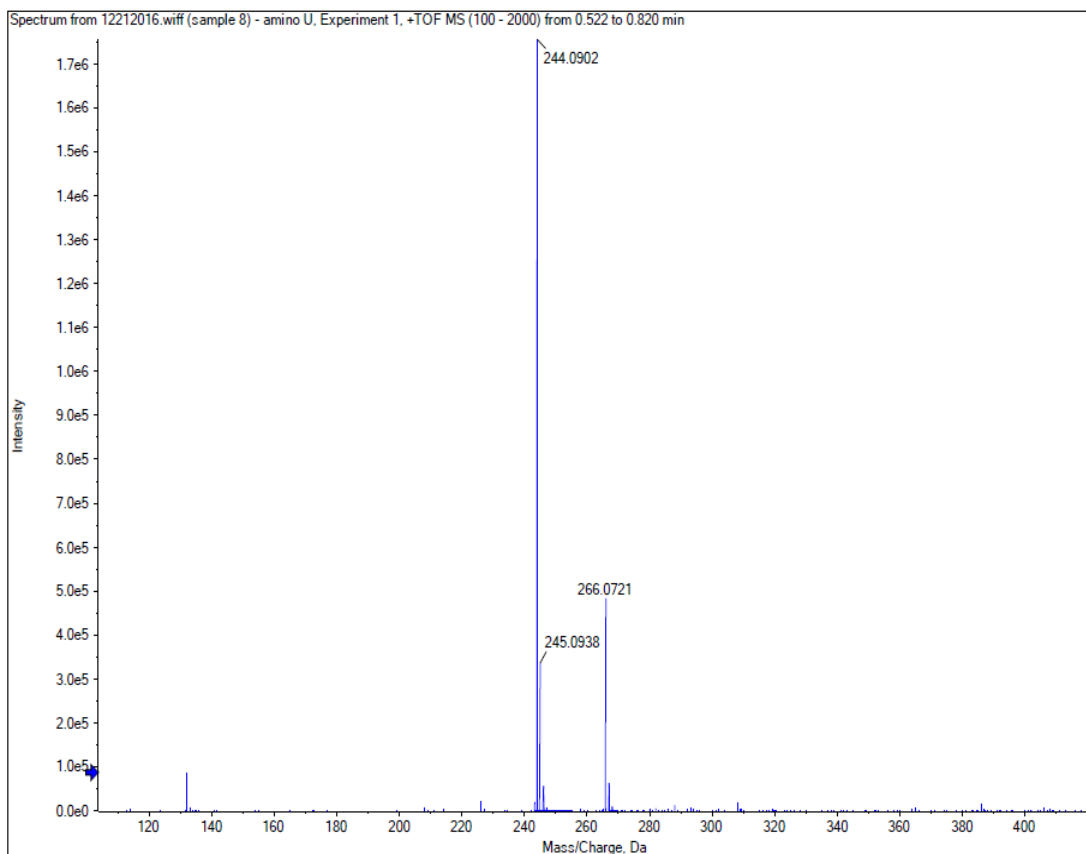
Figure S3.7 (+)-HR-ESI-MS (positive mode) of purified Mur20 product amino uridine, **4a** (expected (M+H)$^+$ ion at *m/z* = 244.0934, found: 244.0902).
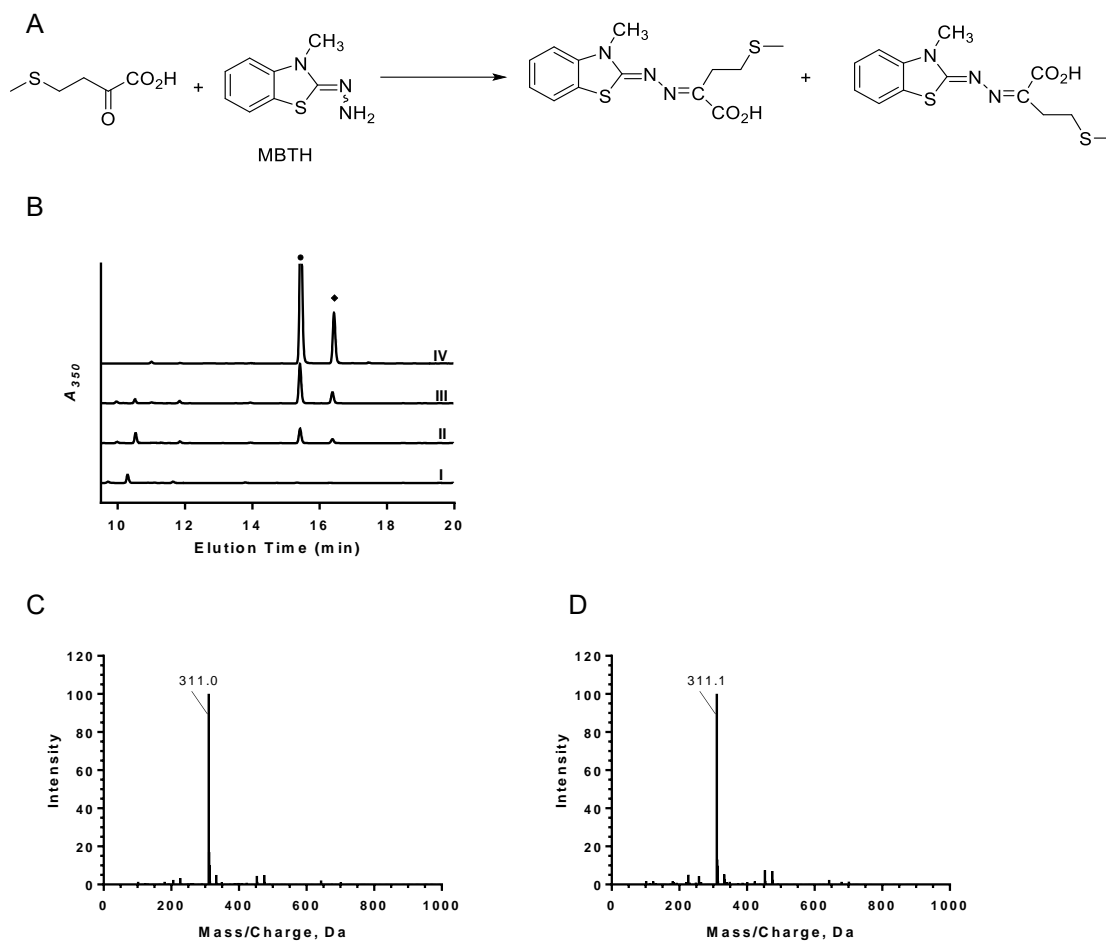
Figure S3.8 LC-MS analysis of MBTH modified Mur20 catalyzed reactions.
(A) α-keto-γ-methylthiol butyric acid reacts with MBTH. (B) LC traces of MBTH modified reaction. I, control reaction without Mur20; II, MBTH modified 6 h reaction with Mur20; III, MBTH modified 6 h reaction with LipO; IV, MBTH modified α-keto-γ-methylthiol butyric acid. (C) Mass spectrum for the ion peak eluting at time t = 15.485 min of MBTH modified Mur20 reaction (MBTH modified α-keto-γ-methylthiol butyric acid, expected $(M+H)^+$ ion at m/z = 310.06, found: 311.0). (D) Mass spectrum for the ion peak eluting at time t = 16.427 min of MBTH modified Mur20 reaction (Found: 311.1).
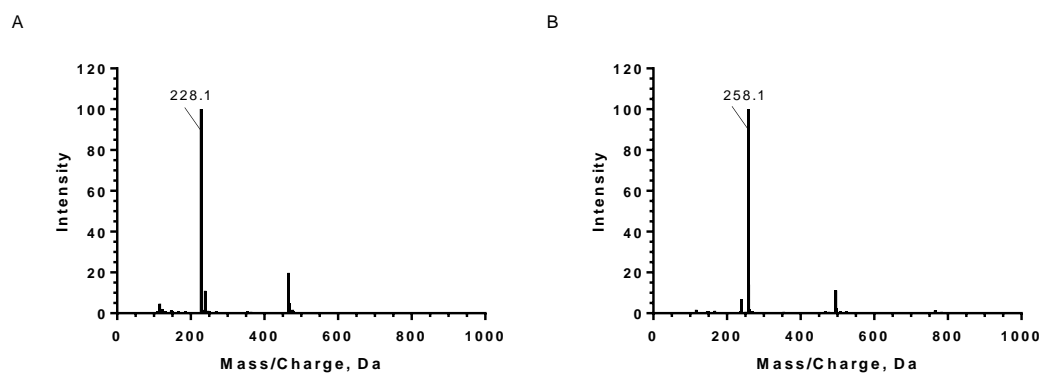
Figure S3.9 LC-MS analysis of Mur20 catalyzed reactions.

(A) Mass spectrum for the ion peak eluting at time t = 7.824 min of Mur20 reaction with 2′-deoxy uridine aldehyde, **2b** (2′, 5′-dideoxy-5′-amino uridine,**4b**, expected (M+H)$^+$ ion at $m/z =$ 228.10, found: 228.1). (B) Mass spectrum for the ion peak eluting at time t = 7.824 min of Mur20 reaction with 2′-deoxy uridine aldehyde, **2c** produced by Mur16 with **1c** (2′-methoxy-5′-deoxy-5′-amino uridine, **4c**, expected (M+H)$^+$ ion at $m/z =$ 258.11, found: 258.1).
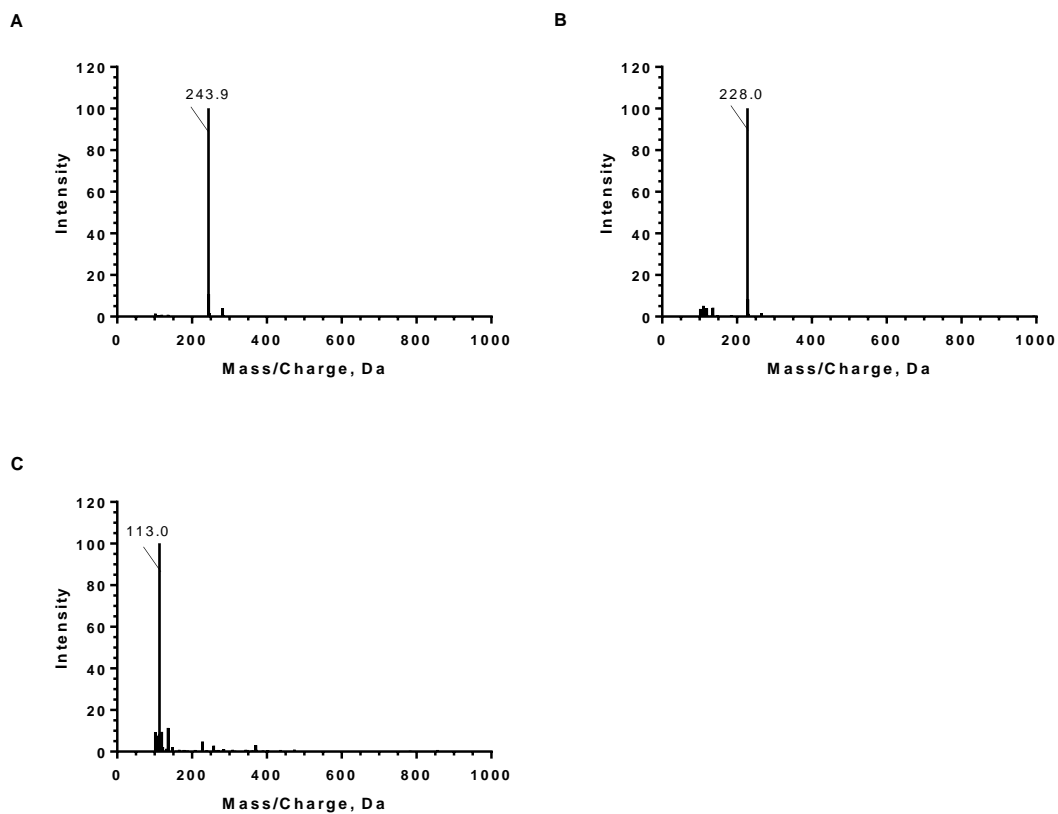
Figure S3.10 LC-MS analysis of Mur26 catalyzed reactions.
(A) Mass spectrum for the ion peak eluting at time t = 8.289 min of Mur26 reaction with **4a** (**4a**, (M+H)$^+$ ion at m/z = 244.10, found: 243.9). (B) Mass spectrum for the ion peak eluting at time t = 12.971 min of Mur26 reaction with **4b** (**4b**, (M+H)$^+$ ion at m/z = 228.1, found: 227.9). (C) Mass spectrum for the ion peak eluting at time t = 16.276 min of Mur26 reaction with **4a** (**6**, (M+H)$^+$ ion at m/z = 113.03, found: 113.0).
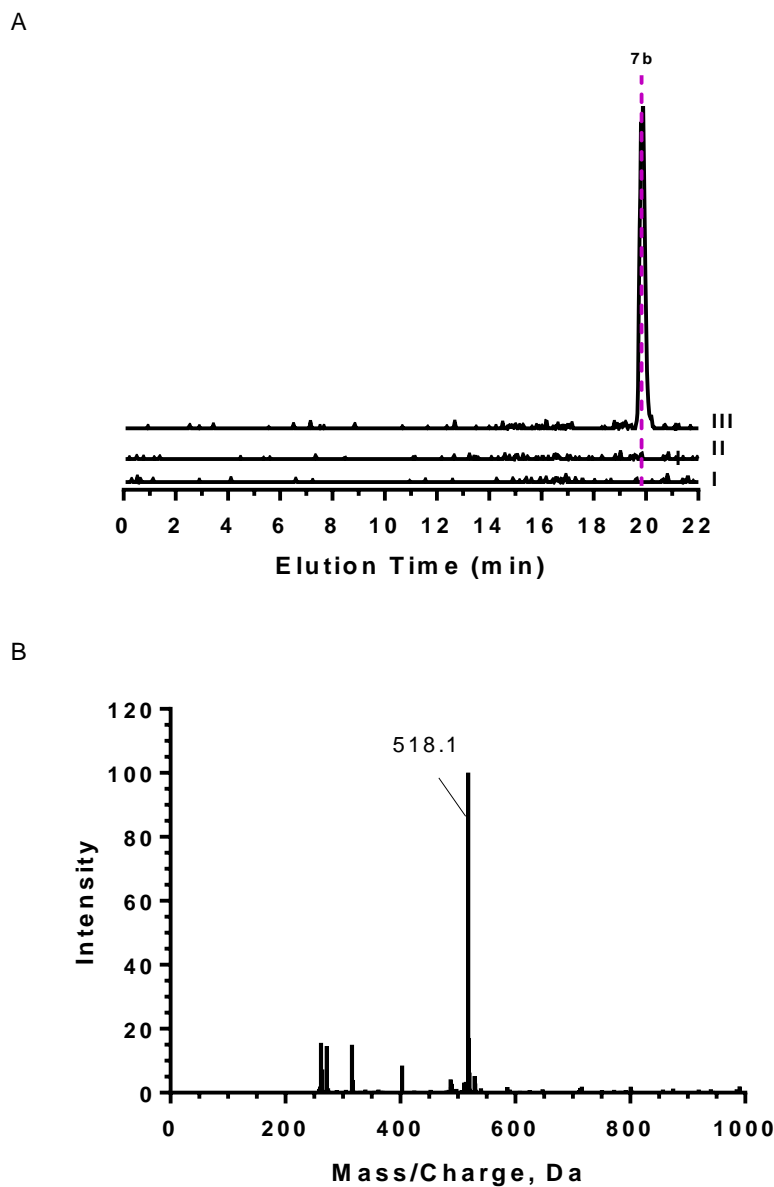
Figure S3.11 LC-MS analysis of Mur26 and Mur18 catalyzed reactions with HILIC column. (A) Extracted ion chromatograms showing the production of **7b**. I, 6 h reaction w/o enzyme; II, 6 h reaction w/ Mur26; III, 6 h reaction w/ Mur26 and Mur18. (B) Mass spectrum for the ion peak eluting at time t = 19.867 min of Mur26 and Mur18 reaction with **4a** (**7b**, (M-H)⁻ ion at *m/z* = 518.06, found: 518.1).
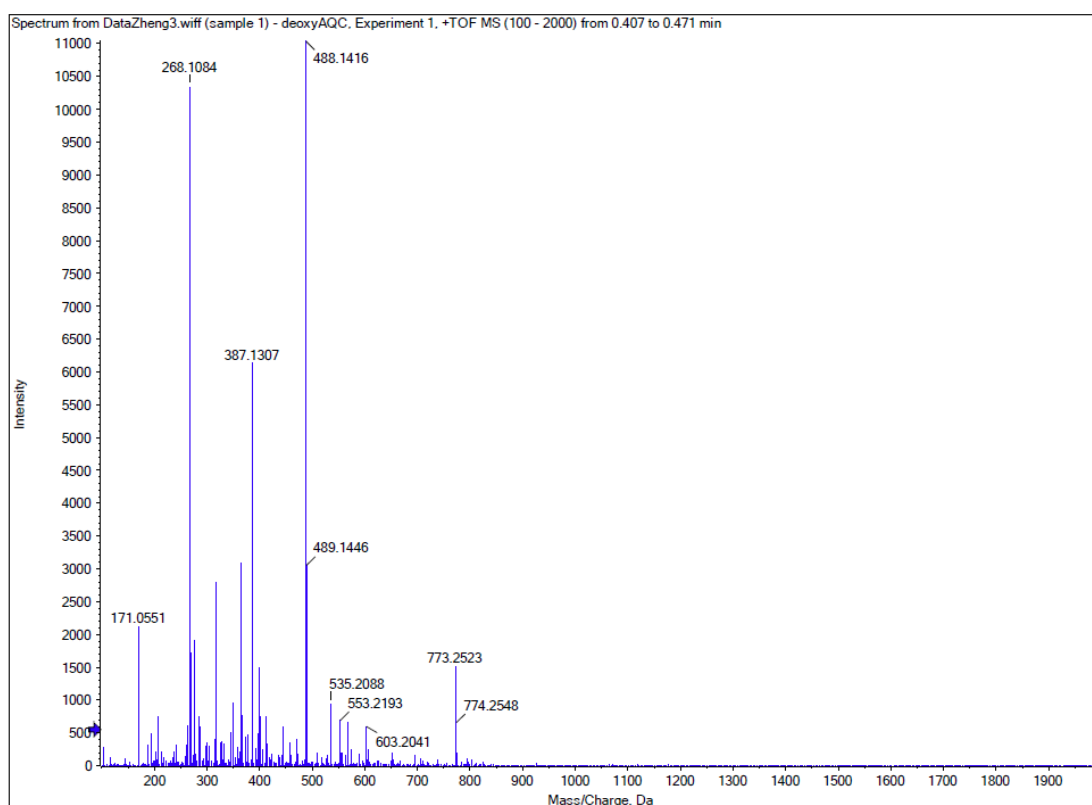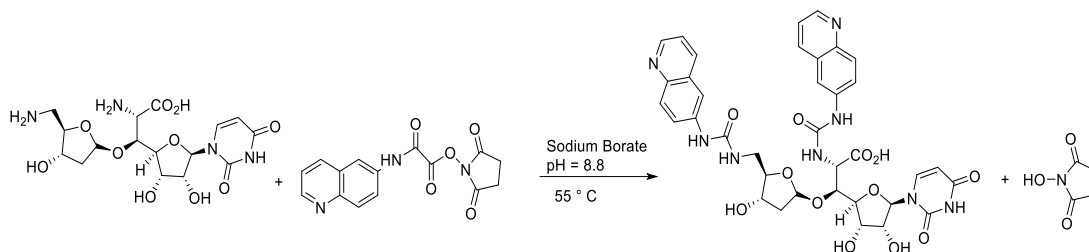
Figure S3.12 (+)-HR-ESI-MS (positive mode) of purified AQC modified **8b** (expected (M+H)$^+$ ion at *m/z* = 773.2524, found: 773.2523).
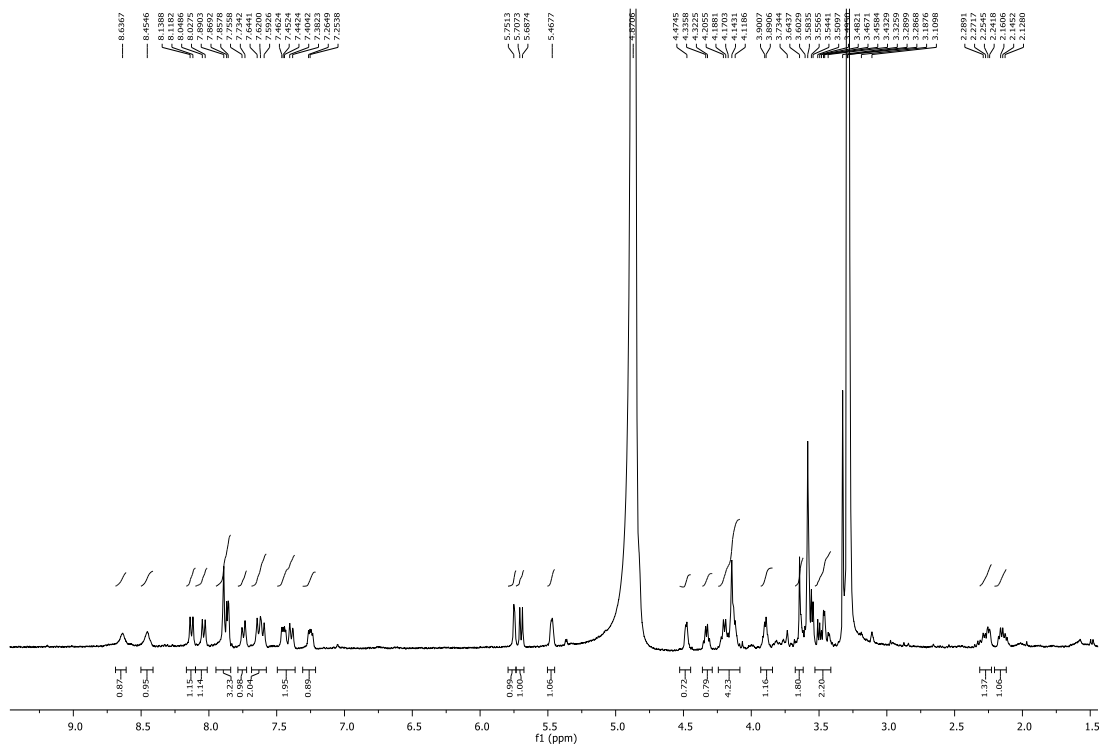
Figure S3.13 ^{1}H NMR spectrum (D$_2$O, 400 MHz) of AQC modified **8b**.
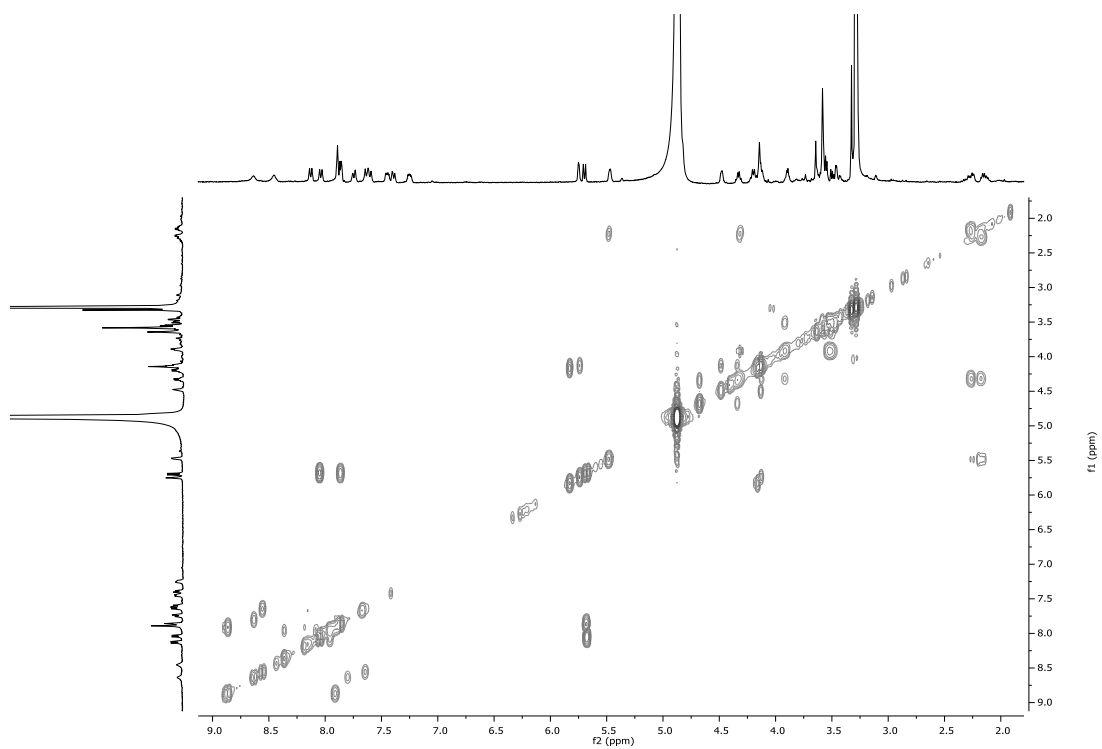
Figure S3.14 ^{1}H-^{1}H COSY spectrum (D$_2$O, 400 MHz) of AQC modified **8b**.

89

Chapter 4 : Self-Resistance During Muraymcyin Biosynthesis: A Complementary

Nucleotidyltransferase and Phosphotransferase with Identical Modification Sites and

Distinct Temporal Order

4.1 Introduction

Muraymycins, produced as a mixture of nearly 20 congeners by *Streptomyces* sp. NRRL 30471 (also known as *Streptomyces* sp. LL-AA896), are peptidyl nucleoside antibiotics that were discovered using a screen to identify inhibitors of the lipid cycle of peptidoglycan cell wall biosynthesis.[1-2] Detailed investigations into their mechanism of action has subsequently revealed muraymycins to be potent and selective inhibitors of translocase 1 (MraY), which catalyzes the initiating step of the lipid cycle.[7, 40] As a consequence of MraY inhibition, many muraymycin congeners are endowed with antibacterial activity. Notably, muraymycin A1, one of the more active of the congeners, displays a relatively broad antibacterial spectrum with modest activity against Gram-positive bacteria including strains of *Staphylococcus aureus* and *Mycobacterium tuberculosis* and Gram-negative bacteria including strains of *Escherichia coli* and *Pseudomonas aeruginosa*.[7-8, 25]

Structurally, muraymycins belong to a larger family of peptidyl nucleoside MraY inhibitors that share a common core consisting of a 5′-C-glycyluridine (GlyU) that is appended with a 5″-amino-5″-deoxyribose (ADR) moiety via a standard O-glycosidic bond (ADR-GlyU disaccharide, Figure 4.1). FR-900493 is structurally the simplest of this family known to be endowed with antibacterial activity, and consists of the ADR-GlyU disaccharide core that is 6′-N-alkylated with an aminopropyl group.[57] A-90289s, caprazamycins, and liposidomycins

(herein collectively termed A-90289-type),[58-60] sphaerimicins,[61] and muraymycins also contain

an aminopropyl group that is further modified leading to structural distinctions among these

three (Figure 4.1). Notably, muraymycins are the sole member of this family to have a linear

peptide attached to the aminopropyl linker, and variations within this peptide lead to the

different series of muraymycin congeners that were initially reported.[1] The D series of

muraymycins contain L-Leu as part of the peptide, while the C series contain a β-hydroxylated

L-Leu that can be acylated with an aliphatic, branched chain fatty acid (B series) or an acyl

group containing a terminal-guanidium (A series). In addition to the standard 2″-OH version of

the ADR moiety that is exemplified in muraymycin D2, congeners have also been isolated with

a 2″-methoxy ADR (for example, muraymycin D1) or a 2″-deoxy ADR (for example,

muraymycin D3). Although they tend to be the least potent, the D series muraymycins are

nonetheless strong inhibitors of MraY with IC_{50}s near 10 nM depending upon the source of

MraY.[7, 14] Hydroxylation and acylation that leads to the A-C series, however, significantly

improves the IC_{50} to the low picomolar range.[45]
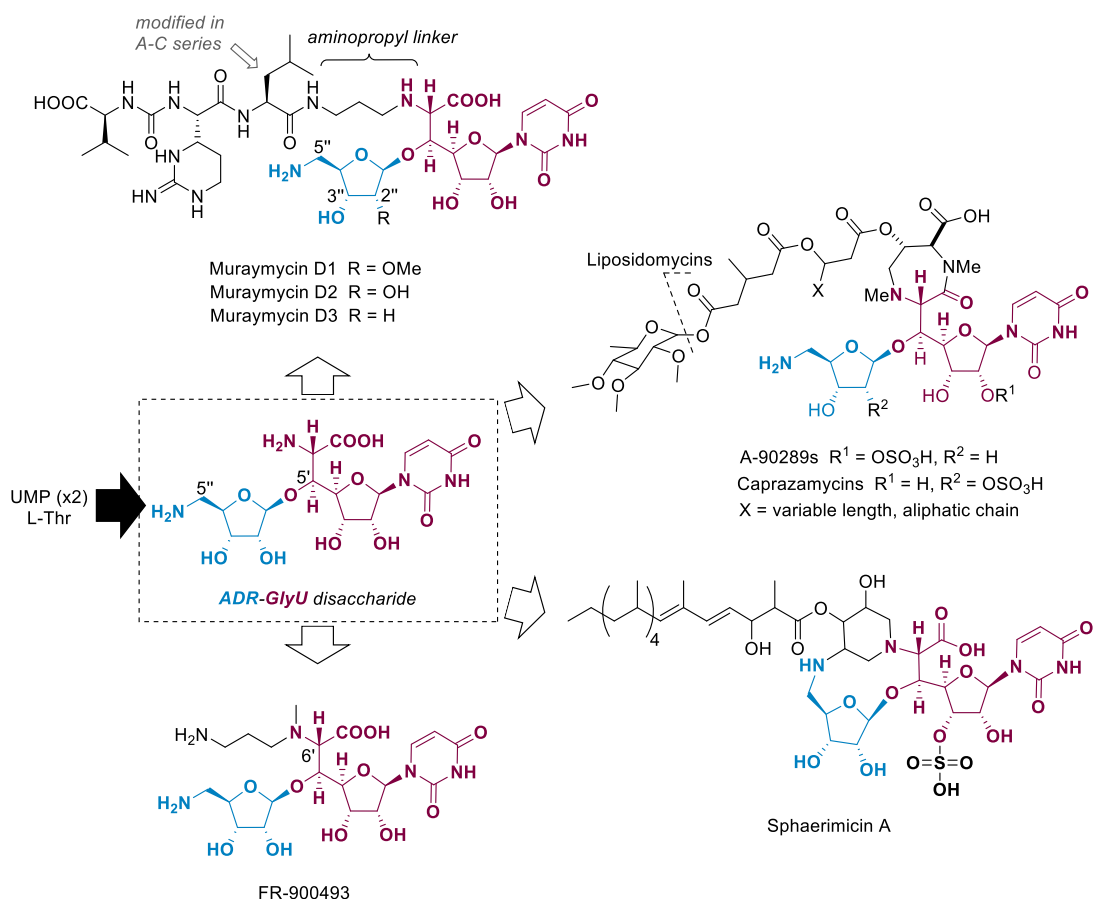
Figure 4.1 Structure of representative peptidyl nucleoside antibiotics consisting of an ADR-GlyU disaccharide core.

Recently, a new muraymycin (C6) was isolated that was acetylated at the 5″-amine of the ADR moiety, yielding a compound with modestly reduced ($\geq$ 6-fold) IC$_{50}$ against MraY from different strains (Chapter 2). In a separate report, a 3″-O-phosphorylated caprazamycin precursor called caprazol-3″-phosphate was unexpectedly isolated following inactivation of *cpz23* encoding a putative SGNH hydrolase, although in this case the inhibitory or antibacterial activity of the phosphorylated variant was not tested.[62] Covalent modification of these types (phosphorylation and acetylation), along with nucleotidylation, are often found as resistance mechanisms to antibiotics, most notably for aminoglycosides.[63-66] The same types of covalent modifications appear to be utilized by aminoglycoside producing strains, as homologous genes encoding for such resistance enzymes are often clustered with the biosynthetic genes.[67-69]

However, the reported muraymycin gene cluster lacked any candidate gene encoding for an acetyltransferase.[22] Instead, the gene cluster does encode for a pair of proteins—Mur29 and Mur28—that potentially catalyze the remaining two types of covalent modifications that are commonplaces for aminoglycoside resistance, namely nucleotidylation and phosphorylation, respectively. Of the known biosynthetic gene clusters for peptidyl nucleoside MraY inhibitors, Mur28 homologs are encoded in all of the biosynthetic gene clusters with two homologs encoded within the gene cluster for A-90289-type MraY inhibitors[46, 51, 70-71]. The only exception to this is the sphaerimicin gene cluster, which lacks a Mur28 homolog. Conversely, a Mur29 homolog is only encoded within the sphaerimicin gene cluster[61].

As part of our goal to elucidate potential resistance mechanisms toward the peptidyl nucleoside antibiotics, we now provide *in vitro* data to support the functional assignment of Mur29 and Mur28 as a Mg·ATP-dependent nucleotidyltransferase and a Mg·ATP-dependent phosphotransferase, respectively, that covalently modify the same site: the 3″-OH of the ADR component of muraymycins. Examination of the substrate specificity along with single-substrate kinetic analysis using muraymycins D1-D3 and a hypothetical biosynthetic intermediate prepared through synthesis, however, suggests a distinct temporal order for Mur29 and Mur28 catalysis during biosynthesis. The antimicrobial and MraY inhibitory activity using the adenylated or phosphorylated products compared with the respective unmodified versions are reported, enabling us to propose a distinct and complementary role for Mur29 and Mur28 in the resistance and biosynthesis of muraymycin. Finally, a preliminary attempt to functionally characterization TmrB from *Bacillus subtilis* is reported, and the unexpected results are provided herein.

4.2 Materials and Methods

4.2.1 Chemicals, reagents, and instrumentation

Nucleotides, buffers, salts, and media components were purchased from Sigma-Aldrich (St. Louis, MO) or Alfa-Aesar (Ward Hill, MA, USA). Synthetic oligonucleotides were purchased from Integrated DNA Technologies (Coralville, IA) and are listed in Table S4.2. Genomic DNA from *Streptomyces* sp. NRRL30473 was extracted using UltraClean Microbial DNA Isolation Kit (MoBio laboratories, Inc) following the manufacturer's protocol. DNA quality and concentration were confirmed using Nanodrop 2000c spectrophotometer (Thermo Scientific) and gel electrophoresis. The *tmrB* gene from *Bacillus subtilis* (accession number WP_042977443) was synthesized by Genscript to give pET28-*tmrB*.

Analytical HPLC was performed with Agilent 1200 series (Agilent Technologies, Santa Clara, CA) or Dionex Ultimate 3000 HPLC system equipped with a diode array detector and an analytical Apollo C18 column (250 x 4.6 mm, 5 μm) purchased from Grace (Deerfield, IL). Semipreparative HPLC was performed with a Waters 600 controller and pump (Milford, MA) equipped with a 996 diode array detector, 717 plus autosampler, and an Apollo C18 column (250 × 10 mm, 5 μm). LC-MS was conducted with an Agilent 6120 Quadrupole MSD mass spectrometer (Agilent Technologies, Santa Clara, CA) equipped with an Agilent 1200 Series Quaternary LC system and an Eclipse XDB-C18 column (150 × 4.6 mm, 5 μm). HR-ESI-MS spectra were acquired with an AB SCIEX Triple TOF 5600 System (AB Sciex, Framingham, MA, USA). All solvents used were minimally of ACS grade and purchased from Pharmco-AAPER (Brookfield, CT) or Fisher Scientific (Pittsburgh, PA). NMR data were recorded at 400

MHz for ^{1}H and 100 MHz for ^{13}C with a Varian Inova NMR spectrometer (Agilent, Santa Clara, CA).

4.2.2 Cloning Genes of *mur28*, *mur29* and *tmrB*

The genes encoding Mur28 and Mur29 were amplified from genomic DNA extracted from *Streptomyces* sp. NRRL 30473 by PCR using Phusion DNA polymerase. The gene encoding TmrB was amplified from pET28a-*tmrB*. The gel-purified PCR product was inserted into pET-30 Xa/LIC using ligation-independent cloning as described in the provided protocol to yield pET30-*mur28* and pET30-*mur29* or digested with *Nde*I-*Bam*HI and ligated to the identical sites of pXY200 or pDB.His.MBP to yield pXY200-*mur28*, pDB.His.MBP-*mur28*, pDB.His.MBP-*mur29* and pDB.His.MBP-*tmrB*. The identity of the cloned genes was confirmed by DNA sequencing. Plasmids pDB.His.MBP-*mur28*, pDB.His.MBP-*mur29*, pET28-*tmrB* and pDB.His.MBP-*tmrB* were expressed in *E. coli* BL21(DE3) cells and plasmid pXY200-*mur28* was expressed in *S. lividans* TK24.

Plasmids were introduced into *E. coli* BL21(DE3) cells, and the transformed strains were grown in LB supplemented with 50 μg/mL kanamycin. Following inoculation of 500 mL of LB with 50 μg/mL kanamycin, the cultures were grown at 37 °C until the cell density reached an $OD_{600} \sim 0.5$ when expression was induced with 0.1 mM IPTG. Cells were harvested after an overnight incubation at 18 °C and lysed in Buffer A (100 mM KH_2PO_4, 300 mM NaCl, 10 mM imidazole, pH 8.3) using a Qsonica sonicator (Qsonica LLC, Newtown, CT) for sonication for a total of 6 min at 40% amplitude with 30 s pulses separated by 30 s rest periods. Following centrifugation the protein was purified using affinity chromatography with HisPurTM Ni-NTA

agarose (Thermo Scientific, Rockford, IL), and proteins were eluted with increasing

concentrations of imidazole in Buffer A. Purified proteins were concentrated and buffer

exchanged into Buffer B (25 mM KH_2PO_4, 100 mM NaCl, pH 8.3) using Amicon Ultra 10000

MWCO centrifugal filter (Millipore) and stored as glycerol stocks (40%) at -20 °C. Protein

purity was assessed by 12% acrylamide SDS-PAGE; His_6-tagged proteins were utilized without

further modifications. Protein concentration was determined using UV/Vis spectroscopy, and

the extension coefficients were calculated using the ProtParam tool available from ExPASY.

Plasmids were transformed into *Streptomyces lividans* TK-24 using PEG-mediated

protoplast transformation and plated on R2YE supplemented with 50 μg/mL apramycin. After

6 days at 28 °C, positive transformants were confirmed by colony PCR using InstaGene Matrix

from Bio-Rad (Hercules, CA) and LA-Taq polymerase with GC buffer I. The recombinant

strain was utilized to inoculate 50 mL R2YE containing 50 μg/mL apramycin, grown for 3 days

at 28 °C at 250 rpm, and 2 mL transferred to fresh 100 mL containing 50 μg/mL apramycin.

Following growth for 3 days at 28 °C at 250 rpm, protein expression was induced by addition

of thiostrepton (5 μg/mL) and the culture was incubated for another 24 h before harvesting. The

cells from 400 mL of culture were collected by centrifugation. The pellet was thoroughly

resuspended in ice-cold Buffer A supplemented with 4 mg/mL of lysozyme. After incubation at

30 °C for 30 min, the cell suspension was mixed by pipetting and lysed using a Qsonica

sonicator (Qsonica LLC, Newtown, CT) for sonication for a total of 10 min at 40% amplitude

with 30 s pulses separated by 30 s rest periods. Protein purification and storage was described

above.

4.2.3 Production of muraymycin D congeners

Streptomyces sp. NRRL 30475 was cultivated in 250 mL Erlenmeyer flasks containing 50 mL TSBG [Tryptic soy broth (Difco) supplemented with 20 g/L glucose] at 30 °C on a rotary shaker (250 rpm) for 72 h. The seed culture was used to inoculate flasks (250 mL) containing 50 mL PM-1 medium. PM-1 was composed of glucose 2%, soluble starch 1%, pressed yeast 0.9%, peptone (Bacto) 0.5%, meat extract (Fluka) 0.5%, NaCl 0.5%, $CaCO_3$ 0.3% and CB-442 (NOF Co., Ltd.) 0.01% (pH 7.4, before sterilization). The fermentation was continued for 7 days at 23 °C on a rotary shaker (210 rpm).

All culture flasks were combined and centrifuged at 5000 rpm for 15 min to separate the mycelium and water phase. The mycelial-cake portion was extracted with methanol by sonication, and the organic phase was evaporated to obtain brown crude extract. Amberlite XAD-16 (4%) resin was added to the water phase and stirred for 12 h. The resin was washed with water until the effluent became colorless, and then eluted with methanol. The methanol extract was concentrated under reduced pressure to obtain a crude extract. Components of the mycelium crude extract and water phase crude extract were subjected to Sephadex LH-20 (25-100 μm, GE Healthcare) column, and methanol was used to elute compounds at a flow rate at 2 mL/min. The major fraction was further purified by using semipreparative HPLC. A series of linear gradients was developed from 0.025% trifluoroacetic acid in water (A) to 0.025% trifluoroacetic acid in acetonitrile (B) in the following manner: 0 min, 10% B; 0-25 min, 22% B; 25-26 min, 100% B; 26-31 min, 100% B; 31-32 min, 10% B; and 31-32 min, 10% B (beginning time and ending time with linear increase to % B). The flow rate was kept constant at 3.5 mL/min.

4.2.4 Enzyme reactions

Reactions consisted of 50 mM Tris (pH 7.5), 10 mM $MgCl_2$, 1 mM NTP (ATP, dATP, dTTP, GTP, CTP or UTP) or dATP, 1 mM muraymycin D1, D2, D3 or 0.5 mM ADR-GlyU disaccharide and 1 µM Mur29, Mur28, or TmrB at 30 °C. The reaction was terminated by adding twice volume of methanol followed by centrifugation (14000 rpm, 30 min) to remove the precipitated protein. Following centrifugation to remove protein, the reaction was analyzed by HPLC or LC-MS using one of four gradient programs provided in the Supporting Information.

4.2.5 Single-substrate kinetics

For Mur29 assays consisted of 50 mM Tris (pH 7.5), 10 mM $MgCl_2$, near saturating ATP (1 mM) with variable muraymycin D1 (1 µM–1000 µM), muraymycin D2 (1 µM–1000 µM) or muraymycin D3 (5 µM–500 µM). Reactions were performed at 30 °C with 200 nM Mur29 for 4 h with muraymycin D1, D2 or D3. For Mur28 assays consisted of 50 mM Tris (pH 7.5), 10 mM $MgCl_2$, near saturating ATP (1 mM) with variable muraymycin D2 (1 µM–1000 µM), muraymycin D3 (5 µM–500 µM) or disaccharide (5 µM–500µM). Reactions were performed at 30 °C with 200 nM Mur28 for 4 h with muraymycin D2 or D3 and for 15 min with disaccharide. Product formation was determined using HPLC with GP2. All reactions were analyzed under near initial velocity conditions ($\leq$ 10% product). Each data point represents a minimum of three replicate end point assays; kinetic constants were obtained by nonlinear regression analysis using GraphPad Prism (GraphPad Software, La Jolla, CA) by fitting the data to the following equations depending on the presence of substrate inhibition:

$$v = \frac{V_{max}[S]}{K_m + [S]} \quad \text{or} \quad v = \frac{V_{max}[S]}{K_m + [S] + [S]^2/K_i}$$

4.2.6 Antimicrobial Bioactivity

The protocol used for the determination of the minimum inhibitory concentration (MIC) was as described previously with minor modifications[29]. The bacterial strains *Mycobacterium smegmatis* ATCC 14468, *E. coli* DH5α/*ΔtolC*, and *E. coli* BL21(DE3) introduced with plasmids pET30-*mur28*, pET30-*mur29*, pET28a-*tmrB*, or pET30-*mur20* were used as model strains for antimicrobial susceptibility assays. All strains were grown in appropriate liquid or on agar plates using Middlebrook 7H9 with ADC enrichment for *M. smegmatis* or LB medium supplemented with 50 μg/mL kanamycin for *E. coli*. Individual strains were grown in 5 mL of medium for 16 h at 37 °C with shaking (250 rpm), and then were diluted ×1000 into 4.5 mL of medium and incubated until OD_{600} reaching 0.4. An aliquot of the suspensions was diluted ×1000. Aliquots (90 μL) of each diluted culture and transferred into the individual well of a 96-well plate supplied with 10 μL of the tested compound. Maximum final concentration of 256 μg/mL with serial dilutions was maintained to obtain the antimicrobial activities and compared to the negative control (water). The culture plates were incubated at 37 °C for 16 h with shaking (160 rpm) for *E. coli* and without shaking for *M. smegmatis*. The OD_{600} of each well measured using BioTek™ Synergy™ 2 Multi-Mode Microplate Readers. The acquired OD_{600} values were normalized to the negative control wells (100% viability). Resazurin solution (5 μL) was also added to each well, and the plates were shaken for 10 s and incubated at 37 °C for another 3 h. The minimal concentration of the tested compound that caused growth inhibition was recorded as the MIC.

4.2.7 MraY Inhibition

Inhibition against *Sa*MraY was performed as previously reported (S. Koppermann, Z. Cui, P. D. Fischer, X. Wang, J. Ludwig, J. S. Thorson, S. G. Van Lanen, and C. Ducho, submitted for publication).

4.3 Results

4.3.1 Functional insight through bioinformatic analysis

Mur29 consists of two conserved domains: an N-terminal nucleotidyltransferase domain of DNA polymerase subunit beta and C-terminal DUF4111 superfamily/PRK13746 domain. PRK13746 domain-containing proteins are provisionally annotated as aminoglycoside resistance proteins. Secondary structure-based prediction using HHPred suggested structural similarity to *Salmonella enteric* aminoglycoside O-adenylyltransferase (annotated as AadA; PDB 4CS6), which catalyzes a Mg·ATP-dependent adenylation of spectinomycin and streptomycin[72], and *Staphylococcus aureus* kanamycin nucleotidyltransferase (annotated as ANT(4′); PDB 1KNY), which adenylates several distinct aminoglycosides at the 4′- or 4″-hydroxyl substituent depending upon the identity of the aminoglycoside[73]. Pairwise alignment, however, revealed only 17% sequence identity to these proteins. Sequence alignment of Mur29 and the homologous gene product SphT encoded in the sphaerimicin gene cluster revealed a 48% sequence identity.

Bioinformatic analysis suggests Mur28 likely belongs to the conserved domain of P-loop-containing nucleoside triphosphate hydrolases that include several types of nucleoside/nucleotide kinases. Proteins with the highest sequence identity (~47%)—notably present in both Gram-positive and Gram-negative bacteria—are annotated as tunicamycin resistance proteins, TmrB. Pairwise alignment of Mur28 with *Bacillus subtilis* TmrB (*Bs*TmrB)[74-76], which consists of the same conserved domain and confers resistance to tunicamycin upon heterologous expression of the gene, had a lower sequence identity, yet was

nonetheless significant at 34% (Table S4.1). Sets of homologous genes encoding proteins with similarity to Mur28 are located in each of the A-90289-type gene clusters, represented by LipX (36% sequence identity) and LipI (23% sequence identity) for A-90289 (Table S4.1).

4.3.2 *In vitro* functional assignment and characterization of recombinant Mur29

The three known congeners of the muraymycin D series, which differ only at the 2″ substituent of the ADR-GlyU disaccharide core (Figure 4.1), were isolated from *Streptomyces* sp. NRRL 30475, a previously reported mutant strain of *Streptomyces* sp. NRRL 30471[2]. MS and NMR spectroscopic data were consistent with their identities as muraymycin D1 (Figures S4.2-S4.7), muraymycin D2 (Figures S4.8-S4.12), and muraymycin D3 (Figures S4.13 and S4.14). The ADR-GlyU disaccharide, the likely biosynthetic precursor of muraymycin D1 and D2 as well as the other members of the peptidyl nucleoside MraY inhibitors (Figure 4.1), was prepared using the synthetic methodology developed by Ichikawa with slight modifications[16]. MS and NMR spectroscopic data were comparable to the prior report and likewise consistent with the identity of the disaccharide (Figures S4.15-S4.19).

Mur29 was produced in *E. coli* BL21(DE3) as a maltose-binding protein (MBP)-fusion to obtain soluble protein for *in vitro* assays. Using HPLC analysis to monitor the reaction, incubation of recombinant Mur29 with muraymycin D1 and ATP revealed a new peak eluting with a later retention time relative to muraymycin D1 (Figure 4.2A). HR-MS analysis of the purified product revealed an $(M + H)^+$ ion at m/z = 1259.5045, consistent with the molecular formula of $C_{48}H_{75}N_{16}O_{22}P$, corresponding to a monoadenylated muraymycin D1 (expected m/z = 1259.5052) (Figure S4.20). ^1H NMR spectroscopic data (Figures S4.21 and S4.22) were

likewise consistent with adenylation of muraymycin D1 (Figure 4.2B), and comparison of the

substrate and product spectra revealed a clear downfield shift of the 3″ proton (Figure 4.2C).

Thus, the results are consistent with Mur29 catalyzing a regioselective adenylation to yield the

product, 3″-AMP-muraymycin D1 (D1-AMP).
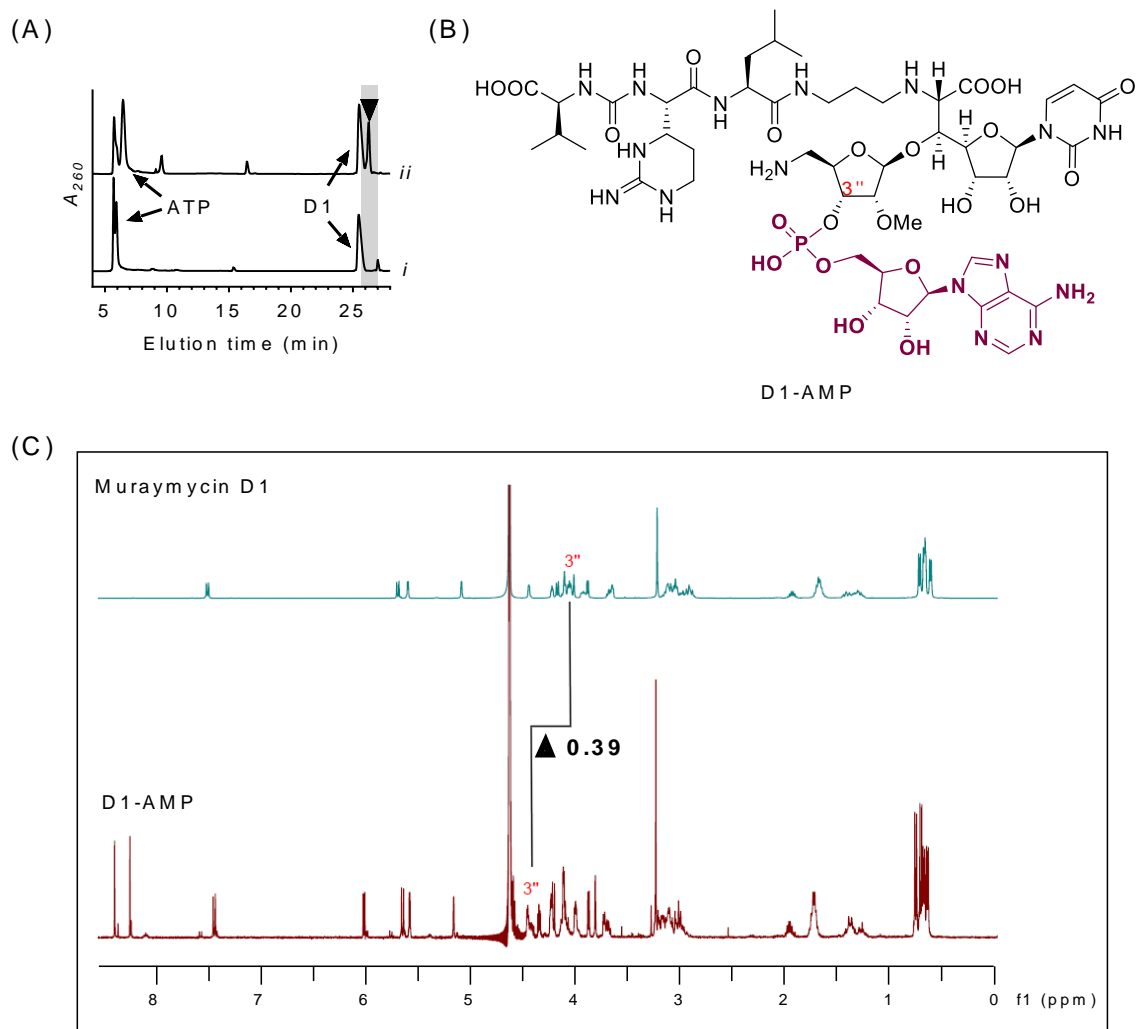
(A) HPLC analysis after (i) 12 h incubation without Mur29 and (ii) 12 h reaction. Data were collected using gradient program 1 (GP1) described in the Supplemental Material. (▼) denotes peak corresponding to D1-AMP; A_{260}, absorbance units at 260 nm. (B) Structure of 3″-monoadenylated muramycin D1. (C) Comparison of the ^{1}H-NMR spectrum for muraymycin D1 and the Mur29 product.

To provide insight into the specificity and timing of adenylation during muraymycin biosynthesis, the activity of Mur29 was tested with the remaining two D series congeners and ADR-GlyU disaccharide. In contrast to the disaccharide, which was not a substrate for Mur29, both muraymycin D2 and muraymycin D3 yielded products with an $(M + H)^+$ ion at $m/z =$ 1246.2 and 1229.2, respectively, consistent with monoadenylated products (expected $m/z =$ 1245.5 for D2-AMP and 1229.5 for D3-AMP) (Figures S4.23 and S4.24). The lack of activity with ADR-GlyU disaccharide is consistent with the Mur29 reaction occurring after the addition of the aminopropyl linker. Single-substrate kinetic analysis with variable muraymycins D1, D2, and D3 revealed non-Michaelis Menten kinetics with modest substrate-inhibition for all three substrates (Figures 4.3A-C). Comparison of the second order rate constants from the extracted kinetic parameters did not reveal a clear substrate preference (Table 4.1).

Specificity toward the nucleoside triphosphate co-substrate was also examined using muraymycin D1 as an acceptor. HPLC and LC-MS analysis revealed that the other canonical ribonucleotide triphosphates could substitute for ATP to generate the corresponding mononucleotide muraymycin D1 (Figures S4.25-S4.27). 2′-deoxy-ATP and 2′-deoxy-TTP were also used by Mur29 as nucleotidyl donors (Figures S4.28 and S4.29). The highest specific activity, however, was realized with ATP (Figure 4.3D). Finally, the addition of magnesium to the reaction was essential for activity. The addition of 20 mM EDTA abolished the reaction. Thus, the data are consistent with the functional assignment of Mur29 as a Mg·ATP:muraymycin 3″-adenylyltransferase.
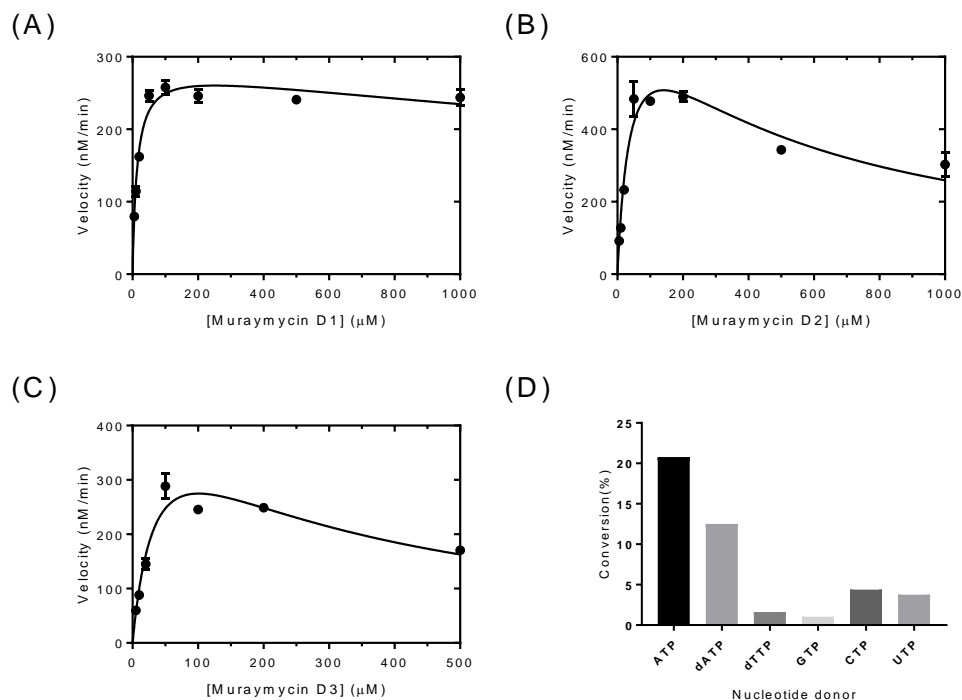
Figure 4.3 Biochemical characterization of Mur29.
Single-substrate kinetic analysis using near saturating ATP and variable (A) muraymycin D1, (B) muraymycin D2, and (C) muraymycin D3. (D) Relative activity of Mur29 with muraymycin D1 and different nucleotide donors.

4.3.3 *In vitro* functional assignment and characterization of Mur28

His$_6$-Mur28 was initially produced in *Streptomyces lividans* TK24 to obtain soluble protein for *in vitro* assays. In contrast to Mur29, incubation of recombinant Mur28 with muraymycin D1 and ATP did not reveal any new peaks. However, HPLC analysis of an overnight reaction of Mur28 with ATP and muraymycin D2, which is the likely direct biosynthetic precursor of muraymycin D1, revealed the appearance of a new peak eluting after muraymycin D2 (Figure 4.4A). The new peak was collected by semipreparative HPLC, and HR-MS analysis of the purified product revealed an $(M + H)^+$ ion at $m/z = 996.4050$, consistent with the molecular formula of $C_{37}H_{62}N_{11}O_{19}P$, corresponding to a monophosphorylated muraymycin D2 (expected $m/z = 996.4034$) (Figure S4.30). ^{1}H NMR spectroscopic data

(Figures S4.31 and S4.32) were likewise consistent with phosphorylation of muraymycin D2 (Figure 4.4B), and similarly to the Mur29-catalyzed adenylation of muraymycin D1, comparison of the substrate and product spectra revealed a clear downfield shift of the 3″ proton (Figure 4.4C). To provide further evidence for a classical kinase activity, the Mur28-catalyzed reaction was performed with [γ-P^{18}O$_4$]ATP. LC-MS analysis of the monophosphorylated product revealed a shift of + 6.0 amu, consistent with the incorporation of the γ-phosphate of ATP into muraymycin D2 (Figure S4.33). Finally, Mur28 was produced as a MBP-fusion protein from *E. coli* BL21(DE3), and comparable results were obtained. Thus, the data are consistent with Mur28 catalyzing a regioselective phosphorylation to yield the product, 3″-phospho-muraymycin D2 (D2-PHOS).
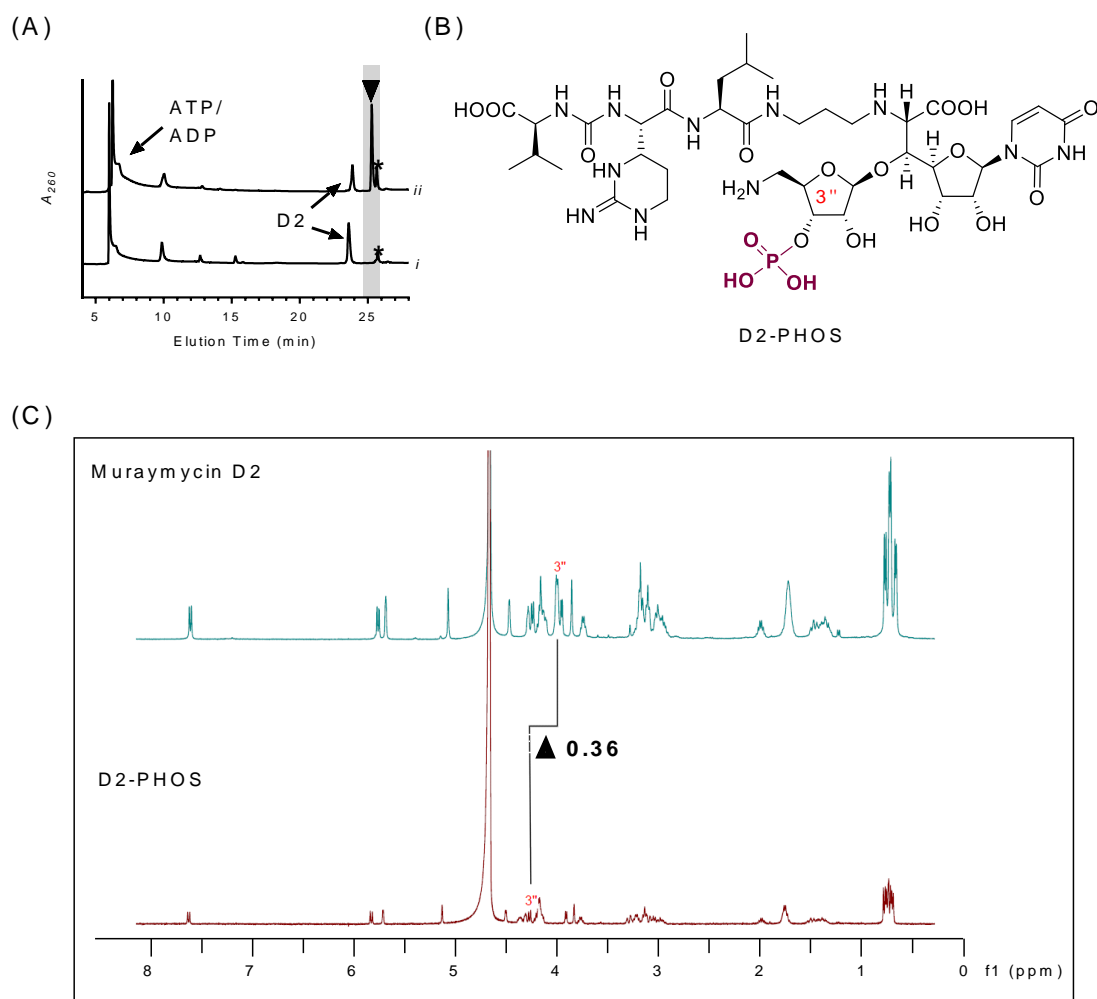
Figure 4.4 Functional assignment of Mur28.
(A) HPLC analysis after (i) 12 h incubation without Mur28 and (ii) 12 h reaction. Data were collected using GP1. (▼) denotes peak corresponding to D2-PHOS; (*) denotes unidentified peak; A_{260}, absorbance units at 260 nm. (B) Structure of 3″-phospho-muramycin D2. (C) Comparison of the ^{1}H-NMR spectrum for muraymycin D2 and the Mur28 product.

The specificity and timing of phosphorylation during muraymycin biosynthesis was subsequently investigated. LC-MS analysis of Mur28 reactions with hypothetical substrates muraymycin D3 or the ADR-GlyU disaccharide yielded new peaks with $(M + H)^+$ ions at m/z = 980.1 and 527.0, respectively, consistent with the formation of a monophosphorylated product (expected m/z = 980.4 for D3-PHOS and 527.1 for ADR-GlyU-PHOS) (Figures S4.34 and S4.35). Single-substrate kinetic analysis with variable muraymycin D2 and D3 revealed non-Michaelis-Menten kinetics with modest substrate-inhibition, while analysis with the ADR-GlyU disaccharide revealed typical Michaelis-Menten kinetics (Figures 4.5A-C). Second order rate constants from the extracted kinetic parameters revealed >60-fold higher catalytic efficiency with ADR-GlyU relative to muraymycin D2, consistent with phosphorylation occurring prior to the attachment of the aminopropyl-linked peptide.

LC-MS analysis of reactions using muraymycin D2 as the acceptor revealed Mur28 uses alternative phosphate donors, results that were similar to Mur29 (Figure S4.36). The highest activity was achieved with ATP, although good conversion was realized with dATP, dTTP, and the remaining ribonucleoside triphosphates (Figure 4.5D). Unexpectedly, ADP was also utilized as a co-substrate, although D2-PHOS was only detected in trace amounts suggesting that this activity is insignificant *in vivo*. Finally, similar to Mur29, the inclusion of magnesium was essential for activity. In total the data are consistent with the functional assignment of Mur28 as a Mg·ATP:ADR-GlyU 3″-phosphotransferase.
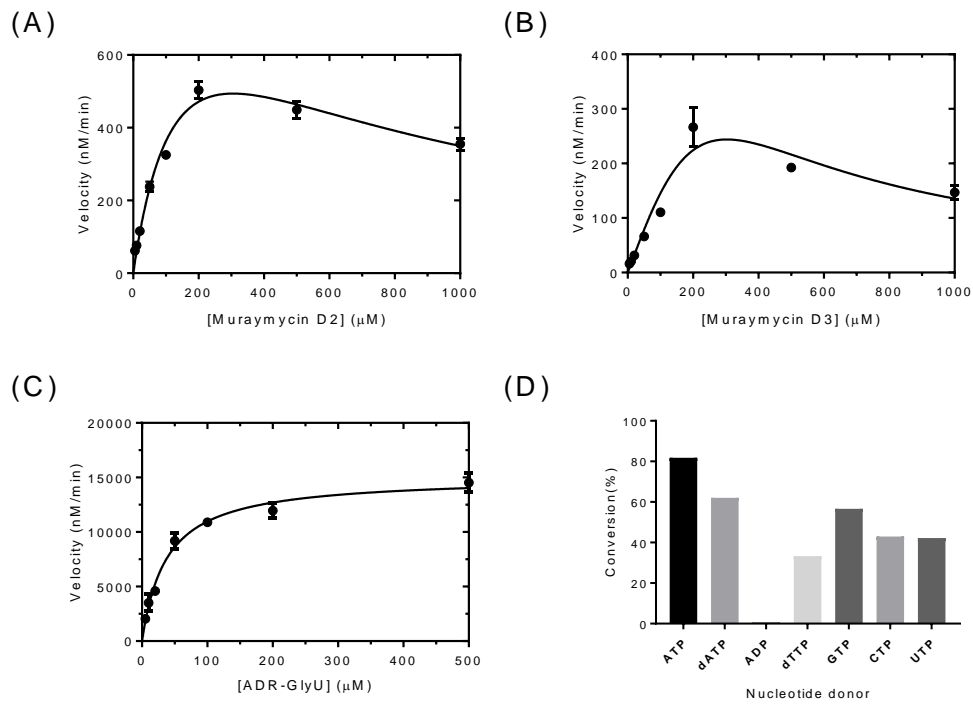
Figure 4.5 Biochemical characterization of Mur28.
Single-substrate kinetic analysis using near saturating ATP and variable (A) muraymycin D2,
(B) muraymycin D3, and (C) ADR-GlyU. (D) Relative activity of Mur28 with muraymycin
D2 and different nucleotide donors.

Table 4.1 Kinetic parameters for Mur29 and Mur28

Enzyme	Substrate	K_M (μM)	K_i (μM)	k_{cat} (min^{-1})	k_{cat}/K_M ($M^{-1} s^{-1}$)	Relative (%)
Mur29	Muraymycin D1	14 ± 2	$(4.6 \pm 1.4) \times 10^3$	1.4 ± 0.1	1.7×10^3	100
	Muraymycin D2	41 ± 8	$(4.9 \pm 1.1) \times 10^2$	4.0 ± 0.4	1.6×10^3	94
	Muraymycin D3	39 ± 10	$(2.6 \pm 0.8) \times 10^2$	2.4 ± 0.4	1.0×10^3	59
	ADR-GlyU	NA	NA	NA	NA	NA
Mur28	Muraymycin D1	NA	NA	NA	NA	NA
	Muraymycin D2	$(1.7 \pm 0.4) \times 10^2$	$(5.6 \pm 1.0) \times 10^2$	5.2 ± 0.7	5.1×10^2	1.5
	Muraymycin D3	ND	ND	ND	ND	ND
	ADR-GlyU	38 ± 4	NA	75 ± 2	3.3×10^4	100

Abbreviations are NA, not applicable; ND, not determined.

4.3.4 Insight into the Function of Mur28-homologs *Bs*TmrB

*Bs*TmrB, which has never been functionally assigned in vitro except for its ability to bind ATP[74, 76] and tunicamycin[75], was initially targeted to serve as a control due to its modest sequence similarity to Mur28. Soluble His$_6$-TmrB and MBP-TmrB fusion protein were obtained using *E. coli* BL21(DE3) as an expression host. Using HPLC to monitor the reaction, recombinant TmrB did not have any phosphotransferase activity when incubated with ATP and commercial tunicamycin. Unexpectedly, however, LC-MS analysis revealed TmrB was able to phosphorylate muraymycin D2 and ADR-GlyU using ATP as the phosphate donor (Figure S4.37). The conversion of both was comparable to the Mur28-catalyzed reaction. Likewise, a trace amount of D2-PHOS was detected with ADP as the phosphate donor. In contrast to Mur28, however, no other nucleotide triphosphates were substrates for *Bs*TmrB.

4.3.5 Potential role of Mur29 and Mur28 in self-resistance

The possibility that Mur29 and/or Mur28 play a role in self-resistance to muraymycins was explored using three approaches. We first examined the antibacterial activity of muraymycin D1 and D2 against *E. coli* BL21(DE3) harboring the *mur29*, *mur28, or tmrB* expression plasmids (Table 4.2). *E. coli* BL21(DE3) harboring an expression plasmid for *mur20*, encoding a putative aminotransferase likely involved in ADR biosynthesis, was used as control. Both muraymycin D1 and D2 have low antibacterial activity against plasmid-free *E. coli* BL21(DE3) or strains expressing *mur20*, with MICs determined in the range of 16-32 μg/mL. A similar MIC for muraymycin D1 (32 μg/mL) was obtained against *E. coli* BL21(DE3) expressing *mur28* or *tmrB*. However, *E. coli* BL21(DE3) expressing *mur29* was resistant to

muraymycin D1 (MIC > 256 μg/mL). *E. coli* BL21(DE3) cells expressing *mur29*, *mur28*, or *tmrB* were likewise all resistant to muraymycin D2 (MIC > 256 μg/mL). These results were consistent with the substrate selectivity of each enzyme that was revealed through in vitro assays.

The purified Mur29 and Mur28 products (D1-AMP and D2-PHOS) were next screened against *Mycobacterium smegmatis* and *E. coli* DH5α/Δ*tolC* (Table 2). Both strains are more sensitive compared to *E. coli* BL21(DE3) with MIC = 4 μg/mL (muraymycin D1 or D2) and 1 μg/mL (muraymycin D1 or D2), respectively. In contrast to the unmodified muraymycins, D1-AMP and D2-PHOS were inactive against *M. smegmatis* (MIC > 256 μg/mL) while both had reduced activity against *E. coli* DH5α/Δ*tolC* (MIC = 16 μg/mL).   The results are consistent with the conferred resistance upon heterologous expression of *mur29* and *mur28* in *E. coli* BL21(DE3).

The third and final approach to examine a potential role in self-resistance was to screen D1-AMP and D2-PHOS for inhibitory activity against recombinant *Staphylococcus aureus* MraY (*Sa*MraY) *in vitro*. In contrast to muraymycin D1 and D2, which were determined to be sub-nanomolar inhibitors of *Sa*MraY with $IC_{50} = 0.48 \pm 0.13$ and 0.39 ± 0.11 nM, respectively, D1-AMP and D2-PHOS were significantly less potent with $IC_{50} = 82 \pm 32$ nM and 20 ± 5 nM, respectively. Therefore, the direct inhibition of the translocase I target is positively correlated with the whole cell antibacterial activity.

Table 4.2 Bacterial MraY assays and antimicrobial activities

compound	*S. aureus* MraY growth inhibition IC$_{50}$ (nM)	*M. smegmatis* growth inhibition MIC (µg/mL)	*E. coli* Δ*tolC* mutant growth inhibition MIC (µg/mL)	*E. coli* BL21(DE3) growth inhibition MIC (µg/mL)	*E. coli* BL21(DE3) *mur28* pET30 growth inhibition MIC (µg/mL)	*E. coli* BL21(DE3) *mur29* pET30 growth inhibition MIC (µg/mL)	*E. coli* BL21(DE3) *tmrB* pET30 growth inhibition MI (µg/mL)	*E. coli* BL21(DE3) *mur20*pET30 growth inhibition MIC (µg/mL)
muraymycin D1	0.48±0.13	4	1	32	32	>256	32	32
muraymycin D2	0.39±0.11	4	1	32	>256	>256	>256	16
muraymycin D1-AMP	82±32	>256	16	>256	na	na	na	na
muraymycin D2-Phos	20±5	>256	16	>256	na	na	na	na

4.4 Discussion

4.4.1 Why We Choose Muraymycin D Series to Test the Activity

We have provided evidence to support the functional assignment of two enzymes that covalently modify known muraymycins or a hypothetical biosynthetic precursor. Twenty-two muraymycin congeners, categorized structurally into four series (A-D), were initially discovered using an enzyme activity-based screen to identify inhibitors of MraY and/or MurG, which catalyze sequential reactions to generate Lipid II intermediate in peptidoglycan cell wall biosynthesis. The D series of congeners were targeted here as representative muraymycins in part due to (i) the relatively decent titres in our hands, (ii) they are structurally the simplest of the independent series, and (iii) this was the only series within which we could isolate the three congeners with variations in the ADR (namely, D1, D2, and D3). Unfortunately, this series also represents the weakest inhibitors of the four, but nevertheless remain potent inhibitors of the

MraY-catalyzed reaction[8, 77] and are modestly active against a few bacterial pathogens. In our

in vitro screen, muraymycin D1 and D2 were very potent inhibitors of recombinant

Staphylococcus aureus MraY with IC_{50} of 0.48 and 0.39 nM, respectively. The details of this

assay and the variability with respect to the literature is reported elsewhere. Given the moderate

sequence identity (~ 40%) and conservation of key motifs of *Sa*MraY and MraY from different

*Streptomyce*s including the muraymycin D2 binding site, we predict that the producing strain's

MraY is equally inhibited.

4.4.2 Distinct Temporal Order for Mur29 and Mur28 Catalysis

The ADR-GlyU disaccharide core of muraymycin is technically an aminoglycoside,

and thus it seemed plausible that our results are consistent with the functional assignment of

Mur29 as an ATP-dependent muraymycin adenylyltransferase and Mur28 as an ATP-dependent

ADR-GlyU phosphotransferase. NMR spectroscopic analyses of each enzyme-catalyzed

product revealed a downfield shift with respect to the C-3″ proton, the magnitude of which is

consistent with other enzymes that adenylate or phosphorylate sugars such as the numerous

aminoglycoside resistance enzymes.[78] Interestingly both Mur29 and Mur28 covalently modify

the ADR with the identical regioselectivity, yet Mur29 did not have any activity with ADR-

GlyU while Mur28 kinetically preferred this muraymycin precursor. The realization of the

substrate preferences suggests that ADR is phosphorylated at an earlier stage in the biosynthetic

pathway, and is potentially utilized as a transient resistance mechanism. The biochemical

data—along with consideration of MraY inhibition—lead us to conclude that ADR-GlyU is the

authentic *in vivo* substrate of Mur28, as the kinetic parameters are in line with other

phosphotransferases and the attachment of the aminopropyl group leads to the first active antibiotic scaffold, FR-900493. Thus, we propose that transient phosphorylation occurs inside the cell and protects the producing strain from MraY self-inhibition during antibiotic maturation. Following phosphorylation, muraymycin biosynthesis is completed by downstream, as-of-yet uncharacterized enzymes, transported outside the cell, and dephosphorylated by an unknown enzyme. In contrast to Mur28, the biochemical data support that Mur29 functions later in the biosynthetic pathway. Therefore, as opposed to a preventive resistance mechanism that is proposed via Mur28-catalyzed phosphorylation, we hypothesize that Mur29-catalyzed adenylation provides a protective resistance mechanism in the case of intracellular accumulation of muraymycin.

4.4.3 Predicted Phosphorylation Position of Tunicamycin by TmrB

Noda et al[79] discovered that *Bs*TmrB, responsible for tunicamycin resistance of *B. subtillis*, confers reisistance to tunicamycin on *E. coli*. The same team also showed that TmrB is an ATP-binding membrane protein[74], and suggested that it could act to lower the intracellular concentration of tunicamycin. Kapp reported the crtystal structure of TmrD (a homolog of TmrB) and suggested that either of the three hydroxyls in ribose moiety of tunicamycin could be the target by structural alignment and modelling with chloramphenicol phosphotransferase.[76] In our experiment, although TmrB did not show any phosphotransferase activity with a commercial mix of tunicamycin congeners, TmrB was able to phosphorylate muraymycin D2 and ADR-GlyU using ATP as the phosphate donor. Recently, MraY tunicamycin complex structure was reported. [80] Based on the comparison of tunicamycin and muraymycin D2 binding

with MraY, ADR-Gly moiety of muraymycin showed similar binding pattern of uridyl moiety of tunicamycin to MraY. The 5′ hydroxyl group of tunicamycin located in the similar position of aminoribose moiety of muraymycin D2, which lead us to propose that TmrB might transfer phosphate from ATP to 5′ hydroxyl group in the ongoing studies.

4.5 Conclusion

In conclusion, we have provided evidence to support the functional assignment of Mur29 as a Mg·ATP-dependent 3″-O-muraymycin adenylyltransferase and Mur28 as a Mg·ATP-dependent ADR-GlyU 3″-phosphotransferase. The biochemical data—along with consideration of MraY inhibition—lead us to conclude that ADR-GlyU is the authentic in vivo substrate of Mur28, as the kinetic parameters are in line with other phosphotransferases and the attachment of the aminopropyl group leads to the first active antibiotic scaffold, FR-900493. Thus, we propose that transient phosphorylation occurs inside the cell and protects the producing strain from MraY self-inhibition during antibiotic maturation. Following phosphorylation, muraymycin biosynthesis is completed by downstream, as-of-yet uncharacterized enzymes, transported outside the cell, and dephosphorylated by an unknown enzyme. In contrast to Mur28, the biochemical data support that Mur29 functions later in the biosynthetic pathway. Therefore, as opposed to a preventive resistance mechanism that is proposed via Mur28-catalyzed phosphorylation, we hypothesize that Mur29-catalyzed adenylation provides a protective resistance mechanism in the case of intracellular accumulation of muraymycin.

4.6 Supporting Information

Table S 4.1 Sequence identity for pairwise sequence alignment with Mur28.

Protein[a,b]	Identity (%)	Protein	Identity (%)
*Bs*TmrB	34		
LipX	36	LipI	23
Cpz27	38	Cpz12	26
LpmY	38	LpmJ	23
Mra06	38	Mra16	22

[a]Accession numbers for proteins are as follows: BsTmrB, WP_042977443; LipX, BAJ05900; LipI, BAJ05885; Cpz27, ACQ63635; Cpz12, ACQ63620; LpmY, ADC96673; LpmJ, ADC96658; Mra06, BAM98967; Mra16, BAM98977

[b]Protein annotations are Lip, A-90289 from *Streptomyces* sp. SANK 60405; Cpz, caprazamycin from *Streptomyces* sp. MK730-62F2; Lpm, liposidomycin from *Streptomyces* sp. SN-1061M; and Mra, muraminomicin from *Streptosporangium amethystogenes*.

Table S 4.2 Primers used in this study.
3

Primer	Sequence	Note
mur28_NdeI	5'-GATAGGCATATG AGCAGGCACGCACACAC-3'	*mur28* expression with pXY200 or pDB.His.MBP vector
mur28_BamHI	5'-CGAGTTGGATCC TCACCGCGCTCCGTCCG-3'	
mur29_NdeI	5'-GATAGGCATATG AGCGTCGTCGACAACG-3'	*mur29* expression with pDB.His.MBP vector
mur29_BamHI	5'-CGAGTTGGATCCTCACGGCAGTAGTGACTCCAG-3'	
mur28_pET30F	5'-GGTATTGAGGGTCGCGTGATCATTTGGATC-3'	Activity assay with *E. coli* BL21(DE3)
mur28_pET30R	5'-AGAGGAGAGTTAGAGCCTCAAAACCTGGCGG-3'	
mur29_pET30F	5'-GGTATTGAGGGTCGCGTGCAAGCCATGAAC-3'	Activity assay with *E. coli* BL21(DE3)
mur29_pET30R	5'-AGAGGAGAGTTAGAGCCTCAGCGGGTCACGTC-3'	
tmrB_NdeI	5'-AAAAAACAT ATGATCATTTGGATCAACGGTGCG-3'	*tmrB* expression with pDB.His.MBP
tmrB_BamHI	5'-AAAAAAGGATCCTTATTTAATACGGATGTGGTTCAGCTTAA-3'	
lipI_pET30F	5'-GGTATTGAGGGTCGCGTGATCATCGTCATCACGGGC-3'	*lipI* expression with pET30 vector
lipI_pET30R	5'-AGAGGAGAGTTAGAGCCTCATGTGGCCGTCCCTGC-3'	
lipX_NdeI	5'-AAAAAACATATGCTGGTGTGGATCAACGG-3'	*lipX* expression with pDB.His.MBP vector
lipX_BamHI	5'-AAAAAAGGATCCTCATGGACGCGAGTCCCTTC-3'	

Table S4.3 Gradient used for muraymycins separation.

Semipreparative HPLC separation of muraymycin D1, muraymycin D2, muraymycin D3, muraymycin D1-AMP and muraymycin D2-Phosphate with an analytical Apollo C18 column (250 $\times$ 10 mm, 5 μm).

Solvent A= ddH$_2$O with 0.025% trifluroacetic acid; Solvent B= acetonitrile; A260

Time (min)	% Solvent B	Flow Rate (mL/min)
0	10	3.5
25	22	3.5
26	100	3.5
31	100	3.5
32	10	3.5
36	10	3.5

Table S4.4 Gradient program 1 (GP1) used for HPLC or LC-MS analysis of reactions with an analytical Apollo C18 column (250 mm x 4.6 mm, 5 μm).

Solvent A= ddH$_2$O with 0.1% formic acid; Solvent B= acetonitrile with 0.1% formic acid; A260

Time (min)	% Solvent B	Flow Rate (mL/min)
0	1	0.5
16	20	0.5
28	100	0.5
37	100	0.5
38	1	0.5
41	1	0.5

Table S4.5 Gradient program 2 (GP2) used for LC-MS analysis of AQC modified reactions with an analytical Apollo C18 column (250 mm x 4.6 mm, 5 μm).

Solvent A= ddH$_2$O with 0.1% formic acid; Solvent B= acetonitrile with 0.1% formic acid; A260

Time (min)	% Solvent B	Flow Rate (mL/min)
0	10	0.4
25	60	0.4
26	100	0.4
36	100	0.4
37	10	0.4
41	10	0.4

Table S4.6 Gradient program 3 (GP3) used for HPLC analysis of reactions with an analytical Apollo C18 column (250 mm x 4.6 mm, 5 μm).

Solvent A = 40 mM acetic acid-triethylamine pH 6.5; Solvent B = 40 mM acetic acid-triethylamine, 20% methanol, pH 6.5; A260

Time (min)	% Solvent B	Flow Rate (mL/min)
0	0	1.0
8	100	1.0
18	60	1.0
19	60	1.0
20	0	1.0
22	0	1.0

Table S4.7 Gradient program 4 (GP4) used for HPLC analysis of reactions with an analytical Apollo C18 column (250 mm x 4.6 mm, 5 μm).

Solvent A = 40 mM acetic acid-triethylamine pH 6.5; Solvent B = 40 mM acetic acid-triethylamine, 20% methanol, pH 6.5; A260

Time (min)	% Solvent B	Flow Rate (mL/min)
0	1	0.5
16	100	0.5
20	100	0.5
21	1	0.5
24	1	0.5

Figure S4.1 SDS-PAGE analysis of purified Mur28, Mur29, TmrB, LipI and LipX.
A, His6-Mur28; B, His6-MBP-Mur28; C, His6-MBP-Mur29; D, His6-TmrB; E, His6-MBP-TmrB; F, His6-LipI; G, His6-MBP-LipX
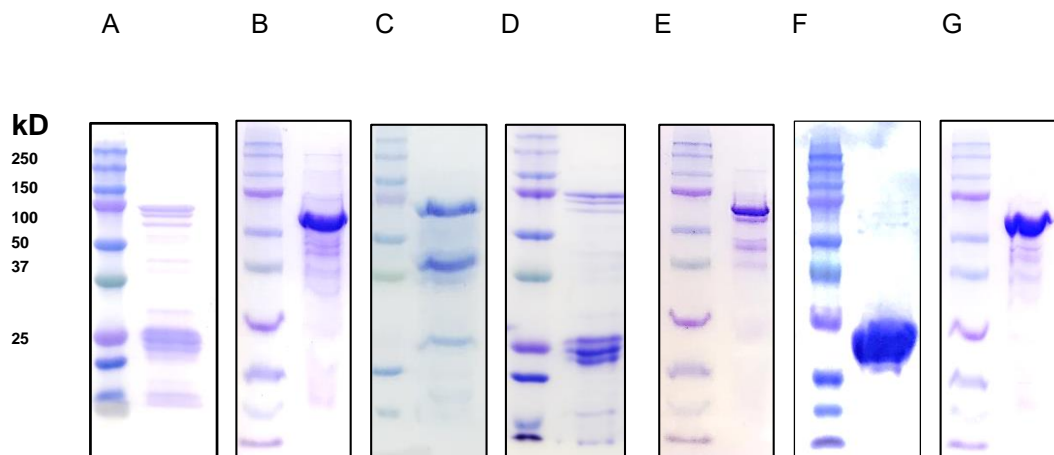
Protein	Size (aa)	Size (kD)
Mur28	184	20.8
Mur29	277	30.5
TmrB	197	22.7
LipI	189	21.2
LipX	188	21.3
MBP Tag	395	43.5
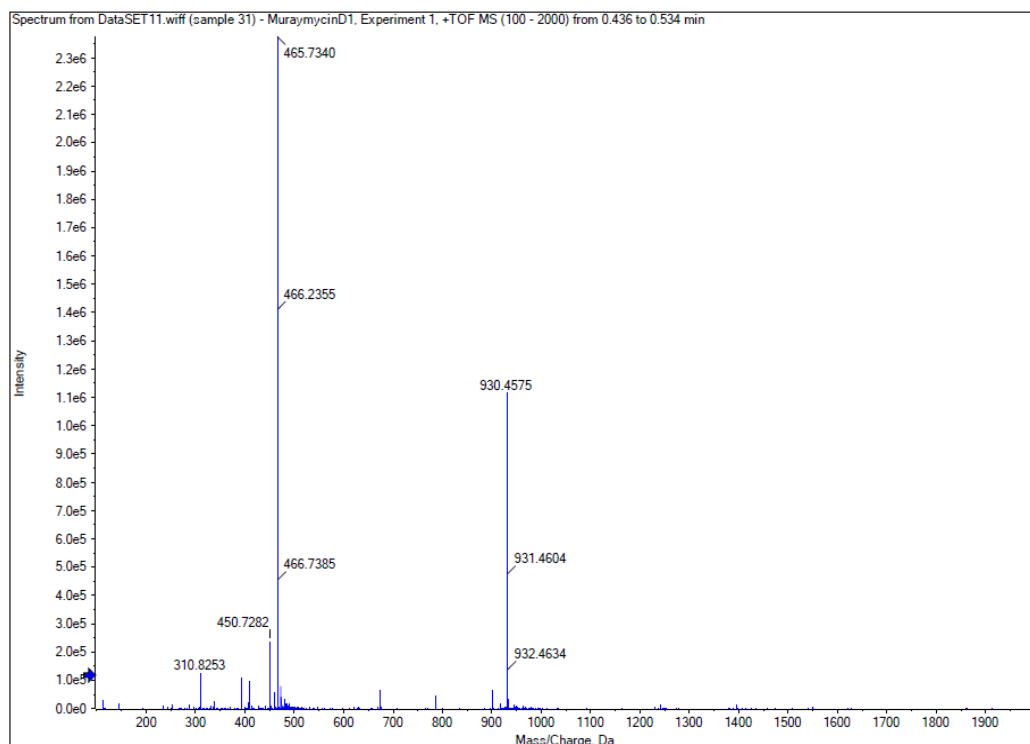
Figure S4.2 (+)-HR-ESI-MS (positive mode) of muraymycin D1
(calcd for C38H63N11O16 expected (M+H)$^+$ ion at m/z = 930.4527, found 930.4575).
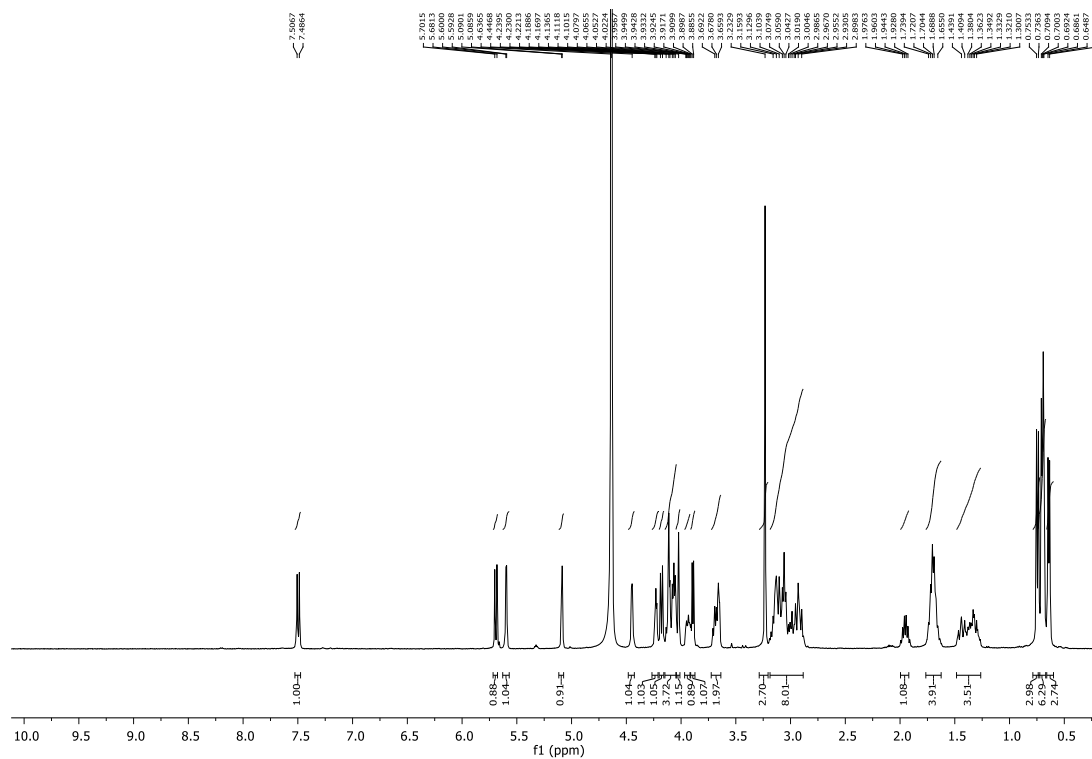
Figure S4.3 ^{1}H NMR spectrum (D2O, 400 MHz) of muraymycin D1.
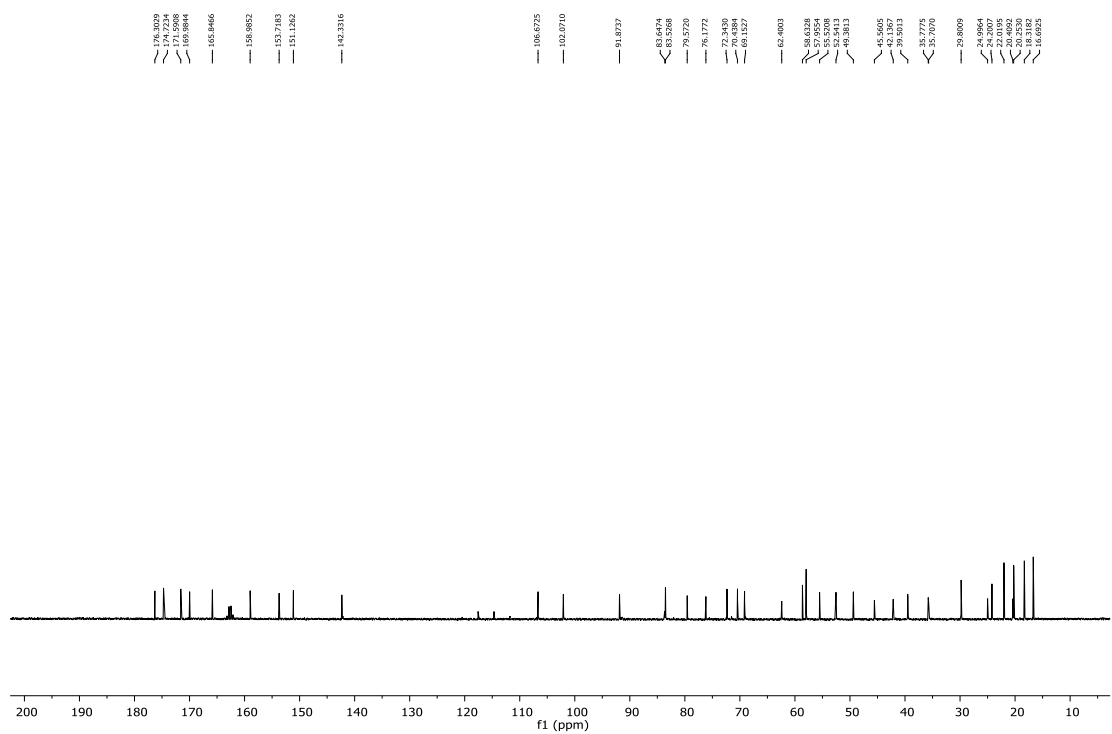
Figure S4.4 ^{13}C NMR spectrum (D$_2$O, 100 MHz) of muraymycin D1.
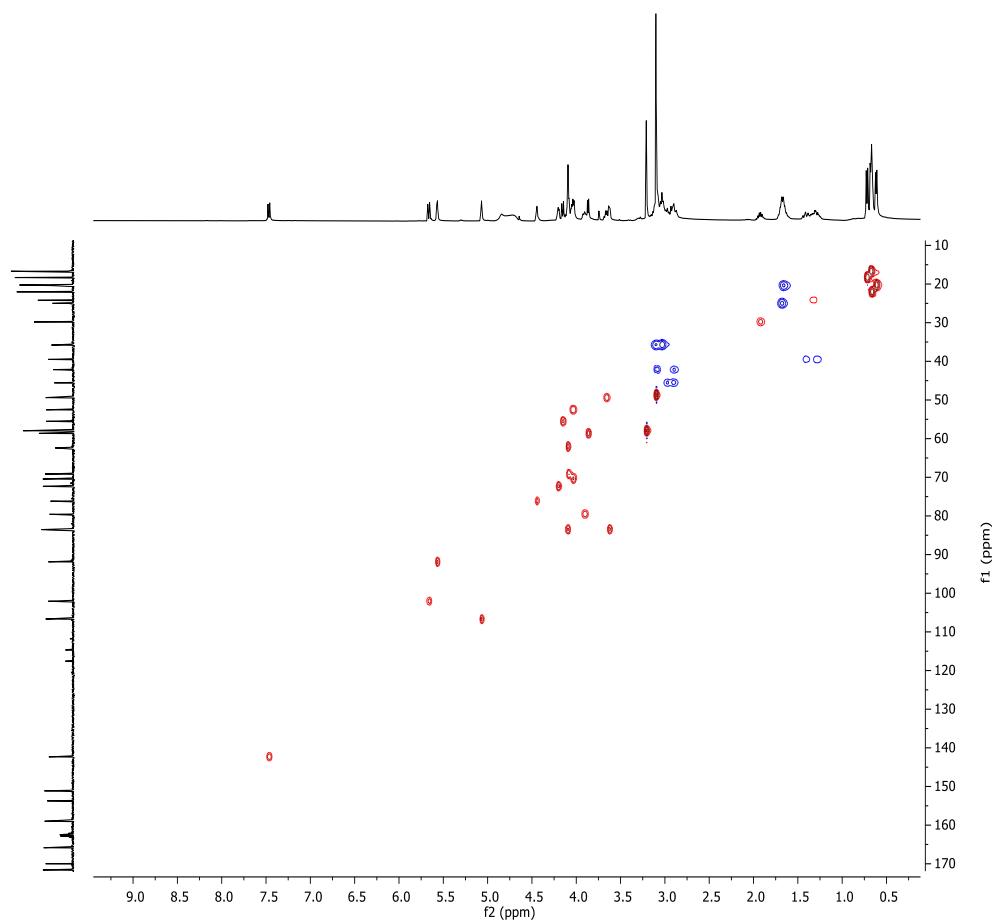
Figure S4.5 HSQC spectrum (D$_2$O, 400 MHz) of muraymycin D1.
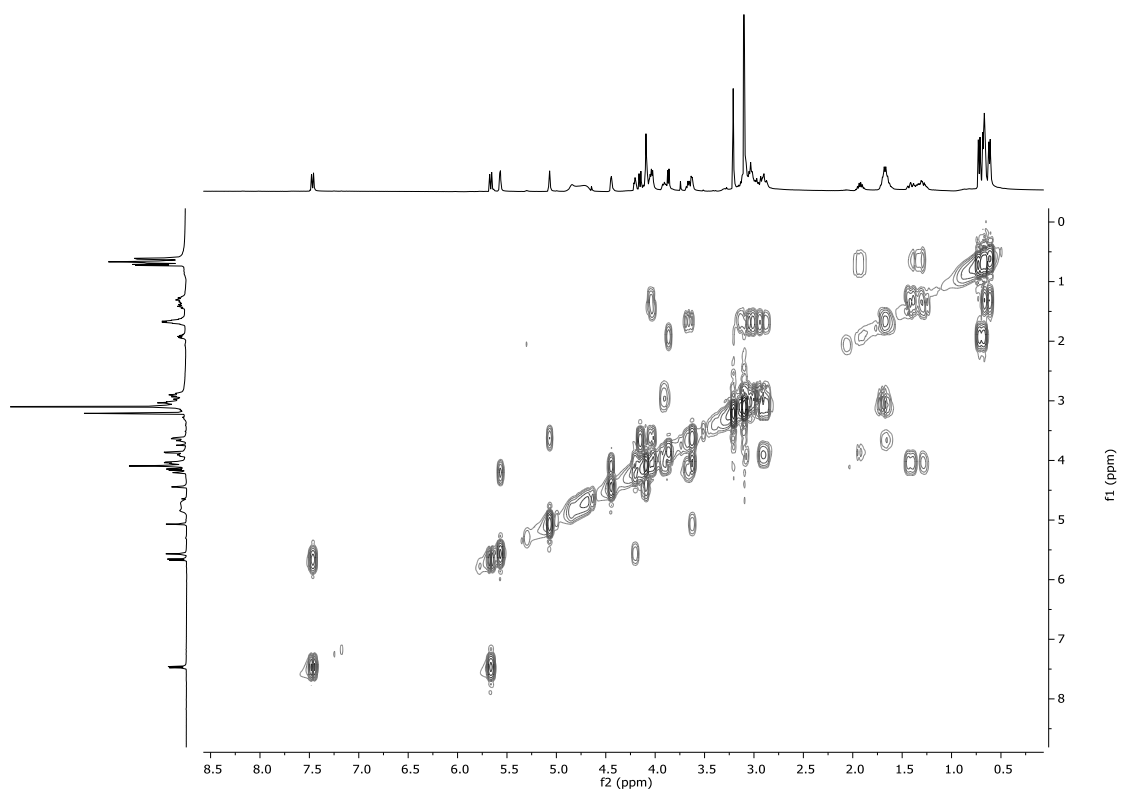
Figure S4.6 ^{1}H−^{1}H COSY spectrum (D$_2$O, 400 MHz) of muraymycin D1.
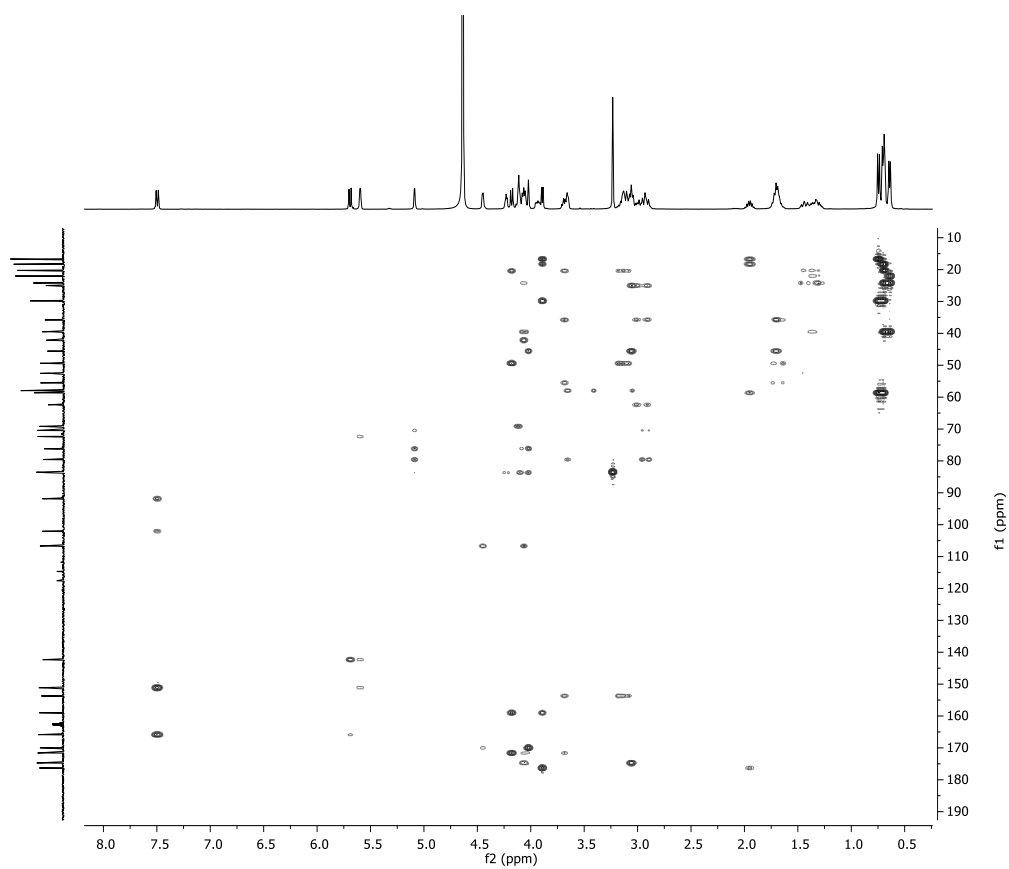
Figure S4.7 HMBC spectrum (D$_2$O, 400 MHz) of muraymycin D1.
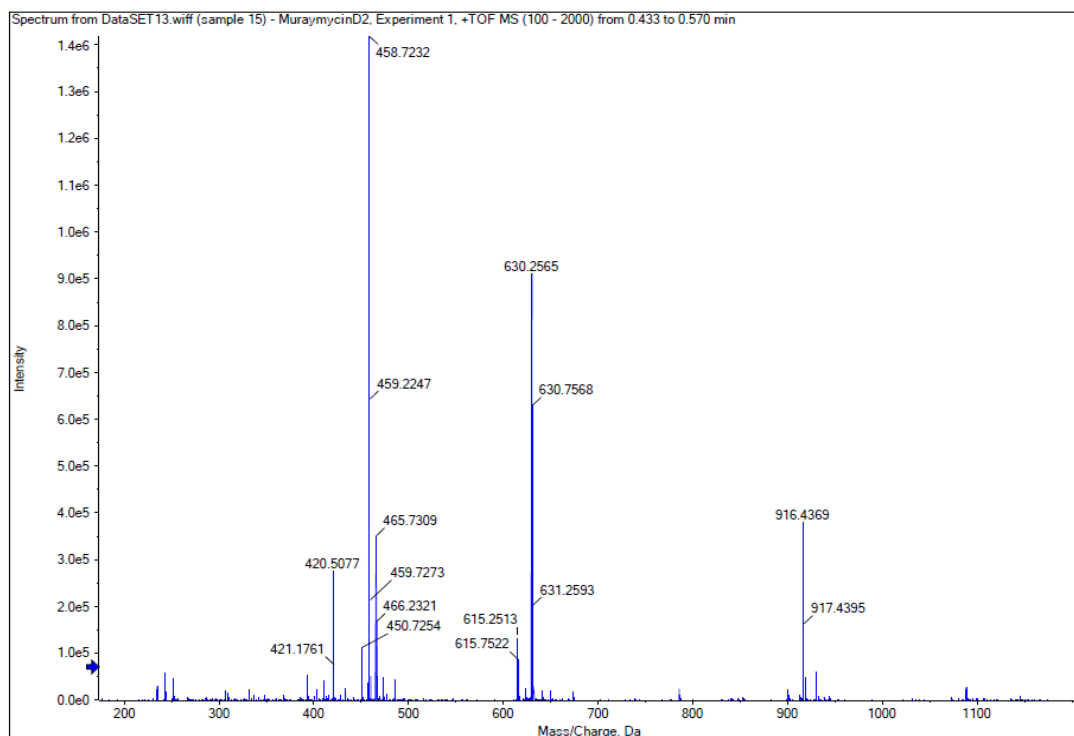
Figure S4.8 (+)-HR-ESI-MS (positive mode) of muraymycin D2
(calcd for C37H61N11O16, expected (M+H)$^+$ ion at m/z = 916.4371, found: 916.4369).
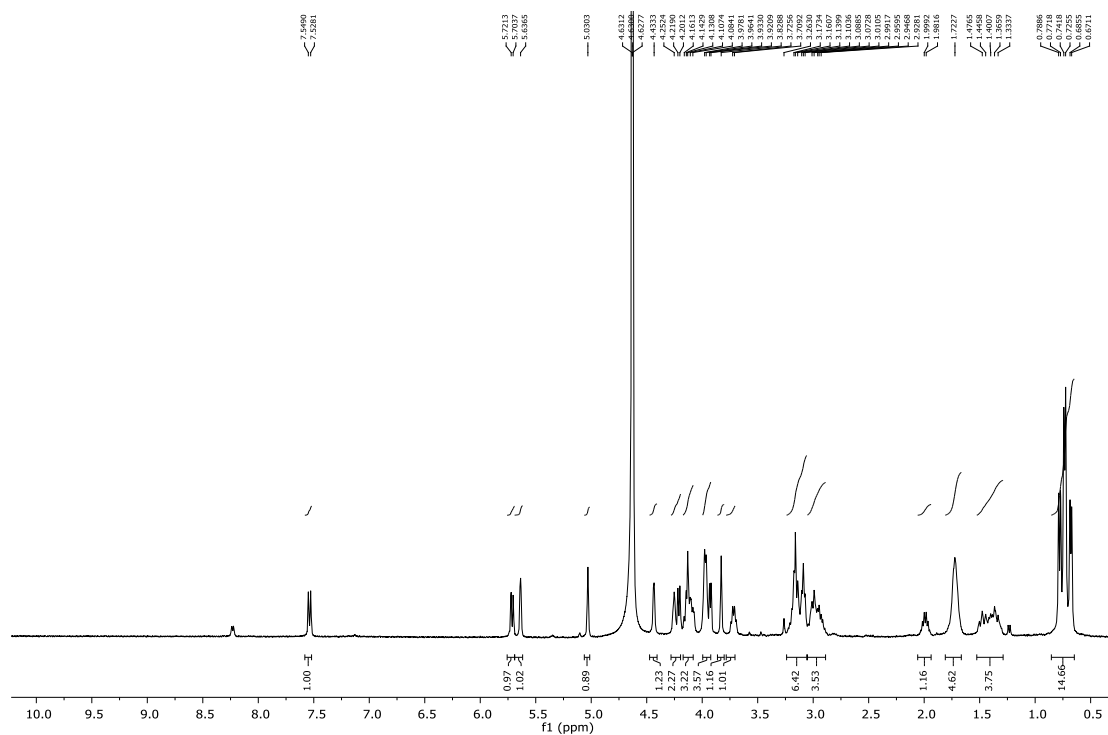
Figure S4.9 ^{1}H NMR spectrum (D$_2$O, 400 MHz) of muraymycin D2.
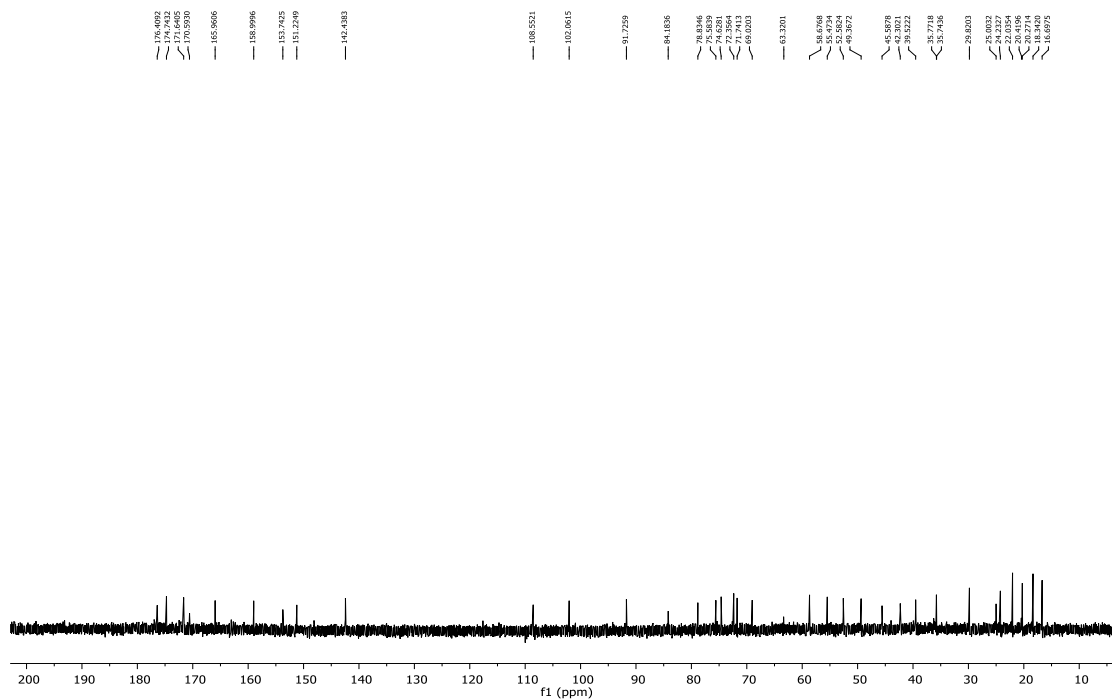
Figure S4.10 ^{13}C NMR spectrum (D$_2$O, 100 MHz) of muraymycin D2.
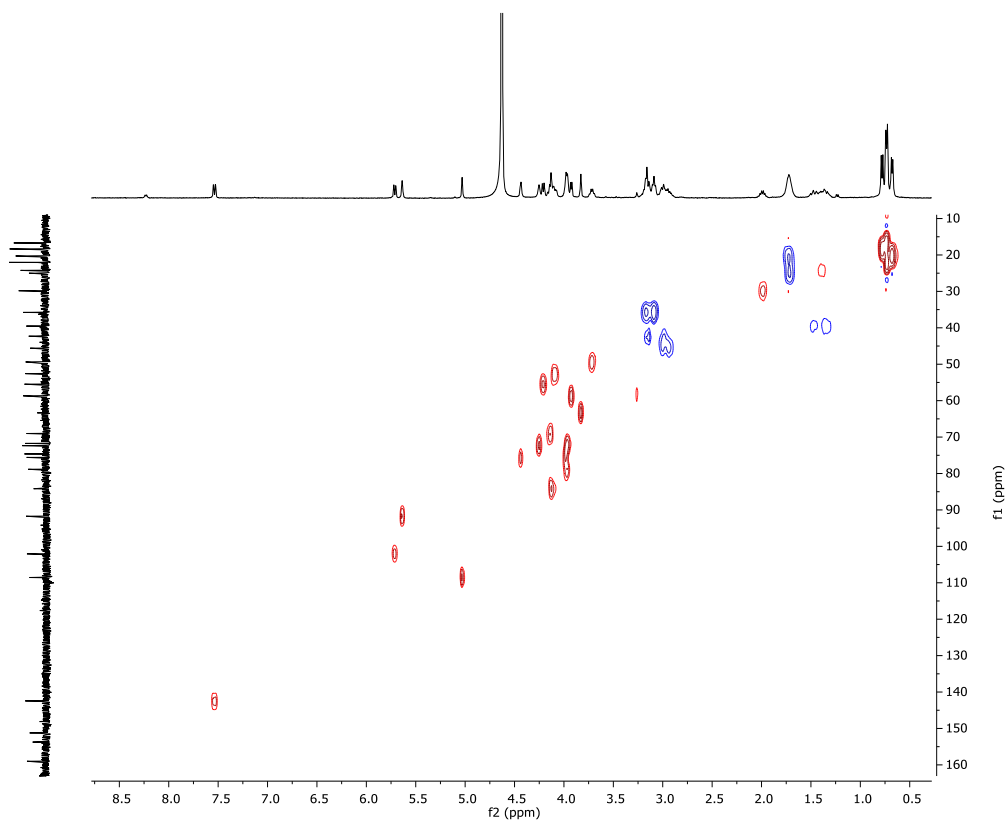
Figure S4.11 HSQC spectrum (D$_2$O, 400 MHz) of muraymycin D2.
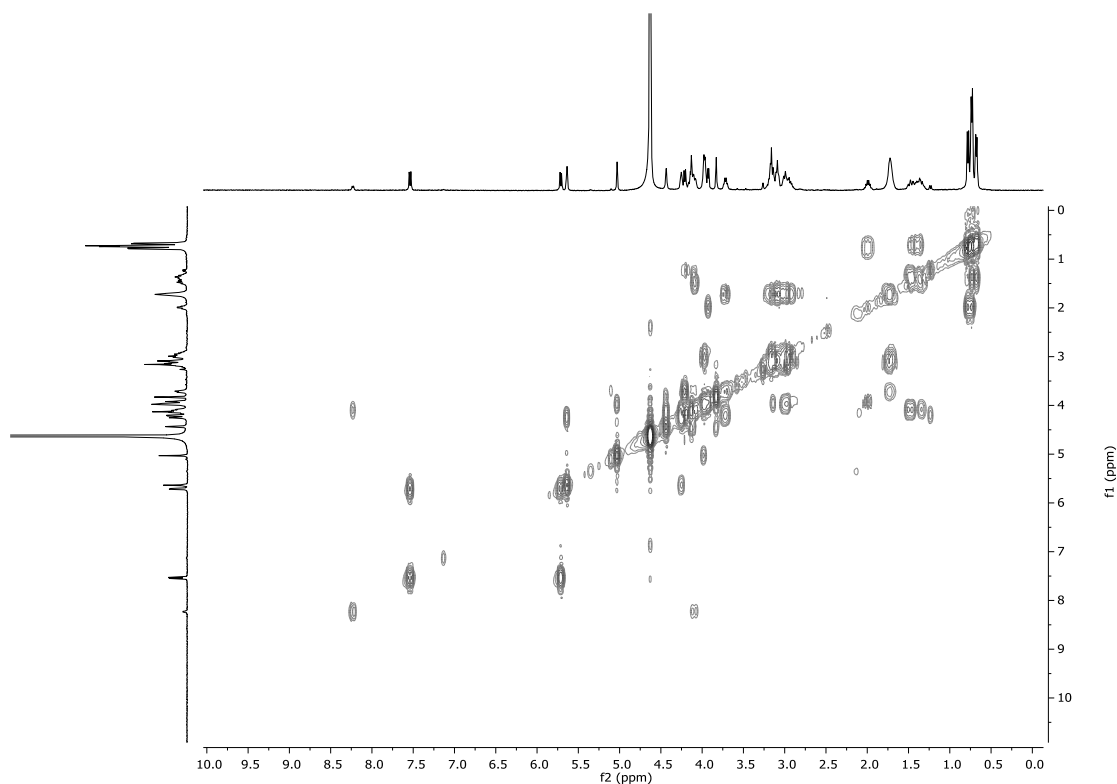
Figure S4.12 ^1H-^1H COSY spectrum (D_2O, 400 MHz) of muraymycin D2.
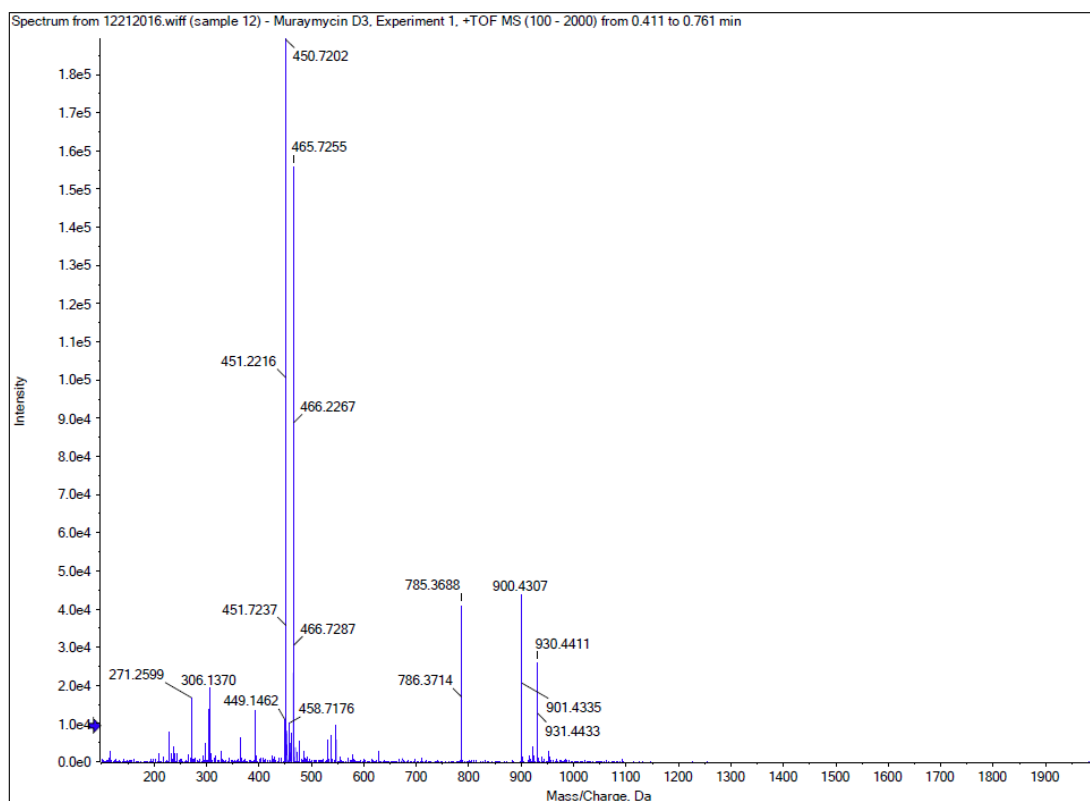
Figure S4.13 (+)-HR-ESI-MS (positive mode) of muraymycin D3. (calcd for C37H61N11O15, expected (M+H)$^+$ ion at m/z = 900.4421, found 900.4307; expected (M+2H)$^{2+}$ ion at m/z = 450.7247, found 450.7202).
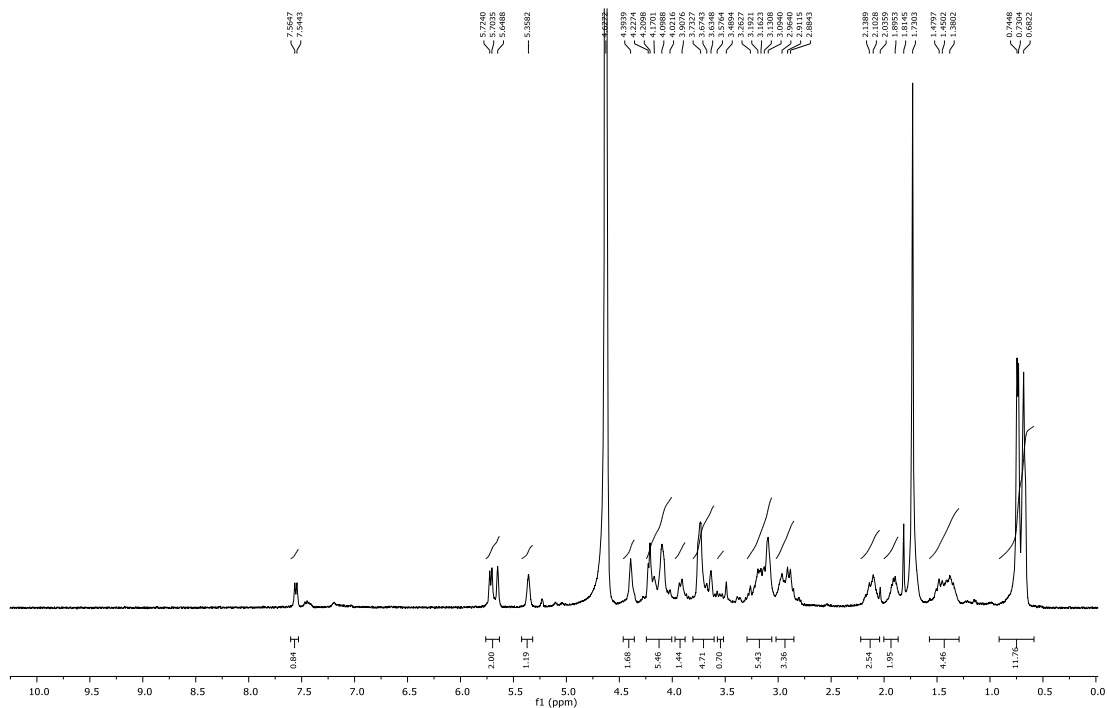
Figure S4.14 ^{1}H NMR spectrum (D$_2$O, 400 MHz) of muraymycin D3.
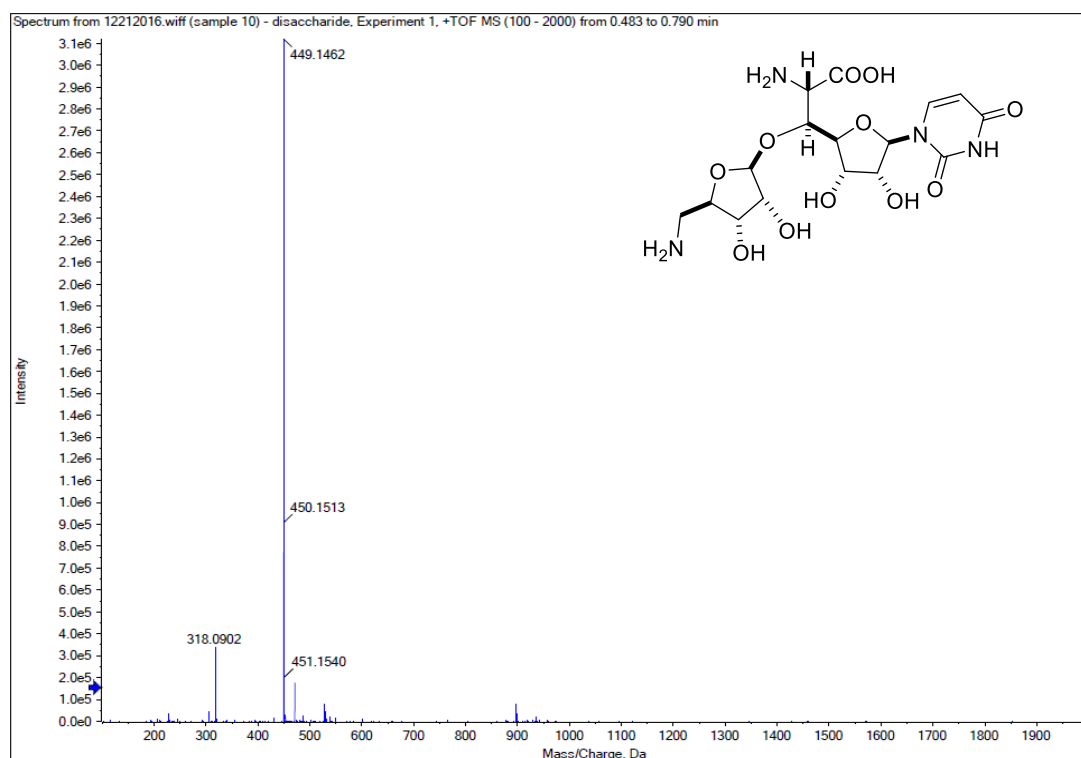
Figure S4.15 (+)-HR-ESI-MS (positive mode) of compound ADR-GlyU
(calcd for C16H24N4O11, expected (M+H)$^+$ ion at m/z = 449.1514, found: 449.1462).
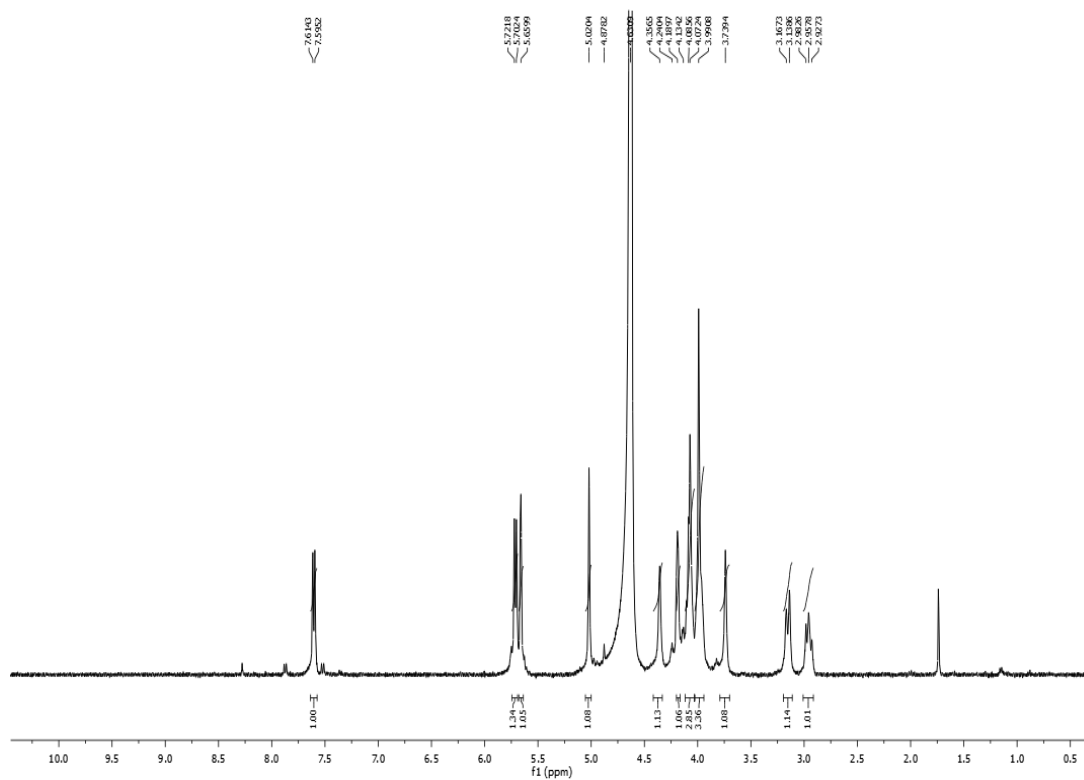
Figure S4.16 ^{1}H NMR spectrum (D$_2$O, 100 MHz) of compound ADR-GlyU.
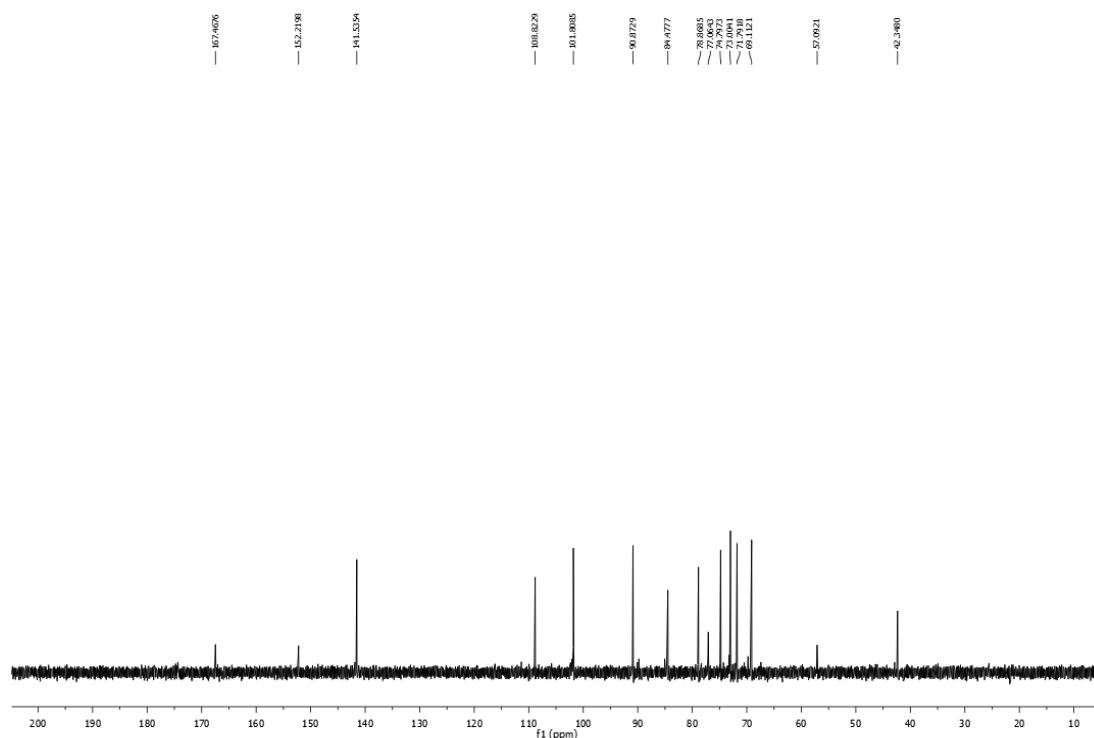
Figure S4.17 ^{13}C NMR spectrum (D$_2$O, 100 MHz) of compound ADR-GlyU.
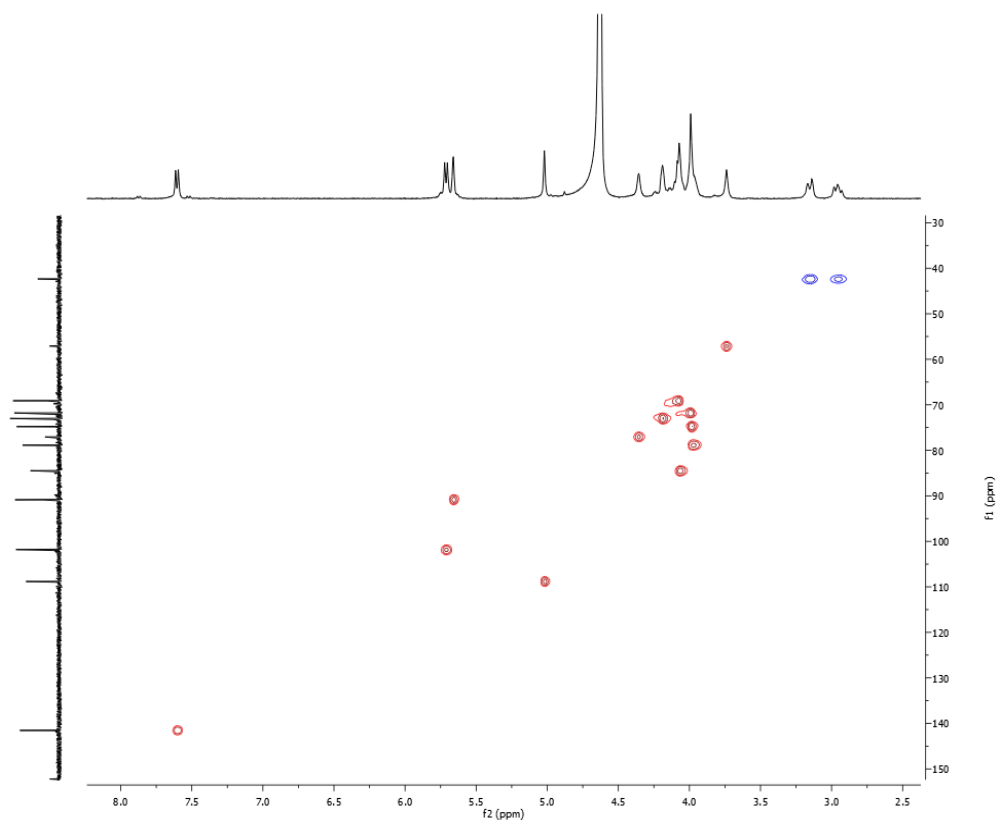
Figure S4.18 HSQC spectrum (D$_2$O, 400 MHz) of compound ADR-GlyU.
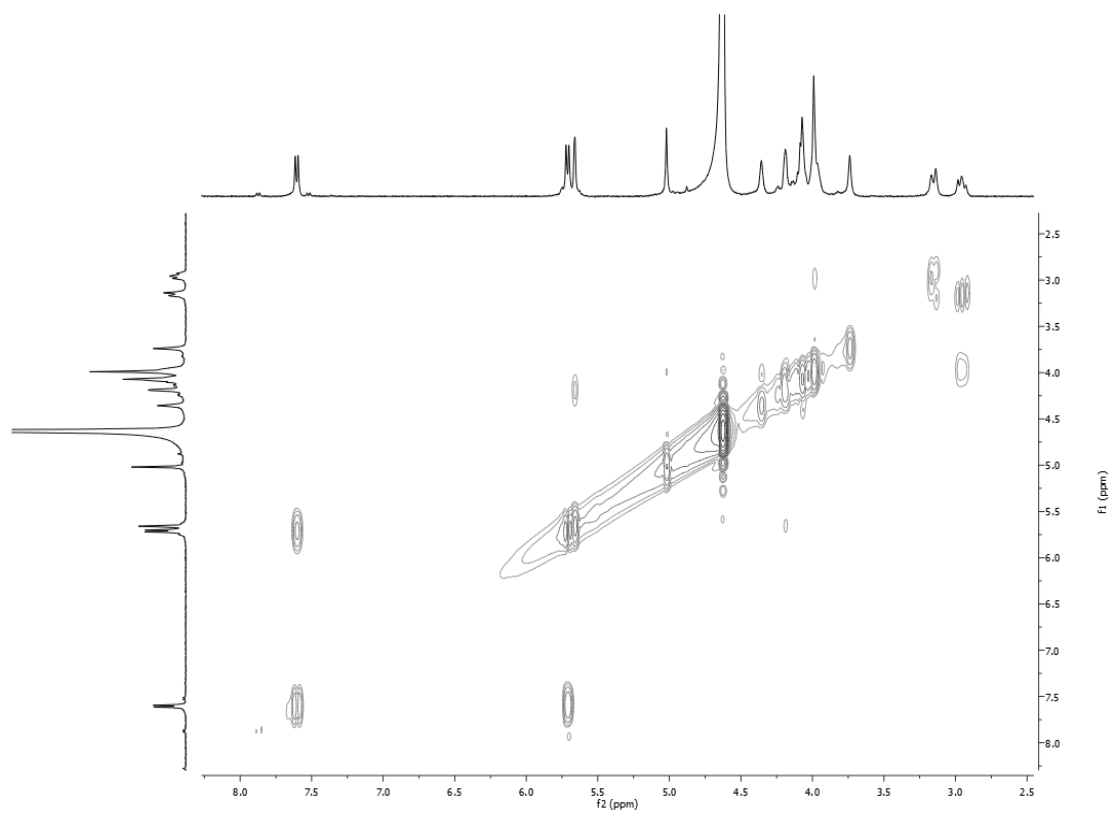
Figure S4.19 ^{1}H-^{1}H COSY spectrum (D$_2$O, 400 MHz) of compound ADR-GlyU.
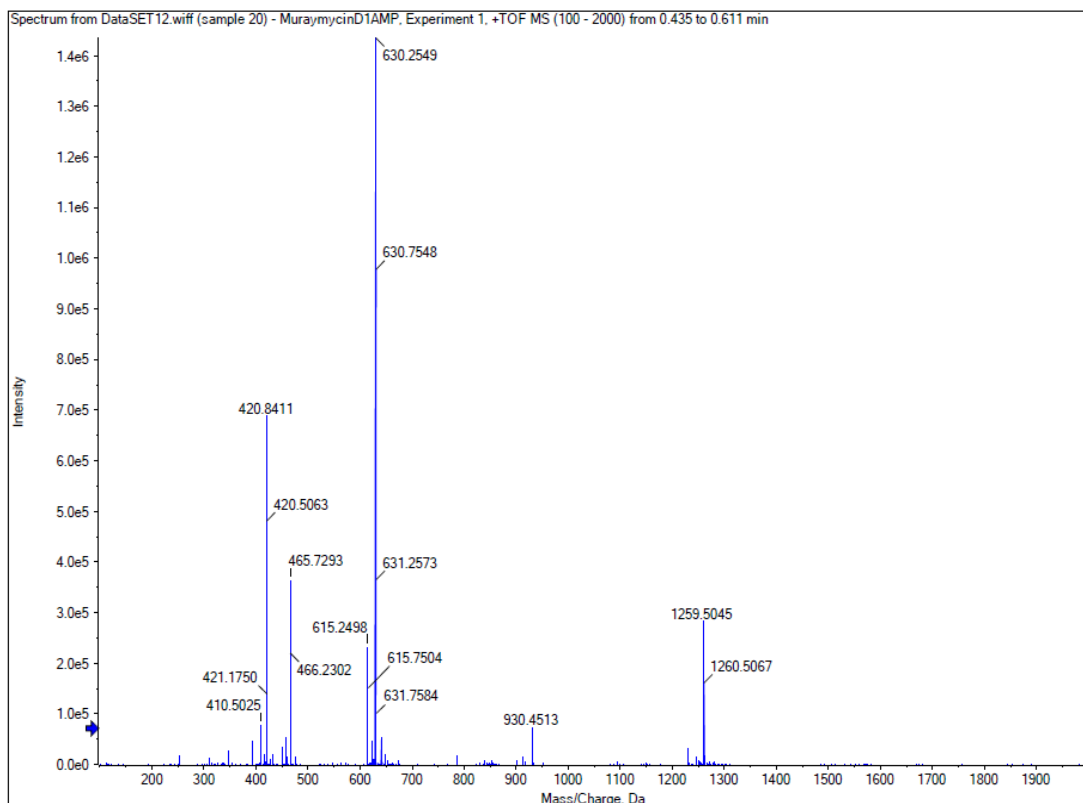
Figure S 4.20 (+)-HR-ESI-MS (positive mode) of compound D1-AMP.
(calcd for C48H75N16O22P, expected (M+H)$^+$ ion at *m/z* =1259.5052, found: 1259.5045).
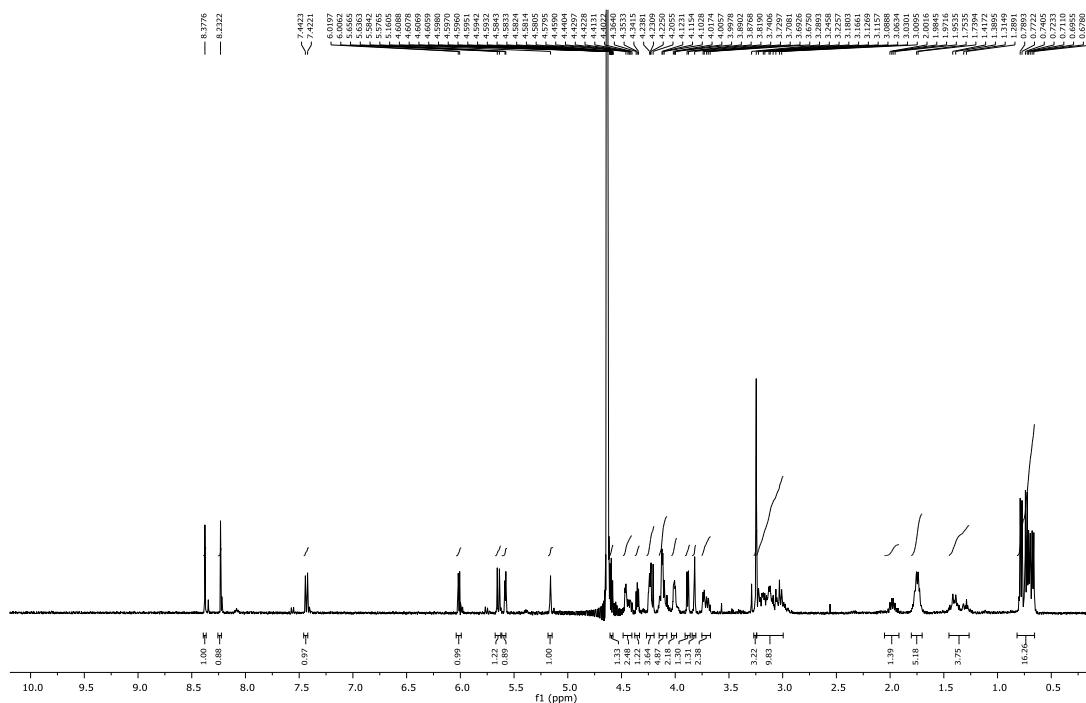
Figure S4.21 ^{1}H NMR spectrum (D$_2$O, 400 MHz) of muramycin D1-AMP.
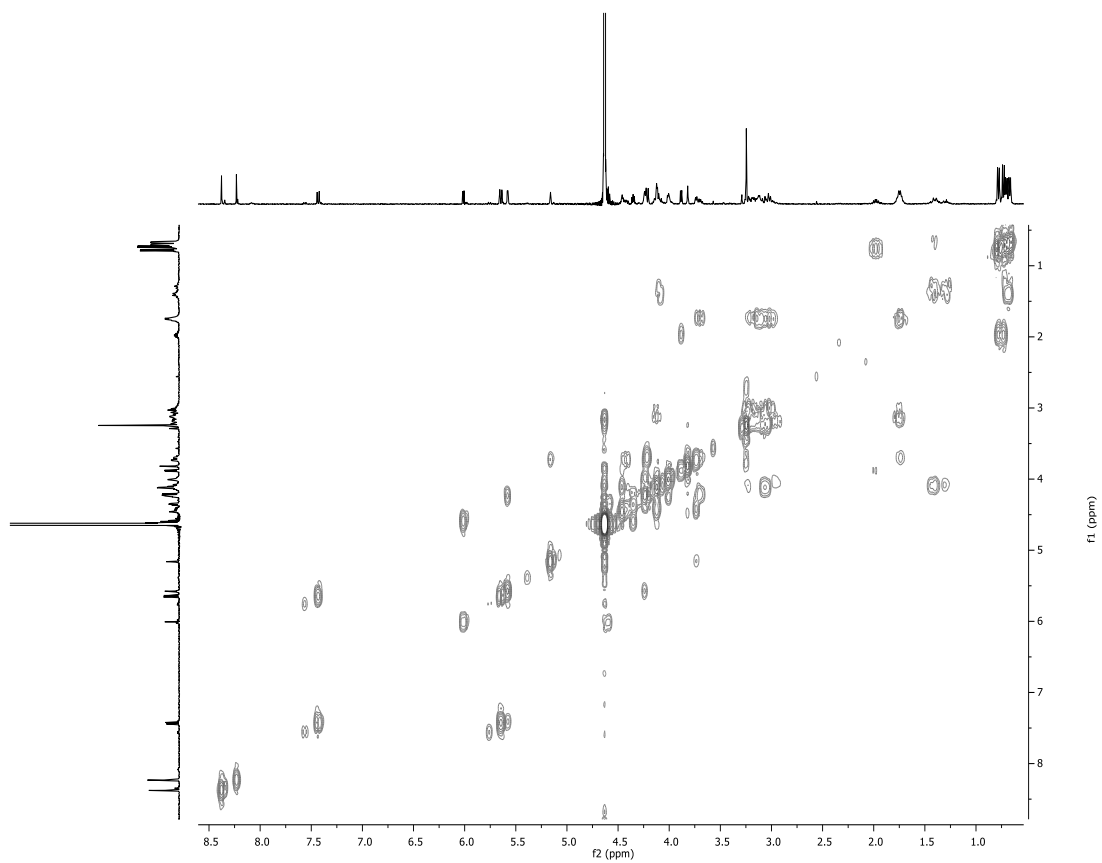
Figure S4.22 ^{1}H-^{1}H COSY spectrum (D$_2$O, 400 MHz) of muramycin D1-AMP.

133
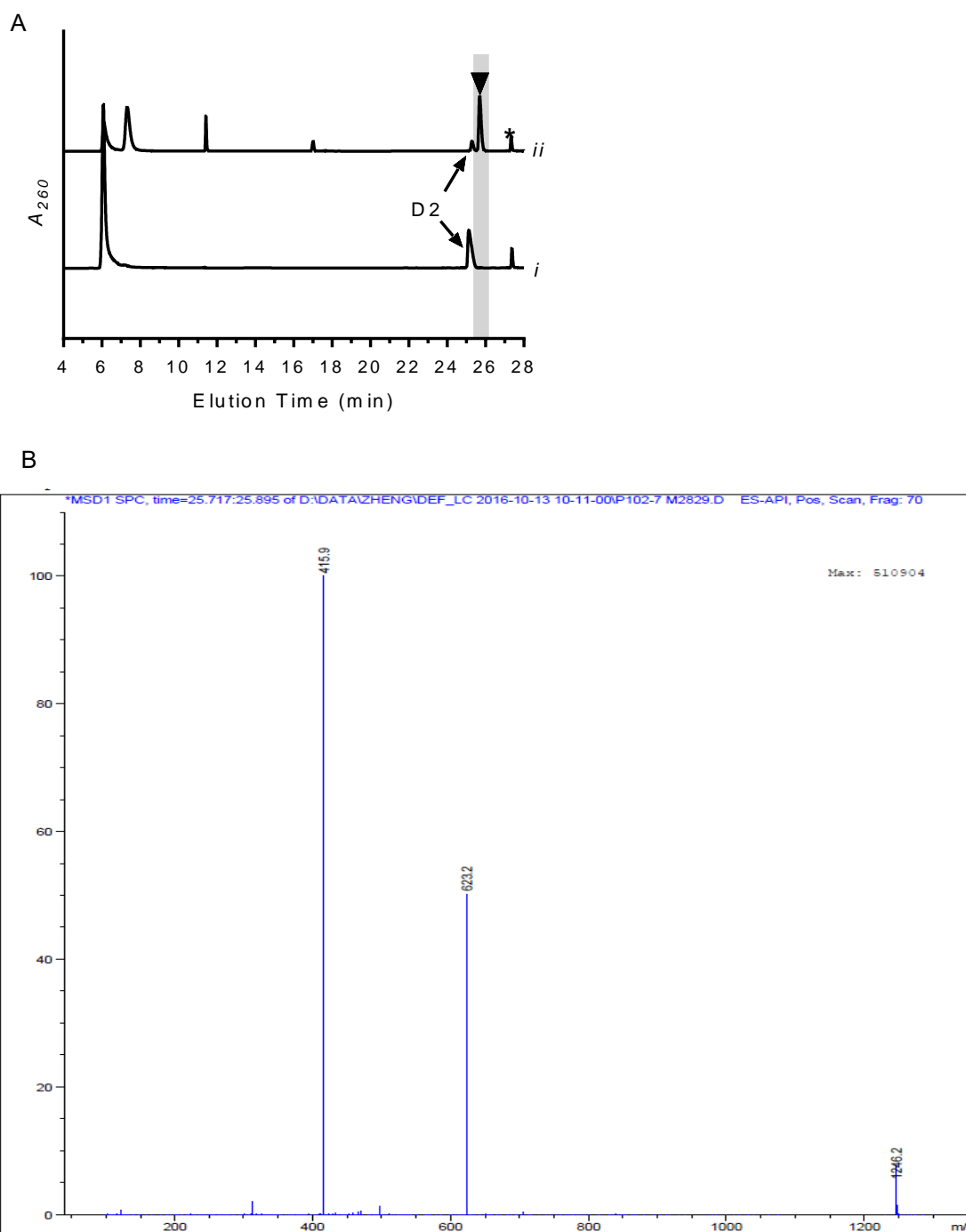
Figure S4.23 Reaction catalyzed by Mur29 with muraymycin D2 and ATP.
(A) LC-MS analysis after (i) 12 h incubation without Mur29 and (ii) 12 h reaction. Data were collected using GP1. (▼) denotes peak corresponding to D2-AMP; (*) denotes unidentified peak; A_{260}, absorbance units at 260 nm. (B) Mass spectrum for the peak eluting at t = 26.0 min (D2-AMP, $C_{47}H_{73}N_{16}O_{22}P$, expected $(M+H)^+$ ion at m/z = 1245.5, found: 1246.2).
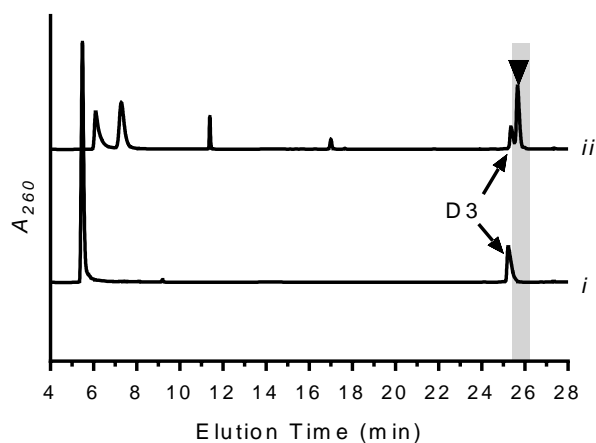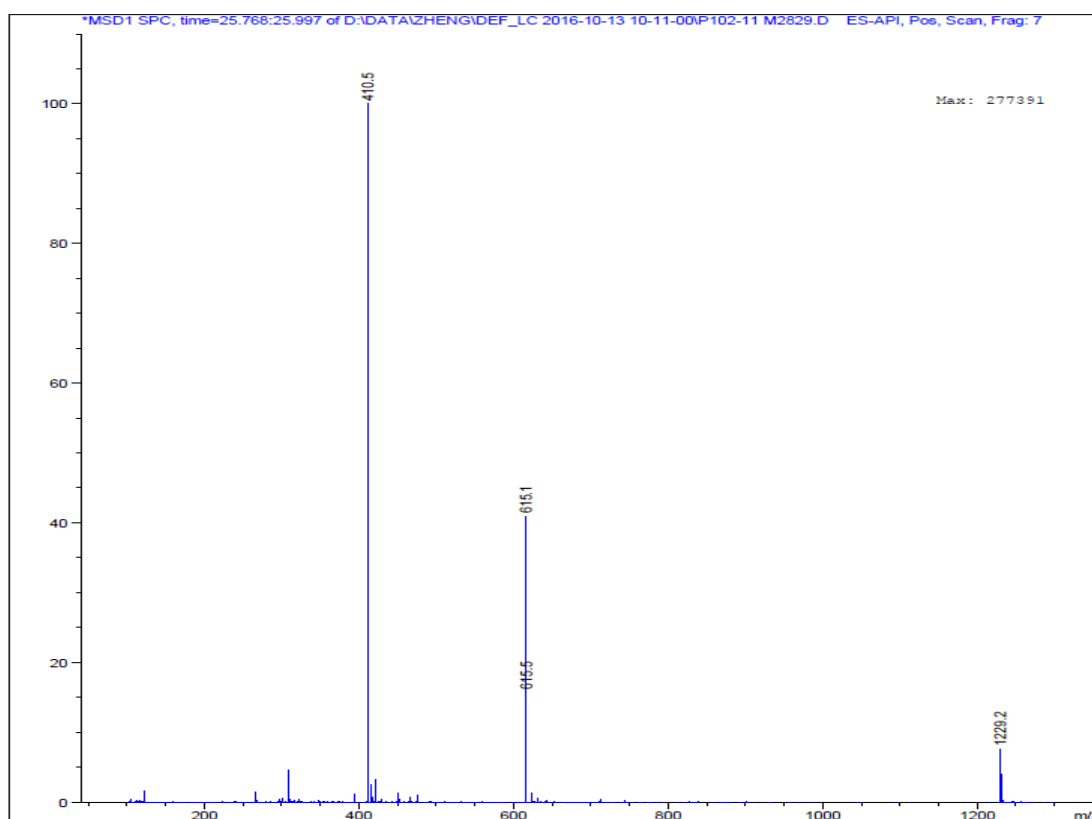
Figure S4.24 Reaction catalyzed by Mur29 with muraymycin D3 and ATP.

(A) LC-MS analysis after (i) 12 h incubation without Mur29 and (ii) 12 h reaction. Data were collected using GP1. (▼) denotes peak corresponding to D3-AMP; A_{260}, absorbance units at 260 nm.   (B) Mass spectrum for the peak eluting at t = 25.9 min (D3-AMP, $C_{47}H_{73}N_{16}O_{21}P$, expected $(M+H)^{+}$ ion at m/z = 1229.5, found: 1229.2).

A
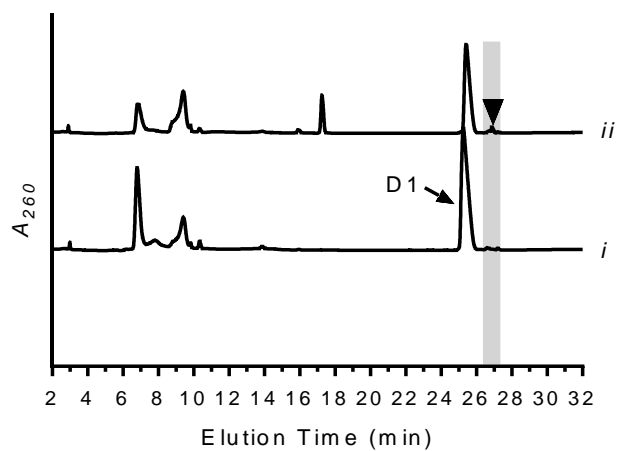
B
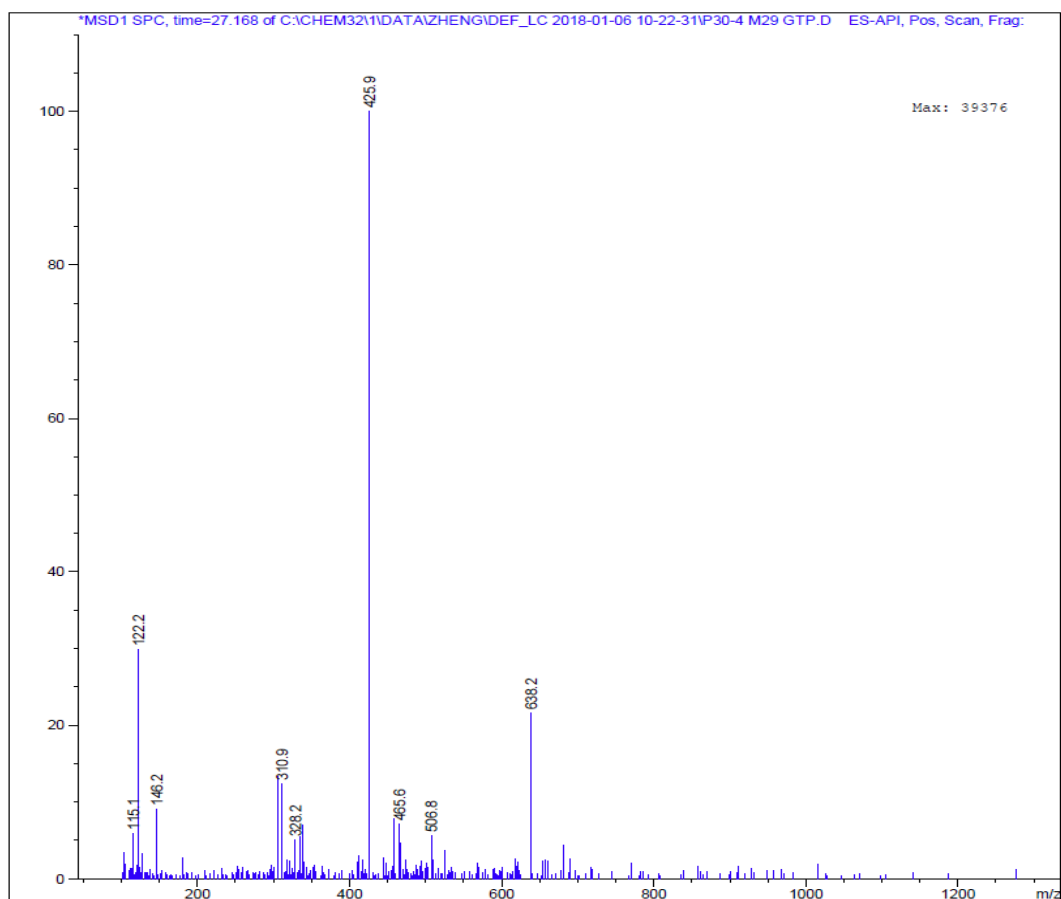
Figure S4.25 Reaction catalyzed by Mur29 with muraymycin D1 and GTP.
A, LC-MS analysis using muraymycin D1 and GTP after (I) 12 h reaction without Mur29, (II) 12 h reaction. B, mass spectrum for the ion peak eluting at time t = 26.926 min of Mur29 reaction with muraymycin D1. (D1-GMP, C48H75N16O23P, , expected (M+2H)$^{2+}$ ion at *m/z* = 638.2, found: 638.2).

A
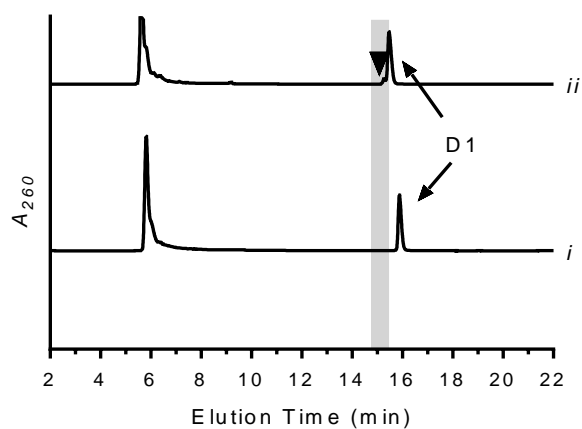
B
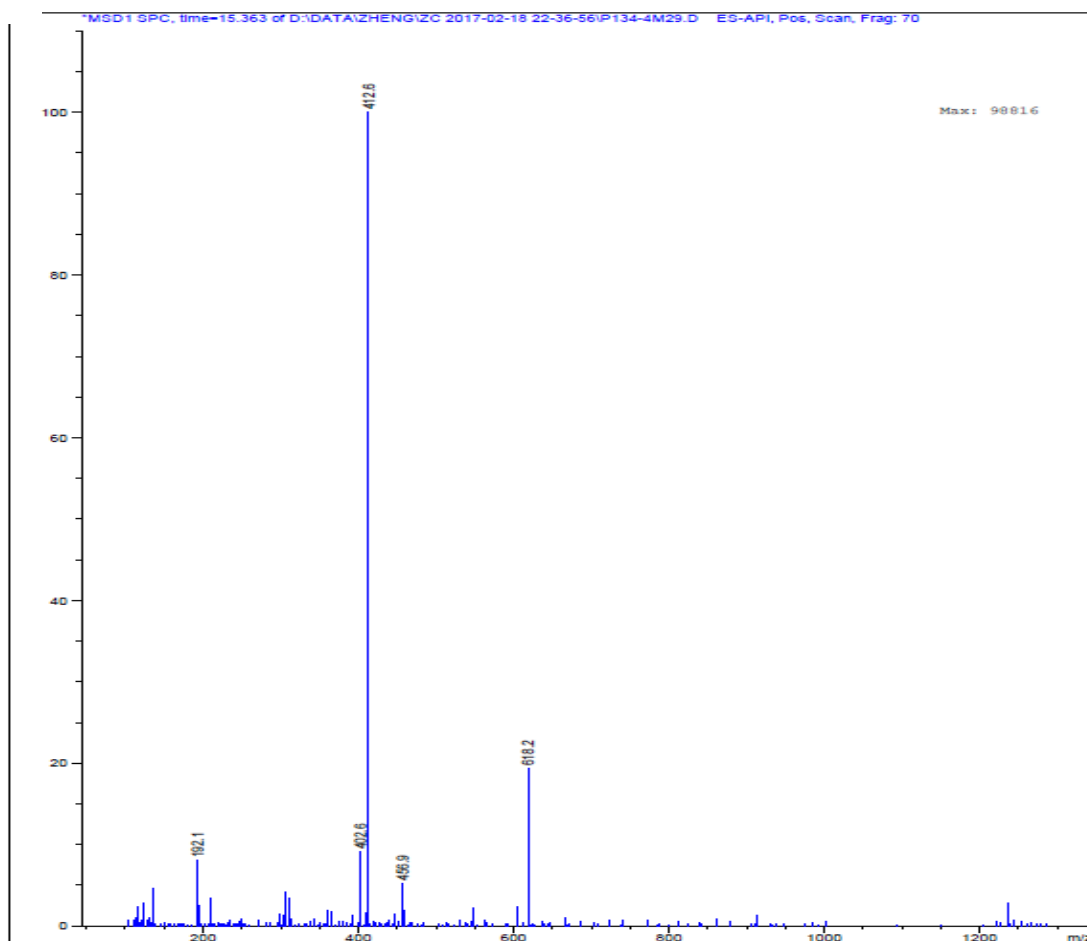
Figure S4.26 Reaction catalyzed by Mur29 with muraymycin D1 and CTP.

A, LC-MS analysis using muraymycin D1 and CTP after (I) 12 h reaction without Mur29, (II) 12 h reaction. B, mass spectrum for the ion peak eluting at time t = 15.363 min of Mur29 reaction with muraymycin D1. (D1-CMP, $C_{47}H_{75}N_{14}O_{23}P$, expected $(M+2H)^{2+}$ ion at m/z = 618.25, found: 618.2).
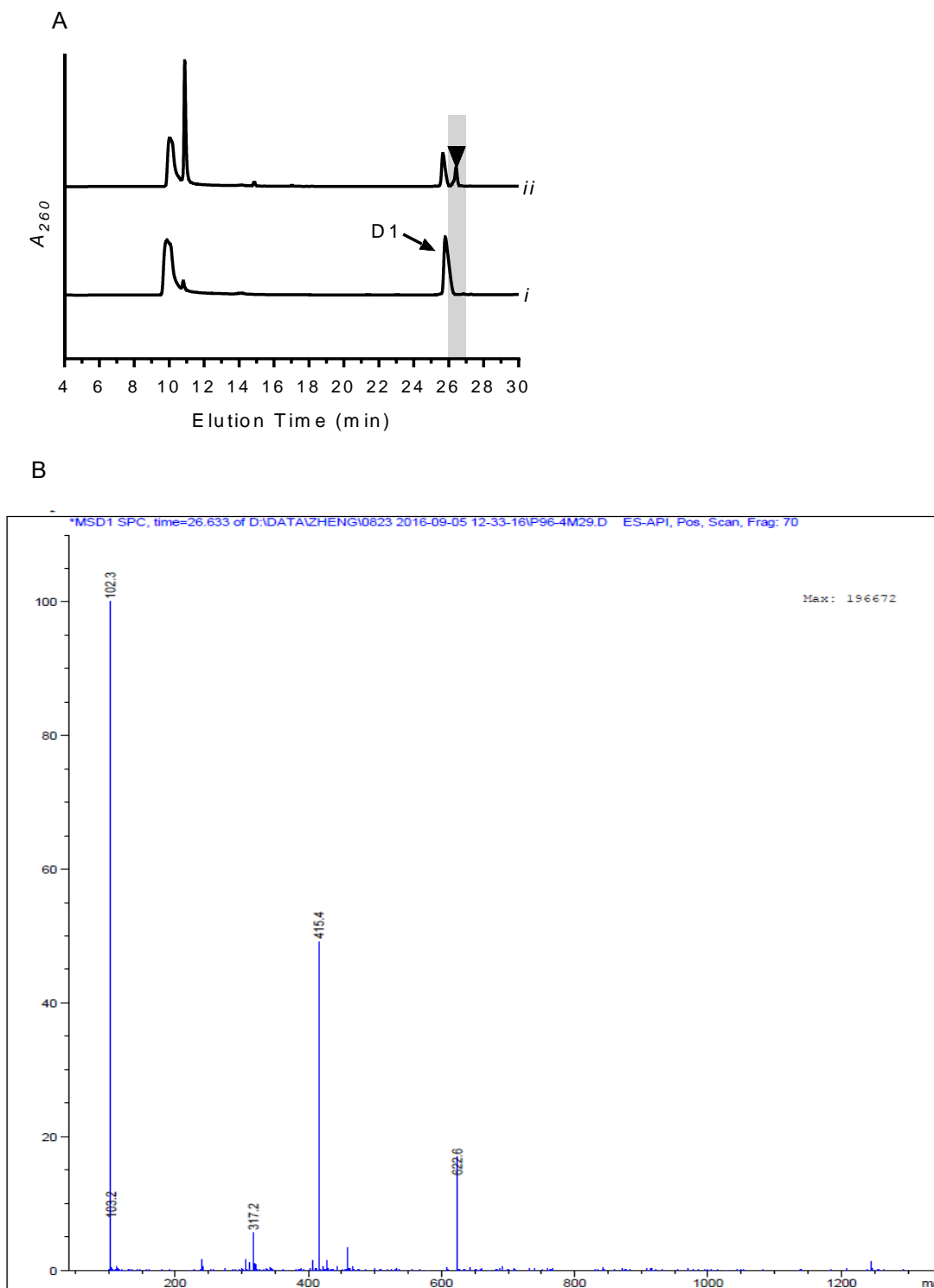
Figure S4.27 Reaction catalyzed by Mur29 with muraymycin D1 and dATP.

A, LC-MS analysis using muraymycin D1 and dATP after (I) 12 h reaction without Mur29, (II) 12 h reaction. B, mass spectrum for the ion peak eluting at time t = 26.633 min of Mur29 reaction with muraymycin D1. (D1-dAMP, C48H75N16O21P, expected $(M+2H)^{2+}$ ion at m/z = 622.25, found:622.6).
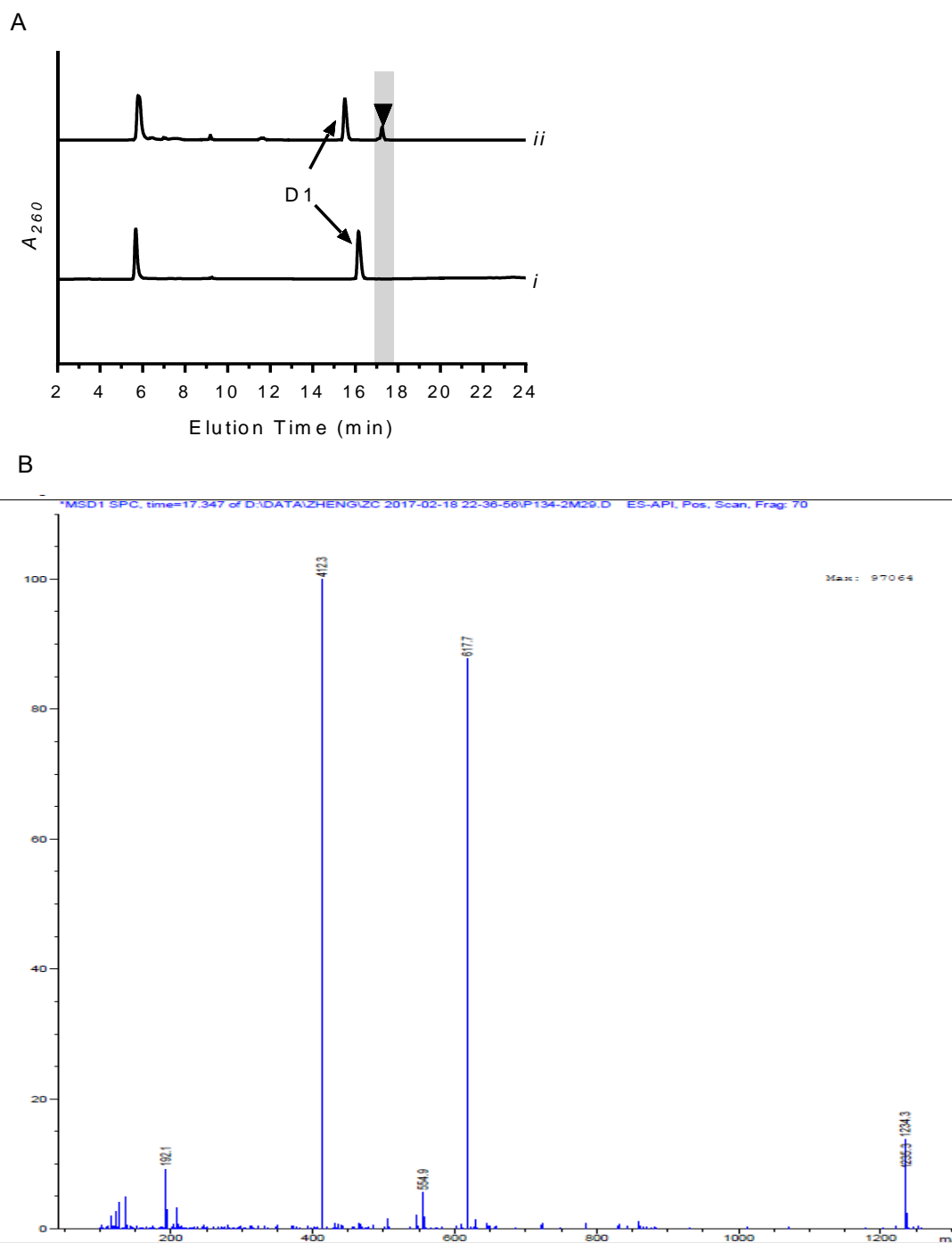
Figure S4.28 Reaction catalyzed by Mur29 with muraymycin D1 and dTTP.
A, LC-MS analysis using muraymycin D1 and dTTP after (I) 12 h reaction without Mur29, (II) 12 h reaction. B, mass spectrum for the ion peak eluting at time t = 17.347 min of Mur29 reaction with muraymycin D1. (D1-dTMP, C48H76N13O23P, expected (M+H)$^+$ ion at m/z = 1234.50, found: 1234.3).
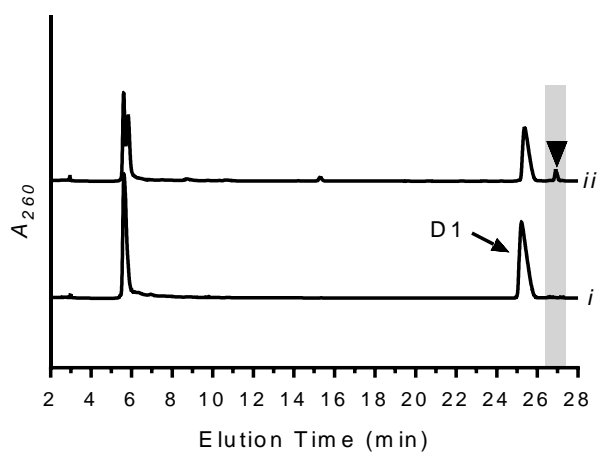
Figure S4.29 Reaction catalyzed by Mur29 with muraymycin D1 and UTP.

A, LC-MS analysis using muraymycin D1 and UTP after (I) 12 h reaction without Mur29, (II) 12 h reaction. B, mass spectrum for the ion peak eluting at time t = 26.986 min of Mur29 reaction with muraymycin D1. (D1-UMP, C47H74N13O24P, expected (M+H)$^+$ ion at m/z = 618.74, found: 618.9).
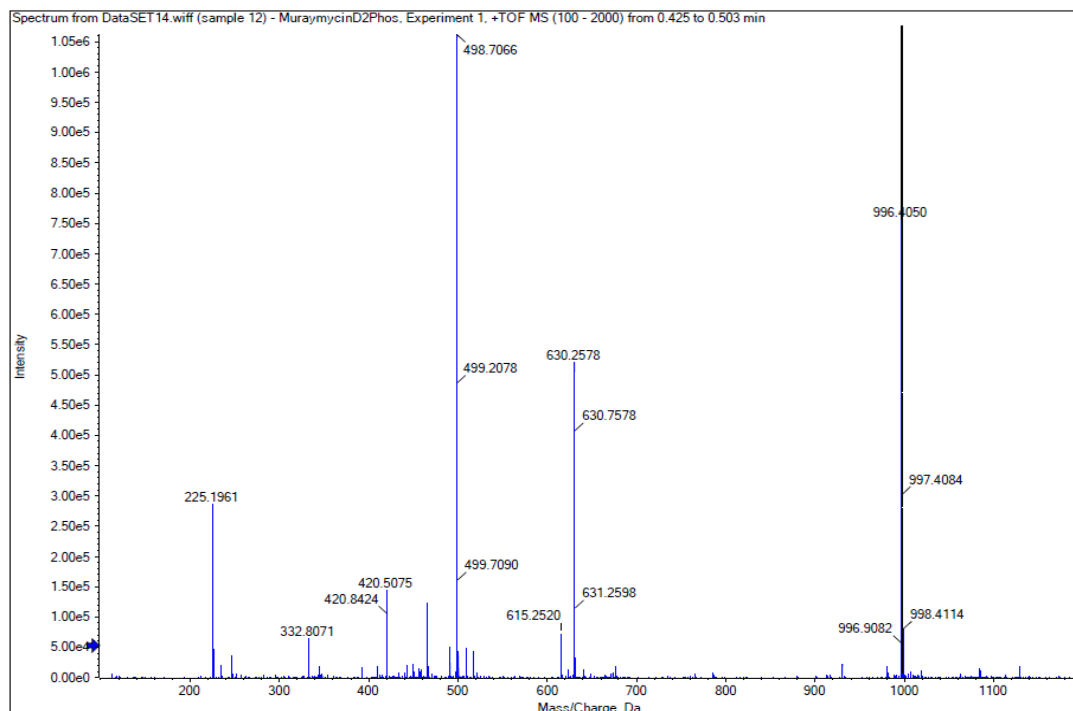
Figure S 4.30 (+)-HR-ESI-MS (positive mode) of compound D2-PHOS
(calcd for C37H62N11O19P, expected (M+H)$^+$ ion at m/z = 996.4034, found: 996.4050).
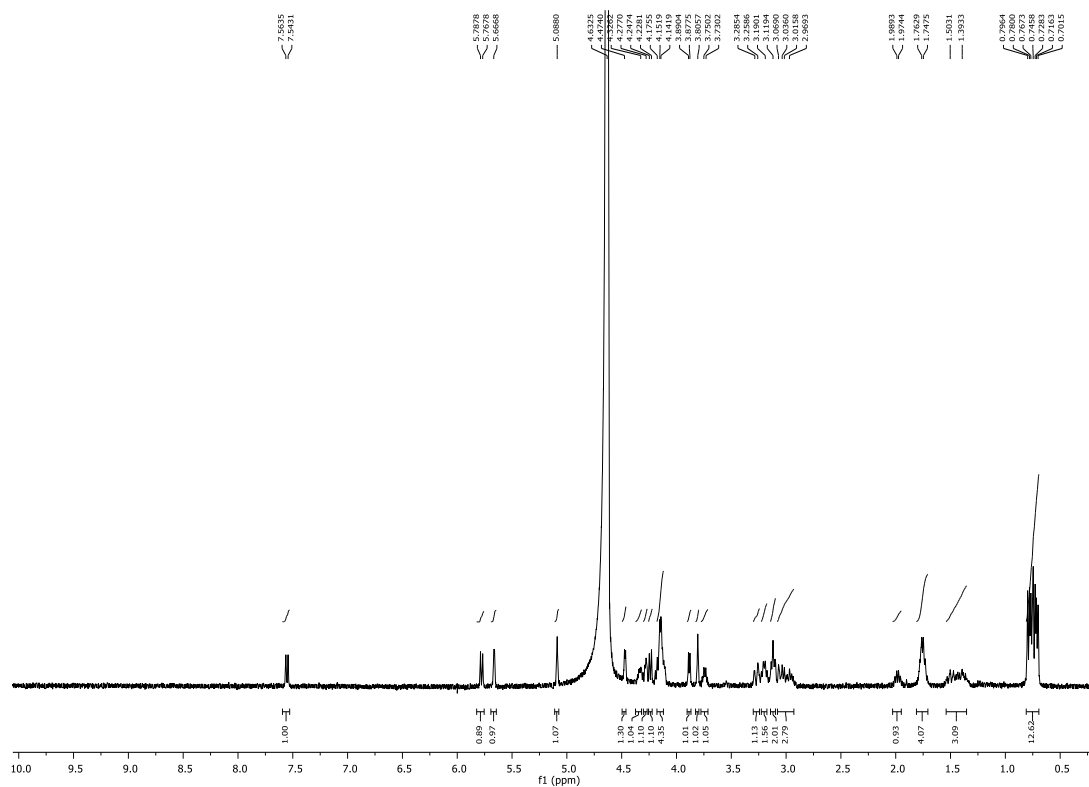
Figure S4.31 ^{1}H NMR spectrum (D$_2$O, 400 MHz) of muramycin D2-PHOS.
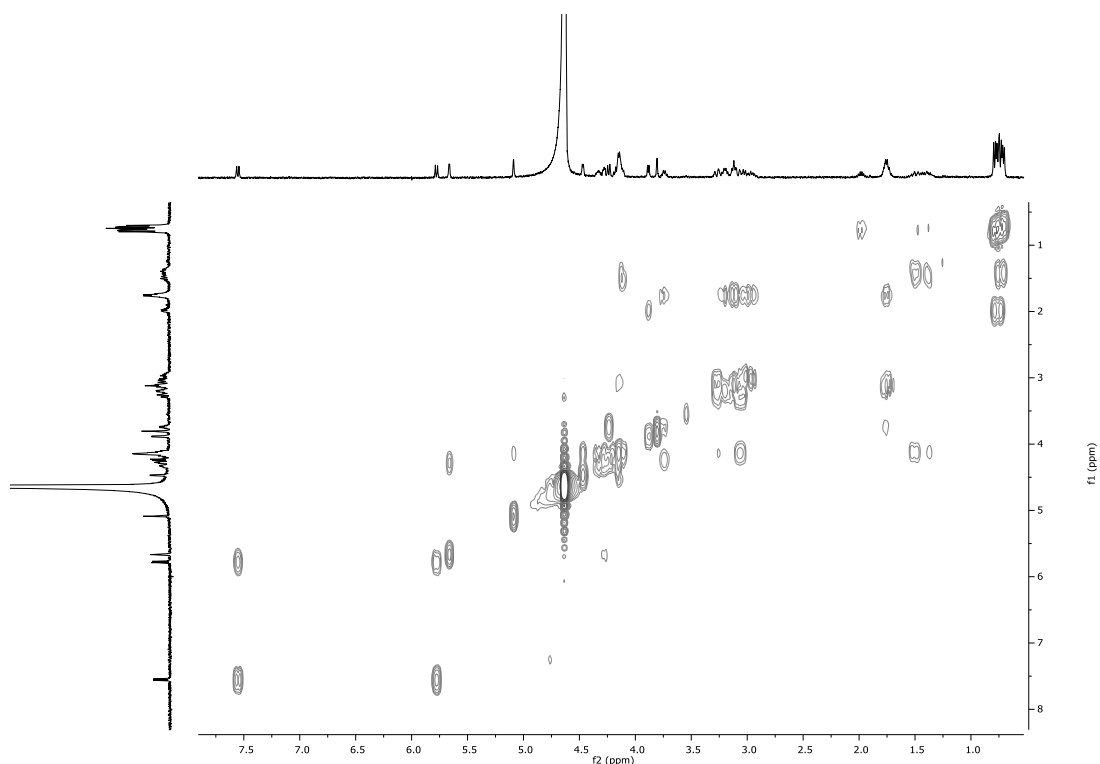
Figure S4.32 ^{1}H-^{1}H COSY spectrum (D$_2$O, 400 MHz) of muramycin D2 -PHOS.
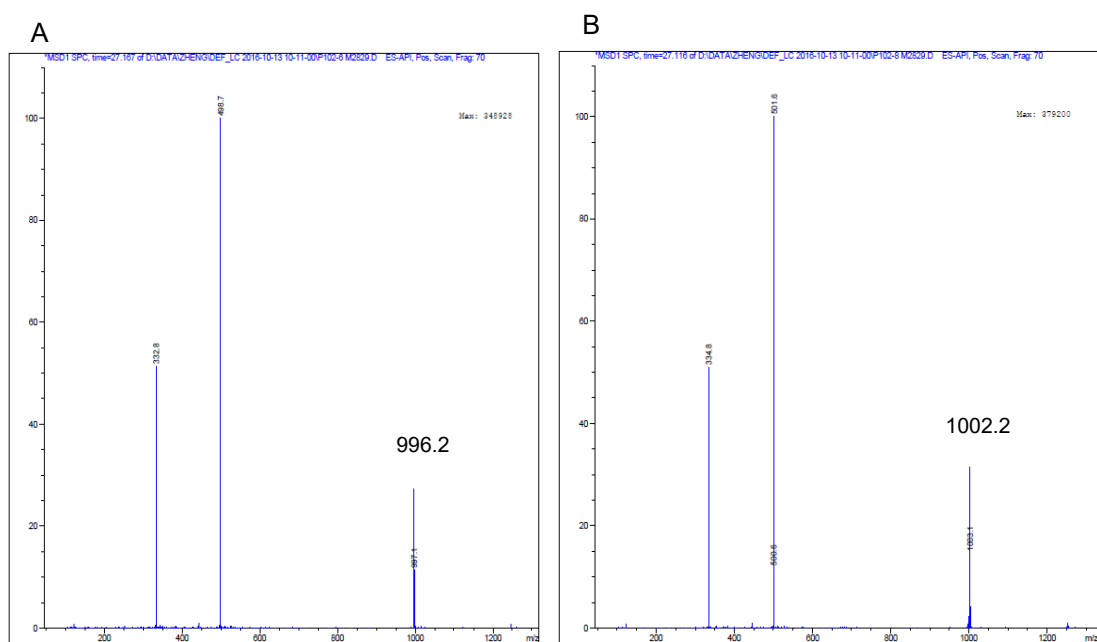
Figure S4.33 Reaction catalyzed by Mur28 with D2 and [γ-P^{18}O$_4$]ATP.
A, mass spectrum for the ion peak eluting at time t = 27.167 min of Mur28 reaction with muraymycin D2 and ATP. B, mass spectrum for the ion peak eluting at time t = 27.116 min of Mur28 reaction with muraymycin D2 and [γ-P^{18}O$_4$]ATP (*m/z* increased by 6 amu).
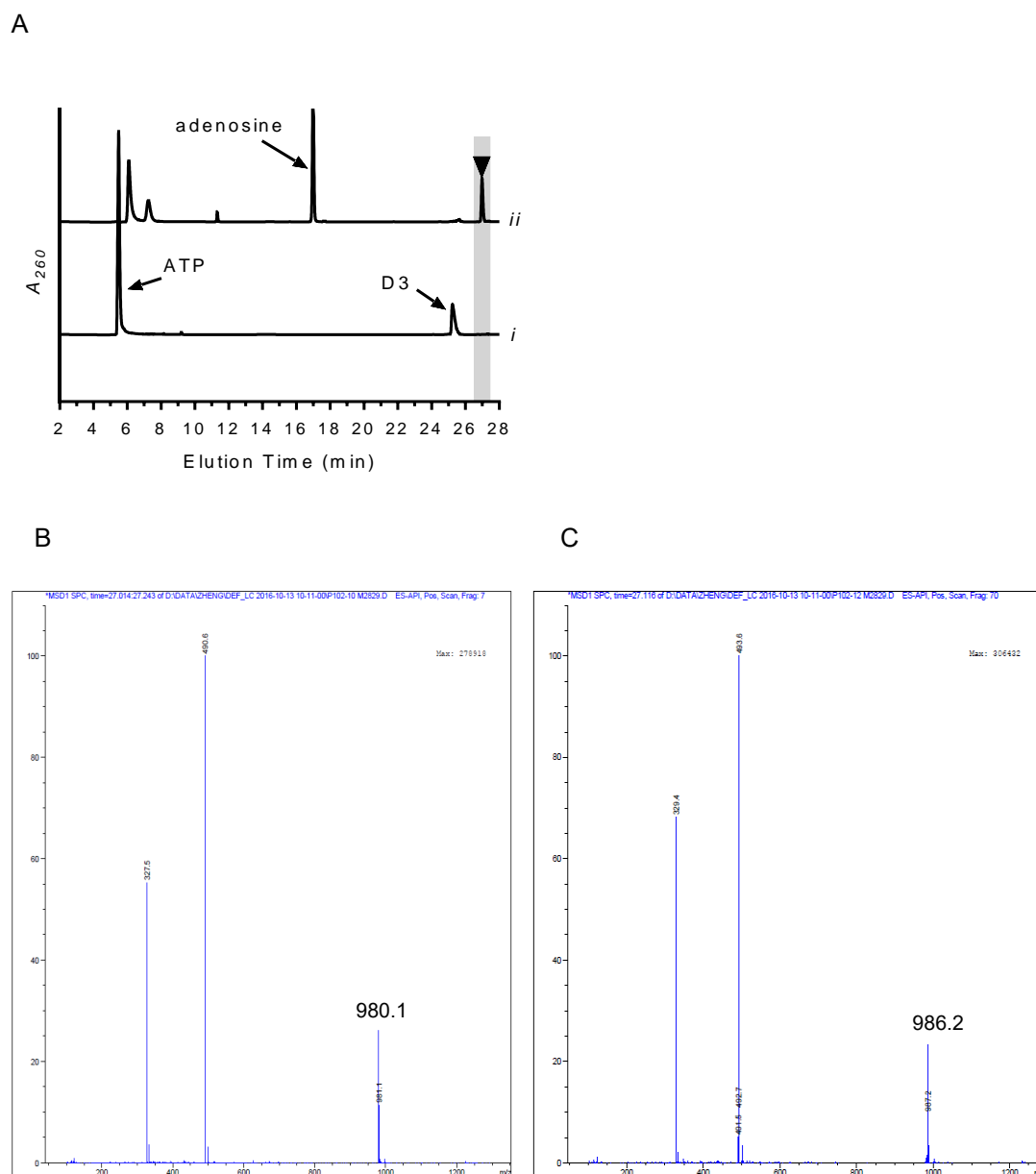
Figure S4.34 Reaction catalyzed by Mur28 with muraymycin D3 and ATP.
(A) LC-MS analysis using muraymycin D3 and ATP after (i) 12 h incubation without Mur29 and (ii) 12 h reaction. Data were collected using GP1. Adenosine was only observed when reactions were performed with excess enzyme and prolonged incubation, suggesting the formation is due to a contaminating phosphatase. (▼) denotes peak corresponding to D3-PHOS; A_{260}, absorbance units at 260 nm. (B) Mass spectrum of the D3-PHOS peak generated with natural-isotope abundance ATP. (C) Mass spectrum of the D3-PHOS peak generated with [γ-P^{18}O$_4$]ATP (m/z increased by 6.1 amu).
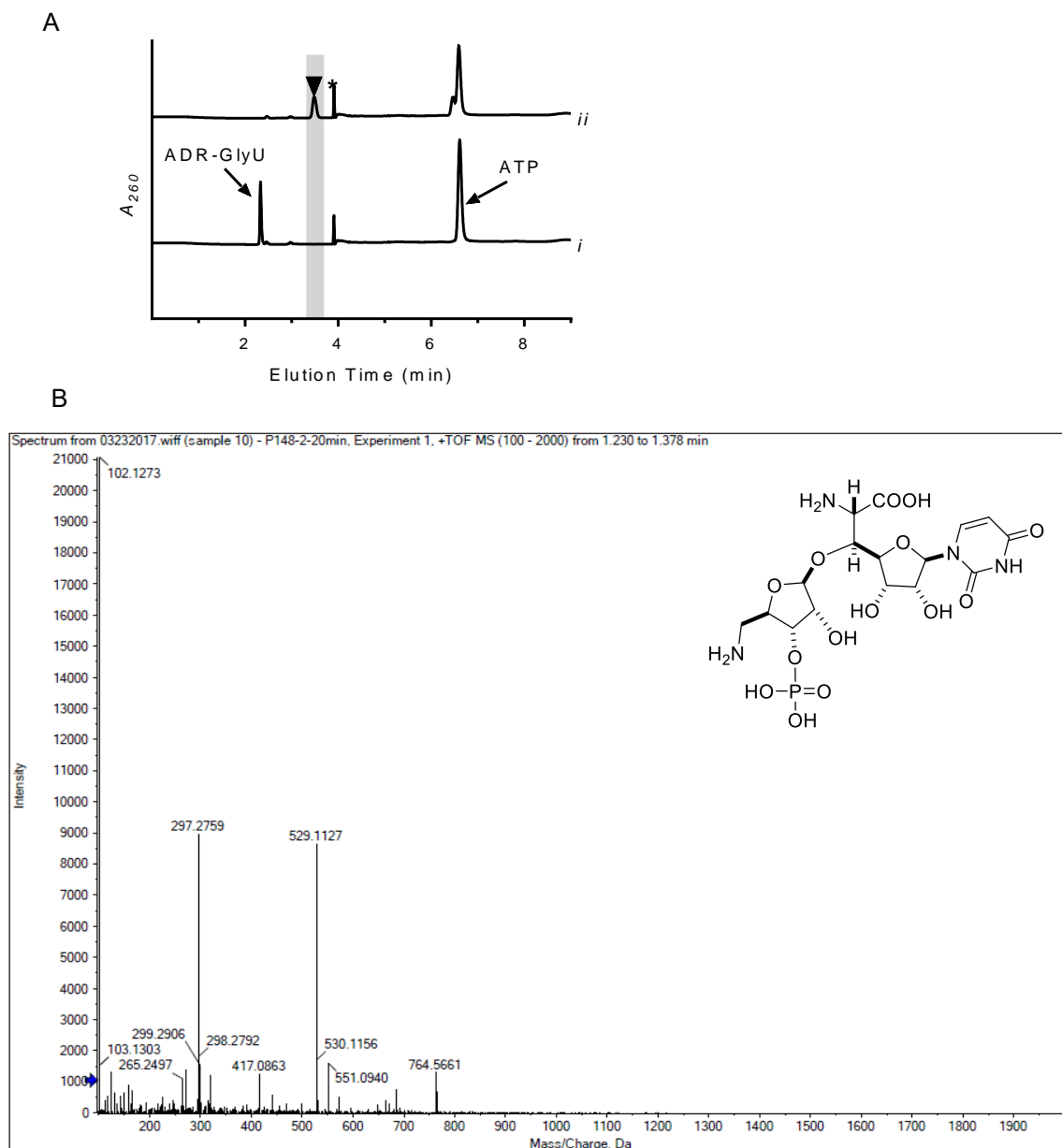
Figure S4.35 Reaction catalyzed by Mur28 with ADR-GlyU and ATP
(A) LC-MS analysis using ADR-GlyU and ATP after (i) 12 h incubation without Mur29 and (ii) 12 h reaction. Data were collected using GP3. (▼) denotes peak corresponding to ADR-GlyU-PHOS; (*) denotes unidentified peak; A_{260}, absorbance units at 260 nm. (B) (+)-HR-ESI-MS of compound ADR-GlyU-PHOS (calcd for $C_{16}H_{25}N_4O_{14}P$, expected $(M+H)^+$ ion at $m/z = 529.1178$, found: 529.1127).
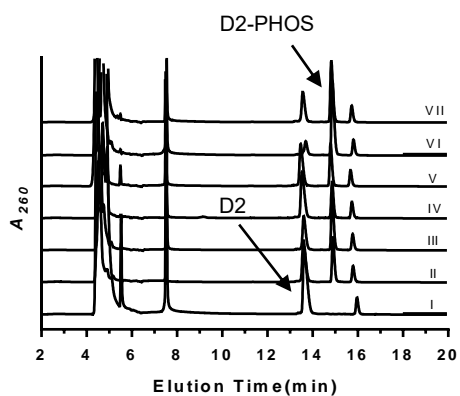
Figure S4.36 Reaction catalyzed by Mur28 with muraymycin D2 and different phosphate donors.
LC-MS analysis after 12 h reactions including (i) all nucleotides and without Mur28, (ii) CTP, (iii) GTP, (iv) TTP, (v) UTP, (vi) ATP, (vii) dATP. Data were collected using GP2. (▼) denotes peak corresponding to D2-PHOS; (*) denotes unidentified peak; A_{260}, absorbance units at 260 nm.
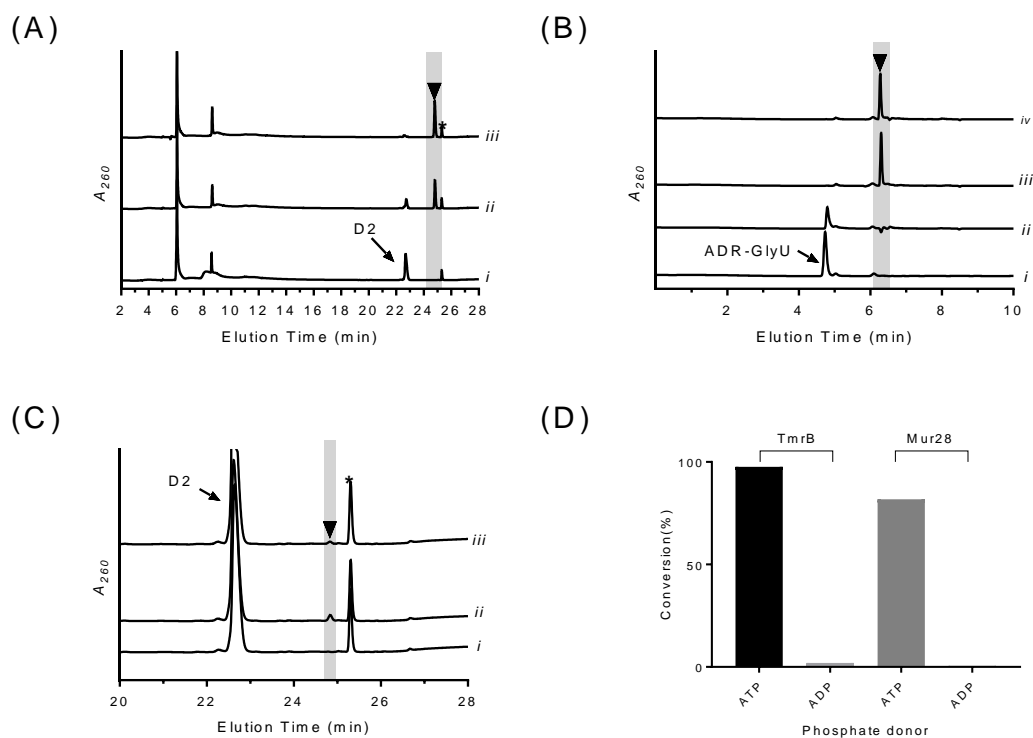
Figure S4.37 Reaction catalyzed by TmrB.

(A) LC-MS analysis using muraymycin D2 and ATP after (i) 12 h incubation without enzyme; (ii) 12 h reaction with Mur28; and (iii) 12 h reaction with TmrB. Data were collected using GP1. (▼) denotes peak corresponding to D2 -PHOS; (*) denotes unidentified peak; A_{260}, absorbance units at 260 nm. (B) LC-MS analysis using ADR-GlyU and ATP with (i) ADR-GlyU control and after (ii) 12 h incubation without enzyme, (iii) 12 h reaction with TmrB, and (iv) 12 h reaction with Mur28. Data were collected using GP4. (▼) denotes peak corresponding to ADR-GlyU-PHOS; A_{260}, absorbance units at 260 nm. (C) LC-MS analysis using muraymycin D2 and ADP after (i) 12 h incubation without enzyme, (ii) 12 h reaction with TmrB, and (iii) 12 h reaction with Mur28. Data were collected using GP1. (▼) denotes peak corresponding to D2 -PHOS; (*) denotes unidentified peak; A_{260}, absorbance units at 260 nm. (D) Comparison of muraymycin D2-PHOS formation with different phosphate donors.

Chapter 5 : A PLP and AdoMet Dependent Strategy for Aminopropyl Group

Incorporation in Nuceloside Antibiotics Biosynthesis

5.1 Introduction

Several nucleoside antibiotics represented by muraymycins from *Streptomyces* sp. NRRL30471[22], A-90289A from *Streptomyces* sp. SANK60405[81], Spharimicins from *Sphaerisporangium* sp. SANK60911[61] and FR-900493 from *Bacillus cereus* No2045[82] are structurally characterized with a high-carbon glycosylated aminopropyl uronic acid (Figure 5.1), which undergoes different modifications to form the final nucleoside antibiotic. SAR studies have shown that the 3-amino-3-carboxypropyl group is essential for the antibacterial activity of muraymycins.[21] Here we present the functional assignment of a butyric acid ribofuranosylated 5′-*C*-glycyluridine synthase and a PLP-dependent butyric acid decarboxylase. The results establish the first known PLP dependent enzymatic strategy for butyric acid incorporation.
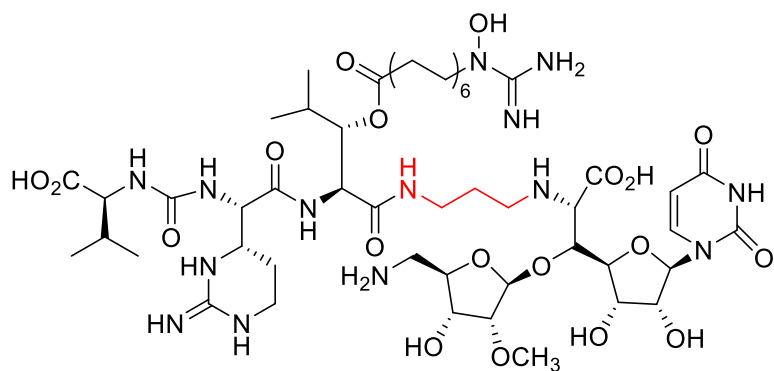
Muraymycin A1
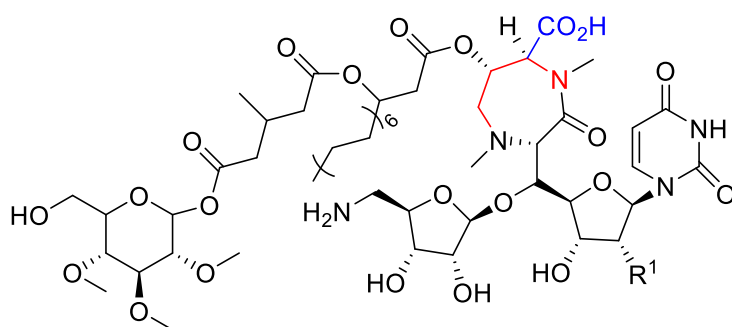
A-90289 A R^1=OSO$_3$H
Caprazamycin A R^1=OH
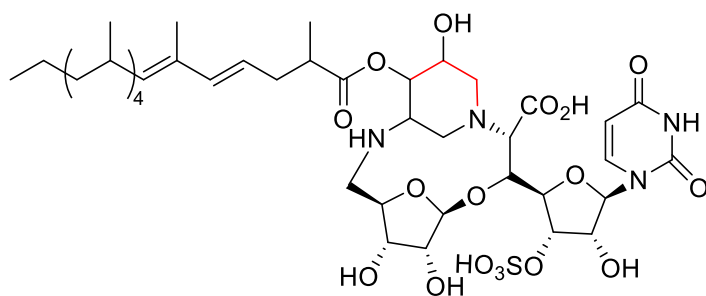
Sphaerimicin A
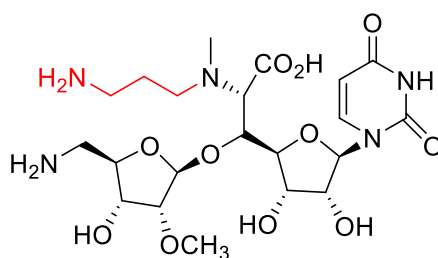
FR-900493

Figure 5.1 Structure of representative nucleoside antibiotics containing an aminopropyl moiety (highlighted in red).

5.2 Materials and Methods

5.2.1 Synthesis

5.2.1.1 Materials and Methods

Hydrogen chloride solution (4.0 M in dioxane), Boc-L-vinylglycine and solvents were purchased from Sigma-Aldrich (St. Louis, MO), and used without further purification. Compound **7** was kindly provided by Prof. Christian Ducho (Department of Pharmacy, Saarland University, Germany). All NMR data was recorded at 400 MHz for ^{1}H and 100 MHz for ^{13}C with a Varian Inova NMR spectrometer (Agilent, Santa Clara, CA). LC-MS was conducted with an Agilent 6120 Quadrupole MSD mass spectrometer (Agilent Technologies, Santa Clara, CA) equipped with an Agilent 1200 Series Quaternary LC system and an Eclipse XDB-C18 column (150 × 4.6 mm, 5 μm). HR-ESI-MS spectra were acquired with an AB SCIEX Triple TOF 5600 System (AB Sciex, Framingham, MA, USA). HPLC analysis was performed on an Agilent 1200 system equipped with a photodiode array (PDA) detector and an analytical ZIC®-HILIC column (250 mm x 4.6 mm, 5 μm).

5.2.1.2 Disaccharide Phosphate, **8**
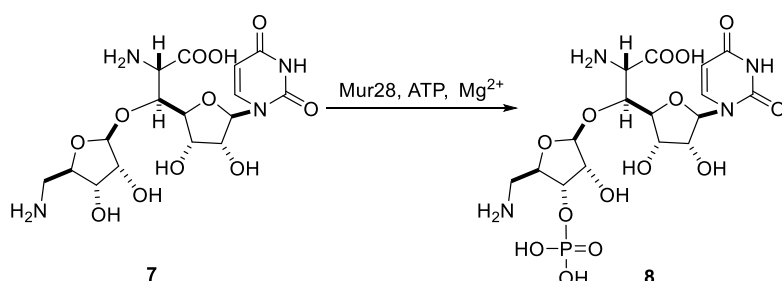
The reaction mixture consisted of 25 mM potassium phosphate (pH 8.5), 500 μM **7**, 2 mM MgCl$_2$, 2 mM ATP and 200 nM Mur28 was incubated at 30 °C. The reaction was terminated

by ultrafiltration using a Microcon YM-3. **8** was purified by HPLC with HILIC column. The separation gradient is shown in Table S5.2. The peak corresponding to the product **8** was collected and freeze-dried as white solid prior to analysis.

5.2.1.3 L- Vinylglycine
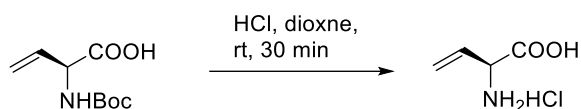
An aliquot (500 μL) of hydrogen chloride solution (4.0 M in dioxane) was added to Boc-L-vinylglycine (10 mg), and the mixture was stirred at room temperature for 30 min. Upon completion of the reaction the volatiles were evaporated and the resulting mixture was dissolved in DI water. The aqueous solution was freeze-dried twice from water as an off-white solid prior to analysis.

5.2.2 Isotopic Enrichment

5.2.2.1 Fermentation, Extraction, Isolation, and Purification of Muraymycin D1

Streptomyces sp. NRRL30475 was cultivated in 250 mL Erlenmeyer flasks containing 50 mL TSBG (Tryptic soy broth (Difco) supplemented with 20 g/L glucose) at 30 °C on a rotary shaker (250 rpm) for 72 h. The seed culture was used to inoculate flasks (250 mL) containing 50 mL PM-1 medium[83]. PM-1 was composed of glucose 2%, soluble starch 1%, pressed yeast 0.9%, peptone (Bacto) 0.5%, meat extract (Fluka) 0.5%, NaCl 0.5%, $CaCO_3$ 0.3% and CB-442 (NOF Co., Ltd.) 0.01% (pH 7.4, before sterilization). The fermentation was continued for 7 days at 23 °C on a rotary shaker (210 rpm).

All culture flasks were combined and centrifuged at 5000 rpm for 15 min to separate

the mycelium and water phase. The mycelial-cake portion was extracted with MeOH by sonication, and the organic phase was evaporated to obtain a brown crude extract.

Amberlite XAD-16 (4%) resin was added to the water phase and stirred for 12 h. The resin was washed with water until the effluent became colorless, and then eluted with methanol. The MeOH extract was concentrated under reduced pressure to obtain a crude extract.

Components of the mycelium crude extract and water phase crude extract were subjected to Sephadex LH-20 (25-100 μm GE Healthcare) column, and MeOH was used to elute compounds at a flow rate at 2 mL/min. The major fraction was further purified by using semipreparative HPLC. The separation gradient used for semipreparative analysis is shown in Table S5.3.

5.2.2.2 Isotopic Enrichment

Fermentation media and growth conditions for *Streptomyces* sp. NRRL30475 are described above. A seed culture was incubated at 30 °C for 72 h, when 2 ml was used to inoculate 50 mL fresh medium. After fermentation for 65 h, 25 mg of filter-sterilized L-[$^{13}C_5$,^{15}N]Met or L- [$^{13}C_4$,^{15}N]Asp (Cambridge Isotope Laboratories, Inc) was added to each flask (50 mL of liquid medium in a 250 mL flask). Fermentation was continued an additional 72 h. Muraymycin D1 were extracted and purified as described in section 5.2.2.1. Purified muraymycin D1 was analyzed by NMR, and relative peak intensities were assigned based on uronic acid C-1 from the natural abundance ^{13}C NMR spectra.

5.2.3 Heterologous Protein Expression

5.2.3.1 Materials and Bacterial Strains

Synthetic oligonucleotides were purchased from Integrated DNA Technologies (Coralville, IA). Phusion DNA polymerase, restriction enzymes and T4 DNA ligase were obtained from New England Biolabs Inc (Ipswich, MA) and used according to the manufacturer's instructions. LA-Taq polymerase were obtained from Takara Bio Inc. (Shiga, Japan). Routine DNA sequencing was carried out at ACGT Inc. Competent *E. coli* NEB® 5-alpha and BL21(DE3) from New England Biolabs (Ipswich, MA) and *S. lividans* TK24 were used for routine cloning and protein expression.

5.2.3.2 Protein Expression Constructs

5.2.3.2.1 Cloning Genes of *mur23*, *mur24 and lipJ*

The gene for *mur23* and *mur24* was amplified from genomic DNA extracted from *Streptomyces* sp. NRRL30473 by PCR using Phusion DNA polymerase (primers listed in Table S5.1). Genomic DNA of *Streptomyces* sp. NRRL30473 was extracted using UltraClean Microbial DNA Isolation Kit (MoBio laboratories, Inc) following manufacturer's protocol. DNA quality and concentration were confirmed using Nanodrop 2000c spectrophotometer (Thermo Scientific) and gel electrophoresis. The gel-purified PCR product was digested with NdeI-BamHI and ligated to the identical sites of pXY200 to yield pXY200-*mur23* and pXY200-*mur24* following the standard protocol and confirmed by DNA sequencing.

5.2.3.2.2 Site-directed Mutagenesis

A K70A point mutation of Mur23, K234A of Mur24 and F201Y of Mur24 was generated by PCR amplification with Q5 hot start high-fidelity DNA polymerase using pET30-*mur23* or pET30-*mur24* as a template, respectively. The template, pET30-*mur23* and pET30-

mur24, was obtained using ligation-independent cloning with pET-30 Xa/LIC vector following the provided protocol. The template DNA after the PCR amplification was digested with 10 units of DpnI for 2 h at 37 °C and transformed into *E. coli* NEB5α competent cells. The sequence of the entire gene with the introduction of the correct point mutation were confirmed by DNA sequencing to yield pET30-*mur23* (K70A), pET30-*mur24* (K234A) and pET30-*mur24* (F201Y), all of which were digested with NdeI-BamHI and the DNA fragment of the expected size was purified and ligated to the identical sites of pXY200 to yield pXY200-*mur23* (K70A), pXY200-*mur24* (K234A) and pXY200-*mur24* (F201Y) were yielded following the same procedure as described above.

5.2.3.3 Heterologous Protein Expression

Plasmids pXY200-*mur23,* pXY200-*mur24,* pXY200-*mur23* (K70A), pXY200-*mur24* (K234A) and pXY200-*mur24* (F201Y) were transformed into *S. lividans* TK24 using PEG-mediated protoplast transformation and plated on R2YE supplemented with 50 μg/mL apramycin. After 6 days at 28 °C, positive transformants were confirmed by colony PCR using InstaGene Matrix from Bio-Rad (Hercules, CA) and LA-Taq polymerase with GC buffer I.

The recombinant strain was utilized to inoculate 50 mL R2YE containing 50 μg/mL apramycin, grown for 3 days at 28 °C at 250 rpm, and 2 mL transferred to fresh 100 mL containing 50 μg/mL apramycin. Following growth for 3 days at 28 °C at 250 rpm, protein expression was induced by addition of thiostrepton (5 μg/mL) and the culture was incubated for another 24 h before harvesting. The cells from 400 mL of culture were collected by centrifugation. The pellet was thoroughly resuspended in ice-

cold Buffer A supplemented with 4 mg/mL of lysozyme was subsequently added to the suspension. After incubation at 30 °C for 30 min, the cell suspension was mixed by pipetting and lysed using a Qsonica sonicator (Qsonica LLC, Newtown, CT) for sonication for a total of 10 min at 40% amplitude with 30 s pulses separated by 30 s rest periods. Cells were harvested after an overnight incubation at 18 °C and lysed in Buffer A (100 mM KH_2PO_4, 300 mM NaCl, 10 mM imidazole, pH 8.3) using a Qsonica sonicator (Qsonica LLC, Newtown, CT) for sonication for a total of 6 min at 40% amplitude with 30 s pulses separated by 30 s rest periods. Following centrifugation the protein was purified using affinity chromatography with HisPurTM Ni-NTA agarose (Thermo Scientific, Rockford, IL), and proteins were eluted with increasing concentrations of imidazole in Buffer A. Purified proteins were concentrated and buffer exchanged into Buffer B (25 mM KH_2PO_4, 100 mM NaCl, pH 8.3) using Amicon Ultra 10000 MWCO centrifugal filter (Millipore) and stored as glycerol stocks (40%) at -20 °C. Protein purity was assessed as by 12% acrylamide SDS-PAGE; His_6-tagged proteins were utilized without further modifications. Protein concentration was determined using UV/Vis spectroscopy, and the extension coefficients were calculated using the ProtParam tool available from ExPASY (Mur23 $\varepsilon_{280} = 44522$ $M^{-1}cm^{-1}$; Mur24 $\varepsilon_{280} = 53922$ $M^{-1}cm^{-1}$.

5.2.4 Enzyme Assays

5.2.4.1 Materials and Methods

S-(5-Adenosyl)-L-methionine chloride dihydrochloride (AdoMet), 1-aminocyclopropanecarboxylic acid (ACC), 3-methyl-2-benzothiazolinone hydrazine

hydrochloride (MBTH), PLP and ATP were purchased from Sigma-Aldrich (St. Louis, MO),

[(3S)-3-amino-3-carboxypropyl] (dimethyl)-sulfonium iodide (SMM) was obtained from VWR

(Radnor, PA), 6-aminoquinolyl-N-hydroxysuccinimidyl carbamate (AQC) was purchased from

Apollo Scientific (Denton, Manchester) and used without further purification. All NMR data

were recorded at 400 MHz for ^{1}H and 100 MHz for ^{13}C with a Varian Inova NMR spectrometer

(Agilent, Santa Clara, CA). LC-MS was conducted with an Agilent 6120 Quadrupole MSD

mass spectrometer (Agilent Technologies, Santa Clara, CA) equipped with an Agilent 1200

Series Quaternary LC system. HR-ESI-MS spectra were acquired with an AB SCIEX Triple

TOF 5600 System (AB Sciex, Framingham, MA, USA). HPLC analysis was performed on an

Agilent 1200 system equipped with a photodiode array (PDA) detector and an analytical ZIC®-

HILIC column (250 mm x 4.6 mm, 5 μm) and an analytical Apollo C18 column (250 mm x 4.6

mm, 5 μm).

5.2.4.2 Tandem Enzymatic Reaction with Mur28, Mur24 and Mur23

The assay mixture for the reaction consisted of 25 mM potassium phosphate (pH 8.3),

500 μM **7**, 500 μM AdoMet, 1 mM ATP, 1 mM MgCl$_2$, 100 μM PLP, and 200 nM Mur28,

Mur24 and Mur23 at 30 °C, and the reaction was subsequently quenched by adding two

volumes of acetonitrile followed by centrifugation (14000 rpm, 30 min) to remove the

precipitated protein. The reaction components were analyzed by HPLC using C-18 reverse-

phase column with gradient shown in Table S5.4 or monitored by HPLC using ZIC®-HILIC

column with the gradient shown in Table S5.2 with detection at 260 nm. 6-aminoquinolyl-N-

hydroxysuccinimidyl carbamate (AQC), a derivatizing reagent for amines, was used for pre-

column derivation. The reaction 20 μL was mixed with 60 μL of 0.2M sodium borate buffer

(pH = 8.8) and 20 μL 3 mg/ mL AQC acetonitrile solution. The mixtures were incubated at 55 °C for 10 min and then allowed to cool to room temperature. The AQC-derivatized samples (50 μL) were applied to LC-MS using C-18 reverse-phase column with detection at 260 nm with gradient shown in Table S5.5.

5.2.4.3 Butyric Acid Incorporation Activity of Mur24

Reactions consisted of 25 mM potassium phosphate (pH 8.3), 500 μM **8**, 500 μM potential aminopropyl donor (AdoMet, SMM, L-VG or ACC), 100 μM PLP and 200 nM enzyme (Mur24, Mur24 (K234A), Mur24 (F201Y) at 30 °C and the reaction was terminated by adding two volumes of acetonitrile followed by centrifugation (14000 rpm, 30 min) to remove the precipitated protein. The reaction was monitored by LC-MS using ZIC®-HILIC column with gradient shown in Table S5.2 with detection at 260 nm. Large scale production of the Mur24 product **9** was identical to the reactions described above and isolated by HPLC using ZIC®-HILIC column.

5.2.4.4 Deaminase Activity of Mur24 or LipJ

Reactions for identification of α-ketobutyrate consisted of 50 mM potassium phosphate (pH 8.3), 500 μM potential aminopropyl donor, 100 μM PLP and 400 nM or 4 μM enzyme at 30 °C and the reaction was terminated by ultrafiltration using a Microcon YM-3. Reaction mixtures were treated with MBTH as follows according to the method described by Tanaka[54]. 50 μL reaction mixtures were mixed with 50 μL of 1 M sodium acetate (pH 5.0) and 50 μL of 8 mM MBTH aqueous solution. The mixtures were then incubated at 50 °C for 30 min and then analyzed by LC-MS with the gradient shown in Table S5.6 with detection at 325 nm.

5.2.4.5 Activity of Mur23

Reactions consisted of 25 mM potassium phosphate (pH 8.3), 500 μM **9**, 100 μM PLP and 200 nM Mur23 or Mur23 (K70A) at 30 °C and the reaction was terminated by adding two volumes of acetonitrile followed by centrifugation (14000 rpm, 30 min) to remove the precipitated protein. The reaction was monitored by LC-MS using ZIC®-HILIC column with the gradient shown in Table S5.2 with detection at 260 nm. Large scale production of the Mur23 product **10** was identical to the reactions described above and was isolated by HPLC using ZIC®-HILIC column.

5.2.4.6 Kinetics of Mur24

Assays consisted of 25 mM potassium phosphate (pH 8.3), 100 μM PLP, near saturating AdoMet (2 mM) with variable **8** (5 μM–500 μM). The reaction was performed at 30 °C with 200 nM Mur24 for 3 h and analyzed under initial velocity conditions. Product formation was determined using HPLC with gradient shown in Table S5.2. Each data point represents a minimum of three replicate end point assays; kinetic constants were obtained by nonlinear regression analysis using GraphPad Prism (GraphPad Software, La Jolla, CA).

5.2.4.7 Kinetics of Mur23

Assays consisted of 25 mM potassium phosphate (pH 8.3), 100 μM PLP with variable **8** (5 μM–1000 μM). The reaction was performed at 30 °C with 50 nM Mur23 for 1 h and analyzed under initial velocity conditions. Product formation was determined using HPLC with gradient shown in Table S5.2. Each data point represents a minimum of three replicate end point assays; kinetic constants were obtained by nonlinear regression analysis using GraphPad Prism

(GraphPad Software, La Jolla, CA).

5.3 Results and Discussion

5.3.1 Bioinformatic Analysis of Mur23 and Mur24

Blast analysis revealed that Mur24 belonged to pyridoxal-5'-phosphate (PLP) dependent aspartate aminotransferase family (type I), members of which have a diverse set of functions including transamination, racemization, decarboxylation, and various side-chain reactions. However, sequence analysis of Mur24 didn't show modest sequence identity (>30%) to any characterized enzyme. Two clues shed light on our proposed function of Mur24, especially after comparison of the biosynthetic gene clusters among other nucleoside antibiotics. One is that Mur24 has 45% sequence identity (Cover 95%) to DNA binding transcription regulator (SCL26195.1) that belongs to MocR family, the mechanism of which hasn't been well understood yet. This similarity, however, suggested that Mur24 potentially uses a nucleoside as a substrate. Another is that Mur24 has 27% sequence identity (Cover 41%) to ACC synthase-like protein (XP0213717 68.1). Mur23 has modest sequence identity to several proteins annotated as PLP dependent diaminopimelate decarboxylase.

Comparison among A-90289, caprazamycin and spharimicin biosynthetic gene cluster revealed that Mur24 homolog is shared by the four gene clusters, while only sphaerimicin gene cluster has Mur23 homolog. Structure comparison of the four nucleoside antibiotics revealed that the four nucleoside antibiotics share the similar aminopropyl group (Figure 5.1 highlighted in red), and both A-90289 and caprazamycin retain the carboxylate group (Figure 5.1 highlighted in blue) while both muraymycin and spharimicin do not. The bioinformatics

158

analysis above led us to propose the pathway that Mur24 catalyzes the aminobutyric acid incorporation, followed with decarboxylation reaction catalyzed by Mur23.

5.3.2 Feeding Experiments: the Source of the Aminopropyl Group

Two potential pathways for incorporation of aminopropyl group were proposed, inspired by the characterized polyamine[84] and staphylopine[85] biosynthetic pathways. From analysis of these two pathways, S-adenosylmethionine or aspartate β-semialdehyde serve as aminopropyl group donors prior to further downstream modification by distinct enzymes.

In order to determine which precursor is the authentic donor of the aminopropyl group in muraymycins, universal labeled L-methionine (L-Met) or L-aspartic acid (L-Asp) was fed to the muraymycin D1 producer *Streptomyces* sp. NRRL30475 at the onset of production. Analysis by ^{13}C NMR spectroscopy revealed enriched resonances (average enrichment = 12%) with fermentation fed with L-Met (Figure 5.2). The ^{13}C-NMR resonances showed four carbon resonances at δ25.0 (t), 35.8 (dd), 45.5 (d) and 57.9 (s) with increased abundance flanking the other natural singlets, indicating that methionine is the origin of C1-C3 of aminopropane moiety and 2′-O-methyl group of the aminoribose moiety of muraymycin. In contrast no significant enrichment was observed with L-Asp. Mass analysis and extraction of the NMR coupling constants were also consistent with retention of the N atom from L-Met in the final muraymycin.
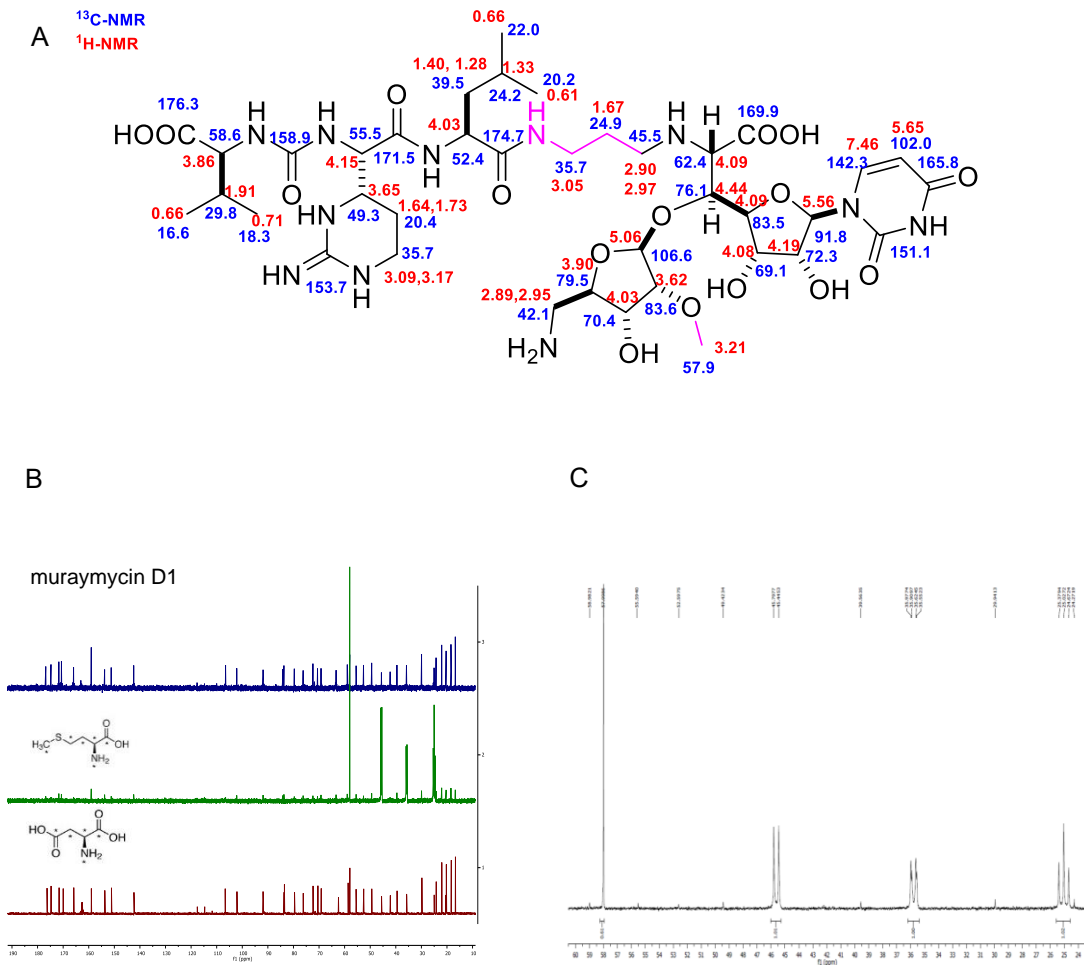
Figure 5.2 ^{13}C NMR spectrum of isotope labelled muraymycin D1.

(A) Chemical shift assignment for muraymycin D1. (B) ^{13}C NMR spectra of muraymycin D1 fed with L-Methionine ([13]C5, 99%; ^{15}N, 98%) and L-Aspartic acid ([13]C4, 99%; ^{15}N, 99%), respectively. (C) Zoom in part of signal of ^{13}C NMR spectra of muraymycin D1 fed with L-methionine.

160

5.3.3 Six-enzyme Biosynthesis of Amino Disaccharide, compound **7**: the Aminopropyl Group Acceptor

Since muraymycin has a similar disaccharide moiety of A-90289, we compared the biosynthetic gene cluster of muraymycin with that of A-90289. Six genes (*mur16*, *mur17*, *mur18*, *mur19*, *mur20*, and *mur26*) have modest similarity to genes in A-90289 that are responsible for the biosynthesis of the disaccharide moiety.[47, 49, 55] However, the glycosyltransferase (LipN) in A-90289 biosynthetic pathway was only confirmed to utilize uridine as a surrogate aminoribose acceptor. The functions of the six enzymes were confirmed individually upon *in vitro* characterization (Figure 5.3) (details shown in chapter 3), and Mur19 was shown to utilize GlyU as an acceptor to produce **7** with in situ generated activated amino ribose **6**. Notably, aminopropyl GlyU cannot be utilized by Mur19 to produce **7**, which suggests that aminopropyl group was added after the formation of **7**.
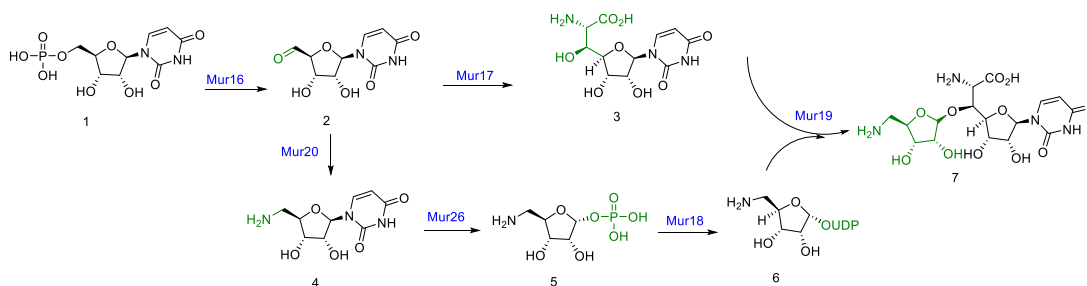
Figure 5.3 Biosynthesis of the amino disaccharide moiety of muraymycins.

5.3.4 Function Assignment of Mur23 and Mur24

To interrogate the mechanism of aminopropane incorporation, Mur23 and Mur24 were expressed in *E. coli*; however, the recombinant protein was completely insoluble under a variety of expression conditions. In contrast, expression in *S. lividans* TK24 yielded soluble proteins (Mur23, 5.8 mg/L, Mur24, 5.1 mg/L) (Figure S5.1A). Mur23 was yellowish and shown to co-

purify with PLP cofactor by UV/vis spectroscopy (Figure S5.1B), while Mur24 was purified

with bound PLP only when purification buffers were supplemented with PLP.

Based on the confirmed biosynthetic pathway of **7**, we initially proposed **7** as the

aminopropyl group acceptor (Figure 5.4A), and incubated Mur24 and Mur23 with **7** and L-Met

derived aminopropyl group donors including L-Met, AdoMet and SMM, but observed no

reaction by both HPLC and LC-MS after pre-column primary amine derivation with 6-

aminoquinolyl-N-hydroxysuccinimidyl carbamate (AQC).

Since the initially proposed product **7** only lacks N-methylation compared to

nucleoside antibiotic FR-900493, we suspected that **7** might also have inhibitory effect to

bacteria and therefore a self-resistance modification of the acceptor might be required before

the incorporation of the aminopropyl group. Careful analysis of the gene cluster of muraymycin,

two ORFs (*mur28* and *mur29*) have sequence similarity to proteins predicted to belong to

aminoglycoside resistance enzymes. In chapter 4, we reported the respective activity of Mur28

and Mur29. To our surprise, by single substrate kinetics we found that Mur28, which was a

kinase, preferred utilizing the precursor of muraymycin, **7**, as its substrate; while a series of

muraymycin congeners showed inhibition to Mur28 at high concentration. However, Mur29, a

nucleotidyltransferase, can only catalyze muraymycins rather than its precursor (details shown

in chapter 4). This discovery led to another proposal that the incorporation of the aminopropyl

group might happen after the phosphorylation of **7** (Figure 5.4B).
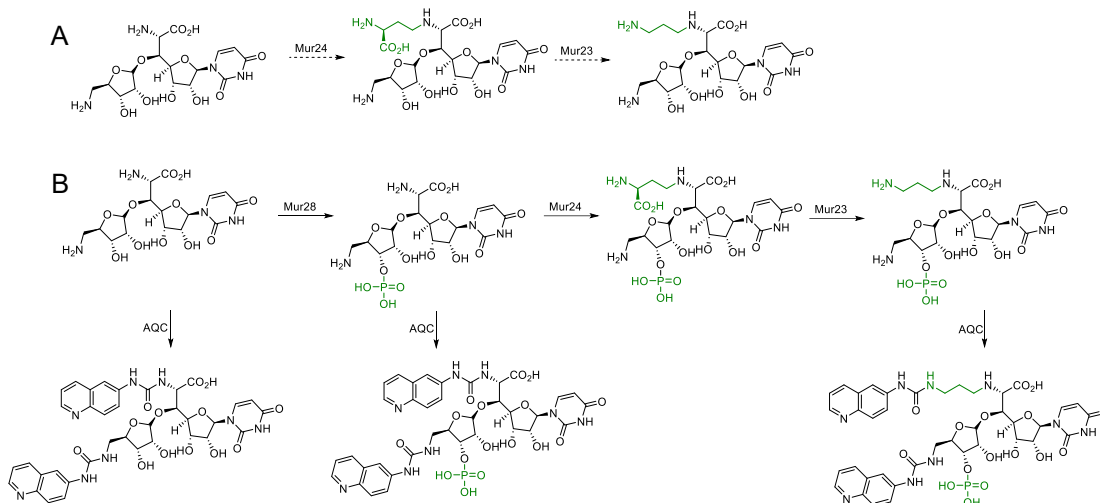
Figure 5.4 Two proposed biosynthetic pathway of the incorporation of aminopropyl moiety of muraymycins.

LC-MS analysis of enzyme coupled reaction by incubating Mur28, Mur24 and Mur23 with **7** after pre-column derivation by AQC yielded an $(M+2H)^{2+}$ ion at m/z = 463.7, consistent with the molecular formula $C_{39}H_{46}N_9O_{16}P$ of an AQC-modified **10** (**10'**), (expected m/z = 463.6) (Figure S5.7). Since a C18 column did not give good separation for the reaction even under ion pairing condition (Figure S5.4) due to the high polarity of the substrate and product, the tandem reactions were analyzed with HILIC column without pre-column derivation (Figure 5.5). In situ generated disaccharide phosphate by Mur28 was clearly processed by Mur24 and a new peak was formed, which was identified as butyric acid disaccharide **9** by HR-ESI-MS with $(M+H)^+$ ion at m/z =630.1643, consistent with the molecular formula $C_{20}H_{33}N_5O_{16}P$ of **9** (expected $(M + H)^+$ ion at m/z = 630.1654) (Figure S5.11). Decarboxylation of in situ generated **9** was also observed when incubating with Mur23. HR-ESI-MS of the purified new peak yielded an $(M + H)^+$ ion at m/z = 586.1735, consistent with the molecular formula $C_{19}H_{33}N_5O_{14}P$ for **10** (expected $(M + H)^+$ ion at m/z = 586.1756) (Figure S5.16).
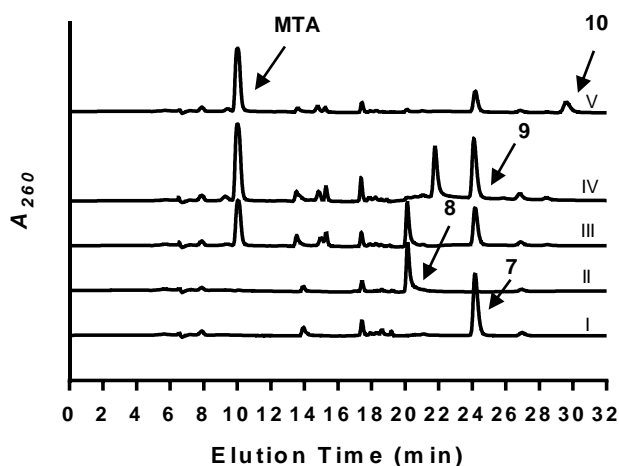
Figure 5.5 HPLC analysis of tandem enzymatic reaction with Mur23, Mur24 and Mur28. I, control reaction with ATP and **7**; II, 6 h reaction with Mur28; III, 6 h reaction with ATP, **7**, AdoMet and Mur28; IV, 6 h reaction with Mur24 and Mur28; V, 6 h reaction with Mur23, Mur24 and Mur28.

Purified **8** was used as substrate to directly test Mur24-catalyzed reaction with AdoMet (Figure 5.6A) to confirm that **8** is the genuine aminopropyl group acceptor. The structure of the product **9** was elucidated by NMR spectroscopy (Figure 5.7, S5.8-S5.10, S5.12-S5.15, S5.17-S5.18). As expected, the connection between the butyric acid group and **8** in **9** was confirmed by ^{1}H-^{13}C HMBC from the proton signal at δ_H 3.79 (H-10) to the carbon signal at δ_C 45.6 (C-17) (Figure S5.15). Accordingly, purified **9** was used as substrate to test the activity of Mur23 (Figure 5.6B). NMR analysis of purified product **10** revealed the decarboxylation at C-19 position as expected.

164
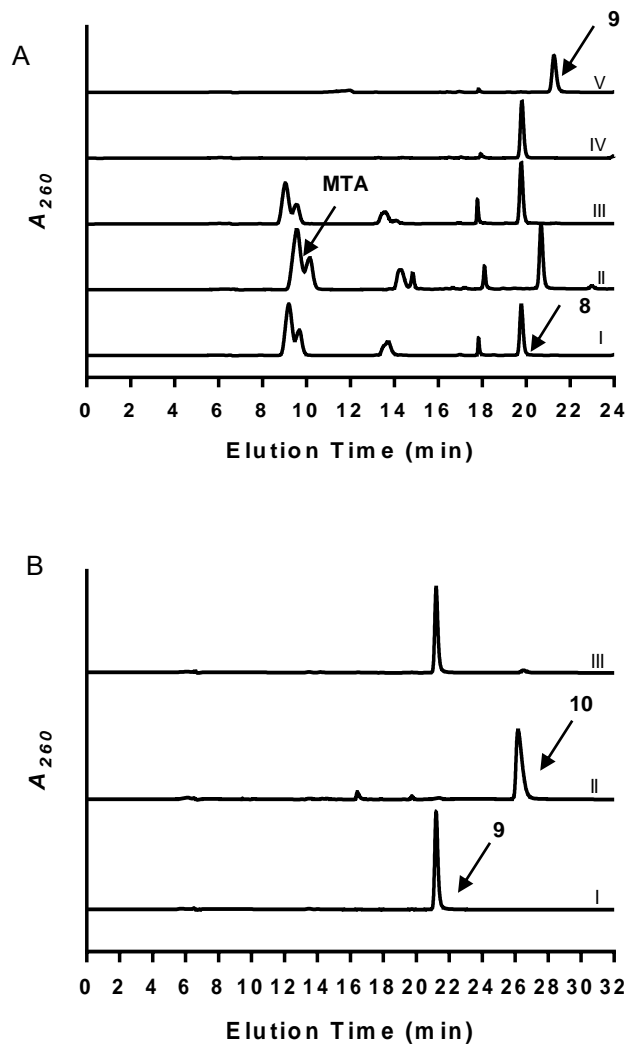
Figure 5.6 Characterization of Mur24 and Mur23.

(A) LC-MS analysis of Mur24 reaction using **8** as substrate. I, control reaction with AdoMet no Mur24; II, 6 h reaction with AdoMet and Mur24; III, 6 h reaction with AdoMet and Mur24 (K234A); IV, 6 h reaction with L-Met and Mur24; V, 6 h reaction with SMM and Mur24. (B) LC-MS analysis of Mur23 reaction using **9** as substrates. I, control reaction without Mur23; II, 6 h reaction with Mur23; III, 6 h reaction with Mur23 (K70A).
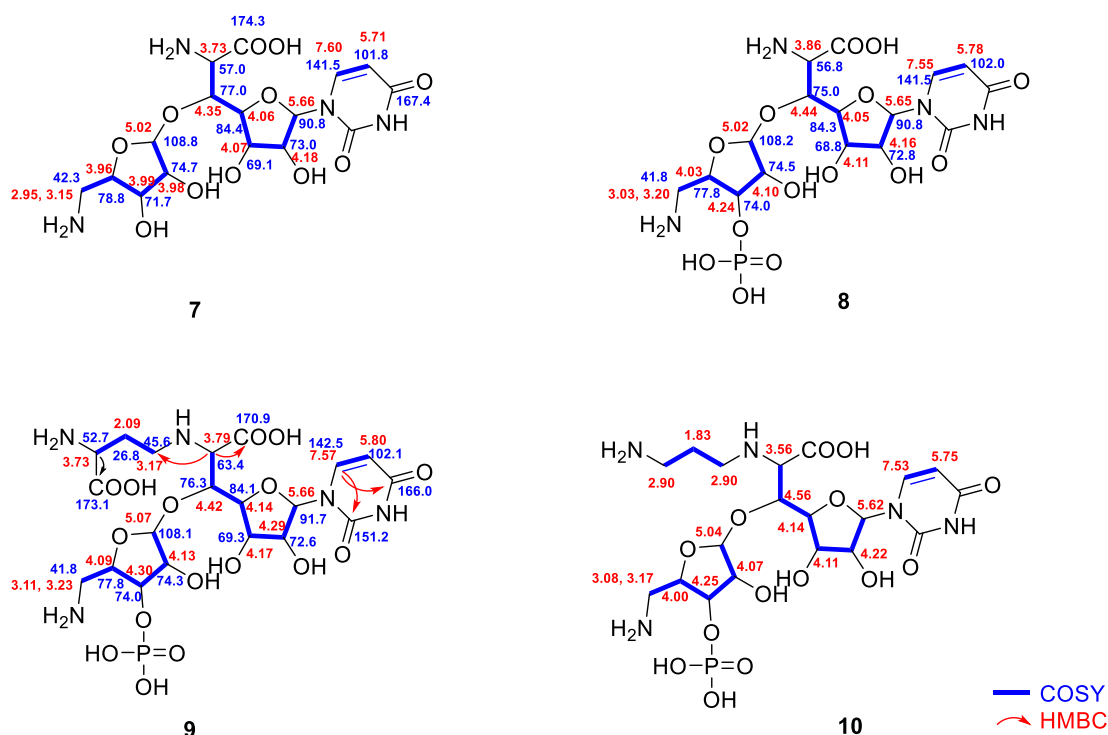
Figure 5.7 Chemical shift assignment for compound **7**, **8**, **9** and **10**.

5.3.5 Kinetic and Mutational Analysis of Mur24 and Mur23

Single-substrate kinetic analysis of Mur24 revealed typical Michaelis−Menten kinetics with respect to varied **8**, yielding kinetic constants of $K_m = 92.3 \pm 7.3$ μM and $k_{cat} = 2.67 \pm 0.08$ min^{-1} (Figure 5.8A). A Mur24 (K234A) mutant was generated by site-directed mutagenesis with the expectation that the point mutation would make the enzyme unable to form an internal aldimine with PLP which is a prerequisite for the catalytic activity, and as expected, incubation of **8** with AdoMet and Mur24 (K234A) revealed no detectable conversion to **9** (Figure 5.6A). Also, absence of adding PLP in the reaction with Mur24 greatly reduced the yield of the product **9** (Figure S5.21), which suggested that Mur24 catalyzed an unusual PLP-dependent reaction to modify the high carbon nucleoside scaffold. Kinetic analysis of Mur23 with respect to **9** also revealed Michaelis-Menten kinetics yielding a $K_m = 701.8 \pm 9.2$ μM and $k_{cat} = 144.8 \pm 1.1$ min^{-1} (Figure 5.8B). Mur23 (K70A) mutant was still yellowish and had a similar UV/Vis profile to

166

wild-type Mur23 (Figure S5.1). The activity of Mur23 (K70A) was significantly reduced when

incubating **9**, suggesting an important—although not essential—role for this Lys residue in the

Mur23 reaction.
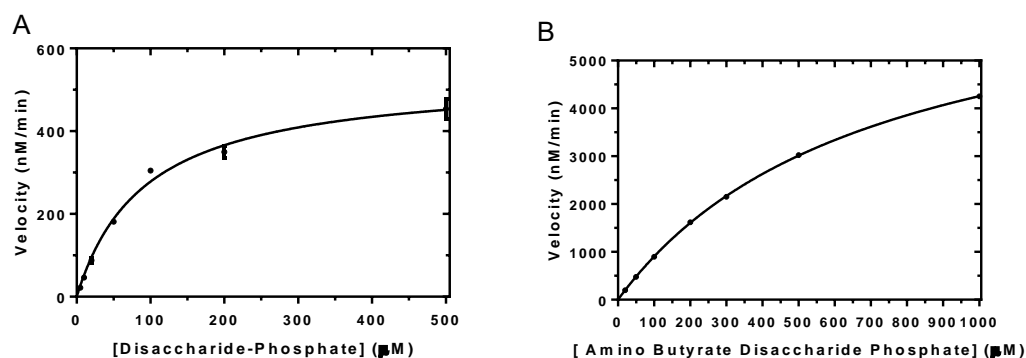
Figure 5.8 Kinetic analysis of Mur24 and Mur23.
(A) Single-substrate kinetic analysis of Mur24 with 2 mM AdoMet and variable **8**. (B) Single-substrate kinetic analysis of Mur23 with variable **9**.

5.3.6 Mechanism Study of Mur24

Formation of **9** can involve in one of a few possible mechanisms (Figure 5.9). The

proposed 'addition' pathway involves an L-VG intermediate as an active vinyl ketamine.

Alternatively, in the 'cyclization' pathway, 1-aminocyclopropanecarboxylic acid (ACC)

involves as an intermediate to form the active aldimine. Moreover, the regular SN2 mechanism

for the aminopropane incorporation is also possible. To distinguish among the proposed

mechanisms, L-VG, ACC and SMM were tested as alternative aminopropane donor in the

reaction with **8** and Mur24. However, activity was only detected when incubating with SMM,

which, although suggested that the adenosyl group is not required for its activity, did not provide

further insight into the mechanism. However, Mur24 did have deaminase activity when **8** was

absent in the reaction, generating α-ketobutyrate (α-KB) (identified by treating with reagent 3-

methyl-2-benzothiazolinone hydrazone hydrochloride (MBTH)) from either AdoMet and SMM.

167

Surprisingly, the formation of α-KB was also observed when incubating L-VG with 10 times more Mur24, but was not observed in reaction with ACC. Mur24 (K234A) revealed no detectable conversion to α-KB with AdoMet and SMM (Figure 5.10, S5.22). The inhibition effect of L-VG to Mur24 was observed when testing its deaminase activity. Although neither L-VG nor ACC can be aminopropyl donor of Mur24, the deaminase activity of Mur24 with L-VG rather than with ACC possibly supported the proposed 'addition' mechanism with L-VG as intermediate for the aminopropyl moiety incorporation reaction. However, since L-VG cannot act as aminopropane donor in this reaction, the regular S_N2 mechanism is still possible for the reaction.
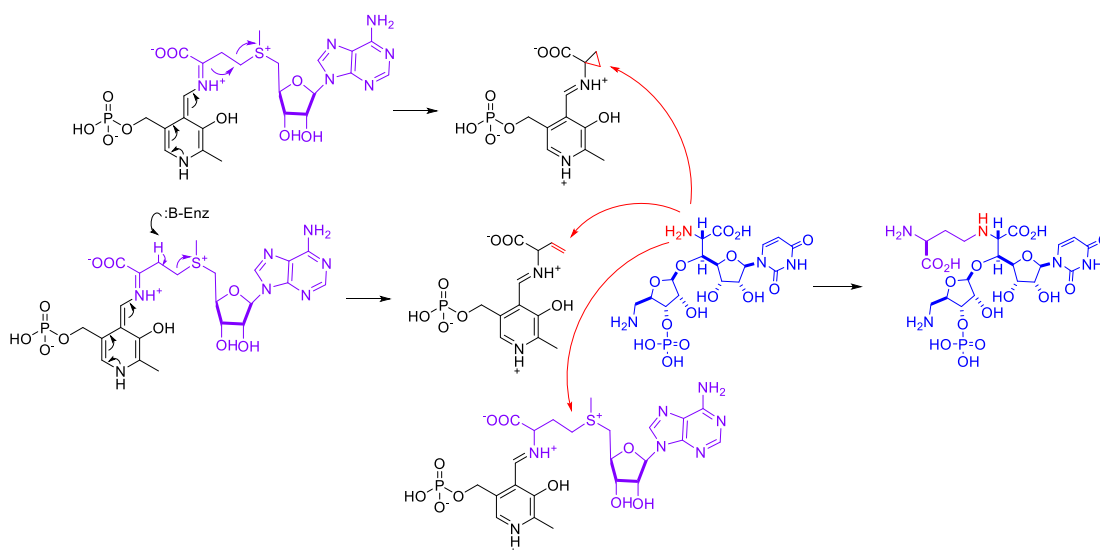
Figure 5.9 Mechanistic proposal for Mur24 catalyzed aminopropyl incorporation reaction.
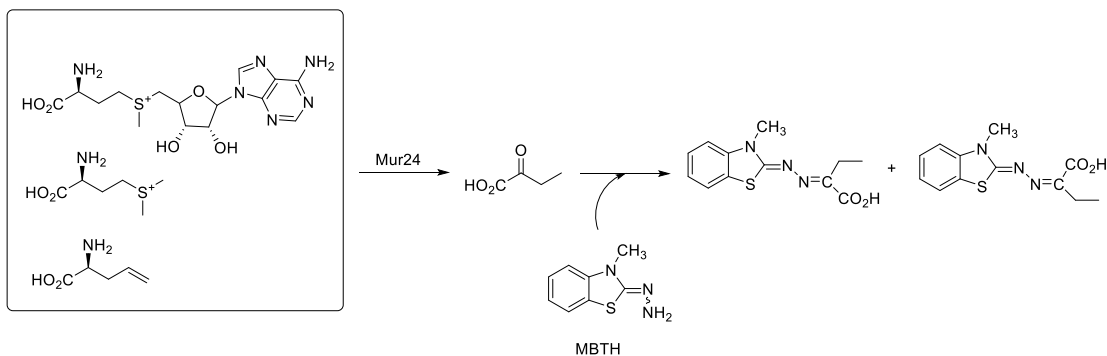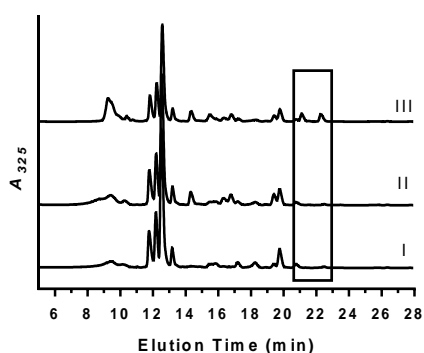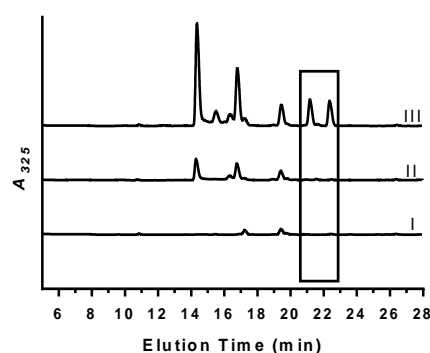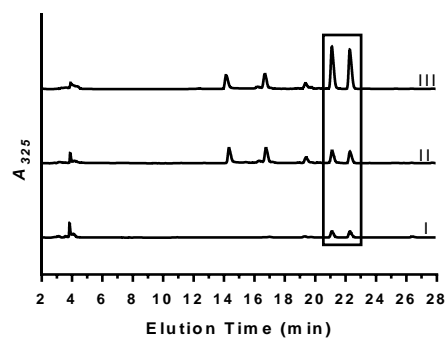
Figure 5.10 LC-MS analysis of MBTH modified Mur24 catalyzed reactions.
(A) α-keto-butyrate reacts with MBTH. (B) LC traces of MBTH modified Mur24 reaction with AdoMet. I, control reaction without enzyme; II, MBTH modified 6 h reaction with Mur24 (K234A); III, MBTH modified 6 h reaction with Mur24. (C) LC traces of MBTH modified Mur24 reaction with SMM. I, control reaction without enzyme; II, MBTH modified 6 h reaction with Mur24 (K234A); III, MBTH modified 6 h reaction with Mur24. (D) LC traces of MBTH modified Mur24 reaction with L-VG. I, control reaction without enzyme; II, MBTH modified 6 h reaction with Mur24 (K234A); III, MBTH modified 6 h reaction with Mur24.

5.4 Discussion

5.4.1 Similarity between ACC Synthase and Mur24

ACC synthase is a PLP dependent enzyme that catalyzes the formation of ACC from AdoMet (Figure 5.11).[86] ACC synthases have only been found in higher plants and fungus. It catalyzes α, γ-elimination from SAM to produce ACC and MTA; it also catalyzes β, γ-elimination to yield L-VG in 1 of 30,000 catalytic cycle.[87] Like Mur24, ACC belongs to α family of PLP-dependent enzymes. It can also transaminate L-VG and SMM to α-ketobutyrate and ammonia.[88-89] Although the aminotransferase activity of ACC synthase is similar to Mur24, ACC synthase can only catalyze AdoMet to form ACC, and SMM cannot be utilized to form ACC. However, Mur24 can utilize both AdoMet and SMM for the butyric acid encorporation.
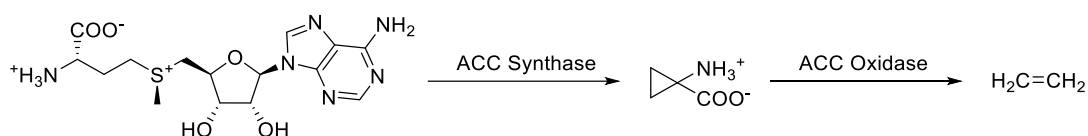
Figure 5.11 The biosynthesis of ethylene.

5.4.2 Relationship of Mur24 and MocR Transcription Regulator

Mur24 has modest sequence identity to PLP dependent MocR/GabR DNA binding transcription regulator, the molecular mechanism of which remains to be elucidated. MocR/GabR DNA binding transcription regulators also have PLP dependent Class I aminotransferase domain but lack the aminotransferase acitivity. Okuda etal[90] reported the spectroscopic studies of the aminotransferase domain of GabR, a PLP dependent transcriptional regulator and revealed that GABA forms an external aldimine with the PLP in the

aminotransferase domain of GabR. It's possible to speculate that Mur24 may also regulate the

transcription of its downstream genes.

5.4.3 Phosphorylation Modification is Also Required in Caprazamycin Biosynthetic Pathway

LipJ, from biosynthetic gene cluster of caprazamycin A-90289 (Figure 5.1), shared 35%

sequence identity to Mur24. Activity tests revealed that, like Mur24, LipJ catalyzes the

incorporation of butyric acid to phosphorylated disaccharide, and also showed deaminase

activity with AdoMet. Recently, Shiraishi etal[62] reported the identification of caprazol-3″-

phosphate (Figure 5.12) in *cpz23*(acyltransferase)-deleted caprazamycin producing strain

mutants. This discovery indicated that the phosphorylation at the 3″ position will also exist in

the following biosynthetic steps.
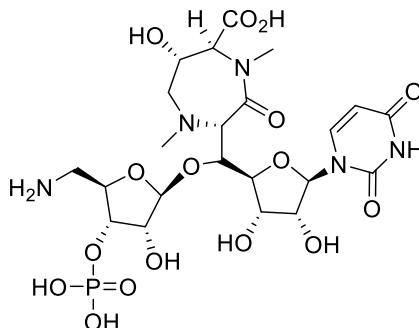
Figure 5.12 Structures of caprazol-3''-phosphate.

5.5 Conclusion

In this chapter, Mur23 and Mur24 were assigned as two enzymes that modify the

cryptic phosphorylated intermediate by attachment of an aminopropyl group. Structures of the

products were elucidated by the cumulative analysis of NMR spectroscopy and HR-ESI-MS.

Three possible catalytic mechanism was proposed. Mur24 catalyzes an unusual β, γ elimination

of AdoMet to form a vinylglycine-bound intermediate that serves as the Michael-type acceptor

of the phosphorylated-disaccharide, or the phosphorylated-disaccharide attacks γ carbon of

AdoMet-bound PLP aldimine via S_N2 to incorporate the butyric acid. Following the butyric

acid incorporation, Mur23 catalyzes a PLP-dependent decarboxylation.

5.6 Supporting Information

Table S5.1 Primers used in this study.

Primer	Sequence	Note
mur23_NdeI	5′-GATAGGCATATG AGCAGGCACGCACACAC-3′	*mur23*
mur23_BamHI	5′-CGAGTTGGATCC TCACCGCGCTCCGTCCG-3′	expression
mur24_NdeI	5′-GATAGGCATATG AGCGTCGTCGACAACG-3′	*mur24*
mur24_BamHI	5′-CGAGTTGGATCCTCACGGCAGTAGTGACTCCAG-3′	expression
mur23_pET30F	5′-GGTATTGAGGGTCGCATGAGCAGGCACGC-3′	*mur23* Site-
mur23_pET30R	5′-AGAGGAGAGTTAGAGCCTCACCGCGCTCCGTC-3′	directed
mur23-K70A_F	5′-CGCCTGTTGTTCAGCGTCGCGGCCAACCGGAGCCGGGCCG-3′	mutagenesis
mur23_K70A_R	5′-CGGCCCGGCTCCGGTTGGCCGCGACGCTGAACAACAGGCG-3′	
mur24_pET30F	5′-GGTATTGAGGGTCGCGTGAGCGTCGTCGAC-3′	*mur24* Site-
mur24_pET30R	5′-AGAGGAGAGTTAGAGCCTCACGGCAGTAGTG-3′	directed
mur24_K234A_F	5′-CTGGCGATGACCCCGTCCGCGGACCTGTCCCTTCCCG-3′	mutagenesis
mur24_K234A_R	5′-CGGGAAGGGACAGGTCCGCGGACGGGGTCATCGCCAG-3′	
pTipA	5′-GAG AAG GGA GCG GAC ATA C-3′	pXY200 sequencing primer

* the engineered Ala or Tyr codon is underlined

Table S5.2 Gradient used for HPLC or LC-MS analysis of Mur28, Mur24, or Mur23 product with an analytical ZIC®-HILIC column (250 mm x 4.6 mm, 5 μm).
Solvent A= ddH$_2$O with 0.1% formic acid; Solvent B= acetonitrile with 0.1% formic acid; A260

Time (min)	% Solvent B	Flow Rate (mL/min)
0	80	0.4
12	50	0.4
26	50	0.4
27	80	0.4
35	80	0.4

Table S5.3 Gradient used for semipreparative HPLC isolation of muraymycin D1 with an Apollo C-18 column (250 mm x 10 mm, 5 μm).
Solvent A= ddH$_2$O with 0.025% trifluoroacetic acid; Solvent B= acetonitrile; A260

Time (min)	% Solvent B	Flow Rate (mL/min)
0	10	3.5
25	22	3.5
26	100	3.5
31	100	3.5
32	10	3.5
36	10	3.5

Table S5.4 Gradient used for HPLC analysis of Mur28, Mur24 and Mur23 tandem reactions with an analytical Apollo C18 column (250 mm x 4.6 mm, 5 μm).
Solvent A= 40 mM acetic acid-triethylamine pH 6.5; Solvent B= 40 mM acetic acid-triethylamine, 20% methanol, pH 6.5; A260

Time (min)	% Solvent B	Flow Rate (mL/min)
0	1	0.5
16	100	0.5
20	100	0.5
21	1	0.5
24	1	0.5

Table S5.5 Gradient used for LC-MS analysis of AQC modified Mur28, Mur24 and Mur23 tandem reactions with an analytical AcclaimTM 120 C18 column (100 mm x 4.6 mm, 5 μm) Solvent A= ddH$_2$O with 0.1% formic acid; Solvent B= acetonitrile with 0.1% formic acid; A260

Time (min)	% Solvent B	Flow Rate (mL/min)
0	1	0.4
40	20	0.4
41	100	0.4
44	100	0.4
45	1	0.4
47	1	0.4

Table S5.6 Gradient used for LC-MS analysis of MBTH modified α-KB production by Mur24 or LipJ with an analytical AcclaimTM 120 C18 column (100 mm x 4.6 mm, 5 μm) Solvent A= ddH$_2$O with 0.1% formic acid; Solvent B= acetonitrile with 0.1% formic acid; A325

Time (min)	% Solvent B	Flow Rate (mL/min)
0	10	0.4
10	40	0.4
20	100	0.4
27	100	0.4
28	10	0.4
30	10	0.4

Table S5.7 ^{1}H NMR (400 MHz) data for **7-10** in D$_2$O (δ in ppm, mult, J in Hz).

7, R$_1$ = H; R$_2$ = H

8, R$_1$ = PO$_3$H$_2$; R$_2$ = H

9, R$_1$ = PO$_3$H$_2$; R$_2$ =

10, R$_1$ = PO$_3$H$_2$; R$_2$ =
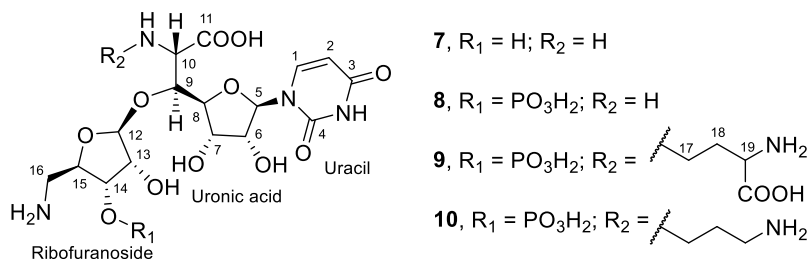
No.	7	8	9	10
1	7.60, d (7.7)	7.55, d (8.0)	7.57, d (7.8)	7.53, d (8.2)
2	5.71, d (7.7)	5.78, d (8.0)	5.80, d (7.8)	5.75, d (8.1)
5	5.66, br s	5.65, br s	5.66, br s	5.62, br s
6	4.18, m	4.16, m	4.29, m	4.22, m
7	4.07, m	4.11, m	4.17, m	4.11, m
8	4.06, m	4.05, m	4.14, m	4.14, m
9	4.35, br s	4.44, br s	4.42, br s	4.55, brs
10	3.73, br s	3.86, br s	3.79, br s	3.56, br s
12	5.02, br s	5.02, br s	5.07, br s	5.04, br s
13	3.98, m	4.10, m	4.13, m	4.07, m
14	3.99, m	4.24, m	4.30, m	4.25, m
15	3.96, m	4.03, m	4.09, m	4.00, m
16a	2.95, t (9.9, 12.2)	3.03, m	3.11, m	3.08, m
16b	3.15, d (11.4)	3.20, m	3.23, m	3.17, m
17			3.17, m	2.90, t (7.4)
18			2.09, m	1.83, m
19			3.73, t (6.3)	2.90, t (7.4)

A   B
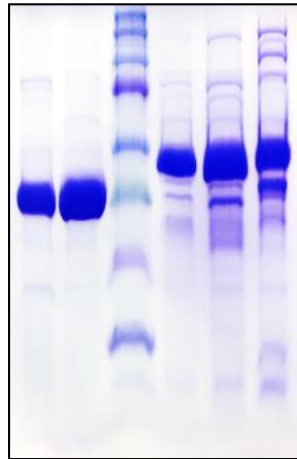
Protein	Size (aa)	Size(kD)
Mur23	388	42
Mur24	433	48
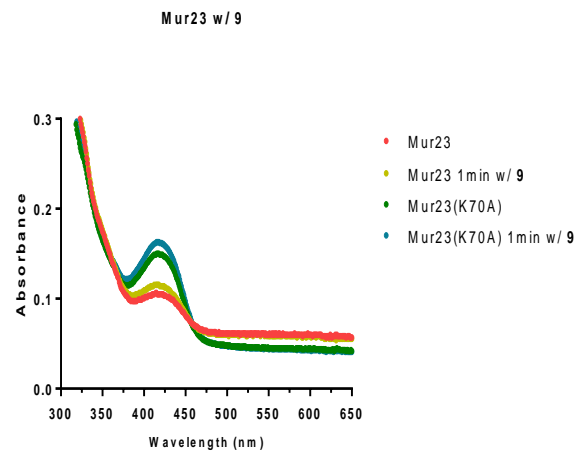
Figure S5.1 SDS-PAGE analysis of purified protein and UV/Vis spectrum of Mur23.
(A) SDS-PAGE analysis of purified His_6-Mur23 (lane 1), His_6-Mur23 (K70A) (lane 2), His_6-Mur24 (lane 3), His_6-Mur24 (234A) (lane 4), His_6-Mur24 (F201Y) (lane 5). (B) UV/Vis spectrum of Mur23 and Mur23 (K70A) with or without **9**.
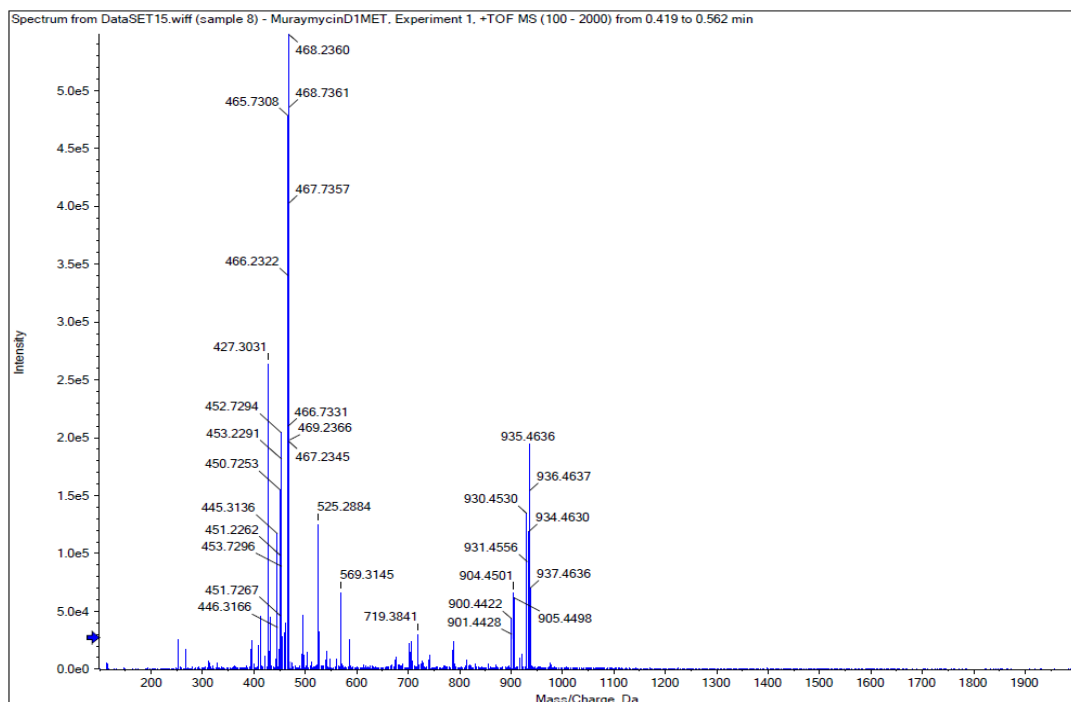
Figure S5.2 (+)-HR-ESI-MS (positive mode) of L-[^{13}C5,^{15}N] Met enriched muraymycin D1.
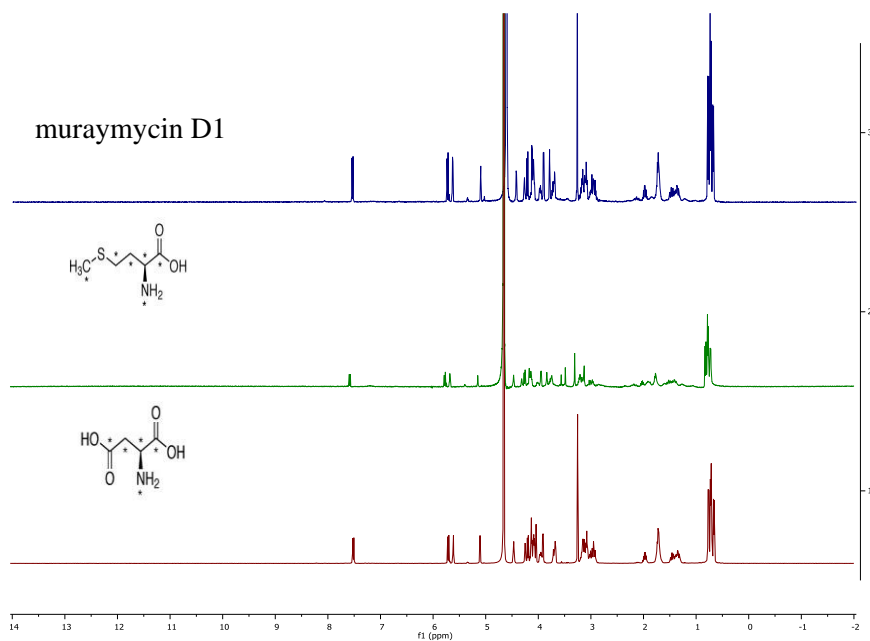
Figure S5.3 ^{1}H NMR spectrum (D$_2$O, 100 MHz) of isotope enriched (L-[^{13}C5, ^{15}N] Met or L-^{13}C4, ^{15}N] Asp) muraymycin D1.

A

B
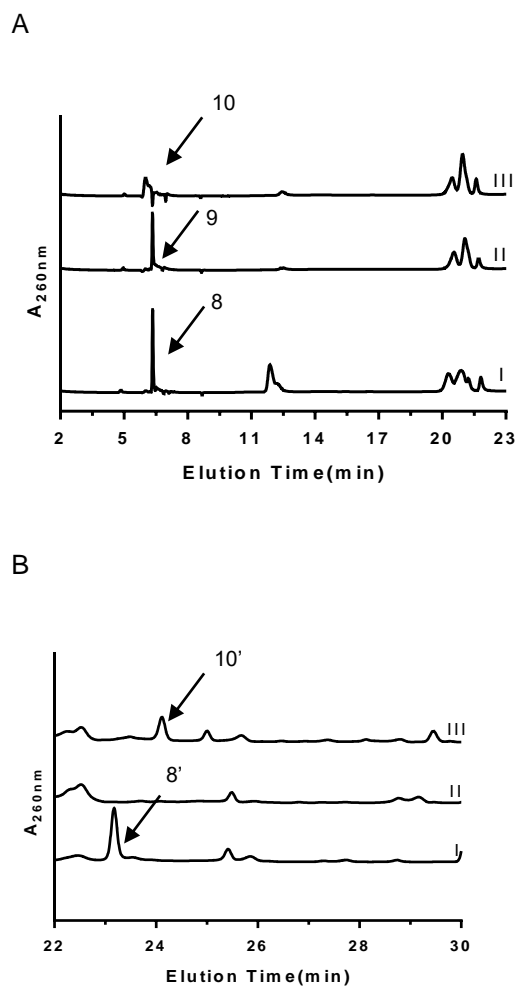
Figure S5.4 Analysis of tandem enzymatic reaction with Mur23, Mur24 and Mur28
(A) HPLC analysis of tandem enzymatic reaction with Mur23, Mur24 and Mur28 using ion pairing condition with C18 column. I, 6 h reaction with **7** and Mur28; II, 6 h reaction with **7**, Mur24 and Mur28; III, 6 h reaction with **7**, Mur23, Mur24 and Mur28. (B) LC-MS analysis of AQC modified tandem enzymatic reaction with Mur23, Mur24 and Mur28. I, 6 h reaction with **7** and Mur28; II, 6 h reaction with **7**, Mur24 and Mur28; III, 6 h reaction with **7**, Mur23, Mur24 and Mur28.
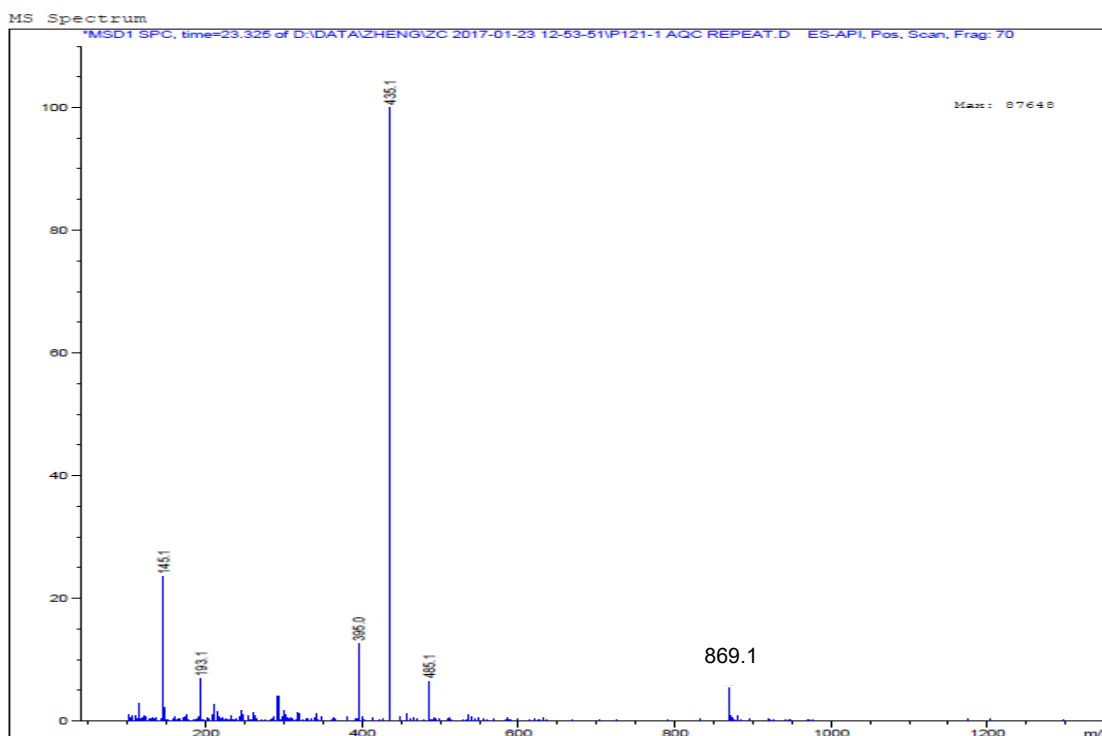
Figure S5.5 ESI-MS spectrum of **7**' eluted at 23.325 min
(calcd for $C_{36}H_{37}N_8O_{16}P$, expected $(M+H)^+$ ion at m/z = 869.21, found 869.1).
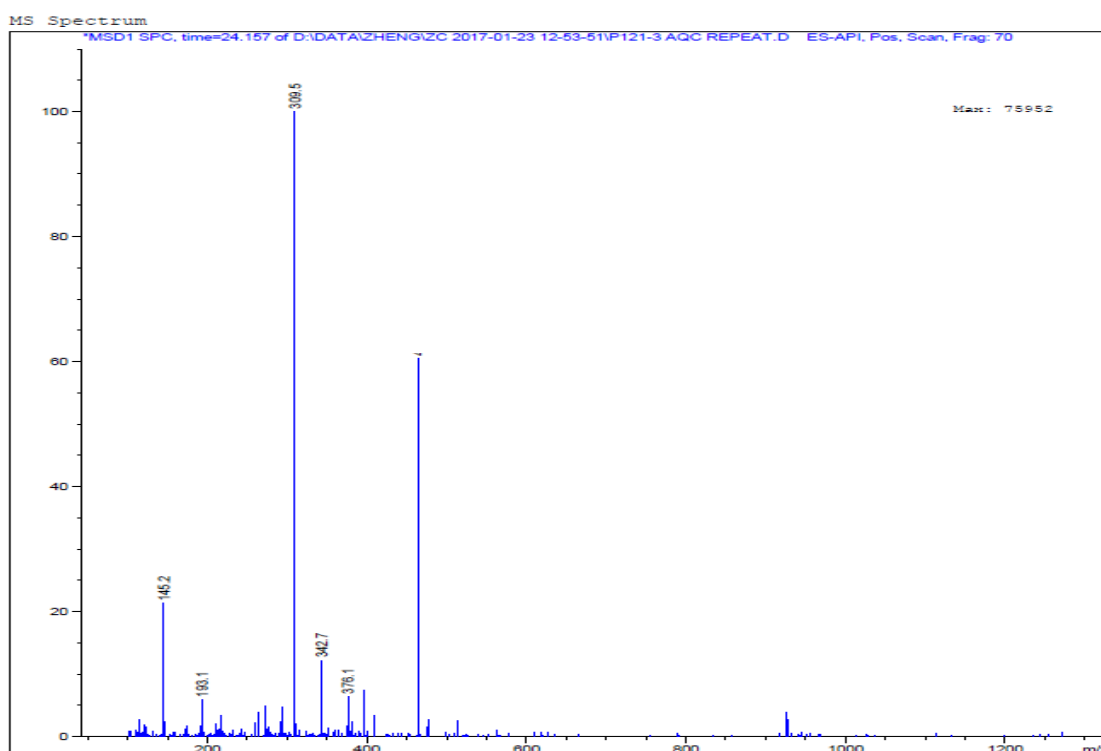
Figure S5.6 ESI-MS of **10**' eluted at 24.157min
(calcd for $C_{39}H_{45}N_9O_{16}P$, expected $(M+2H)^{2+}$: ion at m/z = 463.64, found 463.7).
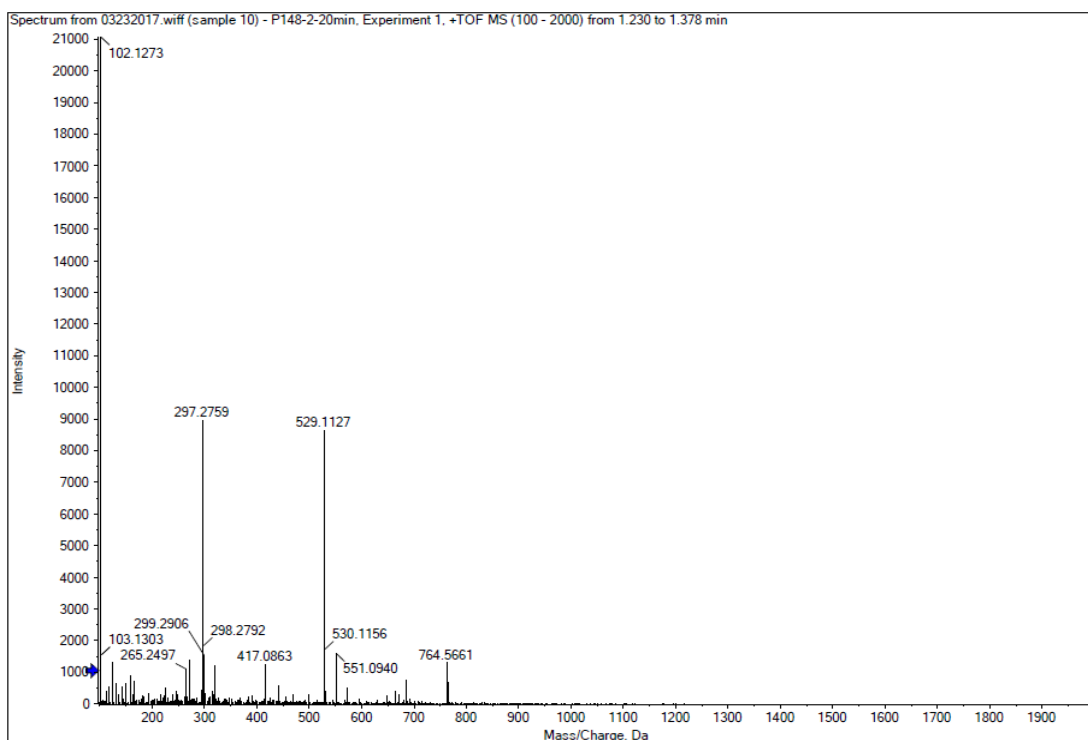
Figure S5.7 (+)-HR-ESI-MS (positive mode) of compound **8**
(calcd for $C_{16}H_{25}N_4O_{14}P$, expected $(M+H)^+$ ion at m/z = 529.1178, found: 529.1127).
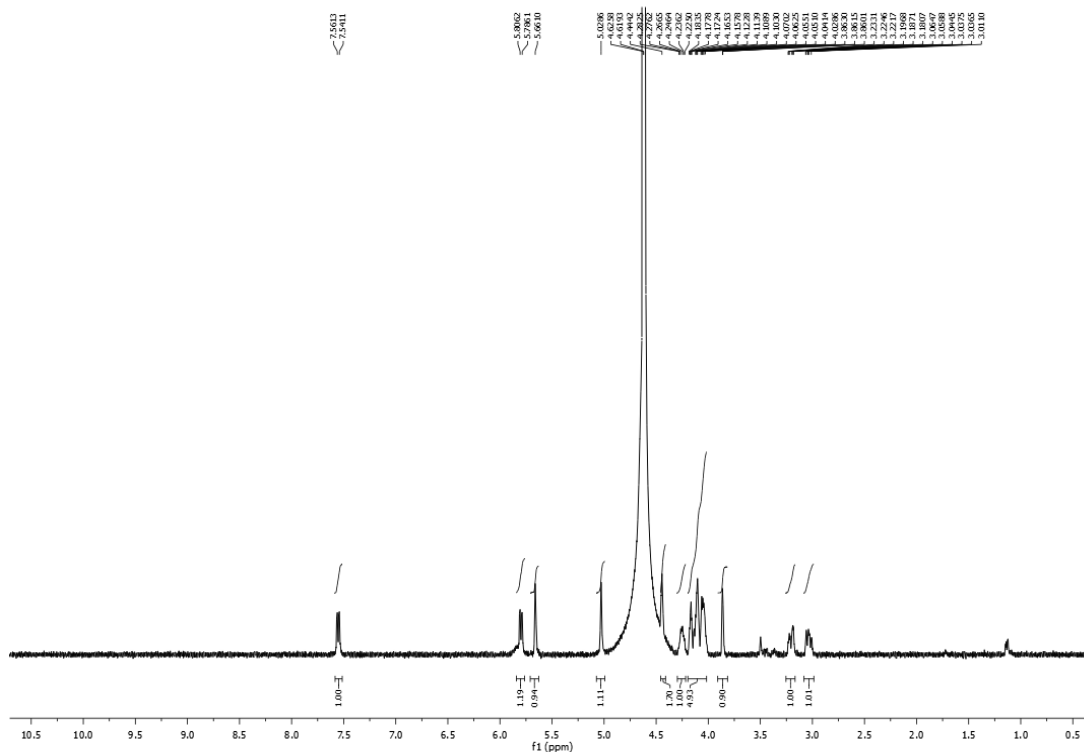
Figure S5.8 ^{1}H NMR spectrum (D_2O, 100 MHz) of compound **8**.
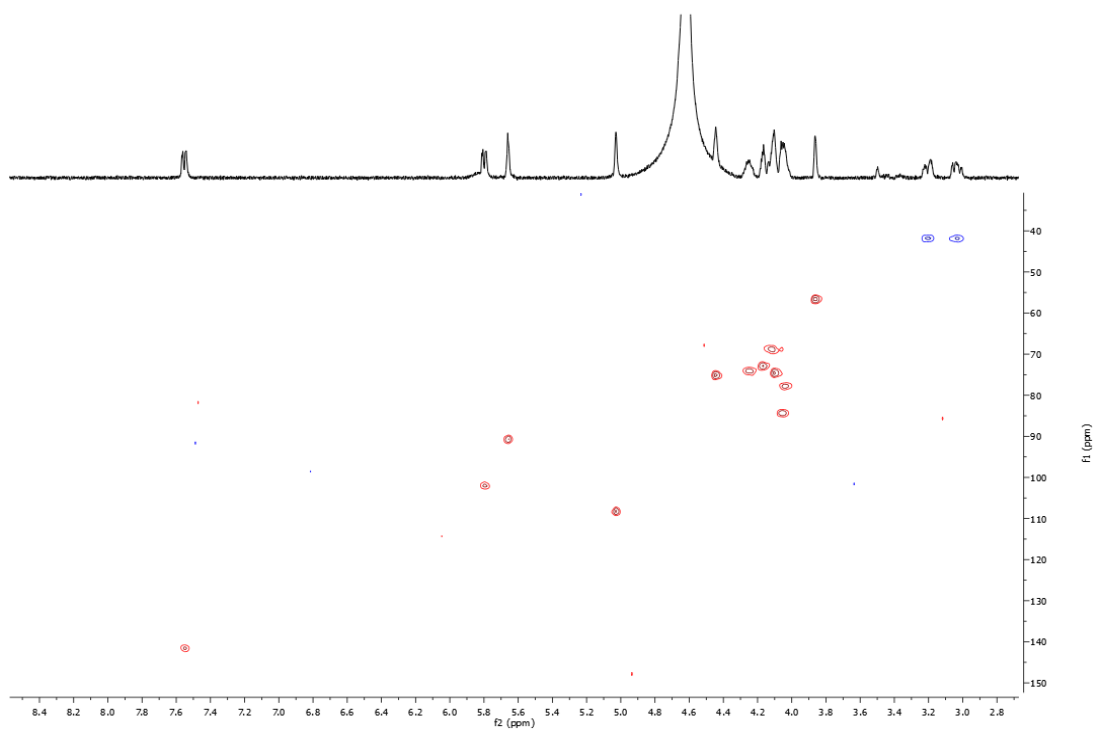
Figure S5.9 HSQC spectrum (D$_2$O, 400 MHz) of compound **8**.
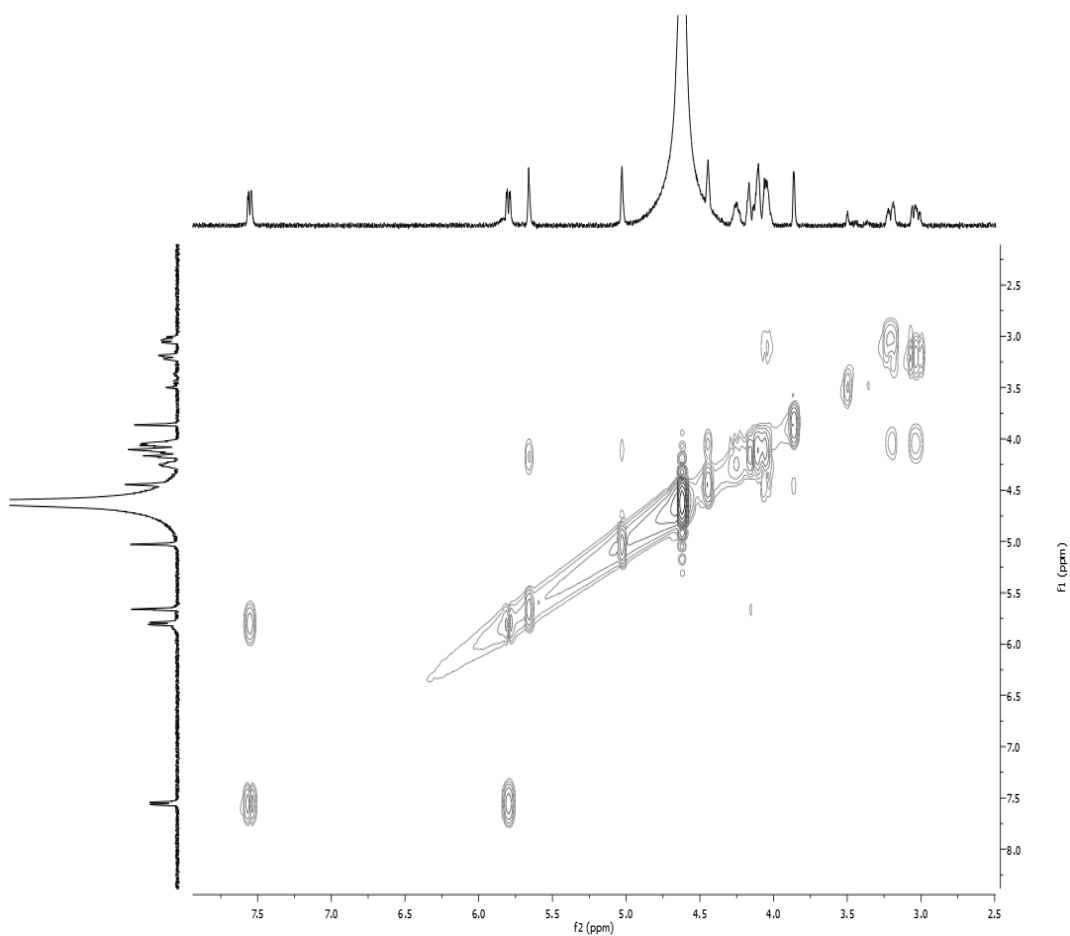
Figure S5.10 ^{1}H-^{1}H COSY spectrum (D$_2$O, 400 MHz) of compound **8**.
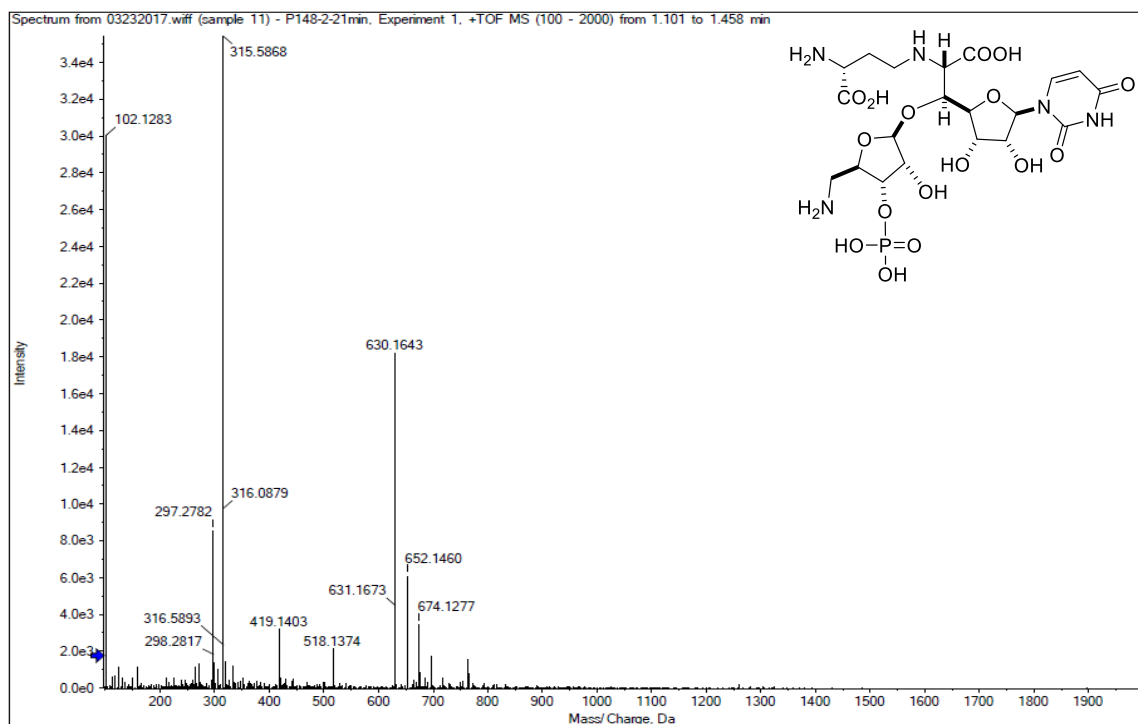
Figure S5.11 (+)-HR-ESI-MS (positive mode) of compound **9**
(calcd for $C_{20}H_{32}N_5O_{16}P$, expected $(M+H)^+$ ion at m/z = 630.1654, found: 630.1643).
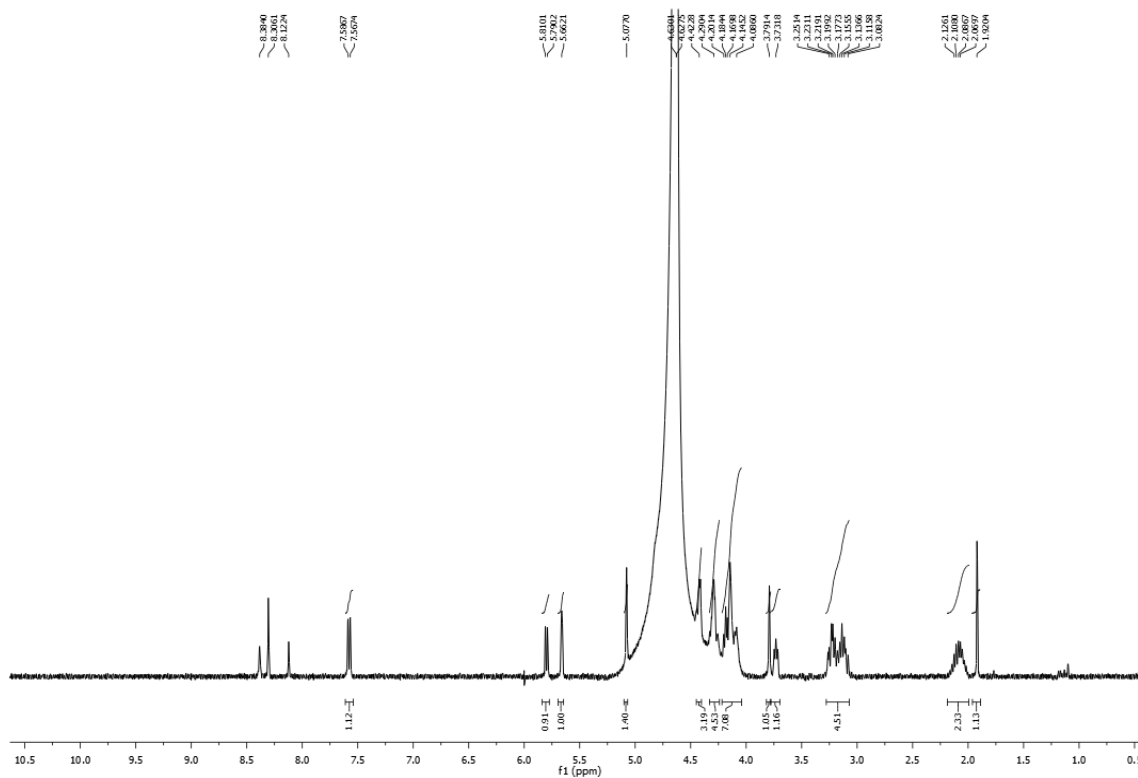
Figure S5.12 ^{1}H NMR spectrum (D_2O, 400 MHz) of compound **9**.
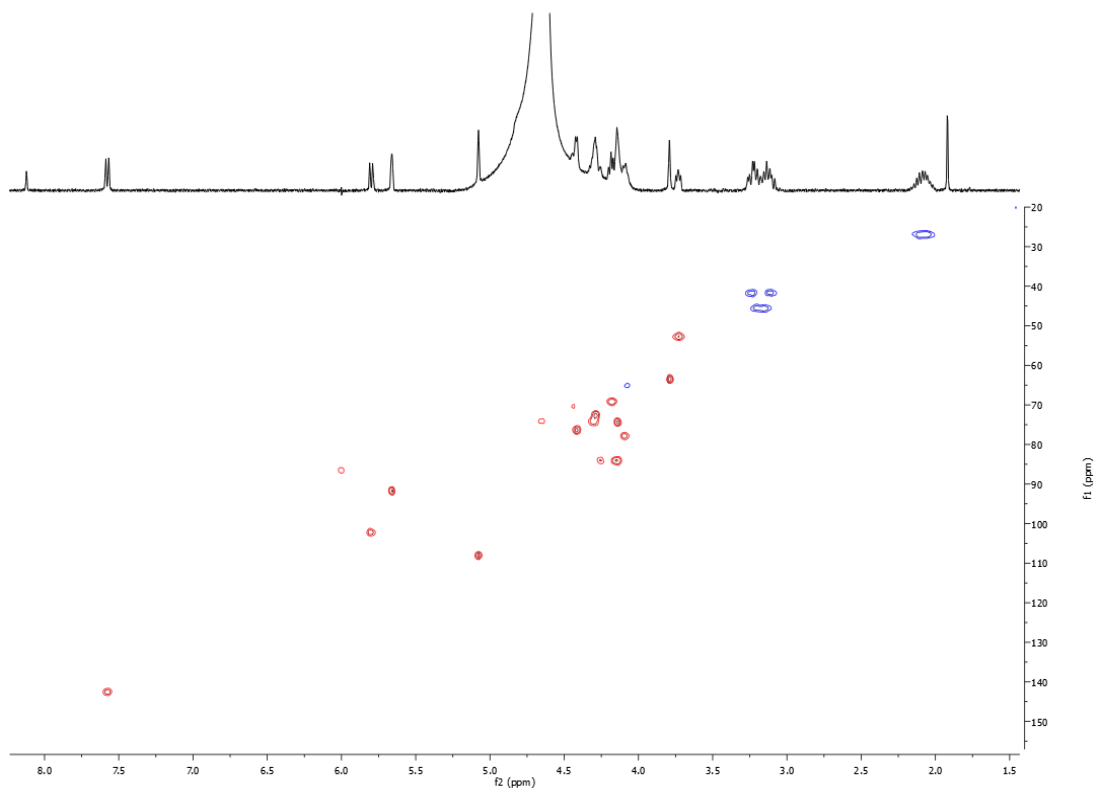
Figure S5.13 HSQC spectrum (D$_2$O, 400 MHz) of compound **9**.
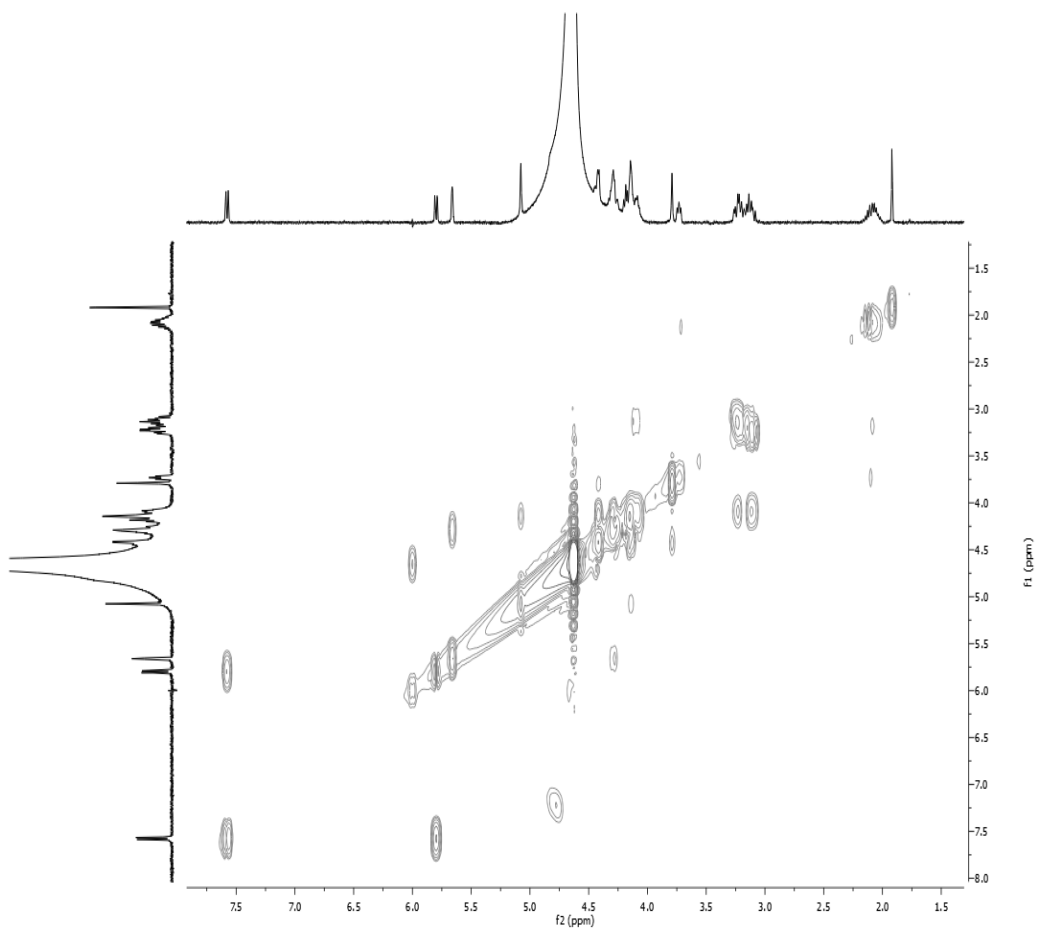
Figure S5.14 ^{1}H-^{1}H COSY spectrum (D$_2$O, 400 MHz) of compound **9**.
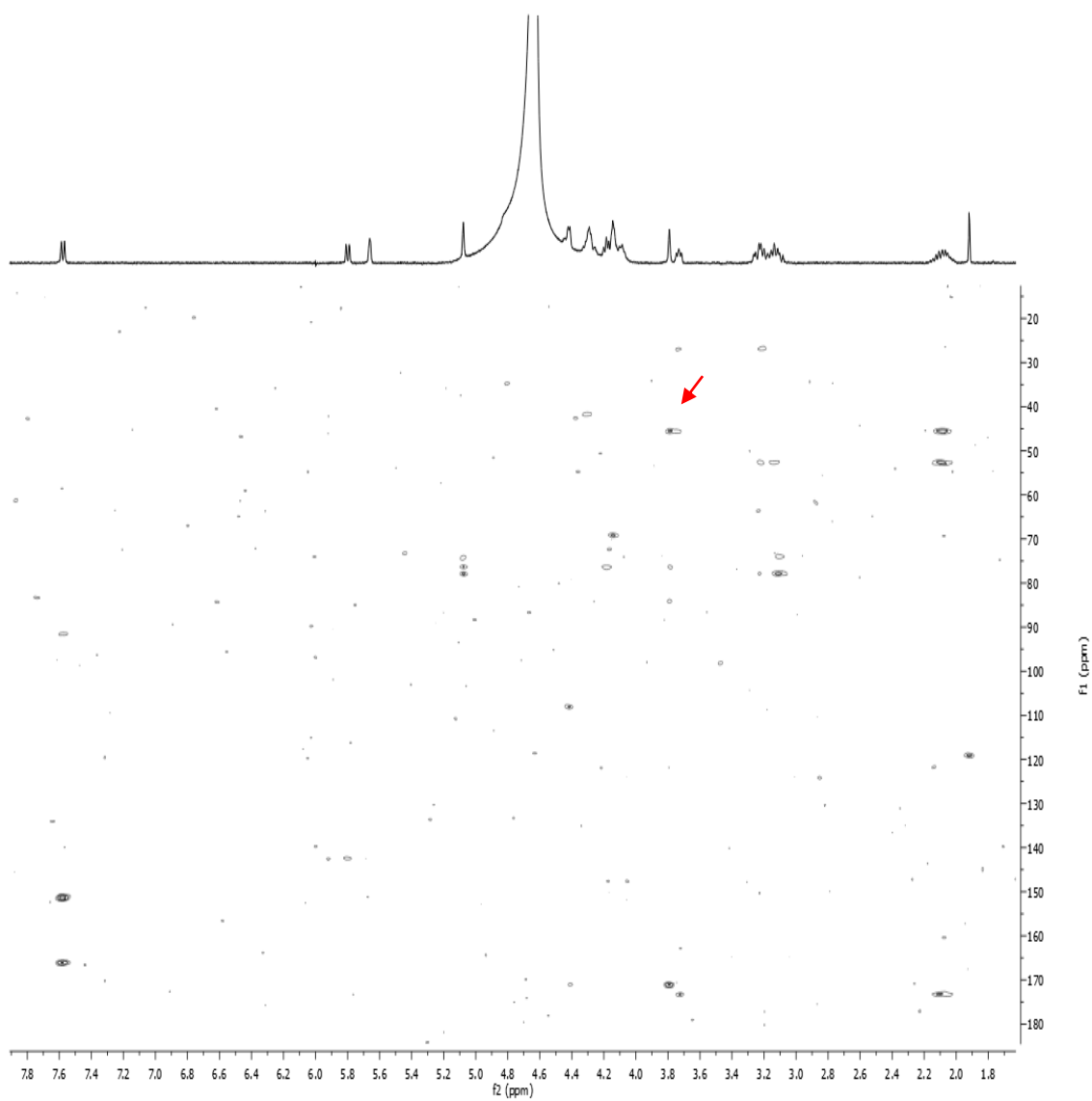
Figure S5.15 HMBC spectrum (D$_2$O, 400 MHz) of compound **9**.
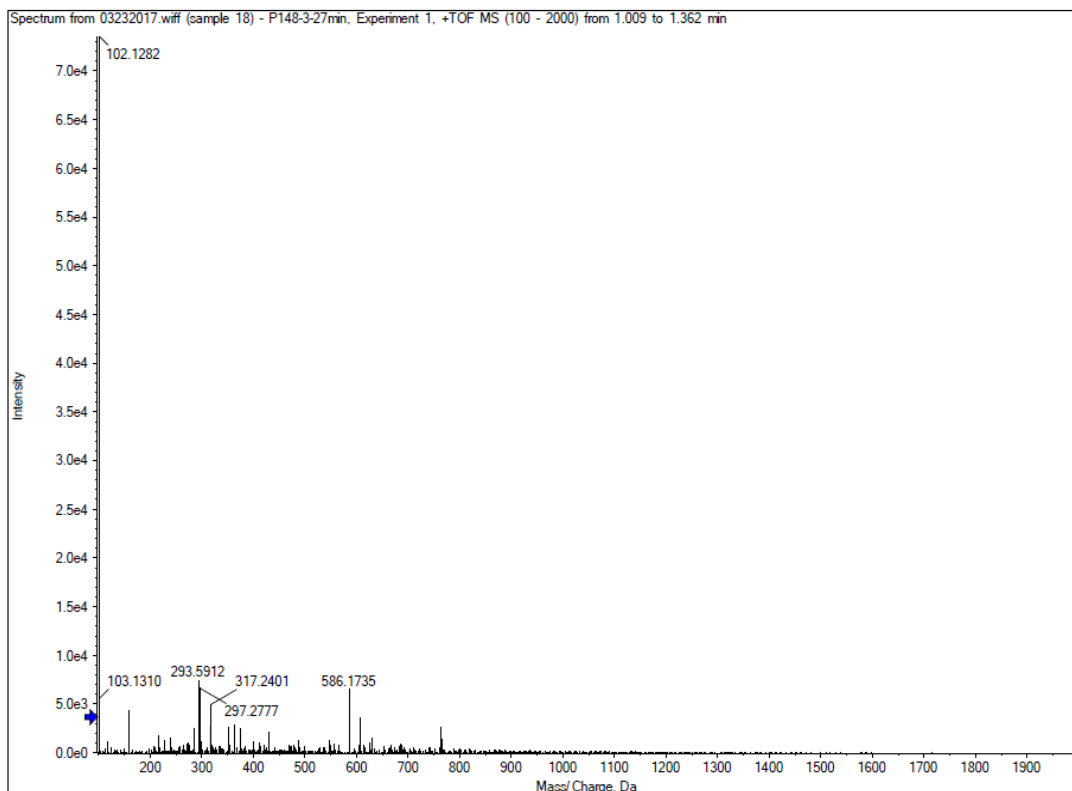
Figure S5.16 (+)-HR-ESI-MS (positive mode) of compound **10**
(calcd for $C_{19}H_{32}N_5O_{14}P$, expected $(M+H)^+$ ion at m/z = 586.1756, found: 586.1735).
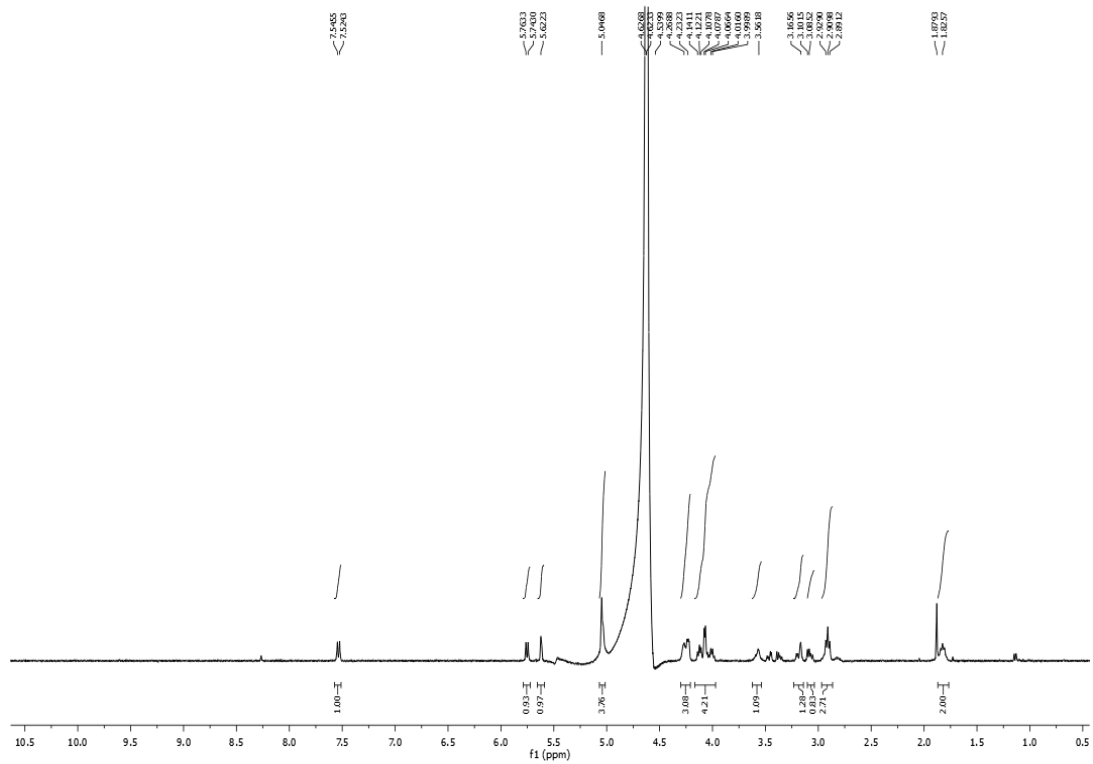
Figure S5.17 ^1H NMR spectrum (D_2O, 400 MHz) of compound **10**.
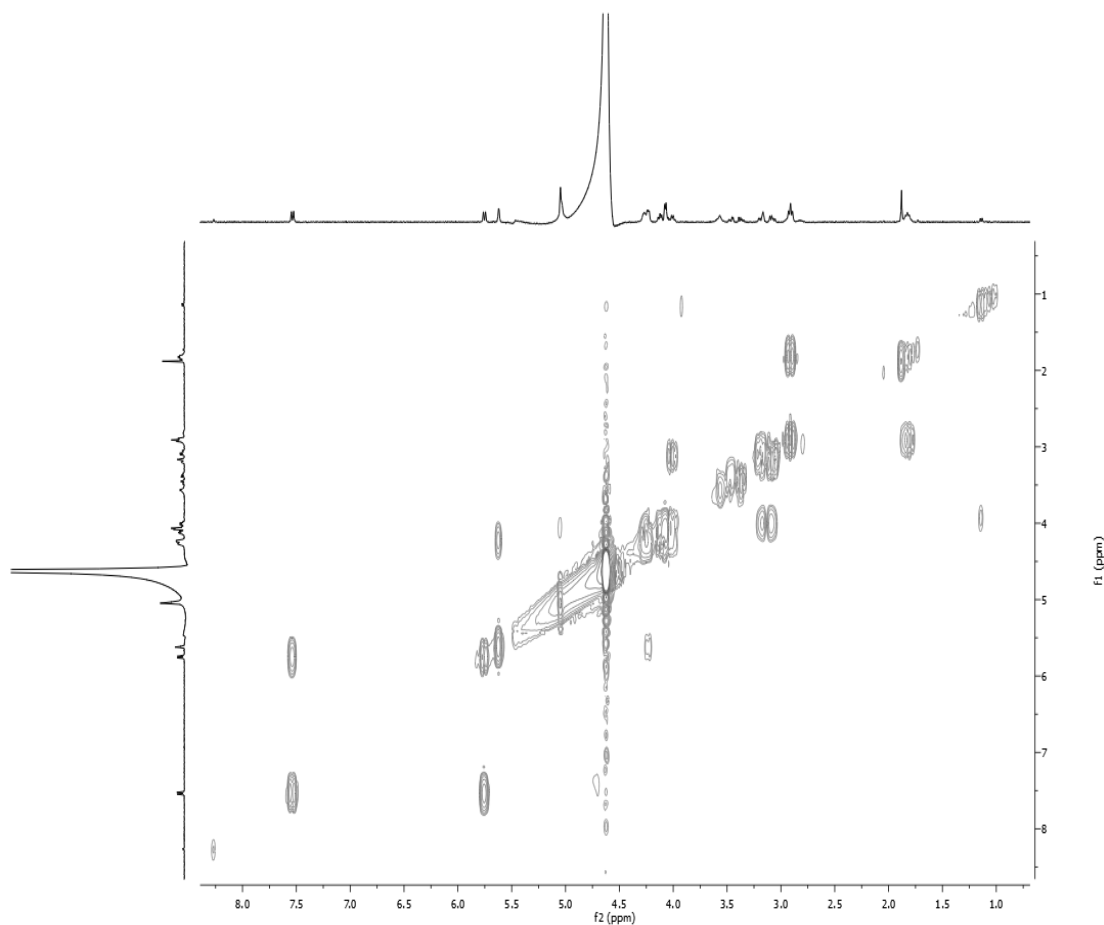
Figure S5.18 ^{1}H-^{1}H COSY spectrum (D$_2$O, 400 MHz) of compound **10**.
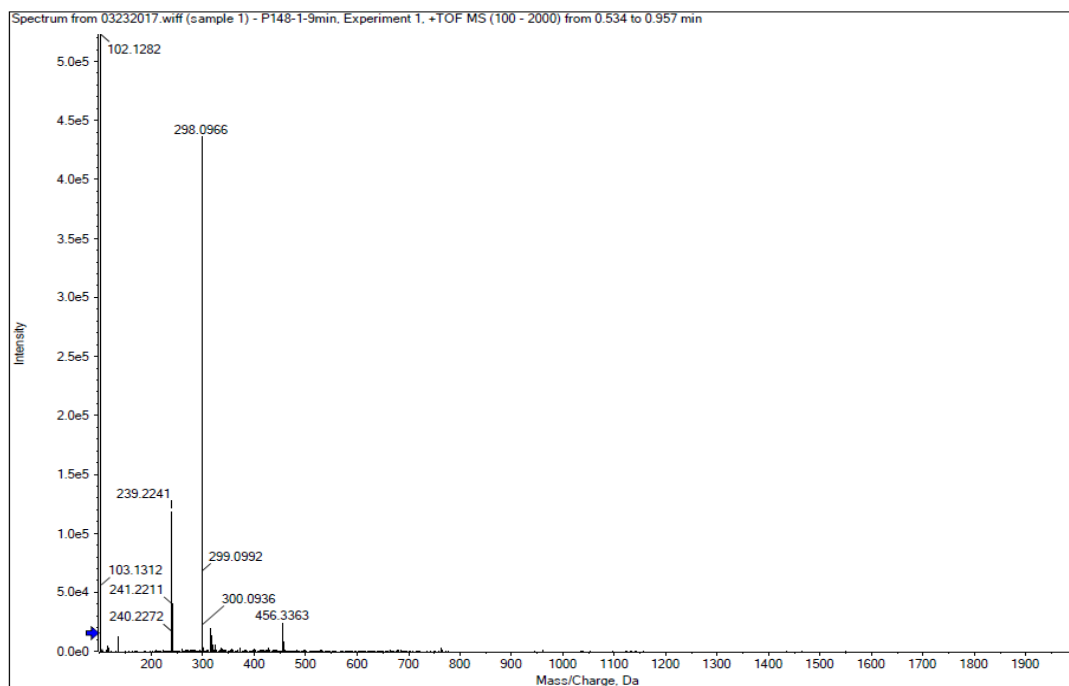
Figure S5.19 (+)-HR-ESI-MS (positive mode) of 5'-deoxy-5'-(methylthio) adenosine (calcd for C$_{11}$H$_{15}$N$_5$O$_3$S, expected (M+H)$^+$ ion at m/z = 298.0968, found: 298.0966).
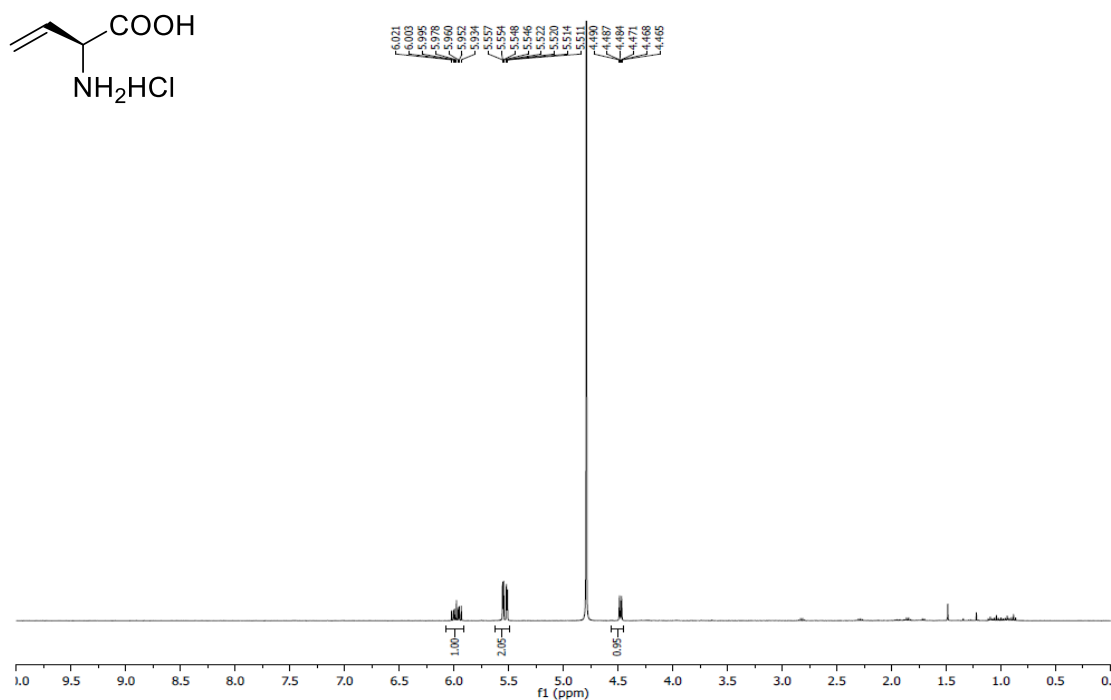
Figure S5.20 ^{1}H NMR spectrum (D$_2$O, 400 MHz) of L-VG.
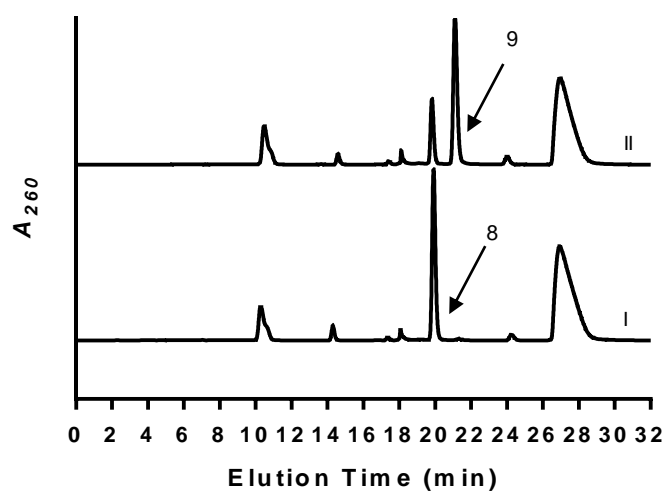
Figure S5.21 HPLC analysis of Mur24 reaction with or without PLP using **8** as substrates. I, 6 h reaction without PLP; II, 6 h reaction with PLP.
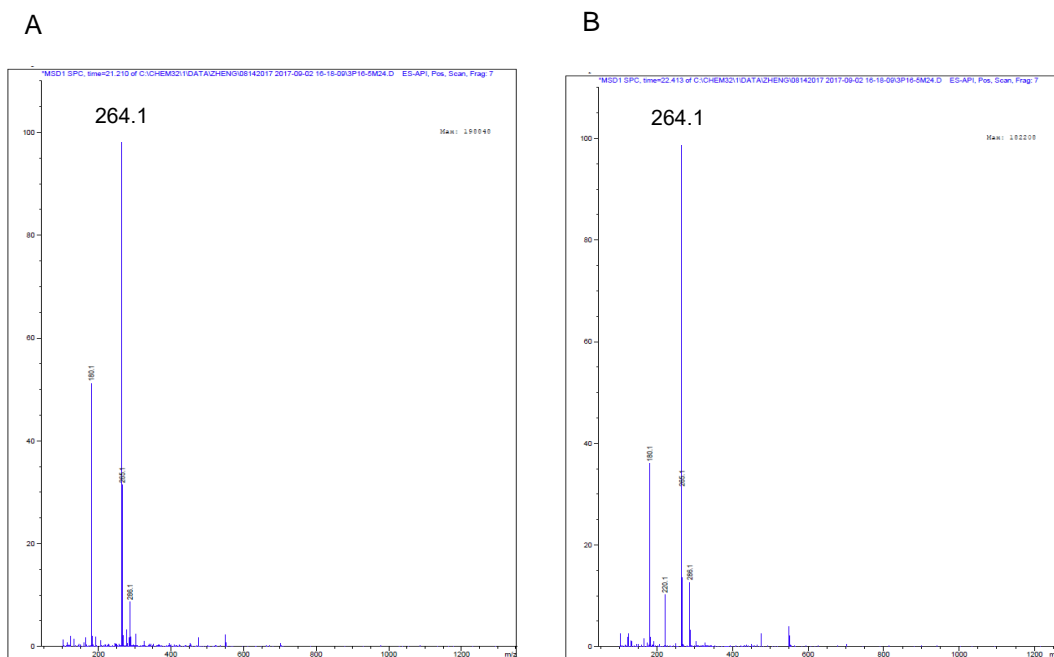
Figure S5.22 LC-MS analysis of MBTH modified Mur24 catalyzed reactions.
(A) Mass spectrum for the ion peak eluting at time t = 21.210 min of MBTH modified Mur24 reaction (MBTH modified α-keto-butyrate expected (M+H)$^+$ ion at m/z = 264.08, found: 264.1).
(B) Mass spectrum for the ion peak eluting at time t = 22.413 min of MBTH modified Mur24 reaction (MBTH modified α-keto-butyrate expected (M+H)$^+$ ion at m/z =264.08, found: 264.1).

Chapter 6 : Characterization of Mur15 as a Non-heme Fe(II), α-Ketoglutarate:

Muraymycin Dioxygenase

6.1 Introduction

The cupin superfamily, which was named on the basis of a conserved β barrel fold of the proteins, is one of the most functionally diverse protein superfamily. The largest subset of this family is the non-heme Fe(II), α-ketoglutarate dependent dioxygenases. In this chapter *in vitro* data are provided to support the functional assignment of Mur15, an enzyme that belongs to cupin superfamily, from the muraymycin gene cluster, as a non-heme, Fe(II)-dependent α-KG: muraymycin dioxygenase that catalyzes the β-hydroxylation of leucine moiety in muraymycin D1 to form muraymycin C1. It can also hydroxylate the γ-position of leucine moiety to muraymycins with fatty acid chain in β-position. To our knowledge, this is the first discovered natural enzyme that catalyzes the γ-hydroxylation of leucine moiety in peptidyl compound.

6.2 Materials and Methods

6.2.1 Cloning, Overexpression and Purification of Proteins

The gene for *mur15* was amplified from genomic DNA extracted from *Streptomyces* sp. NRRL30473 by PCR using Phusion DNA polymerase with primer pairs:

mur15 (forward) 5′-GGTATTGAGGGTCGCGTGAGGAGCCCTCC-3′/

(reverse) 5′-AGAGGAGAGTTAGAGCCTCAGCCGTCCGCGC-3′.

Genomic DNA of *Streptomyces* sp. NRRL30473 was extracted using UltraClean Microbial DNA Isolation Kit (MoBio laboratories, Inc) following manufacturer's protocol. DNA quality and concentration were confirmed using Nanodrop 2000c spectrophotometer (Thermo Scientific) and gel electrophoresis. The gel-purified PCR product of *mur15* was inserted into pET30 Xa/LIC using ligation-independent cloning as described in the provided protocol to yield pET30-*mur15* and confirmed by DNA sequencing. The procedure of protein overexpression and purification from *E. coli* BL21 (DE3) was stated in section 3.2.1.

6.2.2 Fermentation, Extraction, Isolation, and Purification of Muraymycins

Muraymycin producer strains *Streptomyces* sp. NRRL30473, 30475 and 30477 were cultured for the production of muraymycin A1, B2, B6, C1, D1and D2 following the method stated in section 4.2.3.

6.2.3 Activity Assay of Mur15

Reactions consisted of 50 mM HEPES (pH 7.5), 2.5 mM α-KG, 500 μM ascorbic acid, 500 μM $FeCl_2$, 1 mM muraymycin congeners, L-Arg, L-Leu or dipeptide and 1 μM Mur15 at

30 °C. The reaction was terminated by adding twice volume of methanol followed by centrifugation (14000 rpm, 30 min) to remove the precipitated protein. Following centrifugation to remove protein, the reaction was analyzed by HPLC or LC-MS with gradient shown in Table S4.3 or Table S4.4 with detection at 260 nm.

6.2.4 Activity Optimization

Optimal ascorbic acid concentration for activity was determined with assays containing 50 mM HEPES (pH 7.5), 2.5 mM α-KG, 0.25 mM muraymycin D1, 200 μM FeCl$_2$ and 0-2000 μM ascorbic acid and 200 nM Mur15. After identifying the optimal ascorbic acid concentration, the optimal iron concentration was determined with reactions containing 50 mM HEPES (pH 7.5), 2.5 mM α-KG, 0.25 mM muraymycin D1, 500 μM ascorbic acid and 0-1000 μM FeCl$_2$ and 200 nM Mur15. All reactions were carried out at 30 °C, and product formation was analyzed by HPLC with gradient shown in Table S4.3 or Table S4.4 under initial velocity conditions.

6.2.5 Kinetics of Mur15

Assays consisted of 50 mM Hepes (pH 7.5), 500 μM ascorbic acid, 500 μM FeCl$_2$, near saturating muraymycin D1 (0.25 mM) with variable α-KG (5 μM–200μM), or near saturating α-KG (2.5 mM) with variable muraymycin D1 (5 μM–1000μM), or near saturating α-KG (2.5 mM) with variable muraymycin B2 (5 μM–1000 μM). The reaction was performed at 30 °C with 200 nM Mur15 for 2 h and analyzed under initial velocity conditions. Product formation was determined using HPLC with gradient shown in Table S4.3. Each data point represents a minimum of three replicate end point assays; kinetic constants were obtained by nonlinear regression analysis using GraphPad Prism (GraphPad Software, La Jolla, CA).

6.2.6 Antimicrobial Bioactivities

The protocol used for the determination of the minimum inhibitory concentration (MIC) was as described in section 4.2.8.

6.2.7 MraY Inhibition

The assay was carried out by Prof. Christian Ducho's lab in Department of Pharmacy, Pharmaceutical and Medicinal Chemistry, Saarland University. Details are described in section 2.2.5.

6.3 Results and Discussion

6.3.1 Bioinformatic Analysis of Mur15

BLASTP analysis showed that Mur15 belongs to cupin superfamily but has no significant sequence homology to any characterized protein. Proteins in cupin superfamily, which is named after the conserved barrel domain, has diverse functions.[91] Therefore, structural homology search using HHpred was carried out.[92] Mur15 showed structural homology to α-ketoglutarate dependent ribosomal oxygenases YcfD in *E. coli* and nucleolar protein 66 (NO66) in human. YcfD catalyzes arginine hydroxylation in ribosomal protein L16 while NO66 catalyzes histidine hydroxylation in ribosomal protein RPL8.[93] Thus, we proposed that Mur15 may similarly function as an Fe(II) and α-KG dependent dioxygenase to catalyze the hydroxylation of the peptide moiety of muraymycin.

6.3.2 Functional Assignment and Activity Test

Mur15 was cloned as an N-terminal His_6-tagged protein using the genome of

Streptomyces sp. NRRL30473 as template, expressed and purified from *E. coli* BL21(DE3) with a yield of 6.3 mg/L (Figure S6.1). As no hydroxylation of free L-leucine catalyzed by Mur15 could be detected by LC-MS, five muraymycin congeners, muraymycin D1, D2 (from *Streptomyces* sp. NRRL30475), muraymycin A1, B2, B6, C1 (from *Streptomyces* sp. NRRL30473) were isolated from culture medium of *Streptomyces* sp. for activity tests. When Mur15 was incubated with muraymycin D1 and α-KG, HPLC analysis revealed a new peak with concomitant loss of the peak corresponding to D1 (Figure 6.1B). The new peak was confirmed as muraymycin C1 by LC-MS, coinjections with authentic muraymycin C1 and proton NMR comparison (Figure S6.2). No activity was observed when α-KG was omitted in the reaction. Activity of Mur15 was also observed when it was incubated with muraymycin D2 to generate muraymycin C2 (Figure 6.1C). Therefore, Mur15 is preliminarily assigned as an α-KG dependent muraymycin D1 leucine moiety β hydroxylase.
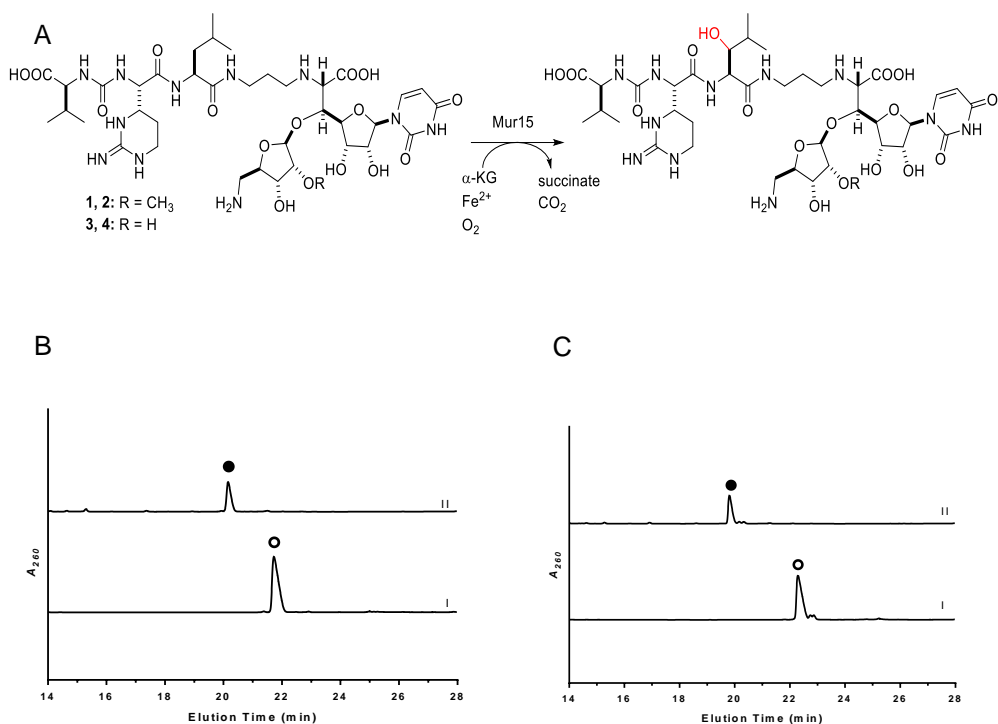
Figure 6.1 Characterization of Mur15 with muraymycin D1 (**1**).
(A) Reaction catalyzed by Mur15 with **1** or **3**. (B) LC-MS analysis using **1** (O) after 6 h without Mur15 (I), 6 h reaction (II). (C) LC-MS analysis using **3** (O) after 6 h without Mur15 (I), 6 h reaction (II).

No activity was detected by HPLC when Mur15 was incubated with C1 and α-KG. However, to our surprise, when Mur15 incubated with muraymycin congeners with fatty acid chain (muraymycin A1, B2 and B6) in β-position, HPLC and LC-MS traces revealed a new peak with 16 amu greater than the substrate (Figure 6.2), indicating that Mur15 also catalyzed the hydroxylation reaction of muraymycins with fatty acid chain. Following large scale purification of the hydroxyl B2 generated by Mur15, ^{1}HNMR revealed absent signal of proton on C4 and downfield shifts of protons on C5 and C6 of leucine moiety, indicating that the hydroxylation occurred at the γ position of leucine moiety (Figure 6.3). To our knowledge, this is the first discovered natural enzyme that catalyzes the γ-hydroxylation of leucine.[94] However, the mass of hydroxyl muraymycin A or B congeners were not found in the reported metabolites of the producer strain.[2]
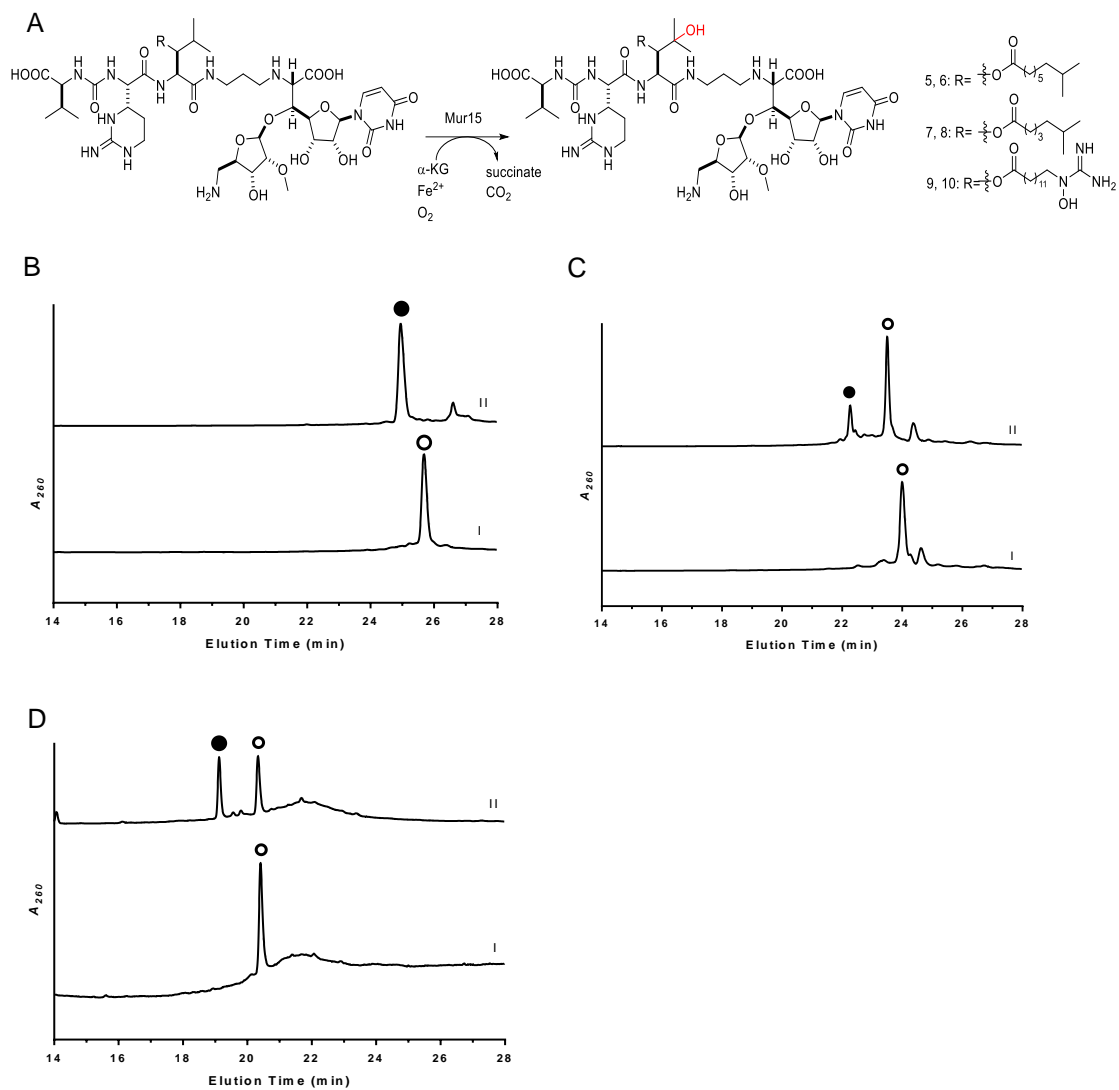
Figure 6.2 Characterization of Mur15 with muraymycin B2 (**5**), B6 (**7**) and A1 (**9**).
(A) Reaction catalyzed by Mur15 with **5** or **7** or **9**. (B) LC-MS analysis using **5** (O) after 6-hr without Mur15 (I), 6 h reaction (II). (C) LC-MS analysis using **7** (O) after 6 h without Mur15 (I), 6 h reaction (II). (D) LC-MS analysis using **9** (O) after 6 h without Mur15 (I), 6 h reaction (II).
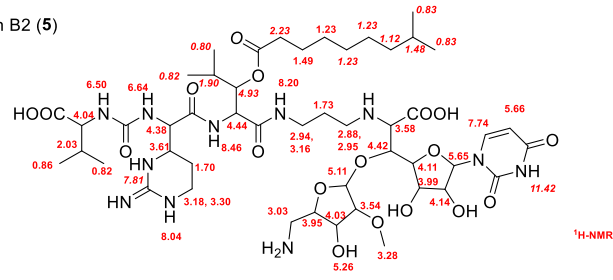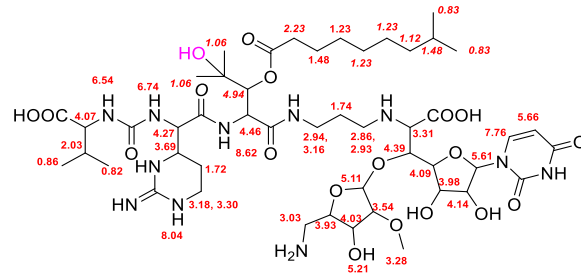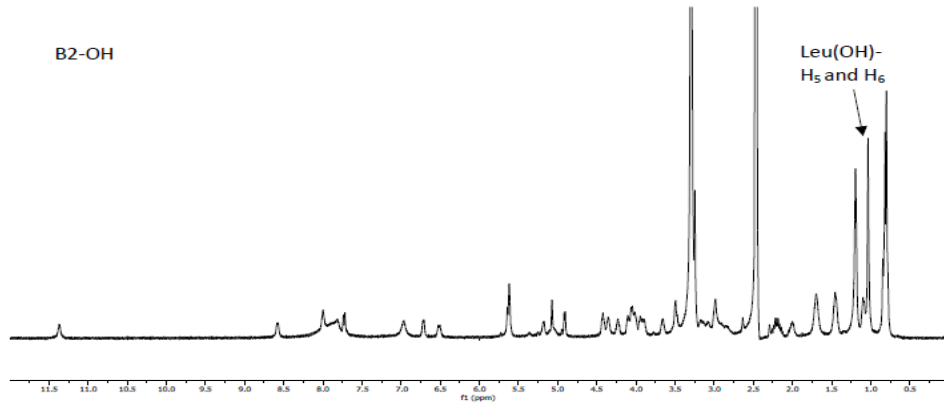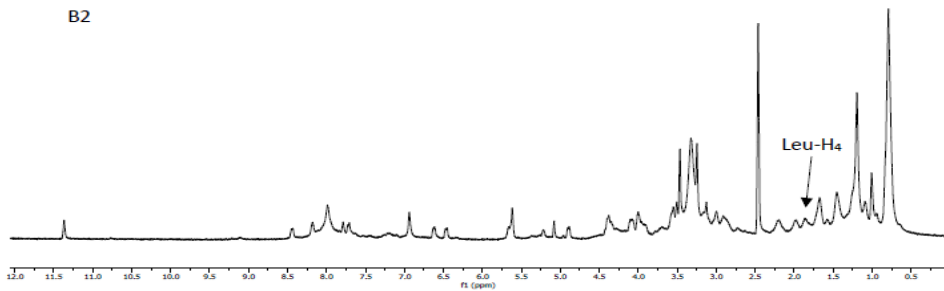
Figure 6.3 Comparison of ¹H NMR (DMSO-d_6, 400 MHz) between muraymycin B2, **5** and Mur15 product hydroxyl muraymycin B2, **6**.

Discovery of the activity promiscuity of Mur15 led us to test the activity of Mur15 with

L-Arg and L-Arg-Leu dipepetide as we proposed that hydroxyl arginine possibly is the

precursor for the biosynthesis of L-epicapreomycidine moiety of muraymycin. No

hydroxylation activity was detected by LC-MS with free L-Arg. However, Mur15 showed

hydrolase activity when incubated with Arg-Leu dipeptide and generated free arginine and

leucine (Figure 6.4). The result didn't exclude the possibility that Mur15 can catalyze the

hydroxylation of nonribosomal peptide synthetase (NRPS) tethered arginine, which is still in

the ongoing NRPS activity study.
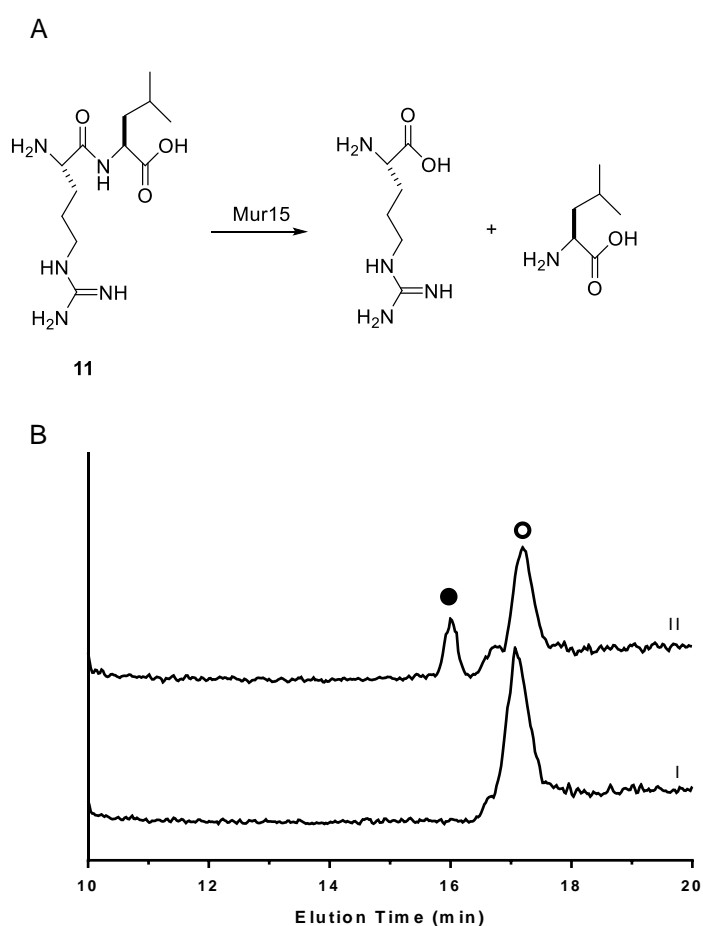
Figure 6.4 Characterization of Mur15 with L-Arg-Leu dipeptide, **11**.
(A) Reaction catalyzed by Mur15 with **11**. (B) LC-MS analysis using **11** (O) after 6 h without
Mur15 (I); 6 h reaction (II). Extracted ion chromatograms showing the production of leucine.

6.3.3 Activity Optimization and Kinetics Analysis

α-KG and O_2 was found to be necessary for the activity of Mur15 while ascorbate or Fe (II) was not essential for the reaction. Optimal activity of Mur15 was achieved in the range of 10-1000 μM $FeCl_2$. With 500 μM $FeCl_2$, Mur15 was found to have optimal activity in the range of 10-1000 μM ascorbate (Figures 6.5 A-B).

Kinetics analysis of Mur15 with muraymycin D1 revealed Michaelis-Menten kinetics yielding a $K_m = 11\pm1$ μM and $k_{cat} = 2\pm0.1$ min^{-1} with respect to α-KG and $K_m = 0.6\pm0.1$ mM and $k_{cat} = 10\pm1$ min^{-1} with respect to muraymycin D1. Kinetics analysis of Mur15 with muraymycin B2 revealed Michaelis-Menten kinetics yielding a $K_m = 0.6\pm0.2$ mM and $k_{cat} = 6 \pm 0.2$ min^{-1} with respect to muraymycin B2 (Figures 6.5 C-E). The catalytic efficiency k_{cat}/K_m with respect to muraymycin D1 is 2.4 times more than that of muraymycin B2, which to some extent predicted that the amount of hydroxyl muraymycin A or B congeners should be relatively low in the metabolites of the producer strain.
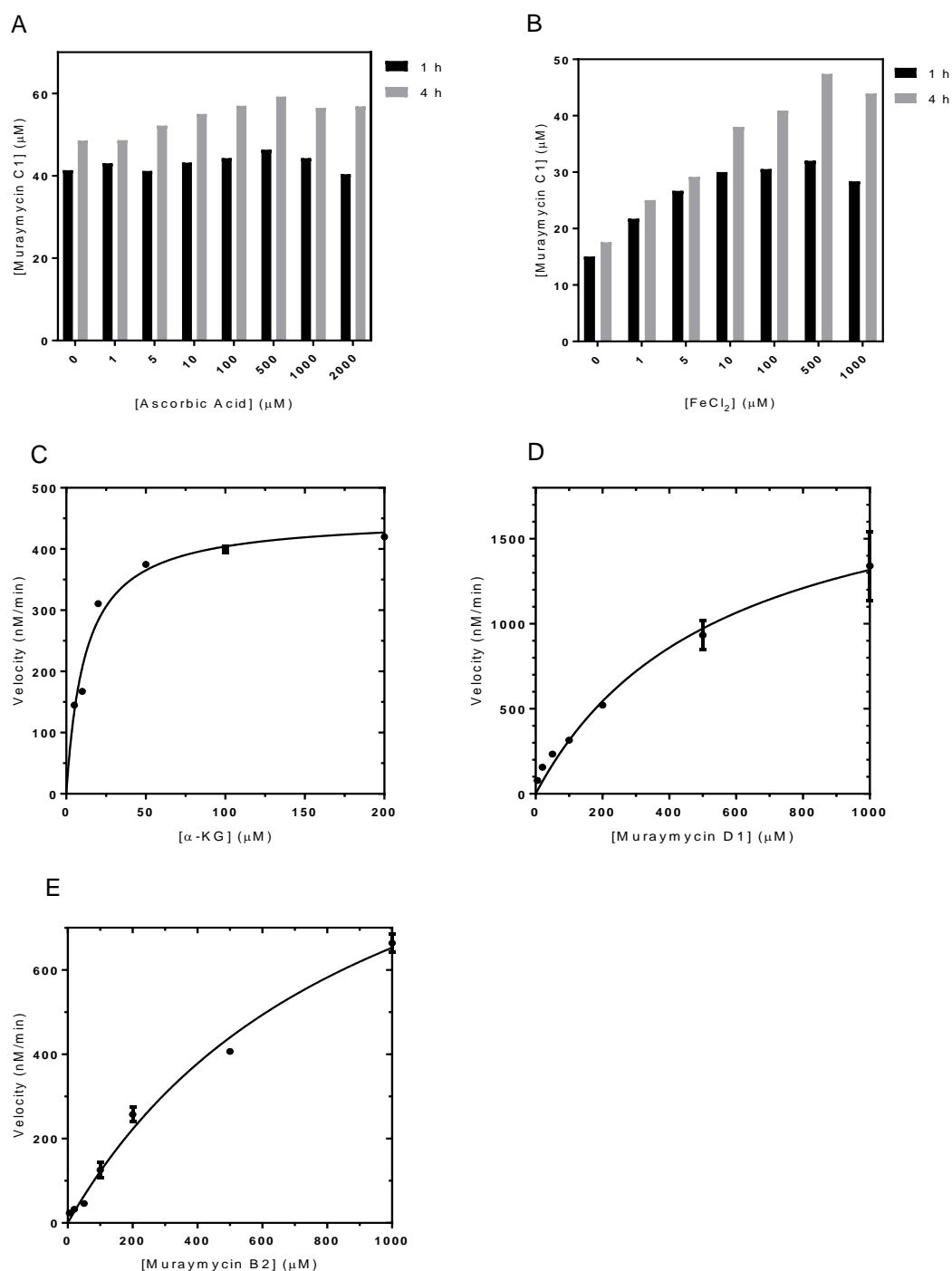
Figure 6.5 Activity optimization and kinetic analysis of Mur15.

(A) Optimal activity of Mur15 with respect to varied ascorbic acid in reactions containing 200 μM FeCl$_2$ and 200 nM Mur15. (B) Optimal activity of Mur15 with respect to varied FeCl$_2$ in reactions containing of 500 μM ascorbic acid and 200 nM Mur15. (C) Single-substrate kinetic analysis using variable α-KG (5 μ-200 μM), near saturating muraymycin D1(250 μM) and 200 nM Mur15. (D) Single-substrate kinetic analysis using variable muraymycin D1 (5 μ-1000 μM), near saturating α-KG (2.5 mM) and 200 nM Mur15. (E) Single-substrate kinetic analysis using variable muraymycin B2 (5 μ-1000 μM), near saturating α-KG (2.5 mM) and 200 nM Mur15. Data represent the average of minimally three independent replicates under initial velocity conditions.

6.3.4 Bioactivity of the Mur15 Products

The isolated Mur15 products, muraymcyin C1 and muraymycin B2-OH were tested for enzyme inhibitory activity against MraY from *S. aureus,* and antimicrobial activity against Gram-positive as well as Gram-negative strains (Table 6.1). To our surprise, muraymycin C1 showed 32 times decrease in IC_{50} against muraymycin D1, suggesting that hydroxylation at β position of muraymycin D1 greatly increased the inhibitory activity against MraY. Enzyme inhibitory activity against MraY *S. aureus* showed comparable IC_{50} of B2 and B2-OH, indicating that the hydroxylation at γ position didn't interfere with its binding to the target protein MraY. Muraymcyin C1 showed comparable antimicrobial activity to muraymycin D1 against *M. smegmatis* and *E. coli*, which indicates that the β hydroxylation didn't affect its antibacterial activity. Considering that muraymycin C1 showed 32 times increased efficacy against the target, hydroxylation at β position of muraymycin D1 possibly interfere its cellular penetration. Importantly, B2-OH didn't show growth inhibitory against *M. smegmatis* ATCC 14468 and *E. coli* BL21(DE3). However, B2-OH showed similar antibacterial activity to B2 against *E. coli* Δ*tolC* mutant, which further indicated that the hydroxylation possibly interfered with the cellular uptake.

Table 6.1 Bacterial MraY assays and antimicrobial activities of the substrate and product of Mur15.

compound	*S. aureus* MraY inhibition IC_{50} (pM)	*M. smegmatis* growth inhibition MIC (μg/mL)	*E. coli* Δ*tolC* mutant growth inhibition MIC (μg/mL)	*E. coli* BL21(DE3) growth inhibition MIC (μg/mL)
muraymycin B2	10±2	8	1	32
muraymycin B2-OH	16±3	>256	1	>256
muraymycin D1	$(4.8 \pm 1.3) \times 10^2$	4	1	16
muraymycin C1	16±2	4	1	8

6.4 Discussion

6.4.1 Timing of Hydroxylation in Muraymycin Biosynthetic Pathway

The discovery of muraymycin D and muraymycin C congeners indicates that the hydroxylation reaction occurred in the biosynthetic pathway. There are three possibilities of when the hydroxylation of the leucine moiety occurs in the biosynthetic pathway of muraymycin. I, hydroxylation of free leucine before the peptide assembles. Hydroxylation of free amino acid is well known in many biosynthetic pathways of nature products.[95-98] L-leucine was tested with Mur15 at first. However, Mur15 not reacting with free L-leucine exclude this possibility. II, late stage modification of muraymycin D congeners. The discovery of muraymycin D and C congeners also suggests that the hydroxylation may happen after the formation of muraymycin D. Activity assay and kinetic study of Mur15 with muraymycin D congeners both supported this hypothesis. Actually, late stage hydroxylation is also observed in many biosynthetic pathways.[99-100] III, hydroxylation of nonribosomal peptide synthetases (NRPS) tethered leucine moiety. Hydroxylation of NRPS peptidyl carrier protein (PCP)-bound amino acid is also found in many biosynthetic pathways.[101-103] There are several NRPSs in the biosynthetic assembly line of muraymycin, which are proposed to be responsible for the biosynthesis of peptide side chain of muraymycin. Whether or not Mur15 can catalyze the hydroxylation of NRPS tethered amino acid will be explored in the ongoing NRPS activity assays.

6.4.2 Repeated Hydroxylation by Multifunctional Enzyme

Dioxygenase Mur15 showed unusual substrate promiscuity. It catalyzed the hydroxylation of muraymycin D congeners, which are further utilized by acyltransferase to produce different fatty acid chain appended muraymycins (muraymycin A or B congeners). Different lipo-muraymycins can be further oxidized by the same enzyme Mur15 (Figure 6.6). Although oxygenase usually has strong substrate specificity, recently an emerging group of multifunctional dioxygenase have been studied. These enzymes usually catalyze two or more reactions in a very ordered behavior and goes through conformational change to catalyze different reactions.[104] Structure study of Mur15 bound with different muraymycin congeners will offer more information for further study of this unusual repeated hydroxylation reaction.
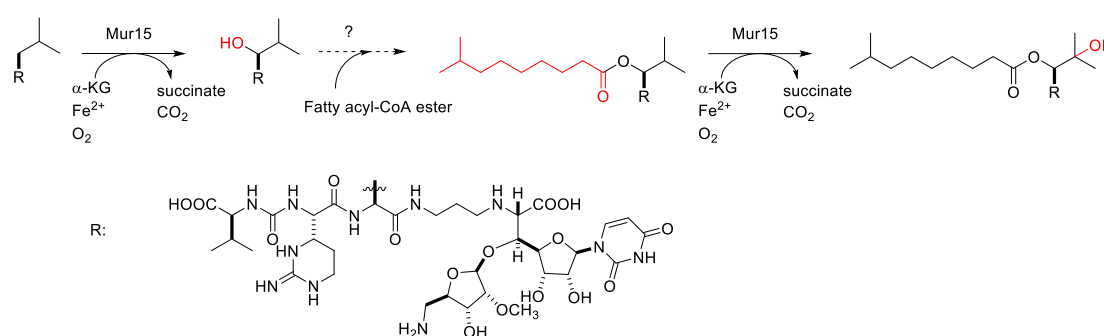
Figure 6.6 Repeated hydroxylation catalyzed by Mur15.

6.5 Conclusion

Enzyme Mur15, which belongs to cupin family and involves in muraymycin late stage modification, is functionally assigned as a non-heme, Fe (II)-dependent α-ketoglutarate dioxygenase that catalyzes the β hydroxylation of leucine moiety in muraymycin D1 to form muraymycin C1. Mur15 can also hydroxylate the γ position of leucine moiety to muraymycins with fatty acid chain in β position. Moreover, Mur15 showed lyase activity to hydrolyze arginine-leucine dipeptide but could not catalyze the single amino acid to its hydroxylated form.

6.6 Supporting Information
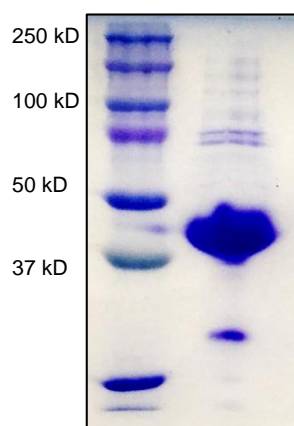
Figure S6.1 SDS-PAGE analysis of purified His$_6$-Mur15 (expected MW of 39 kD).

A
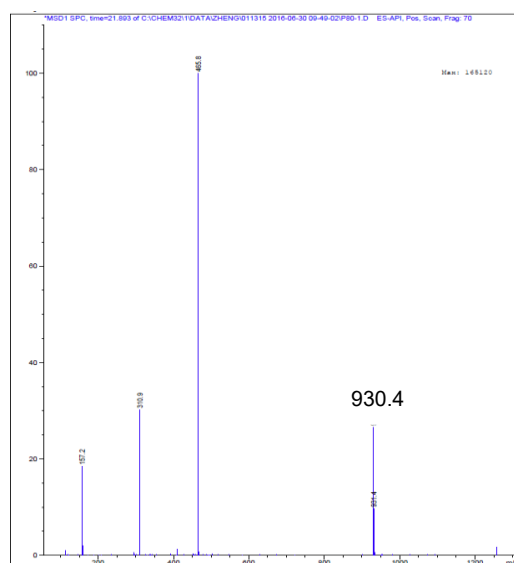
B
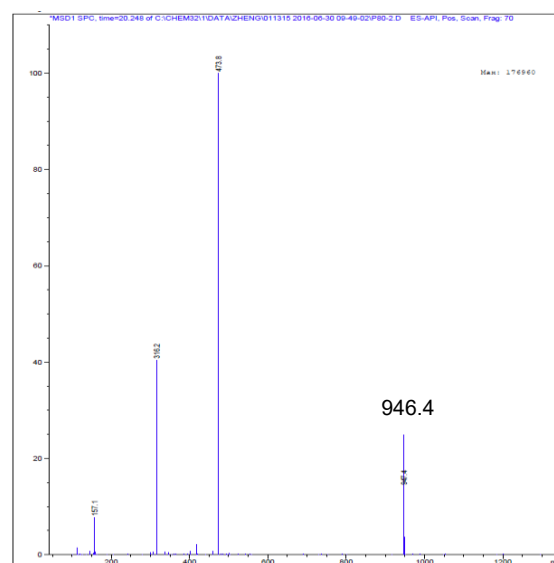
Figure S6.2 Identification of the Mur15 product with **1**.
(A) Mass spectrum for the peak at elution time t = 21.893 min corresponding to **1**. (B) Mass spectrum for the peak at elution time t = 20.248 min corresponding to Mur15 product **2**.

A

B

916.4

932.3
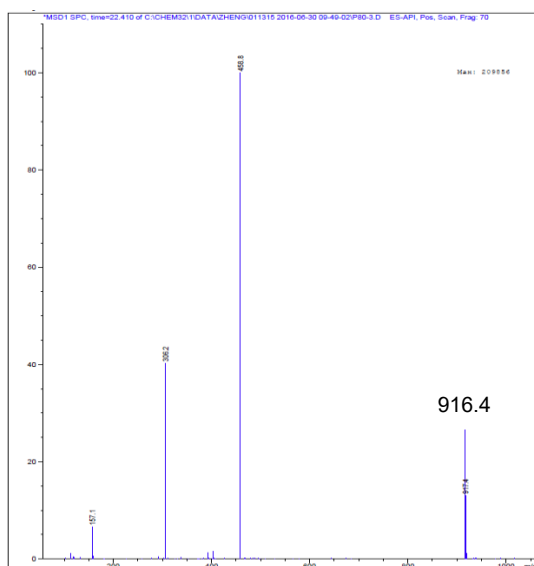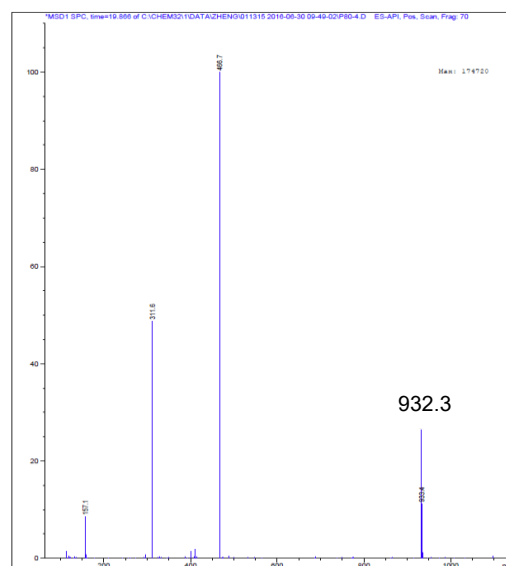
Figure S6.3 Identification of the Mur15 product with **3**.

(A) Mass spectrum for the peak at elution time t = 22.410 min corresponding to **3**. (B) Mass spectrum for the peak at elution time t = 19.866 min corresponding to Mur15 product **4**.
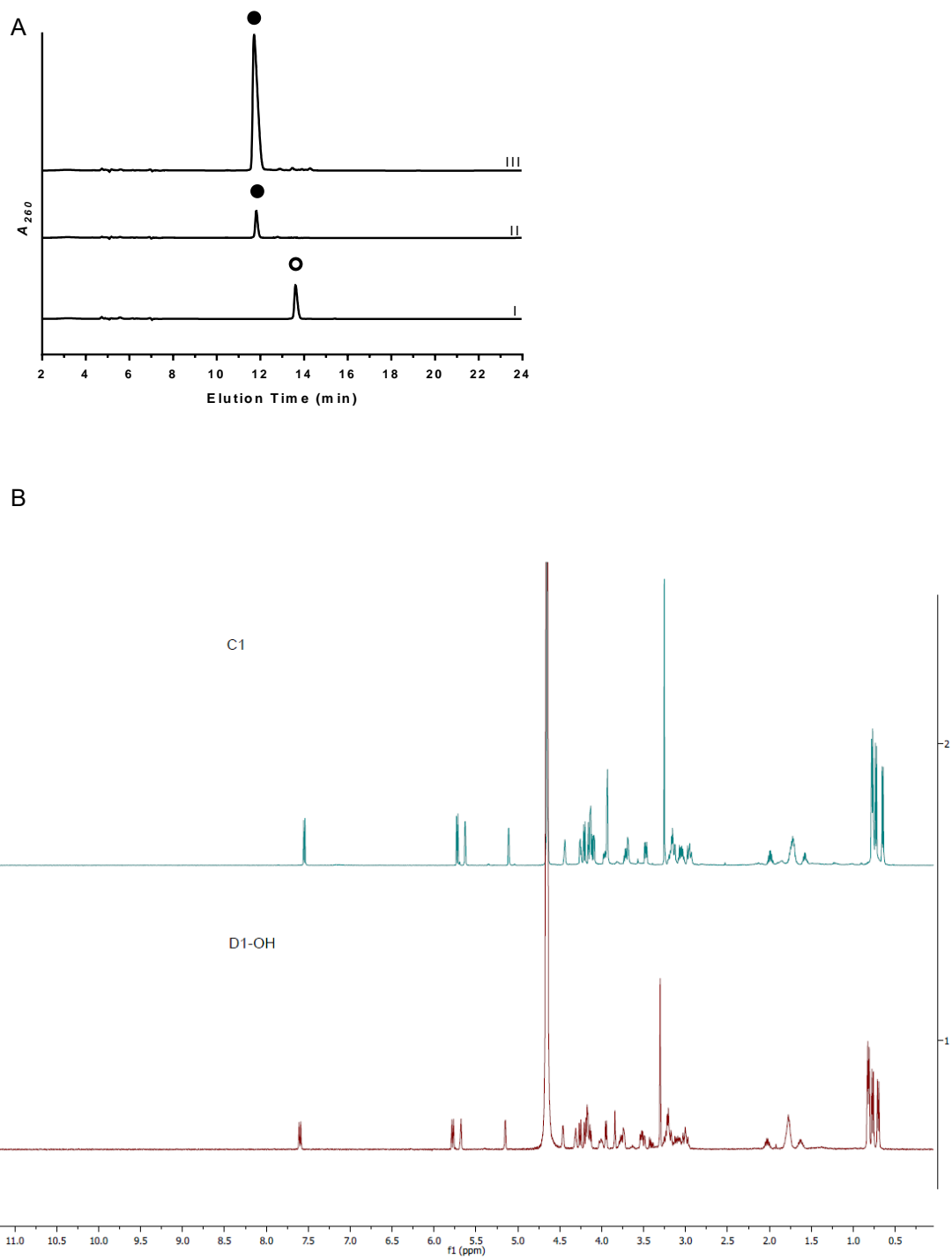
Figure S6.4 Identification of the Mur15 product with **1**.

(A) HPLC analysis using 1 (O) after 6 h without Mur15 (I), 6 h reaction (II), 6 h reaction co-injected with **2** (●) (III). (B) Comparison of ^{1}HNMR between **2** and Mur15 product hydroxyl muraymycin D1.
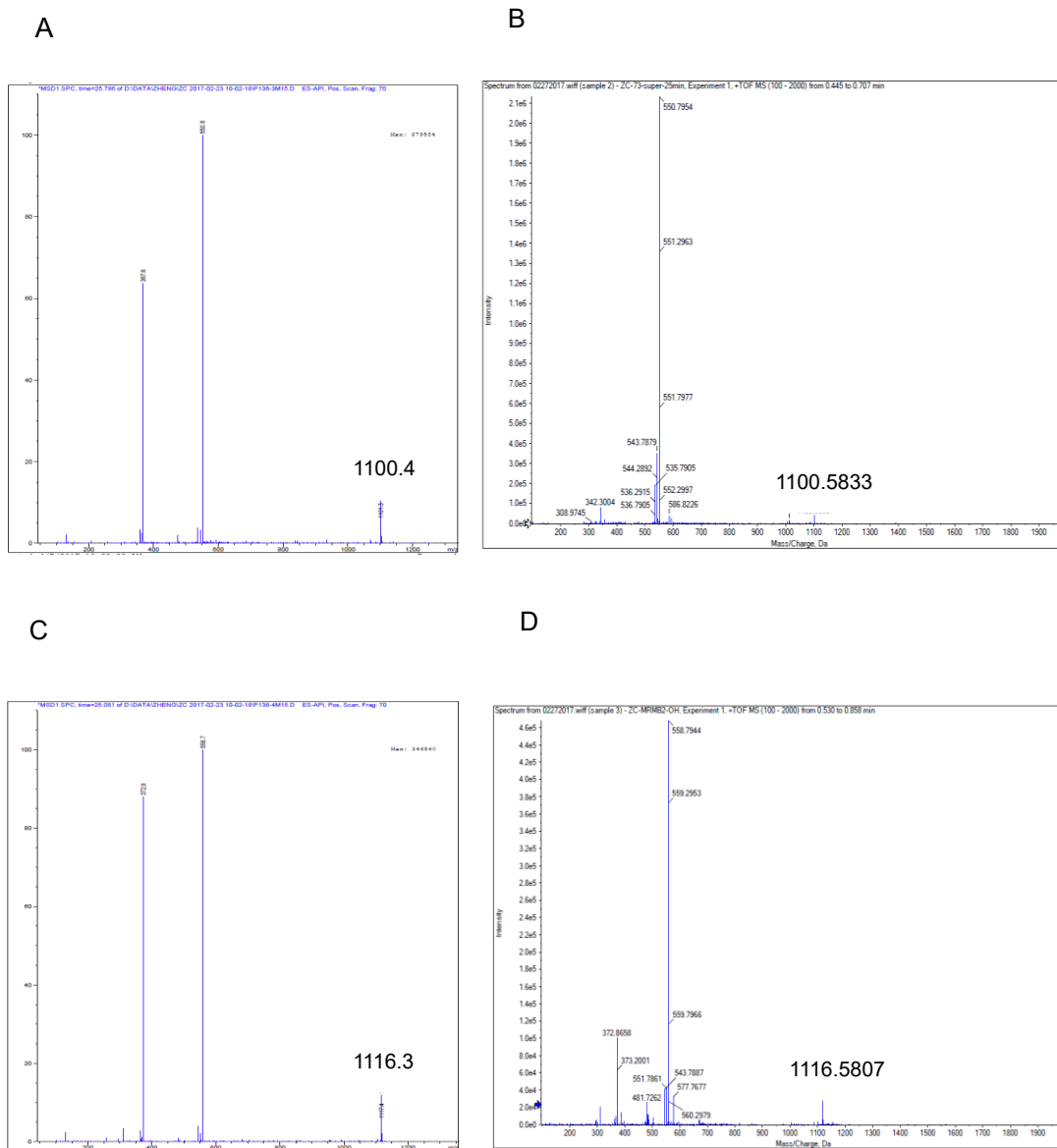
Figure S6.5 Identification of the Mur15 product with **5**.
(A) Mass spectrum for the peak at elution time t = 25.786 min corresponding to **5**. (B) (+)-HR-ESI-MS (positive mode) of **5** (expected (M+H)$^+$ ion at m/z = 1100.5834, found: 1100.5833). (C) Mass spectrum for the peak at elution time t = 25.081 min corresponding to Mur15 product **6**. (D) (+)-HR-ESI-MS (positive mode) of **6**. (expected (M+H)$^+$ ion at m/z = 1116.5783, found: 1116.5807).
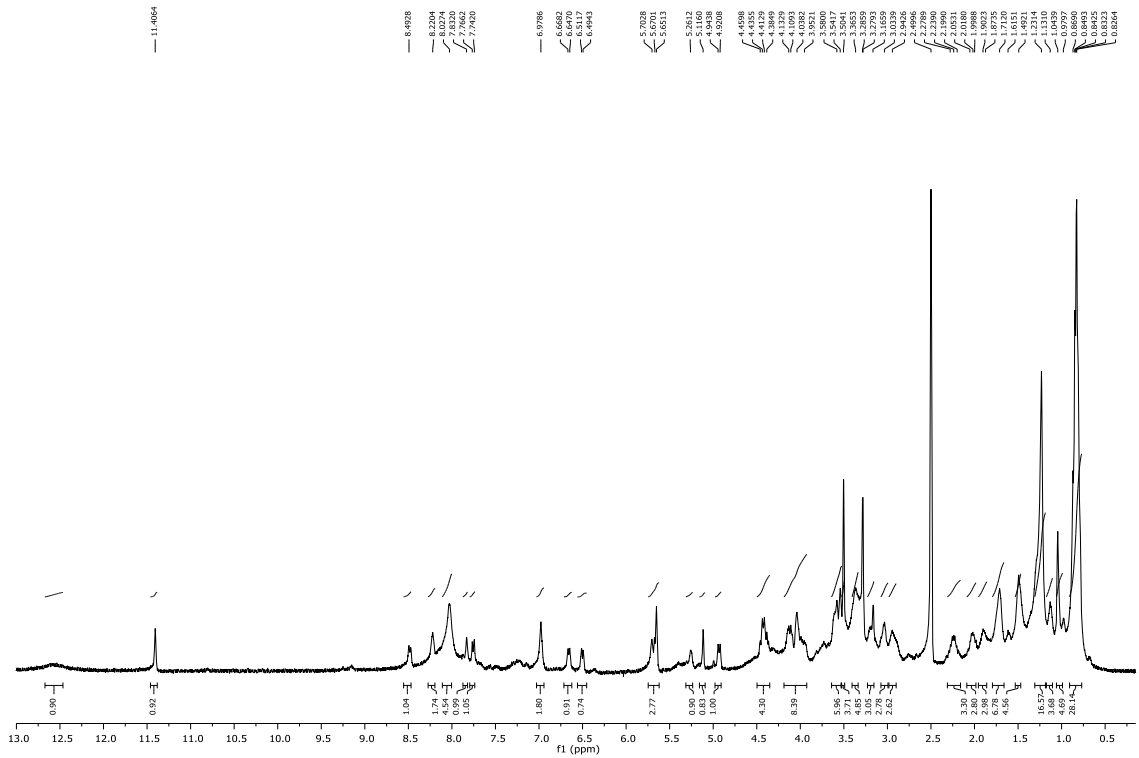
Figure S6.6 ¹H NMR spectrum (DMSO-*d₆*, 400 MHz) of muraymycin B2 (**5**).
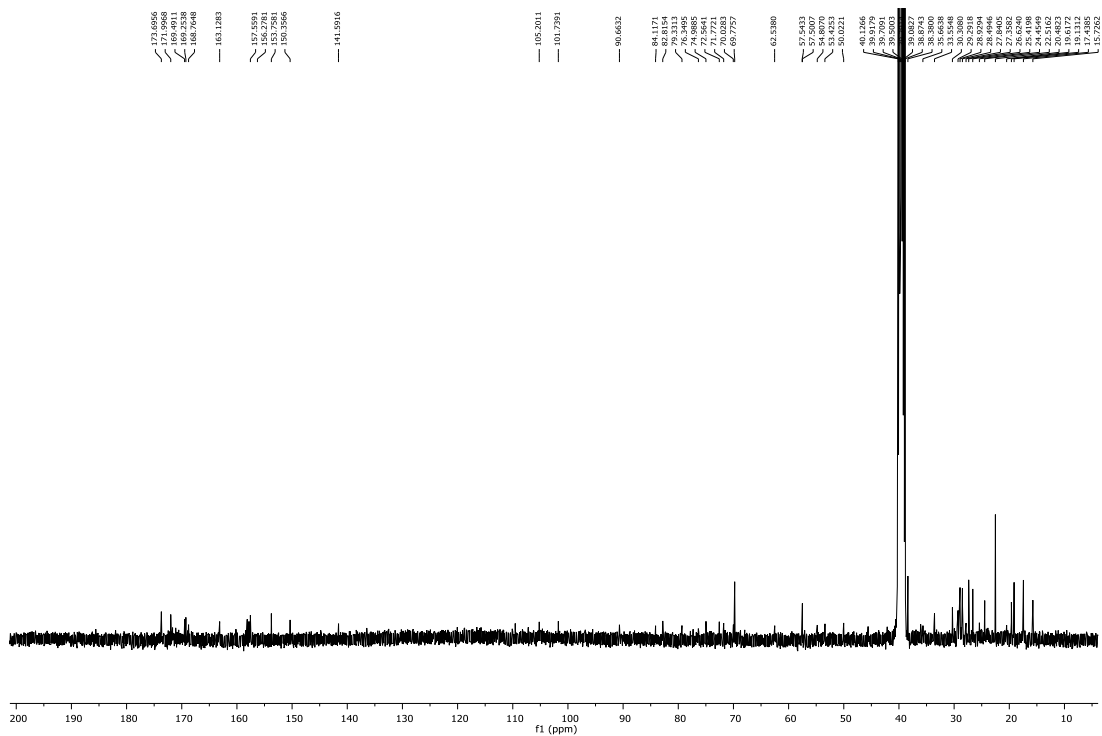
Figure S6.7 ¹³C NMR spectrum (DMSO-*d₆*, 100 MHz) of muraymycin B2 (**5**).
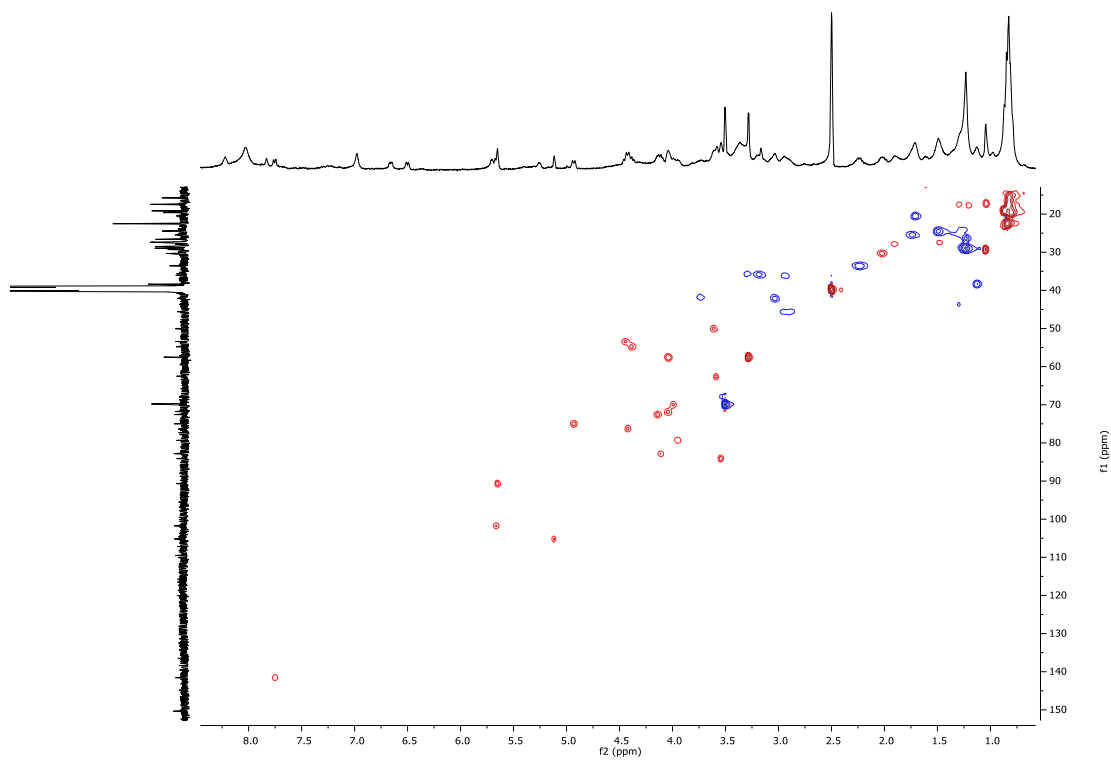
Figure S6.8 HSQC spectrum (DMSO-*d₆*, 400 MHz) of muraymycin B2 (**5**).
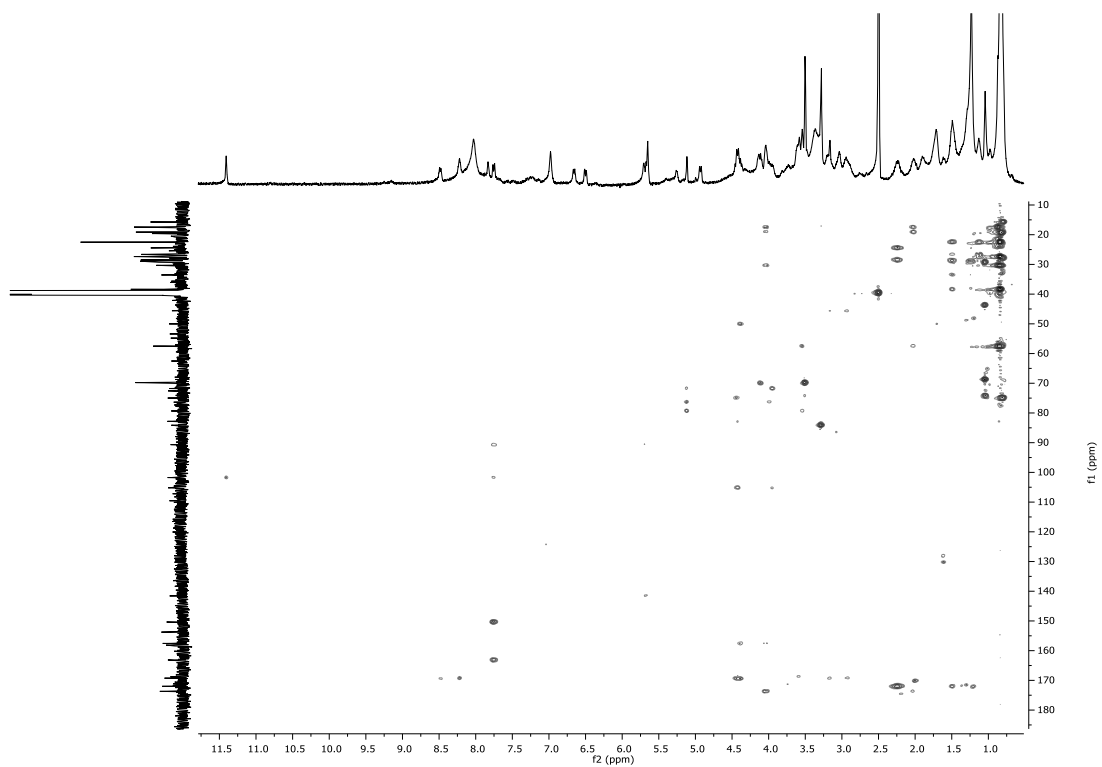
Figure S6.9 HMBC spectrum (DMSO-*d₆*, 400 MHz) of muraymycin B2 (**5**).
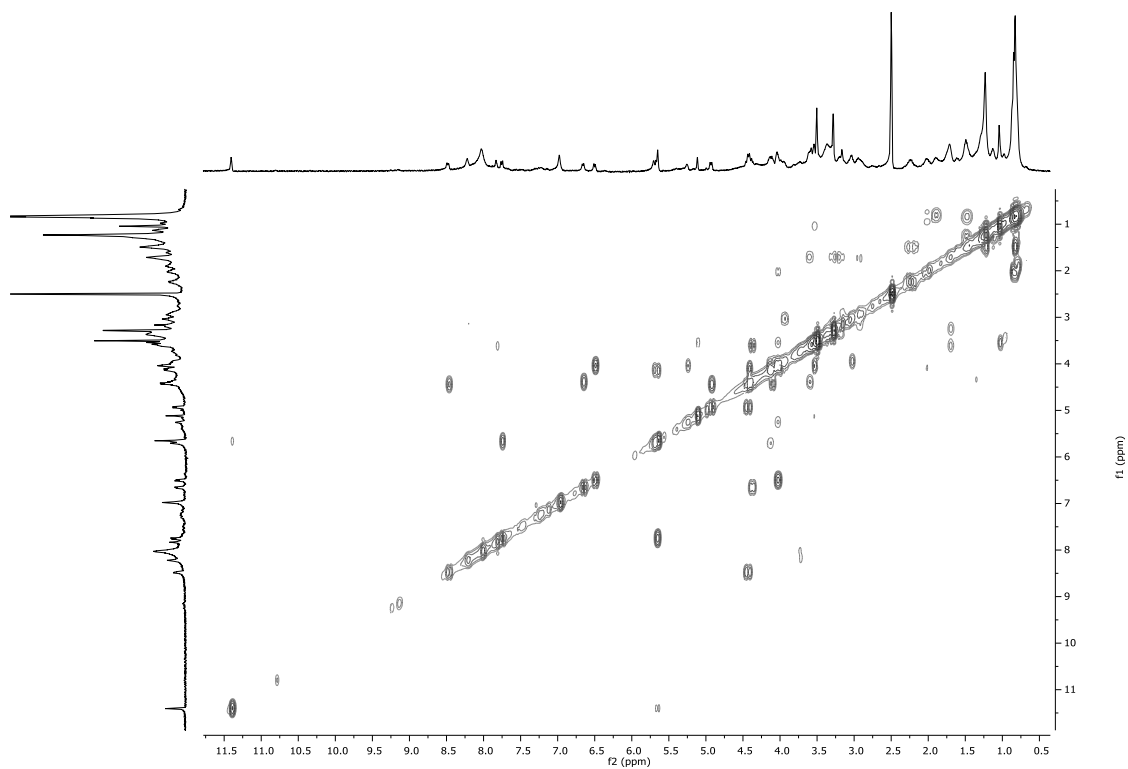
Figure S6.10 ^{1}H-^{1}H COSY spectrum ((DMSO-d_6, 400 MHz) of muraymycin B2 (**5**).
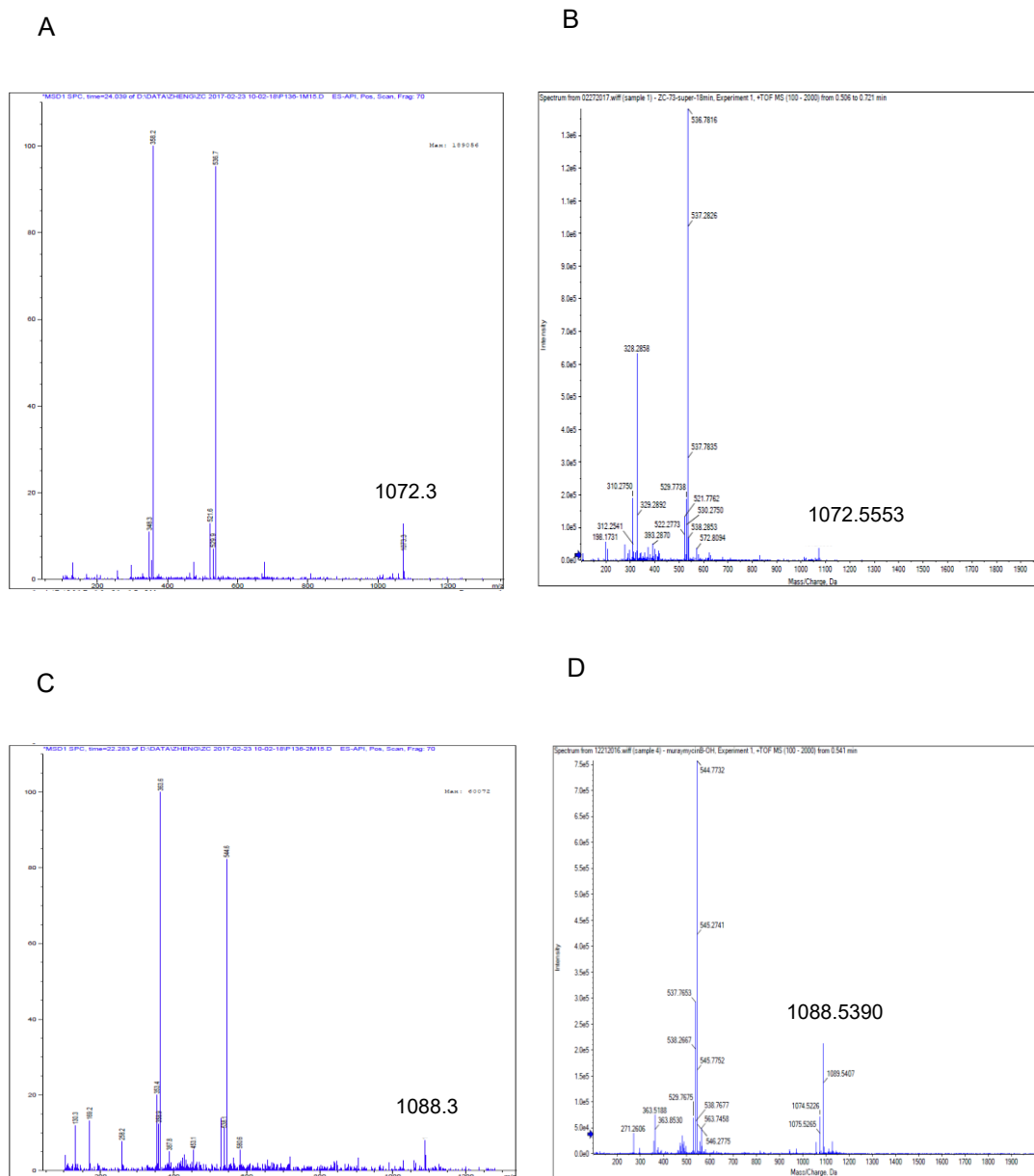
Figure S6.11 Identification of the Mur15 product with **7**.

(A) Mass spectrum for the peak at elution time t = 24.039 min corresponding to **7**. (B) (+)-HR-ESI-MS (positive mode) of **7**(expected $(M+H)^+$ ion at m/z = 1072.5521, found: 1072.5553). (C) Mass spectrum for the peak at elution time t = 22.283 min corresponding to Mur15 product **8**. (D) (+)-HR-ESI-MS (positive mode) of **8**(expected $(M+H)^+$ ion at m/z = 1088.5470, found: 1088.5407).
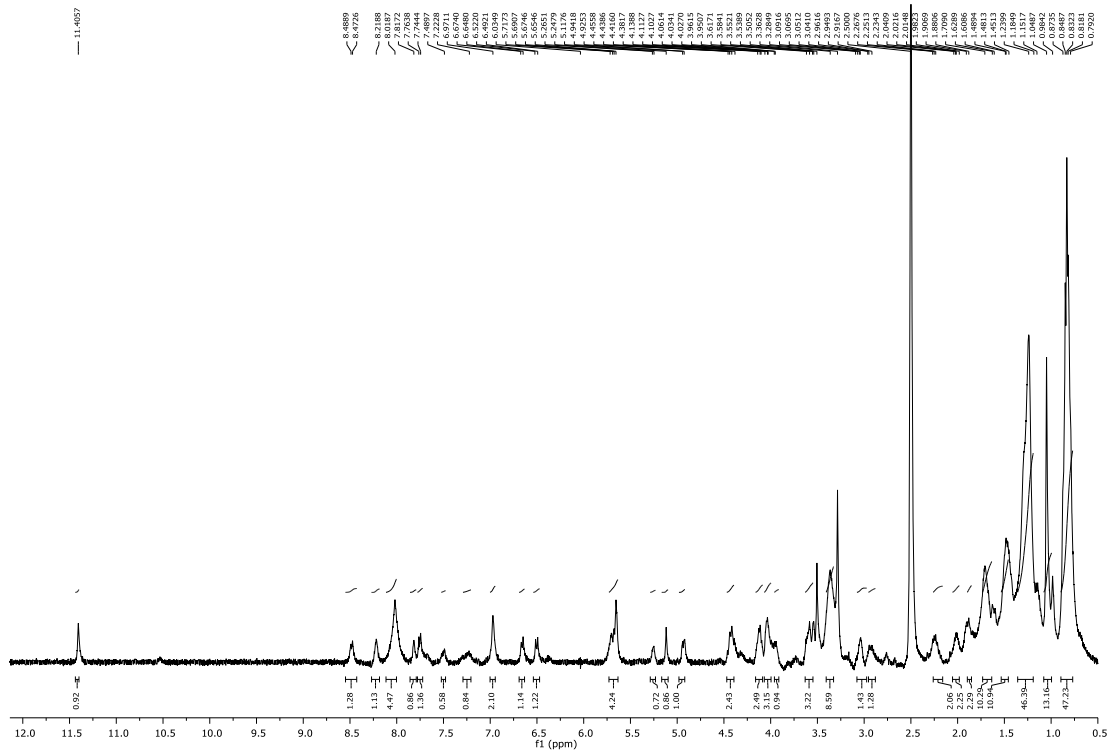
Figure S6.12 ^{1}H NMR spectrum (DMSO-d_6, 400 MHz) of muraymycin B6 (**7**).
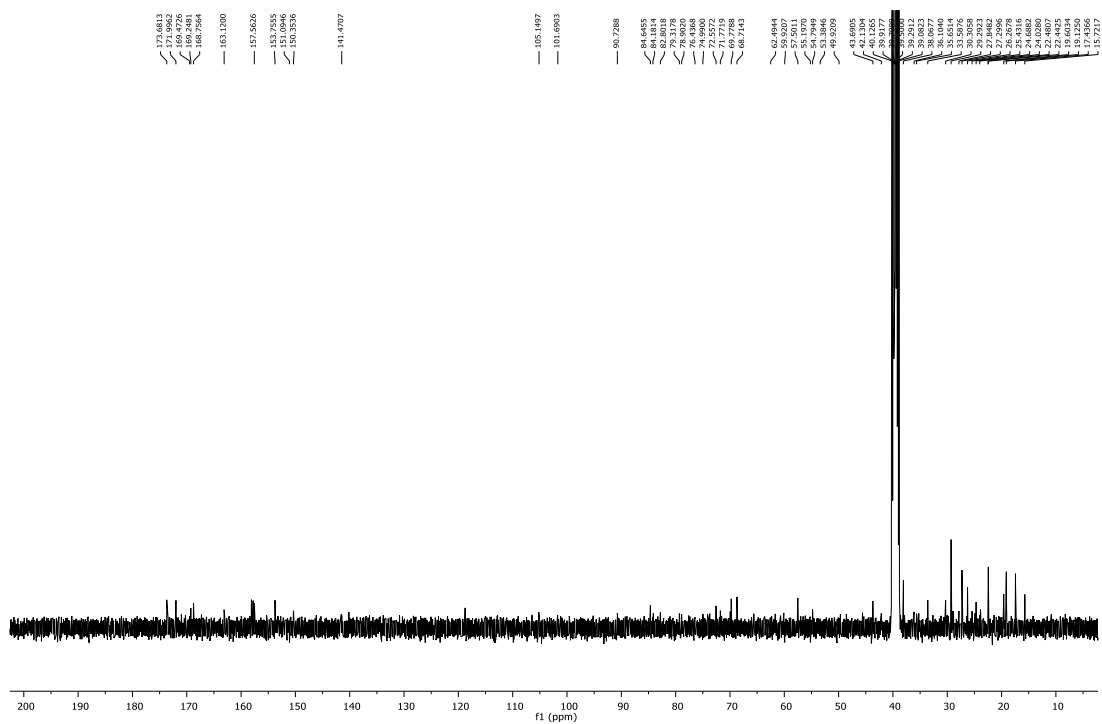
Figure S6.13 ^{13}C NMR spectrum (DMSO-d_6, 100 MHz) of muraymycin B6 (**7**).
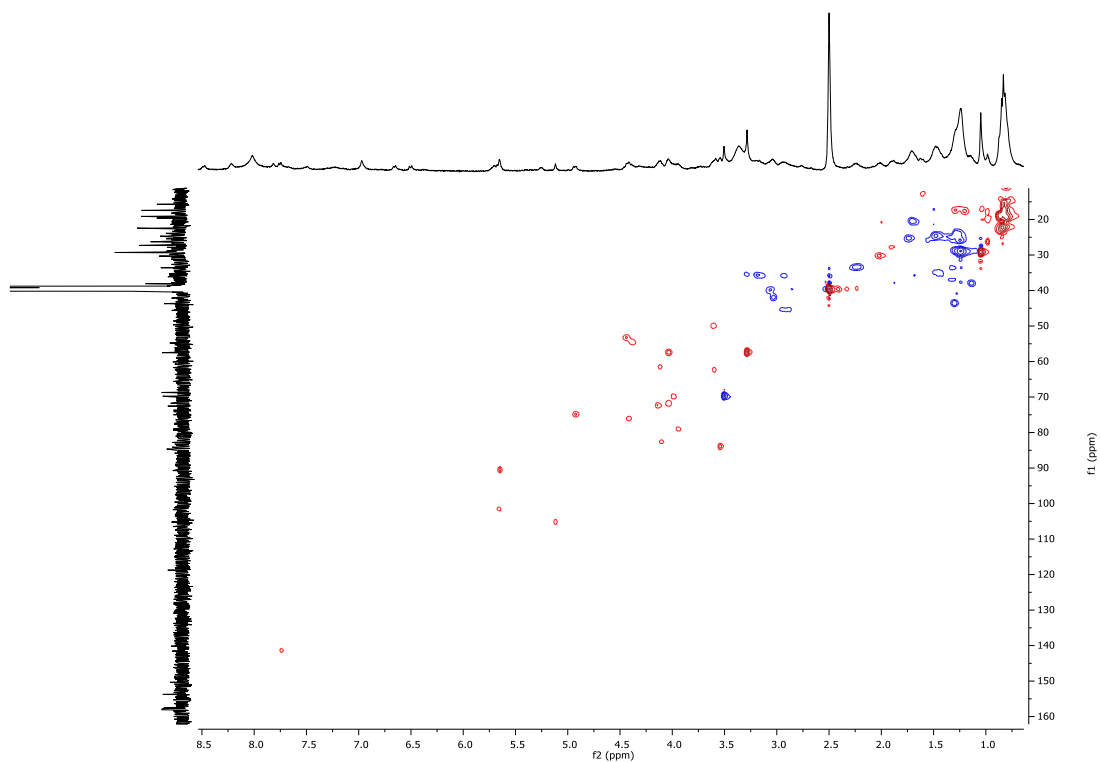
Figure S6.14 HSQC spectrum (DMSO-*d₆*, 400 MHz) of muraymycin B6 (**7**).
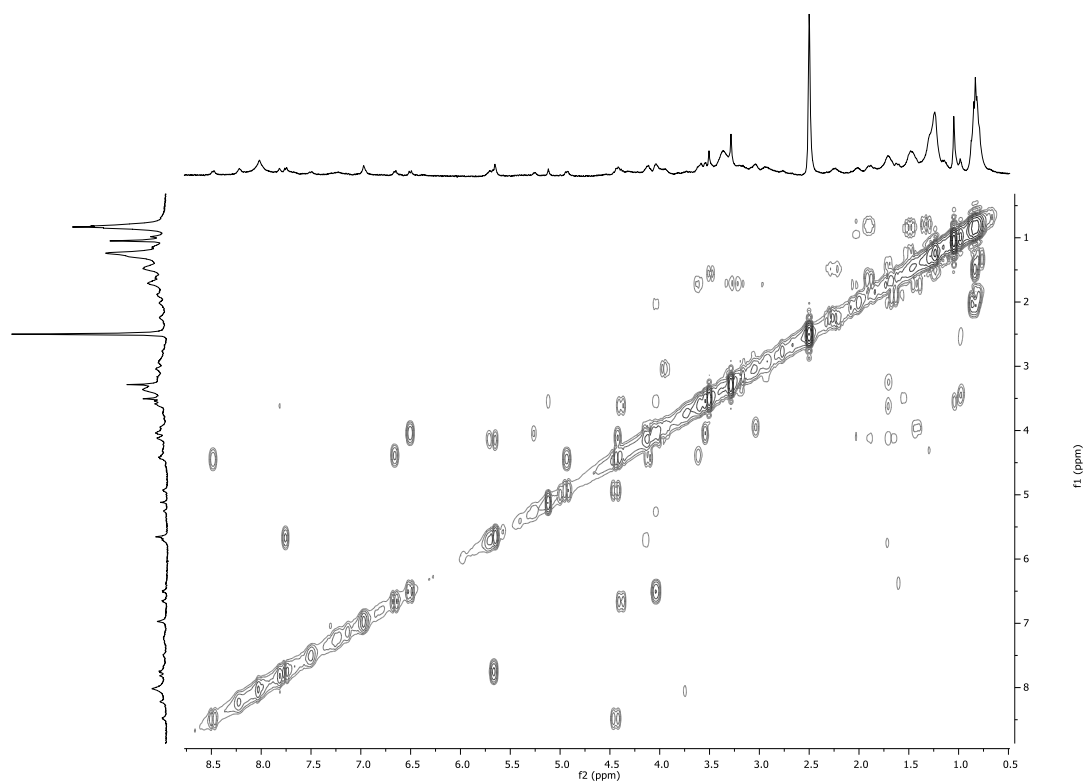
Figure S6.15 HMBC spectrum (DMSO-*d₆*, 400 MHz) of muraymycin B6 (**7**).
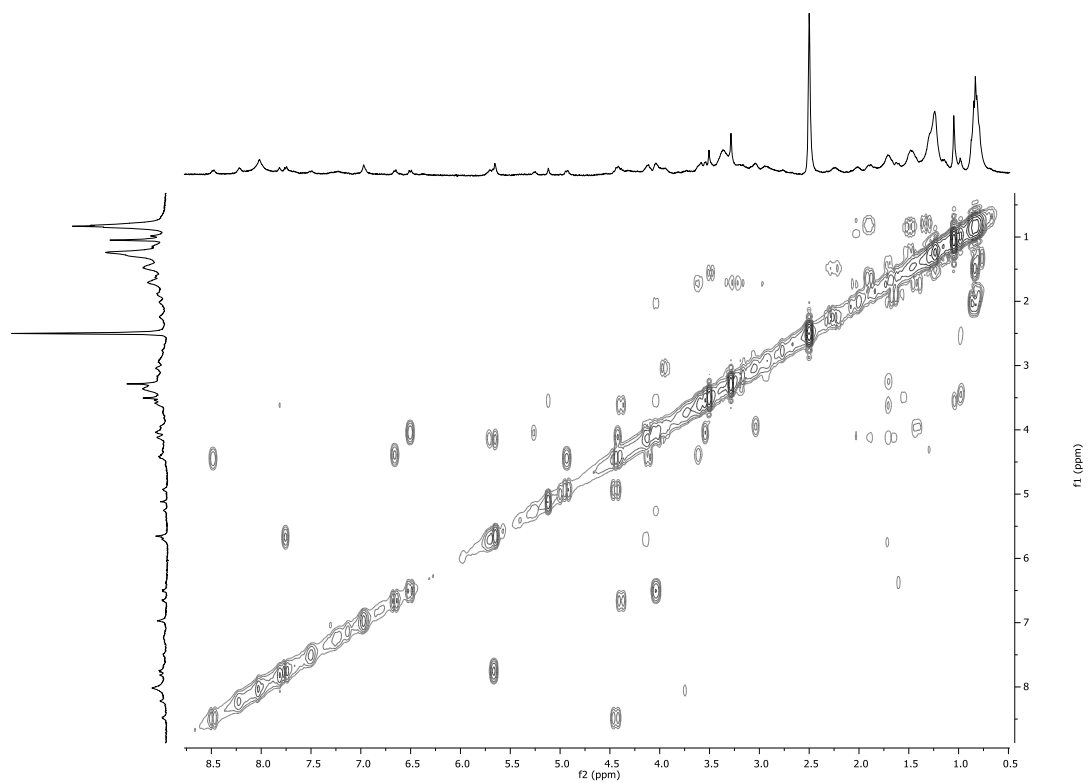
Figure S6.16 ^{1}H-^{1}H COSY spectrum ((DMSO-d_6, 400 MHz) of muraymycin B6 (**7**).
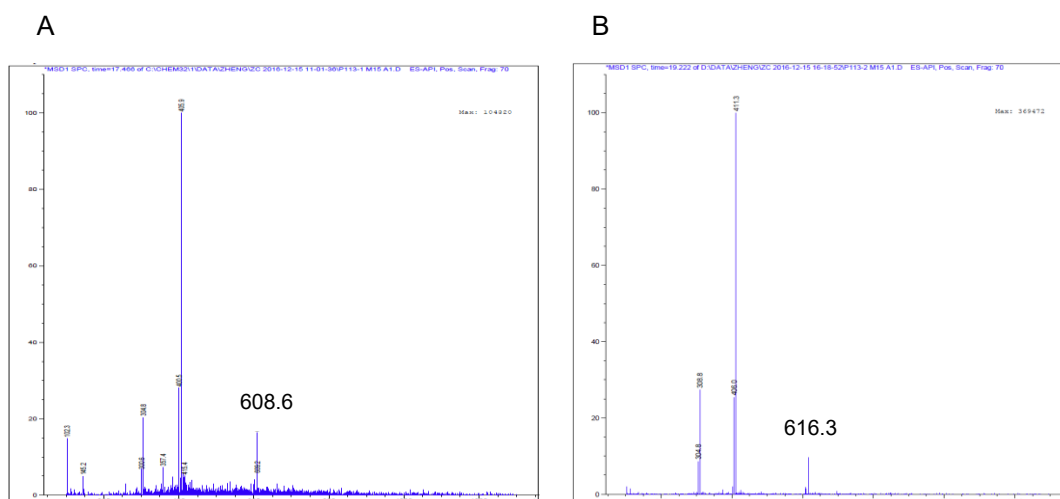
Figure S6.17 Identification of the Mur15 product with **9**.

(A) Mass spectrum for the peak at elution time t = 17.466 min corresponding to **9** (expected (M+H)$^+$ ion at *m/z* = 608.33, found: 608.6). (B) Mass spectrum for the peak at elution time t = 19.222 min corresponding to Mur15 product **10** (expected (M+H)$^+$ ion at *m/z* = 616.33, found: 616.3).
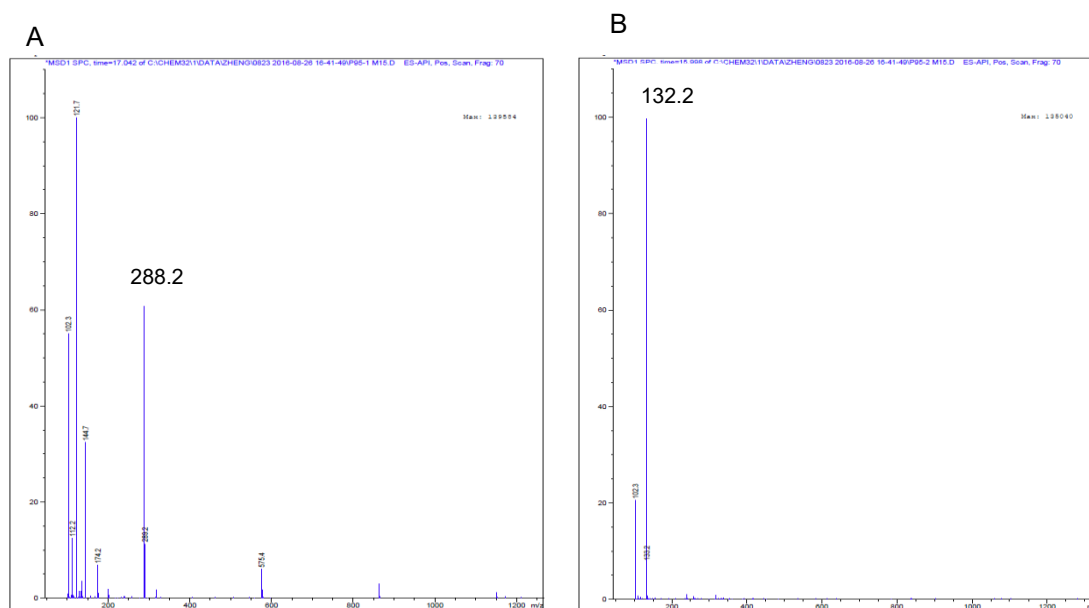
Figure S6.18 Identification of the Mur15 product with **11**.

(A) Mass spectrum for the peak at elution time t = 17.466 min corresponding to **11**(Calc: 288.20, found: 288.2). (B) Mass spectrum for the peak at elution time t = 19.222 min corresponding to Mur15 product L-leucine (expected (M+H)$^+$ ion at *m/z* = 132.10, found: 132.2).

Chapter 7 : Ongoing Studies and Future Directions

7.1 Biosynthetic Mechanism of the NRPS Assembly Line

We have presented the delineation of the biosynthetic pathway for the alkyl aminoribosyl-glycyluridine moiety upon *in vitro* characterization of nine enzymes (Mur16-20, Mur23, 24,26) (Figure 7.1). Next we are going to study the assembly line of the peptidyl moiety of muraymycin, which contains basic amino acid-epicapreomycidine-urea-valine moiety with interesting amino acid-urea-amino acid motif effectively inverting the direction of the peptide chain. Seven enzymes that are proposed to be involved in the NRPS assembly line have been expressed. Isotopic enrichment experiment feeding with leucine, arginine, valine and sodium bicarbonate is carried out. ATP-PP$_i$ exchange assay will be performed to test adenylation domains activity. Covalent loading of the amino acid will be characterized by SDS-gel and HRMS. The condensation of the assembled peptide with the alkyl aminoribosyl-glycyluridine will also be studied.
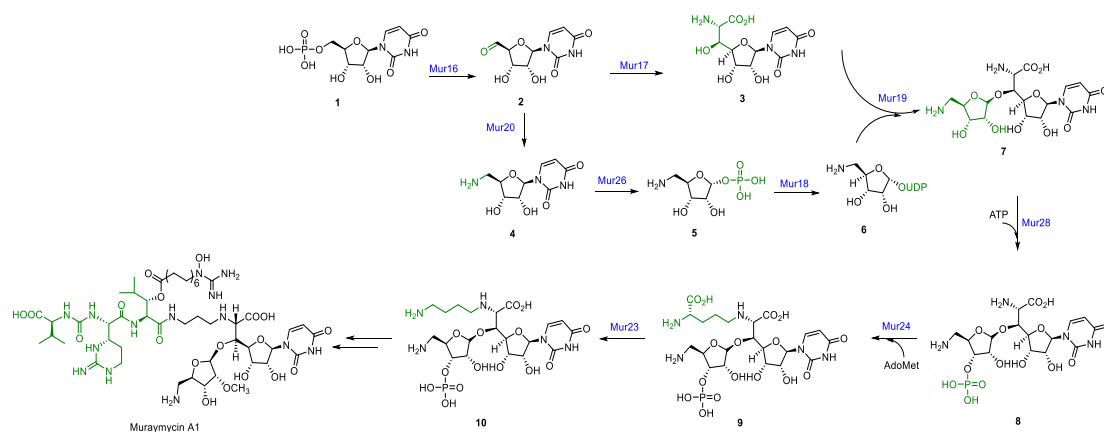
Figure 7.1 Biosynthetic pathway towards alkyl aminoribosyl-glycyluridine moiety of muraymycin.

7.2 Biosynthetic Mechanism of the Formation of the N-methyldiazepanone Moiety of

Caparazamycin Like A-90289

LipJ, from biosynthetic gene cluster of caprazamycin A-90289 (Figure 5.1), shared 35% sequence identity to Mur24. Activity tests revealed that, like Mur24, LipJ catalyzes the incorporation of butyric acid to phosphorylated disaccharide. Proposed biosynthetic pathway of the formation of *N*-methyldiazepanone moiety of A-90289 by BLAST analysis is shown in Figure 7.2. LipG, LipH, LipI and LipQ were expressed in *E. coli* BL21(DE3). Activity tests will be performed accordingly.
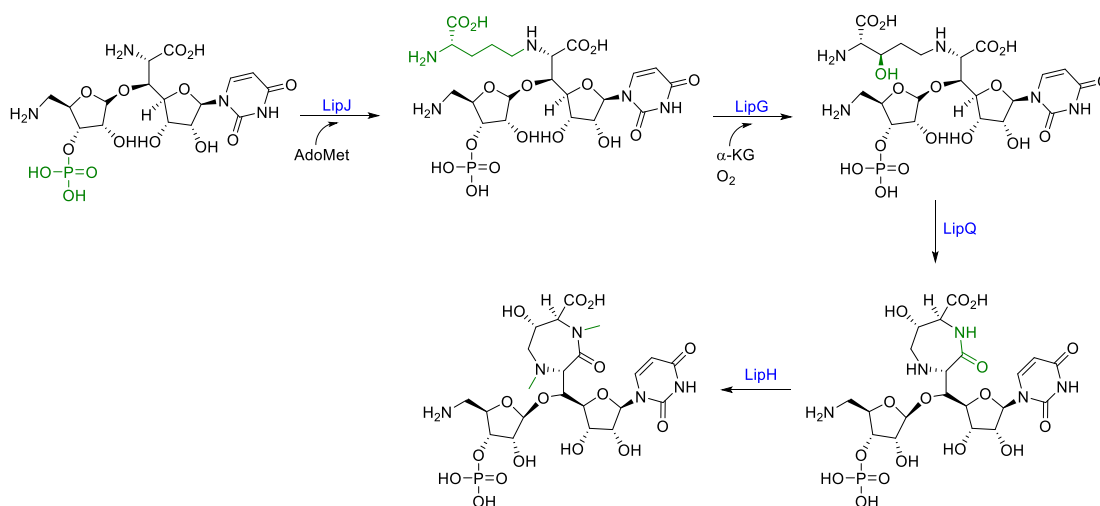
Figure 7.2 Proposed biosynthetic pathway towards N-methyldiazepanone moiety of A-90289.

7.3 Acyltransferase for the Fatty Acid Chain Appendage of Muraymycin

All of muraymycins have a common peptide appended aminoribosyl uronic acid core structure. Members of this family are mainly different in the fatty acid chain. Muraymycin A1, the one with the longest charged fatty acid chain, is the most active one. In chapter 2, we also presented that the structure of the fatty acid chain has great impact on activity of muraymycin. As in chapter 6 we characterized the function of dioxygenase Mur15, which catalyzes the β hydroxylation of muraymycin D1 to form muraymycin C1 (Figure 6.6), we proposed that

acyltransferase will be required to form muraymycins with different fatty acid chain. Therefore, the acyltransferase that is responsible for the fatty acid chain appendage of muraymycin will be characterized. Muraymycins with different fatty acid chains will be made with the acyltransferase in order to obtain more active muraymycin congeners.

References

1. McDonald, L. A.; Barbieri, L. R.; Carter, G. T.; Lenoy, E.; Lotvin, J.; Petersen, P. J.; Siegel, M. M.; Singh, G.; Williamson, R. T., Structures of the Muraymycins, Novel Peptidoglycan Biosynthesis Inhibitors. *Journal of the American Chemical Society* **2002,** *124* (35), 10260-10261.

2. Carter, G.; Lotvin, J.; McDonald, L., Antibiotics AA-896. Google Patents: 2003.

3. Huang, L. Y.; Huang, S. H.; Chang, Y. C.; Cheng, W. C.; Cheng, T. J. R.; Wong, C. H., Enzymatic synthesis of lipid II and analogues. *Angewandte Chemie International Edition* **2014,** *53* (31), 8060-8065.

4. Chung, B. C.; Mashalidis, E. H.; Tanino, T.; Kim, M.; Matsuda, A.; Hong, J.; Ichikawa, S.; Lee, S.-Y., Structural insights into inhibition of lipid I production in bacterial cell wall synthesis. *Nature* **2016,** *533* (7604), 557-560.

5. Chung, B. C.; Zhao, J.; Gillespie, R. A.; Kwon, D. Y.; Guan, Z.; Hong, J.; Zhou, P.; Lee, S. Y., Crystal structure of MraY, an essential membrane enzyme for bacterial cell wall synthesis. *Science* **2013,** *341* (6149), 1012-6.

6. Koppermann, S.; Ducho, C., Natural Products at Work: Structural Insights into Inhibition of the Bacterial Membrane Protein MraY. *Angewandte Chemie International Edition* **2016,** *55* (39), 11722-11724.

7. Mitachi, K.; Aleiwi, B. A.; Schneider, C. M.; Siricilla, S.; Kurosu, M., Stereocontrolled Total Synthesis of Muraymycin D1 Having a Dual Mode of Action against Mycobacterium tuberculosis. *J Am Chem Soc* **2016,** *138* (39), 12975-12980.

8. Takeoka, Y.; Tanino, T.; Sekiguchi, M.; Yonezawa, S.; Sakagami, M.; Takahashi, F.; Togame, H.; Tanaka, Y.; Takemoto, H.; Ichikawa, S.; Matsuda, A., Expansion of Antibacterial Spectrum of Muraymycins toward Pseudomonas aeruginosa. *ACS Medicinal Chemistry Letters* **2014,** *5* (5), 556-560.

9. Tanino, T.; Ichikawa, S.; Al-Dabbagh, B.; Bouhss, A.; Oyama, H.; Matsuda, A., Synthesis and Biological Evaluation of Muraymycin Analogues Active against Anti-Drug-Resistant Bacteria. *ACS Medicinal Chemistry Letters* **2010,** *1* (6), 258-262.

10. Wiegmann, D.; Koppermann, S.; Wirth, M.; Niro, G.; Leyerer, K.; Ducho, C., Muraymycin nucleoside-peptide antibiotics: uridine-derived natural products as lead structures for the development of novel antibacterial agents. *Beilstein journal of organic chemistry* **2016,** *12*, 769-795.

11. Yamashita, A.; Norton, E.; Petersen, P. J.; Rasmussen, B. A.; Singh, G.; Yang, Y.; Mansour, T. S.; Ho, D. M., Muraymycins, novel peptidoglycan biosynthesis inhibitors: synthesis and SAR of their analogues. *Bioorg Med Chem Lett* **2003,** *13* (19), 3345-50.

12. Lin, Y.-I.; Li, Z.; Francisco, G. D.; McDonald, L. A.; Davis, R. A.; Singh, G.; Yang, Y.; Mansour, T. S., Muraymycins, novel peptidoglycan biosynthesis inhibitors: semisynthesis and SAR of Their derivatives. *Bioorganic & Medicinal Chemistry Letters* **2002,** *12* (17), 2341-2344.

13. Spork, A. P.; Büschleb, M.; Ries, O.; Wiegmann, D.; Boettcher, S.; Mihalyi, A.; Bugg, T. D. H.; Ducho, C., Lead Structures for New Antibacterials: Stereocontrolled Synthesis of a Bioactive Muraymycin Analogue. *Chemistry – A European Journal* **2014,** *20* (47), 15292-15297.

14. Tanino, T.; Al-Dabbagh, B.; Mengin-Lecreulx, D.; Bouhss, A.; Oyama, H.; Ichikawa, S.; Matsuda, A., Mechanistic analysis of muraymycin analogues: a guide to the design of MraY inhibitors. *J Med Chem* **2011,** *54* (24), 8421-39.

15. Aleiwi, B. A.; Schneider, C. M.; Kurosu, M., Synthesis of ureidomuraymycidine derivatives for structure-activity relationship studies of muraymycins. *The Journal of organic chemistry* **2012,** *77* (8), 3859-67.

16. Tanino, T.; Ichikawa, S.; Shiro, M.; Matsuda, A., Total synthesis of (-)-muraymycin D2 and its epimer. *The Journal of organic chemistry* **2010,** *75* (5), 1366-77.

17. Spork, A. P.; Ducho, C., Novel 5'-deoxy nucleosyl amino acid scaffolds for the synthesis of muraymycin analogues. *Organic & biomolecular chemistry* **2010,** *8* (10), 2323-6.

18. Tanino, T.; Ichikawa, S.; Al-Dabbagh, B.; Bouhss, A.; Oyama, H.; Matsuda, A., Synthesis and Biological Evaluation of Muraymycin Analogues Active against Anti-Drug-Resistant Bacteria. *ACS Med Chem Lett* **2010,** *1* (6), 258-62.

19. Ichikawa, S.; Yamaguchi, M.; Matsuda, A., Antibacterial Nucleoside Natural Products Inhibiting Phospho-MurNAc-Pentapeptide Translocase; Chemistry and Structure-Activity Relationship. *Current medicinal chemistry* **2015,** *22* (34), 3951-79.

20. Winn, M.; Goss, R. J. M.; Kimura, K.-i.; Bugg, T. D. H., Antimicrobial nucleoside antibiotics targeting cell wall assembly: Recent advances in structure-function studies and nucleoside biosynthesis. *Natural Product Reports* **2010,** *27* (2), 279-304.

21. Kimura, K.-i.; Bugg, T. D. H., Recent advances in antimicrobial nucleoside antibiotics targeting cell wall biosynthesis. *Natural Product Reports* **2003,** *20* (2), 252-273.

22. Cheng, L.; Chen, W.; Zhai, L.; Xu, D.; Huang, T.; Lin, S.; Zhou, X.; Deng, Z., Identification of the gene cluster involved in muraymycin biosynthesis from Streptomyces sp. NRRL 30471. *Molecular BioSystems* **2011,** *7* (3), 920-927.

23. Xu, D.; Liu, G.; Cheng, L.; Lu, X.; Chen, W.; Deng, Z., Identification of Mur34 as the novel negative regulator responsible for the biosynthesis of muraymycin in Streptomyces sp. NRRL30471. *PloS one* **2013,** *8* (10), e76068.

24. Lin, Y. I.; Li, Z.; Francisco, G. D.; Mcdonald, L. A., Antibiotics aa-896. Google Patents: 2002.

25. McDonald, L. A.; Barbieri, L. R.; Carter, G. T.; Kruppa, G.; Feng, X.; Lotvin, J. A.; Siegel, M. M., FTMS structure elucidation of natural products: application to muraymycin antibiotics using ESI multi-CHEF SORI-CID FTMS(n), the top-down/bottom-up approach, and HPLC ESI capillary-skimmer CID FTMS. *Anal Chem* **2003,** *75* (11), 2730-9.

26. Takeoka, Y.; Tanino, T.; Sekiguchi, M.; Yonezawa, S.; Sakagami, M.; Takahashi, F.; Togame, H.; Tanaka, Y.; Takemoto, H.; Ichikawa, S.; Matsuda, A., Expansion of Antibacterial Spectrum of Muraymycins toward Pseudomonas aeruginosa. *ACS Med Chem Lett* **2014,** *5* (5), 556-60.

27. McDonald, L. A.; Barbieri, L. R.; Carter, G. T.; Kruppa, G.; Feng, X.; Lotvin, J. A.; Siegel, M. M., FTMS Structure Elucidation of Natural Products: Application to Muraymycin Antibiotics Using ESI Multi-CHEF SORI-CID FTMSn, the Top-Down/Bottom-Up Approach, and HPLC ESI Capillary-Skimmer CID FTMS. *Analytical Chemistry* **2003,** *75* (11), 2730-2739.

28. Muramatsu, Y.; Arai, M.; Sakaida, Y.; Takamatsu, Y.; Miyakoshi, S.; Inukai, M., Studies on Novel Bacterial Translocase I Inhibitors, A-500359s, V. Enhanced Production of Capuramycin and A-500359 A in Streptomyces griseus SANK 60196. *J Antibiot* **2006,** *59* (9), 601-606.

29. Cai, W.; Wang, X.; Elshahawi, S. I.; Ponomareva, L. V.; Liu, X.; McErlean, M. R.; Cui, Z.; Arlinghaus, A. L.; Thorson, J. S.; Van Lanen, S. G., Antibacterial and Cytotoxic Actinomycins Y6–Y9 and Zp from Streptomyces sp. Strain Gö-GS12. *Journal of natural products* **2016,** *79* (10), 2731-2739.

30.	Wohnig, S.; Spork, A. P.; Koppermann, S.; Mieskes, G.; Gisch, N.; Jahn, R.; Ducho, C., Total Synthesis of Dansylated Park's Nucleotide for High-Throughput MraY Assays. *Chemistry-A European Journal* **2016,** *22* (49), 17813-17819.

31.	Rodolis, M. T.; Mihalyi, A.; Ducho, C.; Eitel, K.; Gust, B.; Goss, R. J.; Bugg, T. D., Mechanism of action of the uridyl peptide antibiotics: an unexpected link to a protein–protein interaction site in translocase MraY. *Chemical communications* **2014,** *50* (86), 13023-13025.

32.	Rodolis, M. T.; Mihalyi, A.; O'Reilly, A.; Slikas, J.; Roper, D. I.; Hancock, R. E.; Bugg, T. D., Identification of a novel inhibition site in translocase MraY based upon the site of interaction with lysis protein E from bacteriophage ϕX174. *ChemBioChem* **2014,** *15* (9), 1300-1308.

33.	Spork, A. P.; Büschleb, M.; Ries, O.; Wiegmann, D.; Boettcher, S.; Mihalyi, A.; Bugg, T. D.; Ducho, C., Lead structures for new antibacterials: stereocontrolled synthesis of a bioactive muraymycin analogue. *Chemistry-A European Journal* **2014,** *20* (47), 15292-15297.

34.	Stachyra, T.; Dini, C.; Ferrari, P.; Bouhss, A.; van Heijenoort, J.; Mengin-Lecreulx, D.; Blanot, D.; Biton, J.; Le Beller, D., Fluorescence detection-based functional assay for high-throughput screening for MraY. *Antimicrobial agents and chemotherapy* **2004,** *48* (3), 897-902.

35.	Brandish, P. E.; Burnham, M. K.; Lonsdale, J. T.; Southgate, R.; Inukai, M.; Bugg, T. D., Slow binding inhibition of phospho-N-acetylmuramyl-pentapeptide-translocase (Escherichia coli) by mureidomycin A. *Journal of Biological Chemistry* **1996,** *271* (13), 7609-7614.

36.	Brandish, P. E.; Kimura, K.-i.; Inukai, M.; Southgate, R.; Lonsdale, J. T.; Bugg, T., Modes of action of tunicamycin, liposidomycin B, and mureidomycin A: inhibition of phospho-N-acetylmuramyl-pentapeptide translocase from Escherichia coli. *Antimicrobial agents and chemotherapy* **1996,** *40* (7), 1640-1644.

37.	Rodolis, M. T.; Mihalyi, A.; Ducho, C.; Eitel, K.; Gust, B.; Goss, R. J.; Bugg, T. D., Mechanism of action of the uridyl peptide antibiotics: an unexpected link to a protein-protein interaction site in translocase MraY. *Chem Commun (Camb)* **2014,** *50* (86), 13023-5.

38.	Rodolis, M. T.; Mihalyi, A.; O'Reilly, A.; Slikas, J.; Roper, D. I.; Hancock, R. E. W.; Bugg, T. D. H., Identification of a Novel Inhibition Site in Translocase MraY Based upon the Site of Interaction with Lysis Protein E from Bacteriophage phi X174. *Chembiochem* **2014,** *15* (9), 1300-1308.

39.	Stachyra, T.; Dini, C.; Ferrari, P.; Bouhss, A.; van Heijenoort, J.; Mengin-Lecreulx, D.; Blanot, D.; Biton, J.; Le Beller, D., Fluorescence detection-based functional assay for high-throughput screening for MraY. *Antimicrobial agents and chemotherapy* **2004,** *48* (3), 897-902.

40.	Tanino, T.; Al-Dabbagh, B.; Mengin-Lecreulx, D.; Bouhss, A.; Oyama, H.; Ichikawa, S.; Matsuda, A., Mechanistic Analysis of Muraymycin Analogues: A Guide to the Design of MraY Inhibitors. *Journal of Medicinal Chemistry* **2011,** *54* (24), 8421-8439.

41.	Medema, M. H.; Blin, K.; Cimermancic, P.; de Jager, V.; Zakrzewski, P.; Fischbach, M. A.; Weber, T.; Takano, E.; Breitling, R., antiSMASH: rapid identification, annotation and analysis of secondary metabolite biosynthesis gene clusters in bacterial and fungal genome sequences. *Nucleic Acids Research* **2011,** *39* (Web Server issue), W339-W346.

42.	Weber, T.; Blin, K.; Duddela, S.; Krug, D.; Kim, H. U.; Bruccoleri, R.; Lee, S. Y.; Fischbach, M. A.; Müller, R.; Wohlleben, W.; Breitling, R.; Takano, E.; Medema, M. H., antiSMASH 3.0—a comprehensive resource for the genome mining of biosynthetic gene clusters. *Nucleic Acids Research* **2015,** *43* (W1), W237-W243.

43. Hiratsuka, T.; Suzuki, H.; Kariya, R.; Seo, T.; Minami, A.; Oikawa, H., Biosynthesis of the Structurally Unique Polycyclopropanated Polyketide–Nucleoside Hybrid Jawsamycin (FR-900848). *Angewandte Chemie International Edition* **2014,** *53* (21), 5423-5426.

44. Tang, M.-C.; Zou, Y.; Watanabe, K.; Walsh, C. T.; Tang, Y., Oxidative Cyclization in Natural Product Biosynthesis. *Chemical Reviews* **2017,** *117* (8), 5226-5333.

45. Stefan Koppermann, Z. C., Patrick D. Fischer,Xiachang Wang, Jannine Ludwig, Jon S. Thorson, Steven G. Van Lanen, and Christian Ducho, Insights into the Target Interaction of Naturally Occurring Muraymycin Nucleoside Antibiotics. *ChemMedChem*.

46. Funabashi, M.; Baba, S.; Nonaka, K.; Hosobuchi, M.; Fujita, Y.; Shibata, T.; Van Lanen, S. G., The Biosynthesis of Liposidomycin-like A-90289 Antibiotics Featuring a New Type of Sulfotransferase. *ChemBioChem* **2010,** *11* (2), 184-190.

47. Chi, X.; Pahari, P.; Nonaka, K.; Van Lanen, S. G., Biosynthetic origin and mechanism of formation of the aminoribosyl moiety of peptidyl nucleoside antibiotics. *Journal of the American Chemical Society* **2011,** *133* (36), 14452-14459.

48. Yang, Z.; Chi, X.; Funabashi, M.; Baba, S.; Nonaka, K.; Pahari, P.; Unrine, J.; Jacobsen, J. M.; Elliott, G. I.; Rohr, J.; Van Lanen, S. G., Characterization of LipL as a Non-heme, Fe(II)-dependent α-Ketoglutarate:UMP Dioxygenase That Generates Uridine-5′-aldehyde during A-90289 Biosynthesis. *Journal of Biological Chemistry* **2011,** *286* (10), 7885-7892.

49. Barnard-Britson, S.; Chi, X.; Nonaka, K.; Spork, A. P.; Tibrewal, N.; Goswami, A.; Pahari, P.; Ducho, C.; Rohr, J.; Van Lanen, S. G., Amalgamation of nucleosides and amino acids in antibiotic biosynthesis: discovery of an L-threonine: uridine-5′-aldehyde transaldolase. *Journal of the American Chemical Society* **2012,** *134* (45), 18514-18517.

50. Yang, Z.; Unrine, J.; Nonaka, K.; Van Lanen, S. G., Chapter Eight - Fe(II)-Dependent, Uridine-5′-Monophosphate α-Ketoglutarate Dioxygenases in the Synthesis of 5′-Modified Nucleosides. In *Methods in enzymology*, Hopwood, D. A., Ed. Academic Press: 2012; Vol. 516, pp 153-168.

51. Chi, X.; Baba, S.; Tibrewal, N.; Funabashi, M.; Nonaka, K.; Van Lanen, S. G., The muraminomicin biosynthetic gene cluster and enzymatic formation of the 2-deoxyaminoribosyl appendage. *MedChemComm* **2013,** *4* (1), 239-243.

52. Imai, K.; Fujii, S.; Takanohashi, K.; Furukawa, Y.; Masuda, T.; Honjo, M., *Phosphorylation. IV. Selective phosphorylation of the primary hydroxyl group in nucleosides*. 1969; Vol. 34.

53. Spork, A. P.; Ducho, C., Stereocontrolled synthesis of 5′-and 6′-epimeric analogues of muraymycin nucleoside antibiotics. *Synlett* **2013,** *24* (03), 343-346.

54. Tanaka, H.; Yamamoto, A.; Ishida, T.; Horiike, K., Simultaneous measurement of d-serine dehydratase and d-amino acid oxidase activities by the detection of 2-oxo-acid formation with reverse-phase high-performance liquid chromatography. *Analytical Biochemistry* **2007,** *362* (1), 83-88.

55. Yang, Z.; Chi, X.; Funabashi, M.; Baba, S.; Nonaka, K.; Pahari, P.; Unrine, J.; Jacobsen, J. M.; Elliott, G. I.; Rohr, J., Characterization of LipL as a non-heme, Fe (II)-dependent α-ketoglutarate: UMP dioxygenase that generates uridine-5′-aldehyde during A-90289 biosynthesis. *Journal of Biological Chemistry* **2011,** *286* (10), 7885-7892.

56. Goswami, A.; Liu, X.; Cai, W.; Wyche, T. P.; Bugni, T. S.; Meurillon, M.; Peyrottes, S.; Perigaud, C.; Nonaka, K.; Rohr, J.; Van Lanen, S. G., Evidence that oxidative dephosphorylation by the nonheme Fe(II), α-ketoglutarate:UMP oxygenase occurs by stereospecific hydroxylation. *FEBS Letters* **2017,** *591* (3), 468-478.

57.   Ochi, K.; Ezaki, M.; Iwani, M.; Komori, T.; Kohsaka, M., FR-900493 substance, a process for its production and a pharmaceutical composition containing the same. Google Patents: 1989.

58.   Fujita, Y.; Kizuka, M.; Funabashi, M.; Ogawa, Y.; Ishikawa, T.; Nonaka, K.; Takatsu, T., A-90289 A and B, new inhibitors of bacterial translocase I, produced by Streptomyces sp. SANK 60405. *The Journal of antibiotics* **2011,** *64* (7), 495-501.

59.   Igarashi, M.; Takahashi, Y.; Shitara, T.; Nakamura, H.; Naganawa, H.; Miyake, T.; Akamatsu, Y., Caprazamycins, novel lipo-nucleoside antibiotics, from Streptomyces sp. II. Structure elucidation of caprazamycins. *The Journal of antibiotics* **2005,** *58* (5), 327-37.

60.   Ubukata, M.; Isono, K.; Kimura, K.; Nelson, C. C.; McCloskey, J. A., The structure of liposidomycin B, an inhibitor of bacterial peptidoglycan synthesis. *Journal of the American Chemical Society* **1988,** *110* (13), 4416-4417.

61.   Funabashi, M.; Baba, S.; Takatsu, T.; Kizuka, M.; Ohata, Y.; Tanaka, M.; Nonaka, K.; Spork, A. P.; Ducho, C.; Chen, W.-C. L.; Van Lanen, S. G., Structure-Based Gene Targeting Discovery of Sphaerimicin, a Bacterial Translocase I Inhibitor. *Angewandte Chemie International Edition* **2013,** *52* (44), 11607-11611.

62.   Shiraishi, T.; Hiro, N.; Igarashi, M.; Nishiyama, M.; Kuzuyama, T., Biosynthesis of the antituberculous agent caprazamycin: Identification of caprazol-3"-phosphate, an unprecedented caprazamycin-related metabolite. *J Gen Appl Microbiol* **2016,** *62* (3), 164-6.

63.   Magnet, S.; Blanchard, J. S., Molecular insights into aminoglycoside action and resistance. *Chem Rev* **2005,** *105* (2), 477-98.

64.   Smith, C. A.; Baker, E. N., Aminoglycoside antibiotic resistance by enzymatic deactivation. *Current drug targets. Infectious disorders* **2002,** *2* (2), 143-60.

65.   Vakulenko, S. B.; Mobashery, S., Versatility of Aminoglycosides and Prospects for Their Future. *Clinical Microbiology Reviews* **2003,** *16* (3), 430-450.

66.   Wright, G. D., Bacterial resistance to antibiotics: Enzymatic degradation and modification. *Advanced Drug Delivery Reviews* **2005,** *57* (10), 1451-1470.

67.   Kudo, F.; Eguchi, T., Biosynthetic enzymes for the aminoglycosides butirosin and neomycin. *Methods in enzymology* **2009,** *459*, 493-519.

68.   Wehmeier, U. F.; Piepersberg, W., Enzymology of aminoglycoside biosynthesis-deduction from gene clusters. *Methods in enzymology* **2009,** *459*, 459-91.

69.   Barka, E. A.; Vatsa, P.; Sanchez, L.; Gaveau-Vaillant, N.; Jacquard, C.; Meier-Kolthoff, J. P.; Klenk, H. P.; Clement, C.; Ouhdouch, Y.; van Wezel, G. P., Taxonomy, Physiology, and Natural Products of Actinobacteria. *Microbiology and molecular biology reviews : MMBR* **2016,** *80* (1), 1-43.

70.   Kaysser, L.; Lutsch, L.; Siebenberg, S.; Wemakor, E.; Kammerer, B.; Gust, B., Identification and manipulation of the caprazamycin gene cluster lead to new simplified liponucleoside antibiotics and give insights into the biosynthetic pathway. *The Journal of biological chemistry* **2009,** *284* (22), 14987-96.

71.   Kaysser, L.; Siebenberg, S.; Kammerer, B.; Gust, B., Analysis of the liposidomycin gene cluster leads to the identification of new caprazamycin derivatives. *Chembiochem* **2010,** *11* (2), 191-6.

72.   Chen, Y.; Nasvall, J.; Wu, S.; Andersson, D. I.; Selmer, M., Structure of AadA from Salmonella enterica: a monomeric aminoglycoside (3")(9) adenyltransferase. *Acta crystallographica. Section D, Biological crystallography* **2015,** *71* (Pt 11), 2267-77.

73.   Pedersen, L. C.; Benning, M. M.; Holden, H. M., Structural investigation of the antibiotic and ATP-binding sites in kanamycin nucleotidyltransferase. *Biochemistry* **1995,** *34* (41), 13305-13311.

74. Noda, Y.; Yoda, K.; Takatsuki, A.; Yamasaki, M., TmrB protein, responsible for tunicamycin resistance of Bacillus subtilis, is a novel ATP-binding membrane protein. *Journal of bacteriology* **1992,** *174* (13), 4302-4307.

75. Noda, Y.; Takatsuki, A.; Yoda, K.; Yamasaki, M., TmrB protein, which confers resistance to tunicamycin on Bacillus subtilis, binds tunicamycin. *Bioscience, biotechnology, and biochemistry* **1995,** *59* (2), 321-322.

76. Kapp, U.; Macedo, S.; Hall, D. R.; Leiros, I.; McSweeney, S. M.; Mitchell, E., Structure of Deinococcus radiodurans tunicamycin-resistance protein (TmrD), a phosphotransferase. *Acta Crystallographica Section F: Structural Biology and Crystallization Communications* **2008,** *64* (6), 479-486.

77. Winn, M.; Goss, R. J.; Kimura, K.; Bugg, T. D., Antimicrobial nucleoside antibiotics targeting cell wall assembly: recent advances in structure-function studies and nucleoside biosynthesis. *Nat Prod Rep* **2010,** *27* (2), 279-304.

78. Ramirez, M. S.; Tolmasky, M. E., Aminoglycoside modifying enzymes. *Drug Resistance Updates* **2010,** *13* (6), 151-171.

79. NODA, Y.; URAKAWA, I.; YODA, K.; YAMASAKI, M., Bacillus subtilis TmrB protein confers resistance to tunicamycin on Escherichia coli. *The Journal of General and Applied Microbiology* **1996,** *42* (4), 343-347.

80. Hakulinen, J. K.; Hering, J.; Branden, G.; Chen, H.; Snijder, A.; Ek, M.; Johansson, P., MraY-antibiotic complex reveals details of tunicamycin mode of action. *Nat Chem Biol* **2017,** *13* (3), 265-267.

81. Fujita, Y.; Kizuka, M.; Funabashi, M.; Ogawa, Y.; Ishikawa, T.; Nonaka, K.; Takatsu, T., A-90289 A and B, new inhibitors of bacterial translocase I, produced by Streptomyces sp. SANK 60405. *The Journal of antibiotics* **2011,** *64* (7), 495-501.

82. Ichikawa, S.; Matsuda, A., Nucleoside natural products and related analogs with potential therapeutic properties as antibacterial and antiviral agents. *Expert Opinion on Therapeutic Patents* **2007,** *17* (5), 487-498.

83. Muramatsu, Y.; Arai, M.; Sakaida, Y.; Takamatsu, Y.; Miyakoshi, S.; Inukai, M., Studies on Novel Bacterial Translocase I Inhibitors, A-500359s. *J Antibiot* **2006,** *59* (9), 601-606.

84. Lee, J.; Sperandio, V.; Frantz, D. E.; Longgood, J.; Camilli, A.; Phillips, M. A.; Michael, A. J., An alternative polyamine biosynthetic pathway is widespread in bacteria and essential for biofilm formation in Vibrio cholerae. *Journal of Biological Chemistry* **2009,** *284* (15), 9899-9907.

85. Ghssein, G.; Brutesco, C.; Ouerdane, L.; Fojcik, C.; Izaute, A.; Wang, S.; Hajjar, C.; Lobinski, R.; Lemaire, D.; Richaud, P.; Voulhoux, R.; Espaillat, A.; Cava, F.; Pignol, D.; Borez ée-Durant, E.; Arnoux, P., Biosynthesis of a broad-spectrum nicotianamine-like metallophore in Staphylococcus aureus. *Science* **2016,** *352* (6289), 1105-1109.

86. Yang, S. F.; Hoffman, N. E., Ethylene biosynthesis and its regulation in higher plants. *Annual review of plant physiology* **1984,** *35* (1), 155-189.

87. Yip, W. K.; Dong, J. G.; Kenny, J. W.; Thompson, G. A.; Yang, S. F., Characterization and sequencing of the active site of 1-aminocyclopropane-1-carboxylate synthase. *Proceedings of the National Academy of Sciences of the United States of America* **1990,** *87* (20), 7930-4.

88. Ko, S.; Eliot, A. C.; Kirsch, J. F., S-methylmethionine is both a substrate and an inactivator of 1-aminocyclopropane-1-carboxylate synthase. *Archives of biochemistry and biophysics* **2004,** *421* (1), 85-90.

89.   Feng, L.; Kirsch, J. F., L-Vinylglycine is an alternative substrate as well as a mechanism-based inhibitor of 1-aminocyclopropane-1-carboxylate synthase. *Biochemistry* **2000,** *39* (10), 2436-2444.

90.   Okuda, K.; Kato, S.; Ito, T.; Shiraki, S.; Kawase, Y.; Goto, M.; Kawashima, S.; Hemmi, H.; Fukada, H.; Yoshimura, T., Role of the aminotransferase domain in Bacillus subtilis GabR, a pyridoxal 5'-phosphate-dependent transcriptional regulator. *Molecular microbiology* **2015,** *95* (2), 245-57.

91.   Dunwell, J. M.; Purvis, A.; Khuri, S., Cupins: the most functionally diverse protein superfamily? *Phytochemistry* **2004,** *65* (1), 7-17.

92.   Soding, J.; Biegert, A.; Lupas, A. N., The HHpred interactive server for protein homology detection and structure prediction. *Nucleic Acids Res* **2005,** *33* (Web Server issue), W244-8.

93.   Chowdhury, R.; Sekirnik, R.; Brissett, N. C.; Krojer, T.; Ho, C. H.; Ng, S. S.; Clifton, I. J.; Ge, W.; Kershaw, N. J.; Fox, G. C.; Muniz, J. R. C.; Vollmar, M.; Phillips, C.; Pilka, E. S.; Kavanagh, K. L.; von Delft, F.; Oppermann, U.; McDonough, M. A.; Doherty, A. J.; Schofield, C. J., Ribosomal oxygenases are structurally conserved from prokaryotes to humans. *Nature* **2014,** *510* (7505), 422-426.

94.   Wu, L.-F.; Meng, S.; Tang, G.-L., Ferrous iron and α-ketoglutarate-dependent dioxygenases in the biosynthesis of microbial natural products. *Biochimica et Biophysica Acta (BBA) - Proteins and Proteomics* **2016,** *1864* (5), 453-470.

95.   Yin, X.; Zabriskie, T. M., VioC is a non-heme iron, alpha-ketoglutarate-dependent oxygenase that catalyzes the formation of 3S-hydroxy-L-arginine during viomycin biosynthesis. *Chembiochem* **2004,** *5* (9), 1274-7.

96.   Katz, E.; Kamal, F.; Mason, K., Biosynthesis of trans-4-hydroxy-L-proline by Streptomyces griseoviridus. *The Journal of biological chemistry* **1979,** *254* (14), 6684-90.

97.   Strieker, M.; Kopp, F.; Mahlert, C.; Essen, L.-O.; Marahiel, M. A., Mechanistic and Structural Basis of Stereospecific Cβ-Hydroxylation in Calcium-Dependent Antibiotic, a Daptomycin-Type Lipopeptide. *ACS Chemical Biology* **2007,** *2* (3), 187-196.

98.   Houwaart, S.; Youssar, L.; Hüttel, W., Pneumocandin Biosynthesis: Involvement of a trans-Selective Proline Hydroxylase. *ChemBioChem* **2014,** *15* (16), 2365-2369.

99.   Almabruk, K. H.; Asamizu, S.; Chang, A.; Varghese, S. G.; Mahmud, T., The α-Ketoglutarate/FeII-Dependent Dioxygenase VldW Is Responsible for the Formation of Validamycin B. *Chembiochem* **2012,** *13* (15), 2209-2211.

100. Bursy, J.; Pierik, A. J.; Pica, N.; Bremer, E., Osmotically induced synthesis of the compatible solute hydroxyectoine is mediated by an evolutionarily conserved ectoine hydroxylase. *The Journal of biological chemistry* **2007,** *282* (43), 31147-55.

101. Strieker, M.; Nolan, E. M.; Walsh, C. T.; Marahiel, M. A., Stereospecific synthesis of threo-and erythro-β-hydroxyglutamic acid during kutzneride biosynthesis. *Journal of the American Chemical Society* **2009,** *131* (37), 13523-13530.

102. Jiang, W.; Cacho, R. A.; Chiou, G.; Garg, N. K.; Tang, Y.; Walsh, C. T., EcdGHK Are Three Tailoring Iron Oxygenases for Amino Acid Building Blocks of the Echinocandin Scaffold. *Journal of the American Chemical Society* **2013,** *135* (11), 4457-4466.

103. Chen, H.; Hubbard, B. K.; O'Connor, S. E.; Walsh, C. T., Formation of β-Hydroxy Histidine in the Biosynthesis of Nikkomycin Antibiotics. *Chemistry & Biology 9* (1), 103-112.

104. Cochrane, R. V.; Vederas, J. C., Highly selective but multifunctional oxygenases in secondary metabolism. *Accounts of chemical research* **2014,** *47* (10), 3148-3161.

Vita

Zheng Cui

Education
2009   B.S., Basic Pharmaceutical Science Base Class, School of Pharmacy, China Pharmaceutical University, Nanjing, Jiangsu, China
2012   M.S., Department of Pharmaceutics, School of Pharmaceutical Sciences, Health Science Center, Peking University, Beijing, China

Research Experience
2007-2009 Research Assistant, School of Pharmacy, China Pharmaceutical University, Nanjing, Jiangsu, China
2009-2012 Resarch Assistant, Department of Pharmaceutics, School of Pharmaceutical Sciences, Health Science Center, Peking University, Beijing, China
2012-2017 Research Assistant, Department of Pharmaceutical Sciences, College of Pharmacy, University of Kentucky, Lexington, KY. USA
2013-2014 Teaching Assistant, PHS 951 (Pharmacological Basics for Therapeutics) Fall 2013, Accommodations coordinator Spring 2014, Department of Pharmaceutical Sciences, College of Pharmacy, University of Kentucky, Lexington, KY. USA

Publications
• **Cui, Z.**, [#] Wang, X., [#] Koppermann, S., Thorson, J. S., Ducho, C., Van Lanen, S. G.,* "Antibiotic muraymycins from mutant strains of *Streptomyces* sp. NRRL 30471, J Nat Prod, accepted. [#] Cui, Z.and Wang, X., contributed equally to this work.
• Koppermann, S., **Cui, Z.**, Fischer, P.D., Wang, X., Ludwig, J., Thorson, J.S., Van Lanen, S.G., Ducho, C.,* Insights into the Target Interaction of Naturally Occurring Muraymycin Nucleoside Antibiotics, ChemMedChem, in press.
• Huang, Y., Liu, X., **Cui, Z**., Wiegmann, D., Niro, G.; Ducho, C., Song, Y., Yang, Z.,* Van Lanen, S. G.,* Pyridoxal-5′-phosphate as an Oxygenase Cofactor: Discovery of a Carboxamide-forming, α-amino acid monooxygenase-decarboxylase, PNAS, 2018**,** 115(5), 974-979.
• Cai, W., Wang, X., Elshahawi, S. I., Ponomareva, L. V., Liu, X., McErlean, M.R., **Cui, Z.**, Arlinghaus, A.L., Thorson, J.S., Van Lanen, S.G., * Antibacterial and Cytotoxic Actinomycins Y6-Y9 and Zp from Streptomyces sp. Strain Gö-GS12, J Nat Prod, 2016, 79(10), 2731-2739.
• Liu, X., Jin, Y., **Cui, Z.**, Nonaka, K., Baba, S., Funabashi, M., Yang, Z., Van Lanen, S.G.,* The Role of a Nonribosomal Peptide Synthetase in l-Lysine Lactamization During Capuramycin Biosynthesis, ChemBioChem, 2016(17), 804-810.
• Khisamutdinov, E.F., Bui, M.N., Jasinski, D., Zhao, Z., **Cui, Z.**, Guo, P.,* Simple Method for Constructing RNA Triangle, Square, Pentagon by Tuning Interior RNA 3WJ Angle from 60° to 90° or 108°, Methods Mol Biol, 2015(1316), 181-193.
• Li, H., Rychahou, P.G., **Cui, Z.**, Pi, F., Evers, B.M, Shu, D., Guo, P.,* Luo, W.,* RNA Nanoparticles Derived from Three-Way Junction of Phi29 Motor pRNA Are Resistant to I-125 and Cs-131 Radiation, Nucleic Acid Ther, 2015(25), 188-197.

• He, S., **Cui, Z.**, Wang, X., Zhang, H., Dai, W., Zhang, Q.,* Cremophor-free Intravenous Self-Microemulsions for Teniposide: Safety, Antitumor Activity *in vitro* and *in vivo*, Int J Pharm, 2015(495), 144-153.

• Gao, W., Lin, Z., Chen, M., Yang, X., **Cui, Z.**, Zhang, X., Yuan, L., Zhang, Q.,* The co-delivery of a low-dose P-glycoprotein inhibitor with doxorubicin sterically stabilized liposomes against breast cancer with low P-glycoprotein expression, Int J Nanomedicine, 2014(9), 3425-3437.

• Zhang, X., **Cui, Z.**, Zhang, X., He, B., Wang, X., Zhang, H., Zhong, Z., Zhang, Q.,* Characteristics, cellular uptake and transepithelial transport of coumarin6 loaded PEO-(hb-PG)-g-PCL miktoarm copolymer micelles, J. Chin. Pharm. Sci., 2013, 22(3), 251-258.

• He, S., **Cui, Z.**, Mei, D., Zhang, H., Wang, X., Dai, W., Zhang, Q.,* A Cremophor-Free Self-Microemulsified Delivery System for Intravenous Injection of Teniposide: Evaluation *in vitro* and *in vivo*, AAPS PharmSciTech., 2012, 13(3), 846-852.

• Zhang, J., He, B., Qu, W., **Cui, Z.**, Wang, Y., Zhang, H., Wang, J., Zhang, Q., * Preparation of the Albumin Nanoparticle System Loaded with Both Paclitaxel and Sorafenib and Its Evaluation *in Vitro* and *in Vivo*, J Microencapsul., 2011, 28(6), 528-536.

• Zhuang, J., Ping, Q.,* Song, Y., Qi, J., **Cui, Z.**, Effects of Chitosan Coating on Physical Properties and Pharmacokinetic Behavior of Mitoxantrone Liposomes, Int J Nanomedicine., 2010, 5, 407-416.

• Zhuang, J., Shi, Y., Ping, Q.,* Su, Z., **Cui, Z.**, Song, Y., 壳聚糖包覆米托蒽醌脂质体在荷瘤小鼠体内的组织分布及药效学 (Tissue Distribution and Pharmacodynamics of Chitosan Coated Mitoxantrone Liposomes in the Tumor Bearing Mice), Journal of China Pharmaceutical University, 2010, 41(4), 353-359.

• Gao, Z., **Cui, Z.**, Kou, J.,* 组胺 H1 受体功能及调节机制研究进展 (Advances on Research of Function and Regulatory Mechanism of Histamine H1 Receptor), Progress in Modern Biomedicine, 2009, 9(19), 3768-3771.

• **Cui, Z.**, Zheng, X., Gao, Z., Cao, F., Ping, Q.,* β-环糊精包合川芎挥发油的制备工艺研究 (Study on Inclusion Technique of *Ligusticum Chuanxiong* Hort Volatile Oil-β-Cyclodextrin Complex by Orthogonal Test), Journal of Chinese Medicinal Materials, 2008, 31(12), 1903-1906.

Zheng Cui